Compensation of Physical Impairments in Multi-Carrier Communications

A Thesis Submitted
to the College of Graduate and Postdoctoral Studies
in Partial Fulfillment of the Requirements
for the Degree of Doctor of Philosophy
in the Department of Electrical and Computer Engineering
University of Saskatchewan

by

Long D. Le

Saskatoon, Saskatchewan, Canada

Permission to Use

In presenting this thesis in partial fulfillment of the requirements for a Postgraduate degree from the University of Saskatchewan, it is agreed that the Libraries of this University may make it freely available for inspection. Permission for copying of this thesis in any manner, in whole or in part, for scholarly purposes may be granted by the professors who supervised this thesis work or, in their absence, by the Head of the Department of Electrical and Computer Engineering or the Dean of the College of Graduate and Postdoctoral Studies at the University of Saskatchewan. Any copying, publication, or use of this thesis, or parts thereof, for financial gain without the written permission of the author is strictly prohibited. Proper recognition shall be given to the author and to the University of Saskatchewan in any scholarly use which may be made of any material in this thesis.

Request for permission to copy or to make any other use of material in this thesis in whole or in part should be addressed to:

Head of the Department of Electrical and Computer Engineering
University of Saskatchewan
57 Campus Drive
Saskatoon, Saskatchewan S7N 5A9
Canada

OR

Dean
College of Graduate and Postdoctoral Studies
University of Saskatchewan
116 Thorvaldson Building, 110 Science Place
Saskatoon, Saskatchewan S7N 5C9
Canada

Acknowledgments

It is a pleasure to thank many people during my studies who made this dissertation possible. A few words mentioned here cannot adequately express my appreciation.

First, I would like to express my deepest gratitude to my supervisor, Professor Ha H. Nguyen, whose expertise, understanding and patience throughout my research program added considerably to my graduate experience. Without him, this thesis would not have been completed.

Second, I would like to also thank the other members of the committee, Professors Rajesh Karki, Joseph Eric Salt, Seok-Bum Ko, Xiongbiao Chen from the University of Saskatchewan and Professor Georges Kaddoum from the University of Quebec for reviewing and evaluating this thesis. Their insightful comments and suggestions have significantly improved the quality of this thesis.

Last but not least, I would like to thank my family for the support that they have provided me throughout my study. Without their love and encouragement, I would not have finished this thesis. My special thanks are extended to all my friends: Peter, Shania, Ali, Khai, Nghia and Botao in Communications Theories Research Group (CTRG) for sharing their knowledge and invaluable assistance.

Abstract

Among various multi-carrier transmission techniques, orthogonal frequency-division multiplexing (OFDM) is currently a popular choice in many wireless communication systems. This is mainly due to its numerous advantages, including resistance to multi-path distortions by using the cyclic prefix (CP) and a simple one-tap channel equalization, and efficient implementations based on the fast Fourier and inverse Fourier transforms. However, OFDM also has disadvantages which limit its use in some applications. First, the high out-of-band (OOB) emission in OFDM due to the inherent rectangular shaping filters poses a challenge for opportunistic and dynamic spectrum access where multiple users are sharing a limited transmission bandwidth. Second, a strict orthogonal synchronization between sub-carriers makes OFDM less attractive in low-power communication systems. Furthermore, the use of the CP in OFDM reduces the spectral efficiency and thus it may not be suitable for short-packet and low-latency transmission applications. Generalized frequency division multiplexing (GFDM) and circular filter-bank multi-carrier offset quadrature amplitude modulation (CFBMC-OQAM) have recently been considered as alternatives to OFDM for the air interface of wireless communication systems because they can overcome certain disadvantages in OFDM. Specifically, these two systems offer a flexibility in choosing the shaping filters so that the high OOB emission in OFDM can be avoided. Moreover, the strict orthogonality requirement in OFDM is relaxed in GFDM and CFBMC-OQAM which are, respectively, non-orthogonal and real-field orthogonal systems. Although a CP is also used in these two systems, the CP is added for a block of many symbols instead of only one symbol as in OFDM, which, therefore, improves the spectral efficiency. Given that the performance of a wireless communication system is affected by various physical impairments such as phase noise (PN), in-phase and quadrature (IQ) imbalance and imperfect channel estimation, this thesis proposes a number of novel signal processing algorithms to compensate for physical impairments in multi-carrier communication systems, including OFDM, GFDM and CFBMC-OQAM.

The first part of the thesis examines the use of OFDM in full-duplex (FD) communication under the presence of PN, IQ imbalance and nonlinearities. FD communication is a

promising technique since it can potentially double the spectral efficiency of the conventional half-duplex (HD) technique. However, the main challenge in implementing an FD wireless device is to cope with the self-interference (SI) imposed by the device's own transmission. The implementation of SI cancellation (SIC) faces many technical issues due to the physical impairments. In this part of research, an iterative algorithm is proposed in which the SI cancellation and detection of the desired signal benefit from each other. Specifically, in each iteration, the SI cancellation performs a widely linear estimation of the SI channel and compensates for the physical impairments to improve the detection performance of the desired signal. The detected desired signal is in turn removed from the received signal to improve SI channel estimation and SI cancellation in the next iteration. Results obtained show that the proposed algorithm significantly outperforms existing algorithms in SI cancellation and detection of the desired signal.

In the next part of the thesis, the impact of PN and its compensation for CFBMC-OQAM systems are considered. The sources of performance degradation are first quantified. Then, a two-stage PN compensation algorithm is proposed. In the first stage, the channel frequency response and PN are estimated based on the transmission of a preamble, which is designed to minimize the channel mean squared error (MSE). In the second stage the PN compensation is performed using the estimate obtained from the first stage together with the transmitted pilot symbols. Simulation results obtained under practical scenarios show that the proposed algorithm effectively estimates the channel frequency response and compensates for the PN. The proposed algorithm is also shown to outperform an existing algorithm that implements iterative PN compensation when the PN impact is high.

As a further development from the second part, the third part of the thesis considers the impacts of both PN and IQ imbalance and proposes a unified two-stage compensation algorithm for a general multi-carrier system, which can include OFDM, GFDM and CFBMC-OQAM. Specifically, in the first stage, the channel impulse response and IQ imbalance parameters are first estimated based on the transmission of a preamble. Given the estimates obtained from the first stage, in the second stage the IQ imbalance and PN are compensated in that order based on the pilot symbols for the rest of data transmis-

sion blocks. The preamble is designed such that the estimation of IQ imbalance does not depend on the channel and PN estimation errors. The proposed algorithm is then further extended to a multiple-input multiple-output (MIMO) system. For such a MIMO system, the preamble design is generalized so that the multiple IQ imbalances as well as channel impulse responses can be effectively estimated based on a single preamble block. Simulation results are presented and discussed in a variety of scenarios to show the effectiveness of the proposed algorithm.

Table of Contents

List of Tables

List of Figures

List of Abbreviations

M-QAM	M-ary Quadrature Amplitude Modulation
5G	The 5th Generation
ADC	Analog-to-Digital Converter
AM/AM	Amplitude to Amplitude Modulation
AM/PM	Amplitude to Phase Modulation
AWGN	Additive White Gaussian Noise
BER	Bit-Error Rate
BPF	Band-Pass Filter
BPSK	Binary Phase Shift Keying
CFBMC	Circular Filter-Bank Multi-Carrier
CFO	Carrier Frequency Offset
CP	Cyclic Prefix
CPE	Common Phase Error
DAC	Digital-to-Analog Converter
DFT	Discrete Fourier Transform
EGF	Extended Gaussian Filter
EPA	Extended Pedestrian A
EVA	Extended Vehicular A
EVM	Error Vector Magnitude
FBMC	Filter-Bank Multi-Carrier
FD	Full-Duplex
FDD	Frequency-Domain Division
FFT	Fast Fourier Transform
FR	Free Running
GFDM	Generalized Frequency-Division Multiplexing
HD	Half-Duplex
IBI	Inter-Block Interference
ICI	Inter-Carrier Interference
IDFT	Inverse Discrete Fourier Transform

IEEE	Institute of Electrical and Electronics Engineers
IFFT	Inverse Fast Fourier Transform
IQ	In-phase and Quadrature
ISI	Inter-Symbol Interference
LMS	Least Mean Square
LNA	Low-Noise Amplifier
LO	Local Oscillator
LS	Least Square
LSE	Least Square Estimation
LUT	Look-Up Table
MF	Matched Filter
MIMO	Multi-Input Multi-Output
MMSE	Minimum Mean-Squared Error
MSE	Mean Squared Error
OFDM	Orthogonal Frequency-Division Multiplexing
OOB	Out-Of-Band
OQAM	Offset Quadrature Amplitude Modulation
PA	Power Amplifier
PER	Packet-Error Rate
PLL	Phase-Locked Loop
PN	Phase Noise
PSD	Power Spectral Density
QPSK	Quadrature Phase Shift Keying
RD	Raised Cosine
RF	Radio Frequency
RSI	Residual Self Interference
S/P	Serial-to-Parallel
SFBC	Space-Frequency Block Code
SI	Self-Interference
SIC	Self-Interference Cancellation

SIR	Signal-to-Interference Ratio
SISO	Single Input Single Output
SNR	Signal-to-Noise Ratio
SRRC	Square-Root Raised Cosine
TDD	Time-Domain Division
VCO	Voltage Controlled Oscillator
WLE	Widely Linear Estimation
ZF	Zero Forcing

1. Introduction

1.1 Motivation

The next generation of wireless communication systems is expected to support not only a wide range of data rates, but also a large number of devices which share a limited transmission bandwidth. Currently, wireless communication techniques can be broadly divided into two categories. One is single-carrier modulation techniques and the other is multi-carrier modulation techniques. Single-carrier modulation techniques have a long development history and have been widely used in many wireless communication systems. However, single-carrier modulation systems use only one radio-frequency (RF) signal (sinusoid) to transmit data symbols and often require complicated multi-tap equalizers to detect the transmitted symbols because of the interferences induced from multi-path fading channels in wireless communications. In contrast to single-carrier modulation techniques, multi-carrier modulation techniques partition the whole channel's frequency band into many sub-channels and the high-rate data stream is divided into many low-rate sub-streams that are transmitted in parallel. If the sub-channels are narrow enough, the associated channel frequency response in each sub-channel is essentially constant, which enables low-complexity detection of the transmitted information.

Multi-carrier transmission has been extensively studied over the last few decades [1]. Currently, orthogonal frequency-division multiplexing (OFDM) is the dominant signaling format for high-speed wireless communication due to its numerous advantages [2]. Specifically, OFDM provides an efficient implementation based on the use of inverse discrete Fourier transform (IDFT) and discrete Fourier transform (DFT) at the transmitter and receiver, respectively. The interferences induced from a dispersive fading channel are completely re-

moved by the use of a cyclic prefix (CP) whose length is longer than the delay spread of the channel. As such, OFDM enables a simple channel equalization. Furthermore, this multi-carrier modulation can be readily applied for multiple-input multiple-output (MIMO) channels. However, OFDM also has its own disadvantages which limit its use in some applications envisioned for the next generation wireless networks. First, the use of IDFT at the transmitter is equivalent to the use of a rectangular pulse shaping filter which leads to an undesirable magnitude response in the frequency domain. As such, this disadvantage prevents OFDM from being applied in non-contiguous spectrum sharing systems [3]. Second, many advantages of OFDM requires the strict orthogonality among sub-carriers, which is, however, hardly achieved in practice due to unavoidable frequency and timing offsets between the transmitter and the receiver. To cope with these impairments, a compensation algorithm is required which, therefore, increases not only the implementation complexity of the transceiver, but also the power spent for orthogonality acquisition. As such, OFDM may not be a suitable choice in applications that demand very low power consumption [4]. Furthermore, since a CP does not carry any useful information, its use results in a loss of spectral efficiency and increased latency. Therefore, the application of OFDM in short-packet and low-latency communication is also limited [5].

Generalized frequency-division multiplexing (GFDM) [6,7] and circular filter-bank multi-carrier offset quadrature amplitude modulation (CFBMC-OQAM) [8] have been recently proposed for next generation wireless networks to overcome the disadvantages of OFDM [9]. The rectangular pulse shaping filter in OFDM is replaced by a better designed prototype filter in GFDM. As such, GFDM is more favorable in non-contiguous spectrum sharing systems. The orthogonality requirement among sub-carriers in OFDM is also removed in GFDM, but it comes at the expense of having interferences induced from one sub-carrier to the other. Therefore, interference cancellation techniques are often used to avoid performance degradation [9]. To overcome the need of having a high-complexity receiver in GFDM, CFBMC-OQAM is proposed. Specifically, CFBMC-OQAM has all advantages of GFDM. The orthogonality is now relaxed in the real domain with the use of OQAM. It has been shown that in the ideal case where there is no channel and noise, CFBMC-OQAM systems are

free of interferences. In GFDM and CFBMC-OQAM, the transmitted signal is constructed in blocks, each consisting of multiple sub-symbols. In this way, the insertion of CP can be implemented in a more spectrally efficient manner compared to OFDM. In particular, the overhead induced from CP is kept minimum in GFDM and CFBMC-OQAM by adding a single CP for the entire block of sub-symbols instead of for every sub-symbols as in OFDM.

Because of their relevance in high-speed communication systems, OFDM, GFDM and CFBMC-OQAM are studied in this thesis. The next section discusses further the main objectives of this research.

1.2 Research Objectives

There are two main objectives in this research:

(i) **Integration of full-duplex communications with OFDM.** Future wireless networks are envisioned to deliver ever-increasing data rates. As such, integration of new techniques into multi-carrier communication systems is inevitable. Current wireless communication systems are designed for devices that operate on a half-duplex (HD) mode in which signal transmission and reception are performed separately by either a time-division or frequency-division duplex. Instead of HD operation, full-duplex (FD) operation has recently been considered to improve the spectral efficiency of a wireless communication system.

The biggest challenge in realizing FD communications is to handle the enormous amount of self-interference (SI), which is caused by the large power difference between the signal imposed by a device's own wireless transmissions and the received desired signal arriving from a remote device. Ideally, a perfect suppression of the SI is plausible since the transmitted signal is always known within the FD device. However, in reality, the actual SI signal is only partially known due to many inherently physical impairments in the transceiver's circuitry such as phase noise (PN), in-phase and quadrature (IQ) imbalance and nonlinearities.

Although PN, IQ imbalance and nonlinearities have been studied for FD communi-

cations, their impacts are often considered separately or as a combination of two or three impairments, and also in either a transmitter or a receiver only. In other words, there is no work considering the joint effects of PN, IQ imbalance and nonlinearity from both the transmitter and receiver in a multi-carrier FD communication system. Moreover, the interference induced from physical impairments is commonly treated as noise in existing research in order to simplify the system model. Different from existing research, we shall consider a bi-directional FD communication system in which PN, IQ imbalance and nonlinearity are present in both transmitter and receiver. Impacts of the physical impairments shall be first analyzed. The obtained analysis is then used to guide the development of an algorithm that can take into account the impacts of PN, IQ imbalance and nonlinearity to effectively mitigate the effect of SI. Performance of the developed algorithm shall be evaluated based on computer simulation and compared with existing algorithms to show whether the developed algorithm can do a better job in canceling SI, leading to improving the decoding performance of the desired signal.

(ii) **Impact of physical impairments and their compensation in multi-carrier systems.** Hardware imperfections can significantly degrade performance of wireless multi-carrier systems by causing distortions, interferences and other random effects. Dealing with physical impairments such as PN, IQ imbalance and nonlinearities will be one of the major design challenges for the next generation wireless communication systems due to conflicting requirements, namely high data rate, low cost and low power consumption. Relying on digital compensation of the imperfections appears to be a very promising approach. Pursuing that path, however, requires thorough understanding of the influence of the RF non-ideal effects on the received signal and the resulting system performance.

The impact of physical impairments and their compensation have been extensively studied for OFDM systems. However, not many studies have been done for GFDM and CFBMC-OQAM systems concerning physical impairments. Recall that, different from OFDM, GFDM and CFBMC-OQAM are, respectively, non-orthogonal and real-domain orthogonal systems. Having different signal processing operations in the

transceiver would result in different impacts of physical impairments on the received signal, and hence require different ways to compensate for them.

In this research, the impact of PN and its compensation shall be first studied in CFBMC-OQAM systems. Specifically, the interferences induced by PN shall be first quantified. Then, an algorithm shall be proposed to compensate for the PN impact which should take into account the interferences. Compensation of PN is even more challenging when the channel is unknown. As such we shall also develop a PN compensation algorithm that can work effectively with the estimated channel.

Along with PN, the impact of IQ imbalance shall also be considered. Furthermore, this part of research shall be considered for a general multi-carrier system, which includes OFDM, GFDM and CFBMC-OQAM as particular cases. We aim to design a preamble so that estimation of the IQ imbalance parameters can be done independently from the channel estimate. Given the IQ imbalance and channel estimates, compensation of the IQ imbalance and PN are then carried out. The developed algorithm shall be further extended to a MIMO system.

1.3 Organization of the Thesis

This thesis is organized in a manuscript-based style. The results obtained are included in the form of published manuscripts. In each chapter, a brief introduction precedes each manuscript in order to connect the manuscript to the main context of the thesis.

This thesis has seven chapters. The first chapter gives a motivation of the research and states the research objectives.

Chapter 2 provides an in-depth look at the single-carrier QAM and multi-carrier systems. The fundamental difference between the two systems will be explained. Discussion of FD communications and physical impairments is also included in this chapter.

In Chapter 3, a bi-directional OFDM-based FD communication scenario is considered. In this work, the implementation of self-interference cancellation (SIC) is affected by the presence of PN, IQ imbalance and power amplifier (PA) nonlinearity. To effectively mitigate

the effect of self-interference (SI), the proposed SIC algorithm in this chapter is operated iteratively in which the processes of SI cancellation and detection of the desired signal aid each other in each iteration. The impairments are also estimated and compensated to improve the decoding performance.

In Chapters 4 and 5, the impact of PN and its compensation are considered in CFBMC-OQAM systems. The source of performance degradation in CFBMC-OQAM in terms of signal-to-interference ratio (SIR) induced from the PN impact is first studied in Chapter 4. Then, an algorithm is proposed to compensate the PN impact by estimating the PN conjugation. Different from Chapter 4 where the channel is assumed to be perfectly known at the receiver, a two-stage algorithm is proposed in Chapter 5 to take into account the channel estimation error while performing the PN compensation.

As a further development from Chapters 4 and 5, the impact of both PN and IQ imbalance is considered in multi-carrier modulation systems in Chapter 6. A two-stage compensation algorithm is first proposed for a single-input single-output (SISO) system in this chapter. Then, the proposed algorithm is further extended to a MIMO system where a spatial diversity technique is deployed.

Finally, Chapter 7 summarizes the contributions of this thesis and suggests potential research problems for future works.

For all the four published manuscripts in Chapters 3 to 6, the research problems were jointly formulated by the student and the supervisor. The student made original and major contributions in addressing these problems, carrying out analysis, writing Matlab programs for computer simulation, obtaining and presenting the results, preparing the first versions of the manuscripts, and implementing revisions required by the reviewers. The supervisor worked closely with the student and provided comments, suggestions, and corrections in all aspects of the research.

References

[1] B. Farhang-Boroujeny: "OFDM Versus Filter Bank Multicarrier", *IEEE Signal Processing Magazine*, vol. 28, no. 3, pp. 92–112, May 2011.

[2] T. Hwang and C. Yang and G. Wu and S. Li and G. Y. Li: "OFDM and Its Wireless Applications: A Survey", *IEEE Transactions on Vehicular Technology*, vol. 58, no. 4, pp. 1673–1694, May 2009.

[3] I. B. F. de Almeida, L. L. Mendes, J. J. P. C. Rodrigues and M. A. A. da Cruz, "5G Waveforms for IoT Applications," *IEEE Communications Surveys & Tutorials*, vol. 21, no. 3, pp. 2554–2567, 2019.

[4] Y. Medjahdi et al., "On the Road to 5G: Comparative Study of Physical Layer in MTC Context," *IEEE Access*, vol. 5, pp. 26556-26581, 2017.

[5] G. Durisi, T. Koch and P. Popovski, "Toward Massive, Ultrareliable, and Low-Latency Wireless Communication With Short Packets," *Proceedings of the IEEE*, vol. 104, no. 9, pp. 1711–1726, Sept. 2016.

[6] G. Fettweis and M. Krondorf and S. Bittner: "GFDM - Generalized Frequency Division Multiplexing", *IEEE 69th Vehicular Technology Conference*, pp. 1–4, April 2009.

[7] N. Michailow and M. Matth and I. S. Gaspar and A. N. Caldevilla and L. L. Mendes and A. Festag and G. Fettweis: "Generalized Frequency Division Multiplexing for 5th Generation Cellular Networks", *IEEE Transactions on Communications*, vol. 62, no. 9, pp. 3045–3061, Sept. 2014.

[8] A. RezazadehReyhani and B. Farhang-Boroujeny: "An Analytical Study of Circularly Pulse-Shaped FBMC-OQAM Waveforms", *IEEE Signal Processing Letters*, vol. 24, no. 10, pp. 1503–1506, Oct. 2017.

[9] A. RezazadehReyhani and A. Farhang and B. Farhang-Boroujeny: "Circularly Pulse-Shaped Waveforms for 5G: Options and Comparisons", *2015 IEEE Global Communications Conference (GLOBECOM)*, pp. 1–7, Dec. 2015.

2. Background

The main purpose of every communication system is to reliably transmit as much information as possible through a propagation channel. Depending on channel characteristics, a communication system can be generally classified as a wired or wireless communication system. In wired communication, signal is transmitted as electrical currents over physical filaments like coaxial cables, or twisted pairs. On the other hand, wireless communication involves the transmission of signals through the air without requiring any wires or cables or electrical conductors. Compared to wired communication, wireless communication has been more widely used nowadays because of its advantages such as there is no need to physically connect the transmitter and receiver in order to transmit or receive messages. Thus wireless communication enables people to communicate with each other virtually regardless of their locations. However, wireless communication has its own disadvantages such as wireless networks are extremely susceptible to noise and interference from other signals being transmitted on the same channel. Also, the range of a wireless network is generally limited. This thesis particularly focuses on studying wireless communication systems.

A typical wireless communication system is depicted in Fig. 2.1. In this figure, the information source is represented as a sequence of bits 0's and 1's. The function of a transmitter is to convert a bit stream to a continuous time signal $x(t)$ before transmitting through a channel. In practice, this process undergoes many stages. Specifically, taking into account the redundancy of the information source, a source encoder represents the information in a more compact form by a compression algorithm. The strategy of a channel encoder, on the other hand, is to add redundancy to the compressed signal so that errors caused by noise and interference during transmission can be corrected at the receiver. To properly represent the

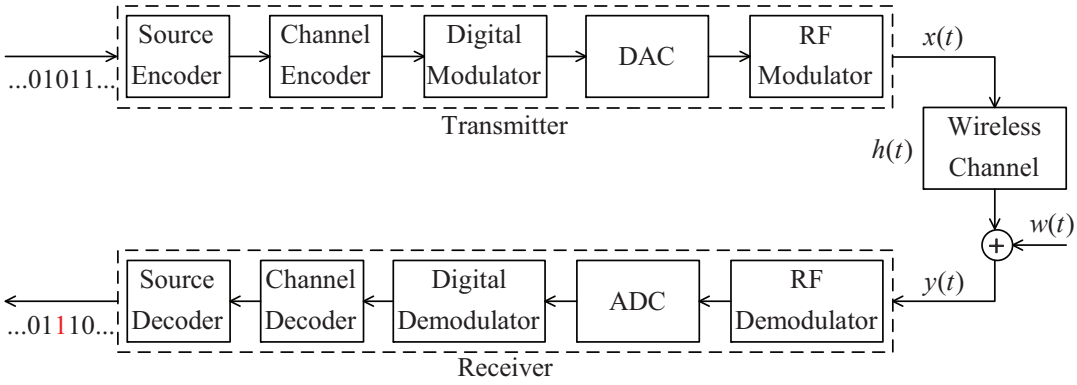

Figure 2.1: A simple block diagram of a wireless communication system.

signal for transmission, the coded bit sequence is further processed by a digital modulator to map the bits into complex symbols.

For efficient transmission over a wireless channel, the complex symbols are further modulated with a very high radio frequency (RF) signal before being sent to the transmit antenna. This RF signal is also called as a carrier because it helps to "carry" information from a transmitter to a receiver over the air. This process is called RF up-conversion. The signals before and after this up-conversion are referred to as baseband and passband signals, respectively. To perform the RF up-conversion, the discrete-time signal from the digital modulator is first passed through a digital-to-analog converter (DAC) to convert the transmitted signal from the discrete-time domain to the continuous-time domain. The output of the DAC is then modulated with the RF signal which is represented by "RF Modulator" block in Fig. 2.1.

The passband signal is then transmitted through a wireless channel. In Fig. 2.1, the channel is represented by an impulse response $h(t)$. Recall that the impulse response of a system refers to the response of that system when its input is an impulse. During transmission, the signal is usually distorted by contamination such as noise or interference from other signals being transmitted over the same channel. This contamination is represented by $w(t)$ in Fig. 2.1.

The main task of a receiver is to reconstruct the information bit sequence from the distorted signal with as less errors as possible. The reconstruction process is performed in the reverse order as what was done at the transmitter. Specifically, the received passband

waveform is first down-converted and sampled to obtain the discrete-time baseband signal, which is performed by the "RF Demodulator" and analog-to-digital converter (ADC) blocks in Fig. 2.1. The discrete-time baseband signal is then processed by a digital demodulator. The coded bit sequence after demodulating is then passed through a channel decoder which is responsible for detecting and correcting erroneous bits. A source decoder eventually reverts the compression process to recover the transmitted information bit sequence.

This thesis mainly focuses on signal processing steps between digital modulation at the transmitter and digital demodulation at the receiver. In this chapter, a single-carrier wireless communication system is first presented in Section 2.1. Then the limitation of this system in dealing with a multi-path channel is discussed to motivate the use of multi-carrier wireless communication, which is described in Section 2.2. Next, an introduction to the impact of physical impairments in communication systems is given in Section 2.3, which is then followed by a description of FD communications in Section 2.4.

2.1 Single-Carrier Wireless Communication Systems

2.1.1 Transmitter

Among various modulation techniques, M-ary quadrature amplitude modulation (M-QAM) is perhaps the most popular technique being used in many communication systems nowadays. Fig. 2.2 shows two M-QAM constellations. The left constellation is 4-QAM, which is more commonly referred to as Quadrature Phase Shift Keying (QPSK), and the right constellation is 16-QAM. It is pointed out that a constellation of an M-ary QAM modulation represents a set of M symbols in a two-dimensional IQ-plane. In this plane, each symbol is represented by a complex number in which the in-phase (I) axis and quadrature (Q) axis represent the real and imaginary components, respectively. The mapping of a bit sequence into a complex symbol in Fig. 2.2 is known as Gray mapping, in which adjacent symbols differ by only one bit. With such a mapping, if a detection error occurs between adjacent constellation points, which is the most probable error in practice, it results in only one bit error. For example, if the input of a 4-QAM modulator is [01 11 00 01], then the output of the modulator is a sequence of complex symbols $[1-j \quad -1-j \quad 1+j \quad 1-j]$.

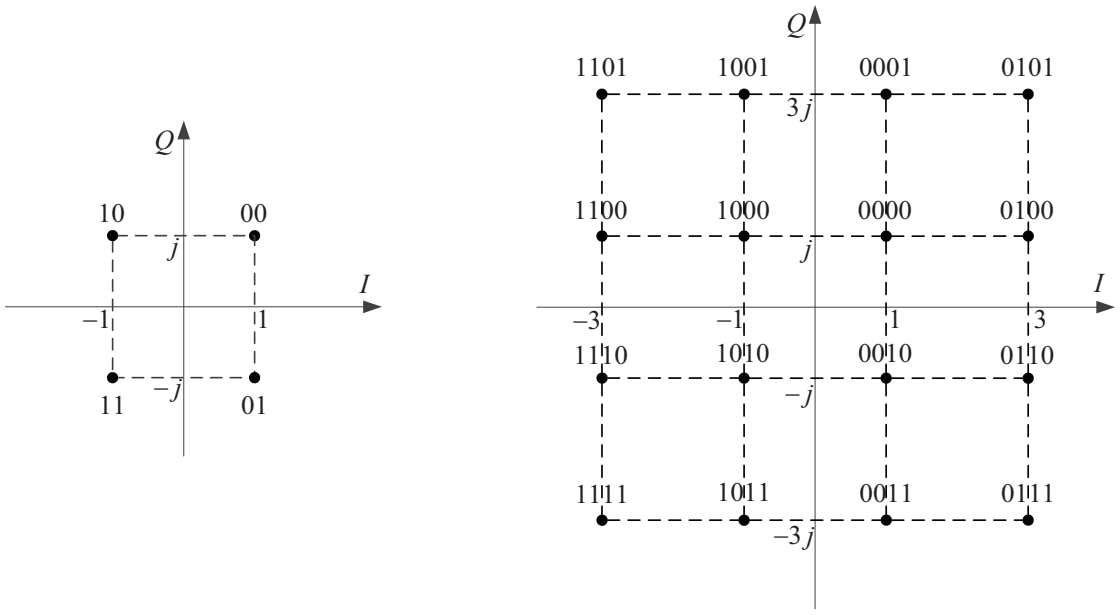

4-QAM or QPSK 16-QAM

Figure 2.2: Examples of QPSK ($M = 4$) and 16-QAM ($M = 16$) constellations.

Fig. 2.3 depicts a block diagram of a single-carrier wireless communication system. At the transmitter, the input bit stream is divided into segments consisting of $\log_2 M$ bits by the serial-to-parallel (S/P) converter. The mapping from a bit segment to a symbol is performed in a look-up table (LUT). For example, based on the mapping from Fig. 2.2, the look-up tables LUT 1 and LUT 2 are shown in Fig. 2.4 for I and Q components for 16-QAM modulation, respectively. From Fig. 2.3, the transmitted M-QAM passband signal can be represented as

$$x(t) = \sum_n \Big(\sqrt{2} x_I[n] p_T(t - nT_s) \cos(\omega_c t) - \sqrt{2} x_Q[n] p_T(t - nT_s) \sin(\omega_c t) \Big) \qquad (2.1)$$

where $p_T(t)$ is the impulse response of the transmit pulse shaping filter, $x_I[n]$ and $x_Q[n]$ are the outputs of LUT 1 and LUT 2, respectively. T_s is the symbol interval, $\omega_c = 2\pi f_c$ and f_c is the frequency of the RF signal. It is pointed out that the DAC block in Fig. 2.1 can be equivalently separated into the "Impulse Modulator" and "Pulse Shaping Filter" blocks in Fig. 2.3. Define $x[n] = x_I[n] + j x_Q[n]$. Then the transmitted signal in (2.1) can be rewritten

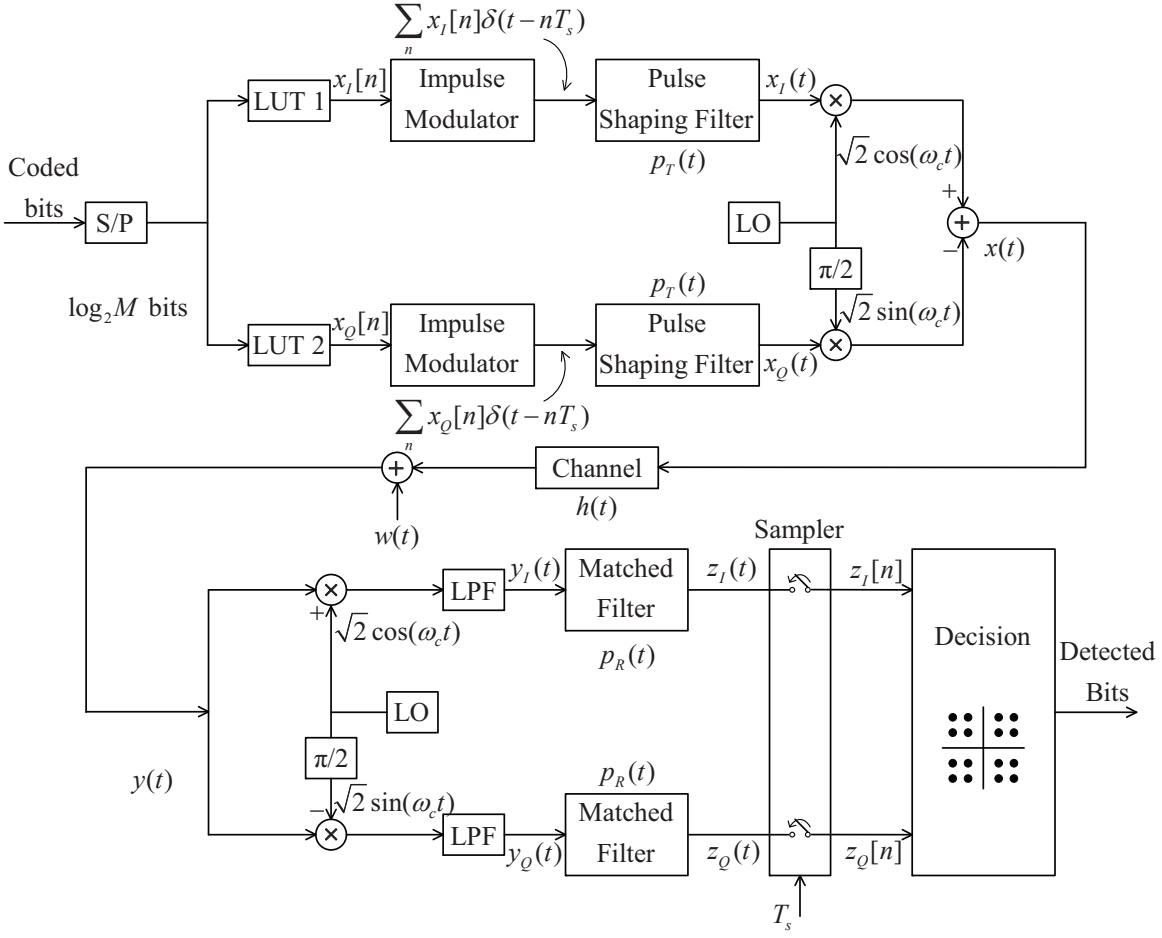

Figure 2.3: Block diagram of a single-carrier wireless communication system.

as

$$x(t) = \sqrt{2}\Re\left\{\sum_n x[n]p_T(t-nT_s)\mathrm{e}^{j\omega_c t}\right\}. \tag{2.2}$$

Next, the passband signal $x(t)$ is propagated through a wireless channel.

2.1.2 Wireless Channel

In Fig. 2.3, the wireless channel is characterized by an impulse response $h(t)$. A defining characteristic of a wireless channel is the variation of channel strength over time and frequency. This variation can be broadly divided into two different types as large-scale fading and small-scale fading. A classification of fading channels is illustrated in Fig. 2.5. Large-scale fading occurs when a mobile device moves through a large distance, for example, a distance of the order of a cell size. It is caused by path loss of signal as a function of distance

LUT 1	
0000	1
0001	1
0010	1
0011	1
0100	3
0101	3
0110	3
0111	3
1000	−1
1001	−1
1010	−1
1011	−1
1100	−3
1101	−3
1110	−3
1111	−3

LUT 2	
0000	1
0001	3
0010	−1
0011	−3
0100	1
0101	3
0110	−1
0111	−3
1000	1
1001	3
1010	−1
1011	−3
1100	1
1101	3
1110	−1
1111	−3

Figure 2.4: Look-up tables for 16-QAM modulation.

and shadowing by large objects such as buildings or hills. On the other hand, small-scale fading refers to a rapid variation of signal levels due to constructive and destructive interference of multiple signal paths (multi-paths) when the mobile moves over short distances. For small-scale fading, as the mobile terminal moves, depending on the transmission scheme

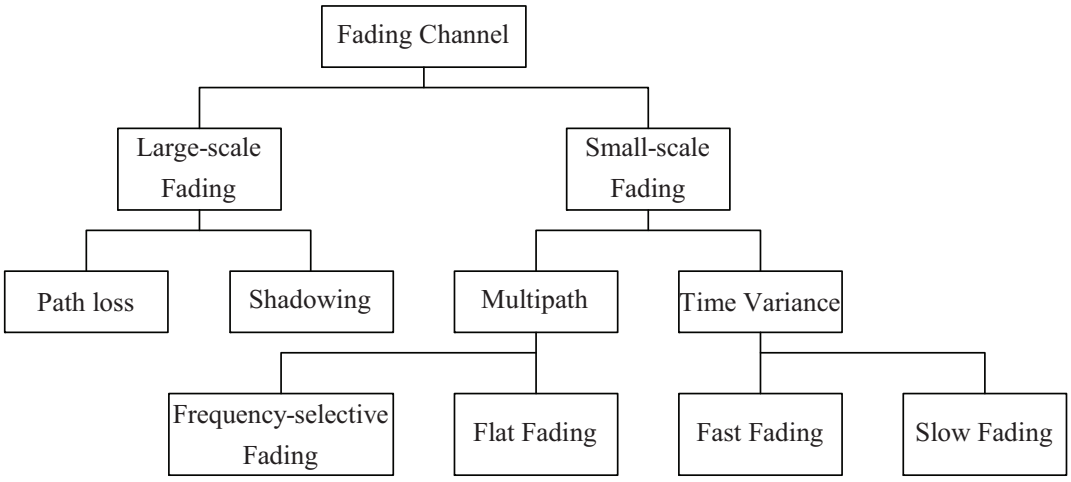

Figure 2.5: A classification of fading channels.

and channel characteristics, there are some specific types of fading as indicated in Fig. 2.5. A transmission scheme is specified with signal parameters such as signal bandwidth B_s and symbol period T_s. Meanwhile, a wireless channel is characterized by two important param-

eters, multi-path delay spread T_d and Doppler spread D_s.

Multi-path delay spread is defined as the difference in propagation time between the longest and shortest paths, counting only the paths with significant power. Define $W_c = \frac{1}{2T_d}$ as the coherence bandwidth. Then, when bandwith of the input signal B_s is considerably less than W_c, the channel is usually referred to as flat fading. In this case, the delay spread T_d is much less than the symbol interval T_s, and the channel impulse response $h(t)$ can be represented by an one-tap filter. Whereas, when bandwidth B_s is much larger than W_c, the channel is said to be frequency selective, and it has to be represented by a multi-tap filter.

Doppler spread is a measure of spectral broadening caused by the rate of change of the mobile radio channel and is defined as a range of frequencies over which the received Doppler spectrum is essentially nonzero. Define $T_c = \frac{1}{4D_s}$ as the coherence time. Then, when the symbol interval T_s is much greater than the coherence time T_c, the channel is referred to as fast fading. Otherwise, the channel is referred to as slow fading.

2.1.3 Receiver

At the receiver, the received signal is corrupted by noise and interferences, which are all together represented as $w(t)$. Hence, the received signal can be written as

$$y(t) = h(t) * x(t) + w(t) \tag{2.3}$$

where $*$ denotes linear convolution operator. The received signal $y(t)$ is first down-converted to baseband by mixing with $\sqrt{2}\cos(\omega_c t)$ and $-\sqrt{2}\sin(\omega_c t)$, and then passed through low-pass filters to obtain $y_I(t)$ and $y_Q(t)$ corresponding to the in-phase and quadrature signal components, respectively. The resulting signals are further forwarded to matched filters, which are characterized by an impulse response $p_R(t)$, to produce $z_I(t)$ and $z_Q(t)$. The resulting signals are sampled by a sampler at every T_s seconds to obtain discrete-time signals $z_I[n]$ and $z_Q[n]$. These signals are then forwarded to the decision block to detect the transmitted bits.

The communication occurs in the passband domain. However, most of the processing, such as coding/decoding, modulation/demodulation, is performed in the baseband domain.

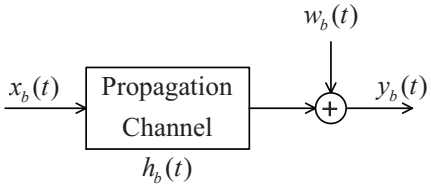

Figure 2.6: The complex baseband equivalent model.

Therefore, from the system design point of view, it is useful to have a baseband equivalent representation of the system. Define $x_b(t) = \sum_n x[n]p_T(t - nT_s) = x_I(t) + jx_Q(t)$ as the complex baseband equivalent of the passband signal $x(t)$. From (2.1), one obtains

$$x(t) = \sqrt{2}\Re\left\{x_b(t)\mathrm{e}^{j\omega_c t}\right\} \tag{2.4}$$

Similarly, define $y(t) = \sqrt{2}\Re\left\{y_b(t)\mathrm{e}^{j\omega_c t}\right\}$ and $w(t) = \sqrt{2}\Re\left\{w_b(t)\mathrm{e}^{j\omega_c t}\right\}$, where $y_b(t)$ and $w_b(t)$ are the complex baseband equivalents of $y(t)$ and $w(t)$, respectively. Then (2.3) can be rewritten as

$$\Re\left\{y_b(t)\mathrm{e}^{j\omega_c t}\right\} = h(t) * \left(\Re\left\{x_b(t)\mathrm{e}^{j\omega_c t}\right\}\right) + \Re\left\{w_b(t)\mathrm{e}^{j\omega_c t}\right\}, \tag{2.5}$$

which is further written as

$$\begin{aligned}\Re\left\{y_b(t)\mathrm{e}^{j\omega_c t}\right\} &= \int_{-\infty}^{\infty} h(\tau)\Re\left\{x_b(t-\tau)\mathrm{e}^{j\omega_c(t-\tau)}\right\}\mathrm{d}\tau + \Re\left\{w_b(t)\mathrm{e}^{j\omega_c t}\right\} \\ &= \int_{-\infty}^{\infty} \Re\left\{\left[h(\tau)x_b(t-\tau)\mathrm{e}^{-j\omega_c\tau}\right]\mathrm{e}^{j\omega_c t}\right\}\mathrm{d}\tau + \Re\left\{w_b(t)\mathrm{e}^{j\omega_c t}\right\}.\end{aligned} \tag{2.6}$$

By defining $h_b(\tau) = h(\tau)\mathrm{e}^{-j\omega_c\tau}$, then one obtains

$$y_b(t) = \int_{-\infty}^{\infty} h_b(\tau)x_b(t-\tau)\mathrm{d}\tau + w_b(t) = x_b(t) * h_b(t) + w_b(t). \tag{2.7}$$

Equation (2.7) implies that the original passband model in (2.3) can be equivalently represented as in Fig. 2.6. Furthermore, one can prove that $y_I(t) = \Re\{y_b(t)\}$ as follows:

$$
\begin{aligned}
y_I(t) &= \mathrm{LPF}\left\{\sqrt{2}y(t)\cos\left(\omega_c t\right)\right\} \\
&= \mathrm{LPF}\left\{\sqrt{2}\int_{-\infty}^{\infty} h(\tau)x(t-\tau)\cos\left(\omega_c t\right)\mathrm{d}\tau\right\} + \mathrm{LPF}\left\{\sqrt{2}w(t)\cos\left(\omega_c t\right)\right\} \\
&= \mathrm{LPF}\left\{2\int_{-\infty}^{\infty} h(\tau)\left(x_I(t-\tau)\cos\left(\omega_c(t-\tau)\right) - x_Q(t-\tau)\sin\left(\omega_c(t-\tau)\right)\right)\cos\left(\omega_c t\right)\mathrm{d}\tau\right\} \\
&\qquad + \mathrm{LPF}\left\{2\Re\left\{w_b(t)\mathrm{e}^{j\omega_c t}\right\}\cos\left(\omega_c t\right)\right\} \\
&= \int_{-\infty}^{\infty} h(\tau)\left(x_I(t-\tau)\cos\left(\omega_c\tau\right) + x_Q(t-\tau)\sin\left(\omega_c\tau\right)\right)\mathrm{d}\tau + \Re\left\{w_b(t)\right\} \\
&= \int_{-\infty}^{\infty} h(\tau)\Re\left\{x_b(t-\tau)\mathrm{e}^{-j\omega_c\tau}\right\}\mathrm{d}\tau + \Re\left\{w_b(t)\right\} \\
&= \Re\left\{\int_{-\infty}^{\infty} h_b(\tau)x_b(t-\tau)\mathrm{d}\tau + w_b(t)\right\} \\
&= \Re\left\{y_b(t)\right\}
\end{aligned}
\tag{2.8}
$$

A similar proof can show that $y_Q(t) = \Im\{y_b(t)\}$. Thus $y_b(t) = y_I(t) + jy_Q(t)$.

Let $x_d(t) = \sum_n \left(x_I[n]\delta(t-nT_s) + jx_Q[n]\delta(t-nT_s)\right)$ and $z(t) = z_I(t) + jz_Q(t)$ be the outputs of the impulse modulator and the matched filter blocks, respectively, then $z(t)$ can be written as

$$
\begin{aligned}
z(t) = \left(y_I(t) + jy_Q(t)\right) * p_R(t) &= y_b(t) * p_R(t) \\
&\overset{(2.7)}{=} x_b(t) * h_b(t) * p_R(t) + w_b(t) * p_R(t) \\
&= x_d(t) * p_T(t) * h_b(t) * p_R(t) + w_b(t) * p_R(t)
\end{aligned}
\tag{2.9}
$$

Define $p(t) = p_T(t) * h_b(t) * p_R(t)$ and $w_d(t) = w_b(t) * p_R(t)$. Then,

$$
z(t) = x_d(t) * p(t) + w_d(t) = \int_{-\infty}^{\infty} x_d(\tau)p(t-\tau)\mathrm{d}\tau + w_d(t) \tag{2.10}
$$

Sampling $z(t)$ at every interval T_s at the receiver results in

$$
z(nT_s) = \int_{-\infty}^{\infty} x_d(\tau)p(nT_s-\tau)\mathrm{d}\tau + w_d(nT_s) \tag{2.11}
$$

However, it is noted that $x_d(t)$ is the output of the impulse modulator whose values are only non-zero at multiples of T_s, thus the above equation can be rewritten as

$$
z(nT_s) = \sum_k x_d(kT_s)p(nT_s-kT_s) + w_d(nT_s) \tag{2.12}
$$

It can be seen from (2.12) that the received signal at the receiver is obtained individually at multiples of sample interval T_s. Thus a discrete-time model for the communication systems in Fig. 2.3 can be written as

$$z[n] = \sum_k x_d[k]p[n-k] + w_d[n] = x_d[n] * p[n] + w_d[n] \tag{2.13}$$

Equation (2.13) can be rewritten as

$$z[n] = x_d[n]p[0] + \sum_{k \neq n} x_d[k]p[n-k] + w_d[n] \tag{2.14}$$

From the above equation, it can be seen that the received signal at time slot n not only depends on the transmitted symbol at time slot n, i.e., $x_d[n]$, but also depends on the transmitted signals from previous time slots. This results in the so-called ISI. In order to eliminate ISI, $p[n]$ should satisfy the following condition

$$p[n] = \begin{cases} 1, & \text{if} \quad n = 0 \\ 0, & \text{otherwise.} \end{cases} \tag{2.15}$$

It can be shown that the Fourier transform of $p(t)$ satisfies

$$\sum_{k=\infty}^{\infty} P\left(f - \frac{k}{T_s}\right) = T_s. \tag{2.16}$$

The above conditions are known as the Nyquist criterion. Fig. 2.7 illustrates the Nyquist criterion in the frequency domain.

One of the most popular function that satisfies the condition (2.16) is the raised cosine (RC) function, given as

$$p_{\mathrm{RC}}(t) = \mathrm{sinc}\left(\frac{t}{T_s}\right) \frac{\cos\left(\frac{\pi\beta t}{T_s}\right)}{1 - \left(\frac{2\beta t}{T_s}\right)^2}, \tag{2.17}$$

where $0 \leq \beta \leq 1$ is the roll-off factor. The corresponding frequency response which is the Fourier transform of $p_{\mathrm{RC}}(t)$ is

$$P_{\mathrm{RC}}(f) = \begin{cases} T_s, & |f| \leq \frac{1-\beta}{2T_s} \\ \frac{T_s}{2}\left\{1 + \cos\left[\frac{\pi T_s}{\beta}\left(|f| - \frac{1-\beta}{2T_s}\right)\right]\right\}, & \frac{1-\beta}{2T_s} \leq |f| \leq \frac{1+\beta}{2T_s}. \\ 0, & \text{otherwise} \end{cases} \tag{2.18}$$

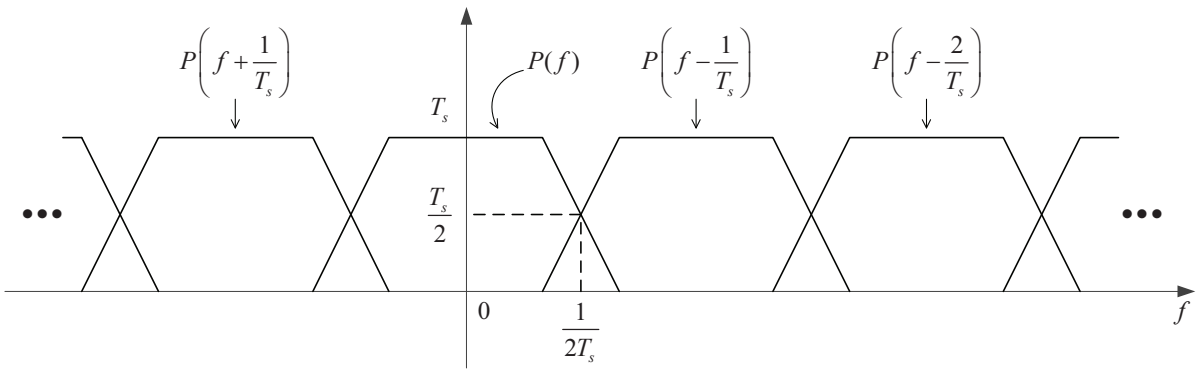

Figure 2.7: Illustration of the Nyquist criterion in the frequency domain.

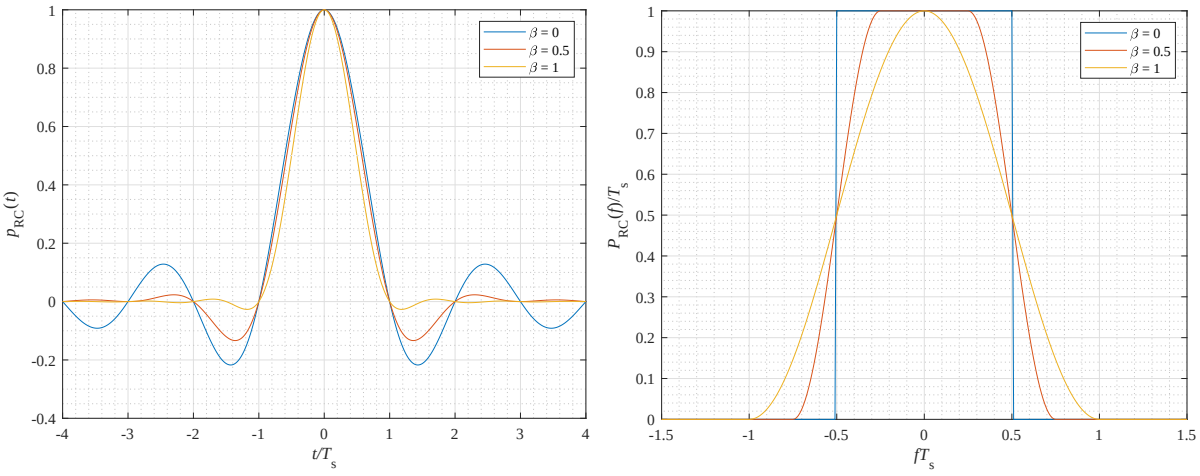

(a) Impulse response.

(b) Frequency response.

Figure 2.8: The raised cosine function.

Plots of $p_{\text{RC}}(t)$ and $P_{\text{RC}}(f)$ are shown in Fig. 2.8a and Fig. 2.8b, respectively.

Design of Transmit and Receive Filters

As shown above, in order to eliminate ISI in single-carrier wireless communications, the equivalent impulse response $p(t)$ should satisfy the Nyquist condition in (2.15). Since $p(t)$ is a convolution of $p_T(t)$, $h_b(t)$ and $p_R(t)$, to design the filters $p_T(t)$ and $p_R(t)$, the complex baseband equivalent channel impulse response $h_b(t)$ should be known, which is not always possible in practice. As such, a common approach is to assume an ideal channel, i.e., $h_b(t) = \delta(t)$, and design the filters to maximize the signal-to-noise ratio (SNR) at the output of the receive filter $p_R(t)$. For the case of additive white Gaussian noise (AWGN), it can be shown that the optimal design is to split the Nyquist impulse response $p(t)$ evenly between the transmitter and receiver [1]. In the frequency domain, this means that

$$P_R(f) = P_T^*(f) \tag{2.19}$$

The pair of filters that are related according to (2.19) are referred to as matched filters. Since $p(t) = p_T(t) * p_R(t)$, it follows that $P(f) = |P_T(f)|^2 = |P_R(f)|^2$, or

$$|P_T(f)| = |P_R(f)| = \sqrt{P(f)}. \tag{2.20}$$

If $P(f)$ is chosen as a RC spectrum in (2.18), then the spectra (i.e., Fourier transforms) of $p_T(t)$ and $p_R(t)$ are square-root raised cosine (SRRC). The continuous-time impulse response of a SRRC filter is given as [1]:

$$p_{\text{SRRC}}(t) = \frac{\sin\left((1-\beta)\frac{\pi t}{T_s}\right) + \frac{4\beta t}{T_s}\cos\left((1+\beta)\frac{\pi t}{T_s}\right)}{\frac{\pi t}{T_s}\left(1 - \left(\frac{4\beta t}{T_s}\right)^2\right)}. \tag{2.21}$$

Fig. 2.9 shows the SRRC function for various roll-off factors β.

Detection Rule

Now, if the transmit and receive filters are designed to satisfy the Nyquist criterion, for example as in (2.21), the received signal sample at $t = nT_s$ is given as

$$z[n] = x[n] + w_d[n] \tag{2.22}$$

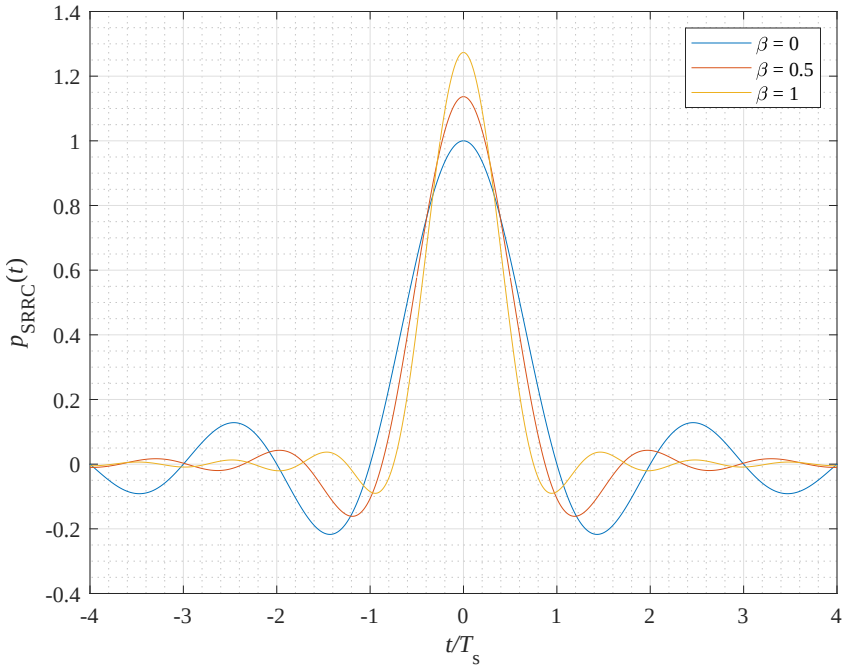

Figure 2.9: Impulse response of the square root raised-cosine function.

where $w_d[n]$ represents noise, which is a zero-mean complex Gaussian random variable with variance N_0. The quantity N_0 comes from the power spectral density (PSD) of AWGN, which is $N_0/2$ watts/Hz.

The equivalent discrete-time channel model in (2.22) is known as an AWGN channel model. For such a channel model, the optimal detection rule that minimizes the probability of error at the receiver can be shown to be the minimum-distance rule if the transmitted symbol $x[n]$ is equally likely to be selected from a QAM constellation [1]. The minimum-distance decision rule is expressed as:

$$\hat{x}[n] = \arg\max_{x[n]} \|z[n] - x[n]\|. \tag{2.23}$$

The above decision rule means that to detect the transmitted symbol based on the received signal, the receiver looks among all possible $x[n]$ to find the signal point that is closest to the received signal $z[n]$ in Euclidean distance.

Using the above minimum-distance receiver, the probability of symbol error can be com-

puted for a square M-QAM constellation (i.e., $M = 2^\lambda$ and λ is an even number) as [1]:

$$P[\text{symbol error}] = 4\left(1 - \frac{1}{\sqrt{M}}\right) Q\left(\sqrt{\frac{3\gamma}{(M-1)}}\right) \tag{2.24}$$

where $\gamma = \frac{E_s}{N_0}$ and E_s is the average transmitted energy of the M-QAM constellation. For a constellation, the energy of each symbol can be computed as a square of the distance between the symbol and the origin [1]. For example, the energy of symbol $(1 - j)$ in the 16-QAM constellation in Fig. 2.2 is $1^2 + (-1)^2 = 2$ joules. Therefore, the average symbol energy for 16-QAM is computed as

$$E_s = \frac{1}{16}\left[4(1^2 + 1^2) + 8(1^2 + 3^2) + 4(3^2 + 3^2)\right] = 10. \tag{2.25}$$

Depending on how a constellation is defined, the value of E_s can be different.

If Gray mapping is used to map a sequence of λ coded bits into a QAM symbol, then two adjacent symbols differ in only a single bit. Since the most probable errors due to noise result in the erroneous selection of a signal adjacent to the true signal, most symbol errors contain only a single-bit error. It follows that the bit error rate (BER) of M-QAM under an AWGN channel can be approximately as

$$\begin{aligned} P[\text{bit error}] \approx \frac{1}{\lambda} P[\text{symbol error}] &= \frac{4}{\lambda}\left(1 - \frac{1}{\sqrt{M}}\right) Q\left(\sqrt{\frac{3\gamma}{(M-1)}}\right) \\ &= \frac{4}{\lambda}\left(1 - \frac{1}{\sqrt{M}}\right) Q\left(\sqrt{\frac{3\lambda\gamma_b}{(M-1)}}\right), \end{aligned} \tag{2.26}$$

where $\gamma_b = \frac{E_b}{N_0}$ and $E_b = \frac{E_s}{\lambda}$ is the average energy per bit. Fig. 2.10 plots the bit error probability (which is also commonly referred to as the bit error rate (BER)) with respect to E_b/N_0 for a variety of M-QAM constellations. It can be seen from Fig. 2.10 that the performance is degraded when the modulation order M increases. Since a higher order M means a faster transmission bit rate over the same bandwidth, the above observation means that the transmit power needs to be increased to maintain the same system performance in terms of the bit error probability.

The receiver design for the case of non-ideal channels, such as frequency-selective channels, could be much more complicated. This is because, as discussed before, to eliminate

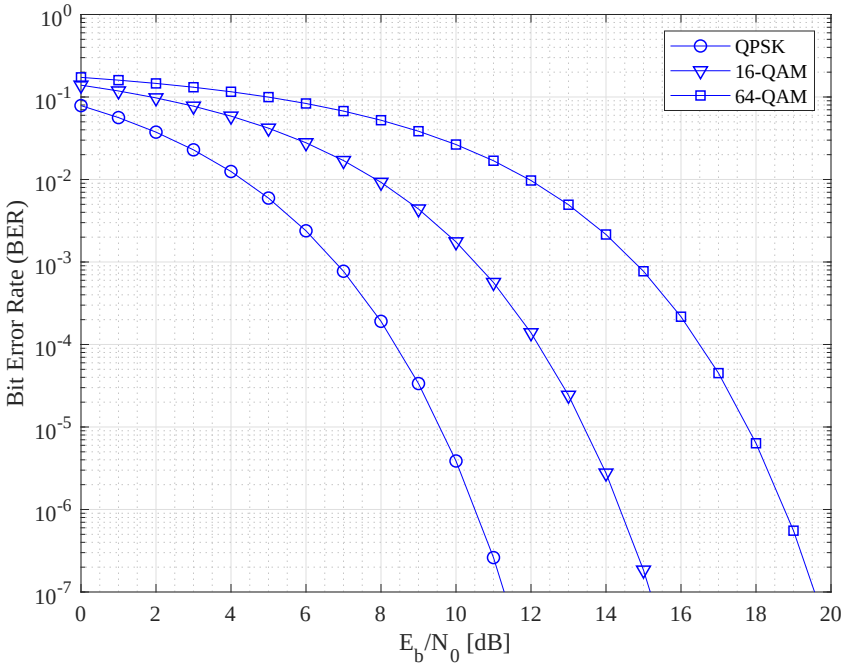

Figure 2.10: Bit error probability of a single-carrier communication system over an AWGN channel.

the ISI induced from the channel, a pair of filters $p_T(t)$ and $p_R(t)$ need to be designed such that the equivalent channel impulse response $p(t) = p_T(t) * h_b(t) * p_R(t)$ satisfies the Nyquist condition in (2.16). Such a design is much more challenging if the channel exhibits a high level of frequency selectivity (equivalently the channel impulse response $h_b(t)$ has a large number of multi-tap components).

Another popular approach to deal with ISI is to convert an ISI channel into non-ISI parallel sub-channels such that a signal transmitted on the sub-channel only experiences a constant gain and thus a simple scalar equalizer for each sub-channel is adequate. This method is commonly known as multi-carrier modulation which is described in the next section.

2.2 Multi-Carrier Wireless Communication Systems

The basic idea of multi-carrier transmission is to split the data stream into different sub-streams and then send them over different sub-channels. Typically the sub-channels are

made orthogonal under ideal propagation conditions. The data rate of each sub-channel is much less than the total data rate. The number of sub-streams is chosen to ensure that each sub-channel has a bandwidth less than the coherence bandwidth of the channel, so that the sub-channels experience relatively flat fading. Thus, ISI on each sub-channel is very small or can be completely canceled.

Fig. 2.11 depicts a transmultiplexer implementing an N-band multi-carrier system, i.e., the channel is divided into N sub-channels. At the transmitter, the transmitted signal is prepared to transmit through N distinct sub-carriers, where each sub-carrier is represented by a filter with the impulse response $f_i(t), i = 0, 1, \cdots, N-1$. At the receiver, there are N corresponding filters $g_i(t)$. The filters are narrow-band with distinct center frequencies, so that the symbols sent over them do not interfere with each other.

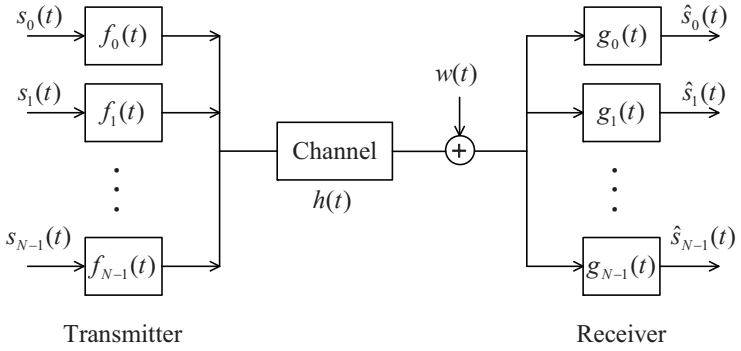

Figure 2.11: General structure of a multi-carrier communication system.

In this section, a detailed description is first provided for a general CP-based multi-carrier systems. Then, OFDM, GFDM and CFBMC-OQAM are discussed as examples of CP-based multi-carrier systems. Each system represents a different class of CP-based multi-carrier systems, either an orthogonal, a non-orthogonal, or a real-domain orthogonal system.

2.2.1 CP-Based Multi-Carrier Systems

Figure 2.12 illustrates a CP-based multi-carrier system. A bit sequence $\mathbf{u}_i$ corresponding to the ith transmission block is first mapped into a symbol sequence $\mathbf{d}_i$ by a QAM mapper. Next, the symbol sequence $\mathbf{d}_i$ is modulated by multiplying with a general multi-carrier

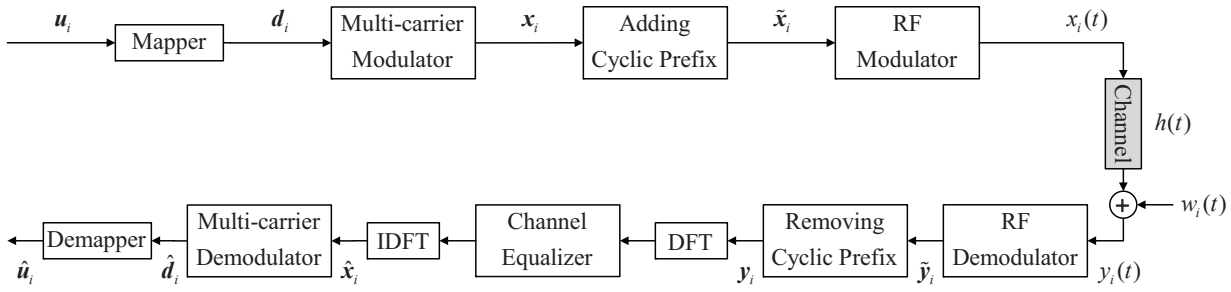

Figure 2.12: A CP-based multi-carrier transceiver.

modulation matrix $\mathbf{G}_t$ to obtain

$$\mathbf{x}_i = \begin{bmatrix} x_i[0] & x_i[1] & \cdots & x_i[N-1] \end{bmatrix}^T = \mathbf{G}_t \mathbf{d}_i. \tag{2.27}$$

Before transmitting over a wireless channel, a CP of length N_g is added into $\mathbf{x}_i$ to obtain $\tilde{\mathbf{x}}_i = \begin{bmatrix} x_i[N-N_g] & \cdots & x_i[N-1] & x_i[0] & \cdots & x_i[N-1] \end{bmatrix}^T$ as

$$\tilde{\mathbf{x}}_i = \mathbf{T}_{\text{cp}} \mathbf{x}_i. \tag{2.28}$$

In (2.28), $\mathbf{T}_{\text{cp}} = \begin{bmatrix} \bar{\mathbf{I}}_{N_g} & \mathbf{I}_N \end{bmatrix}^T$ represents the CP insertion operation, where $\bar{\mathbf{I}}_{N_g}$ contains the last N_g rows of an $N \times N$ identity matrix $\mathbf{I}_N$. The CP essentially is a copy of the last N_g samples of $\mathbf{x}_i$. The resulting signal $\tilde{\mathbf{x}}_i$ is passed through a DAC and then up-converted to a passband signal $x_i(t)$.

The received passband signal is

$$y_i(t) = h(t) * x_i(t) + w_i(t), \tag{2.29}$$

where $h(t)$ is the impulse response of the channel and $w_i(t)$ is thermal noise. The received signal is then down-converted to baseband and lowpass filtered to remove the high-frequency components. The ADC samples the resulting signal to obtain $\tilde{\mathbf{y}}_i = [\tilde{y}_i[0] \quad \tilde{y}_i[1] \quad \cdots \quad \tilde{y}_i[N+N_g-1]]^T$. Let $\mathbf{h} = \begin{bmatrix} h[0] & h[1] & \cdots & h[\mu-1] \end{bmatrix}^T$ be the discrete-time complex baseband equivalent impulse response of the wireless channel. Then

$$\tilde{\mathbf{y}}_i = \mathbf{H}\tilde{\mathbf{x}}_i + \mathbf{G}\tilde{\mathbf{x}}_{i-1} + \tilde{\mathbf{w}}_i \tag{2.30}$$

where $\mathbf{H}$ and $\mathbf{G}$ are, respectively, given as

$$\mathbf{H} = \begin{bmatrix} h[0] & 0 & 0 & \cdots & 0 \\ h[1] & h[0] & 0 & \cdots & 0 \\ \vdots & \vdots & \vdots & \cdots & \vdots \\ 0 & \cdots & h[\mu-1] & \cdots & h[0] \end{bmatrix}_{(N+N_g)\times(N+N_g)} \tag{2.31}$$

and

$$\mathbf{G} = \begin{bmatrix} 0 & \cdots & h[\mu-1] & \cdots & h[1] \\ 0 & \cdots & 0 & \cdots & h[2] \\ \vdots & \cdots & \vdots & \cdots & \vdots \\ 0 & \cdots & 0 & \cdots & h[\mu-1] \\ \vdots & \cdots & \vdots & \cdots & \vdots \\ 0 & \cdots & 0 & \cdots & 0 \end{bmatrix}_{(N+N_g)\times(N+N_g)} \tag{2.32}$$

and $\tilde{\mathbf{w}}_i$ represents Gaussian noise of the ith transmission block. Equation (2.30) indicates that the received signal for the ith transmission block contains not only the desired signal transmitted for the ith transmission block, i.e., $\tilde{\mathbf{x}}_i$, but also the transmitted signal from the previous transmission block, i.e., $\tilde{\mathbf{x}}_{i-1}$. This phenomenon is called inter-block interference (IBI).

In the receiver, the CP is first removed from the received signal before performing the DFT. After removing the CP, the received signal $\mathbf{y}_i$ is written as

$$\mathbf{y}_i = \mathbf{R}_{\text{cp}}\mathbf{H}\mathbf{T}_{\text{cp}}\mathbf{x}_i + \mathbf{R}_{\text{cp}}\mathbf{G}\tilde{\mathbf{x}}_{i-1} + \mathbf{R}_{\text{cp}}\tilde{\mathbf{w}}_i. \tag{2.33}$$

where the CP removal is represented by matrix $\mathbf{R}_{\text{cp}} = \begin{bmatrix} \mathbf{0}_{N\times N_g} & \mathbf{I}_N \end{bmatrix}$. One can verify that when the CP length N_g is longer than the channel length μ, then $\mathbf{R}_{\text{cp}}\mathbf{G} = \mathbf{0}$. It means that the IBI is completely eliminated from the received signal. Furthermore, it can be seen that $\mathbf{R}_{\text{cp}}\mathbf{H}\mathbf{T}_{\text{cp}}$ is an $N \times N$ circulant matrix:

$$\mathbf{H}_{\text{circ}} = \begin{bmatrix} h[0] & 0 & \cdots & h[\mu-1] & \cdots & h[2] & h[1] \\ h[1] & h[0] & \cdots & 0 & \cdots & h[3] & h[2] \\ \vdots & \vdots & \cdots & \vdots & \cdots & \vdots & \vdots \\ 0 & 0 & \cdots & 0 & \cdots & h[1] & h[0] \end{bmatrix}. \tag{2.34}$$

Define $\mathbf{v}_i = \mathbf{R}_{\text{cp}}\tilde{\mathbf{w}}_i$. Then, (2.33) can be rewritten as

$$\mathbf{y}_i = \mathbf{H}_{\text{circ}}\mathbf{G}_t\mathbf{d}_i + \mathbf{v}_i. \tag{2.35}$$

The circulant matrix $\mathbf{H}_{\text{circ}}$ can be represented as $\mathbf{H}_{\text{circ}} = \mathbf{F}^H\mathbf{\Gamma}\mathbf{F}$ where $\mathbf{\Gamma}$ is a diagonal matrix with $\mathbf{\Gamma} = \text{diag}\left\{[h_f[0] \quad h_f[1] \quad \cdots \quad h_f[N-1]]^T\right\}$. $\mathbf{F}$ is the normalized DFT matrix whose (k,m)th element is given as $[\mathbf{F}]_{k,m} = \frac{1}{\sqrt{N}}\text{e}^{-j\frac{2\pi mk}{N}}$. Note that $\mathbf{h}_f = [h_f[0] \quad h_f[1] \quad \cdots \quad h_f[N-1]]^T$ is the N-point DFT of the channel's impulse response $\mathbf{h}$. Therefore, $\mathbf{h}_f$ is exactly the frequency response of the channel evaluated at N carrier frequencies. Then (2.35) can be rewritten as

$$\mathbf{y}_i = \mathbf{F}^H\mathbf{\Gamma}\mathbf{F}\mathbf{G}_t\mathbf{d}_i + \mathbf{v}_i. \tag{2.36}$$

To detect the desired signal, the received signal $\mathbf{y}_i$ is first converted to the frequency domain by the DFT to produce

$$\hat{\mathbf{y}}_i = \mathbf{F}\mathbf{y}_i = \mathbf{\Gamma}\mathbf{F}\mathbf{G}_t\mathbf{d}_i + \hat{\mathbf{v}}_i \tag{2.37}$$

where $\hat{\mathbf{v}}_i = \mathbf{F}\mathbf{v}_i$. It is pointed out that the DFT does not change the statistical characteristics of the noise $\mathbf{v}_i$. Define $\mathbf{s}_i = \mathbf{F}\mathbf{G}_t\mathbf{d}_i$. Then

$$\hat{\mathbf{y}}_i = \mathbf{\Gamma}\mathbf{s}_i + \hat{\mathbf{v}}_i \tag{2.38}$$

The above equation can be further rewritten as

$$\hat{y}_i[n] = h_f[n]s_i[n] + \hat{v}_i[n] \quad \text{for} \quad n = 0, 1, \cdots, N-1. \tag{2.39}$$

It is seen that (2.39) is a set of N independent equations in which each equation represents the received signal in a particular sub-channel. Furthermore, each equation resembles the AWGN channel model in (2.22), albeit with a frequency-dependent channel gain $h_f[n]$. In other words, a CP-based multi-carrier system effectively decomposes the wide-band channel to a set of narrow-band orthogonal sub-channels. Knowing the channel gains $h_f[n]$, $n = 0, 1, \cdots, N-1$, the receiver can recover the original $s_i[n]$ using the minimum-distance rule by first dividing out these gains as $\hat{s}_i[n] = \hat{y}_i[n]/h_f[n]$. This process is called channel equalization. To perform the channel equalization task, the channel state information has to be first estimated based on the transmission of either pilots or preambles in practice [2, 3].

Specifically, preambles are training blocks which are transmitted at the beginning of each transmission frame, while pilots are known symbols which are embedded into transmission blocks based on a specific pattern and transmitted along with the data. Given known preambles or pilots, channel frequency response can be estimated by dividing the received signal by the corresponding preambles or pilots. Since a preamble occupies the entire transmission block, the channel estimation based on a preamble, if well designed, should be better than that obtained based on pilot symbols [2, 3].

After channel equalization, the signal is further passed through an IDFT to obtain $\hat{\mathbf{x}}_i$. The output signal of the IDFT block is demodulated with a bank of filters to obtain

$$\hat{\mathbf{d}}_i = \mathbf{G}_r \hat{\mathbf{x}}_i \tag{2.40}$$

where the multi-carrier demodulation is represented by matrix $\mathbf{G}_r$. The output $\hat{\mathbf{d}}_i$ is finally passed through a demapper to obtain $\hat{\mathbf{u}}_i$.

In the next subsections, three specific designs of CP-based waveforms, namely OFDM, GFDM and CFBMC-OQAM, are first described. After that, brief introduction of the most common physical impairments in communication circuitries, namely phase noise, IQ imbalance and nonlinearity, is presented. An emerging technique to improve the spectral efficiency of wireless communication systems, namely full-duplex communication, is also introduced at the end.

2.2.2 OFDM

For OFDM, the multi-carrier modulation in the transmitter is performed by an IDFT, i.e., $\mathbf{G}_t = \mathbf{F}^H$, and the multi-carrier demodulation in the receiver is performed by a DFT transform, i.e., $\mathbf{G}_r = \mathbf{F}$. In OFDM, $\mathbf{d}_i$ is a set of N *complex* QAM symbols which are related to the output of the multi-carrier modulation as

$$x_i[n] = \frac{1}{\sqrt{N}} \sum_{k=0}^{N-1} d_i[k] \mathrm{e}^{j\frac{2\pi kn}{N}}. \tag{2.41}$$

It can be seen that $x_i[n]$ is a weighted summation of N exponential functions, which represent N different sub-carriers. If synchronization is perfect and there is no channel or noise, then

$\hat{d}_i[n]$ is

$$\hat{d}_i[n] = \frac{1}{\sqrt{N}} \sum_{l=0}^{N-1} x_i[l] \mathrm{e}^{-j\frac{2\pi ln}{N}} \overset{(2.41)}{=} \begin{cases} d_i[n], & \text{if} \quad k = n \\ 0, & \text{otherwise.} \end{cases} \tag{2.42}$$

Equation (2.42) implies that OFDM is an *orthogonal* system.

In OFDM, the use of IDFT and DFT operations in the transmitter and receiver, respectively, as filters helps to divide the whole system bandwidth into orthogonal sub-bands. As such, it makes the signals sent over different sub-carriers not interfering with each other. Furthermore, the use of IDFT and DFT also helps to reduce the implementation complexity.

However, as pointed out in [4], using IDFT is equivalent to using a rectangular pulse shaping filter in the transmitter. The use of a rectangular impulse response leads to an undesirable magnitude response that suffers from large side lobes in the frequency domain. This follows immediately from the fact that the Fourier transform of a rectangular pulse is a sinc function, and it is well-known that the side lobes of a sinc pulse are relatively large. Specifically, the peak of the first side lobe is only 13 dB below the peak of its main lobe. Such high side lobes result in leakage of signal powers into the frequency bands of adjacent systems [4].

The use of OFDM has also been challenged for applications in future generations of wireless networks. Specifically, machine-type communication and machine-to-machine communication require low power consumption, which makes the strict synchronization process required to keep the orthogonality among sub-carriers in OFDM less attractive [5]. Furthermore, the low latency required for vehicle-to-vehicle applications demands for short bursts of data, meaning that OFDM signals with one CP per symbol would present a prohibitive low spectral efficiency [5].

All the above challenges do not favor OFDM as the first choice for the next and future generations of wireless networks. In this context, alternative multi-carrier schemes should be considered. Recently, GFDM and CFBMC-OQAM have emerged as promising techniques to overcome the disadvantages of OFDM. The next sections discuss GFDM and CFBMC-OQAM in more detail.

2.2.3 GFDM

For GFDM, the input of the multi-carrier modulation, $\mathbf{d}_i$, is also a set of N *complex* symbols but it is different from the one in OFDM. Specifically, the symbol sequence after the mapper is first arranged into a block-based structure of M time slots and K sub-carriers so that $N = M \times K$. Then, $\mathbf{d}_i$ is obtained by vectorizing the block-based structure as $\mathbf{d}_i = \begin{bmatrix} \mathbf{d}_i^{(0)} & \mathbf{d}_i^{(1)} & \cdots & \mathbf{d}_i^{(K-1)} \end{bmatrix}^T$ where $\mathbf{d}_i^{(q)} = \begin{bmatrix} d_i^{(q,0)} & d_i^{(q,0)} & \cdots & d_i^{(q,M-1)} \end{bmatrix}^T$ and $d_i^{(k,m)}$ is a QAM symbol at the kth sub-carrier and mth time slot. After the multi-carrier modulation, $x_i[n]$ can be derived as

$$x_i[n] = \sum_{k=0}^{K-1} \sum_{m=0}^{M-1} g_{k,m}[n] d_i^{(k,m)}, \quad n = 0, 1, \cdots, N-1 \tag{2.43}$$

where $g_{k,m}[n] = g\left[n - mK\right]_N \mathrm{e}^{j\frac{2\pi kn}{K}}$ is a time and frequency shifted version of a prototype filter $g[n]$ [5]. In (2.43), $x_i[n]$ is obtained by essentially performing a circular convolution between the prototype filter $g[n]$ and the transmitted symbol sequence. Equation (2.43) can be compactly rewritten as (2.27) where the $(m + kM)$th column of $\mathbf{G}_t$ is written as $\mathbf{G}_t\left[:, m + kM\right] = \begin{bmatrix} g_{k,m}[0] & \cdots & g_{k,m}[N-1] \end{bmatrix}^T$.

Two common methods, namely matched-filter (MF) demodulation where $\mathbf{G}_r = \mathbf{G}_t^H$ and zero-forcing (ZF) demodulation where $\mathbf{G}_r = \mathbf{G}_t^{-1}$, are usually deployed to detect the transmitted signal in GFDM [5, 6]. Assuming that the MF demodulation is deployed, the synchronization is achieved perfectly and there is no channel or noise, then the received signal after the demodulation is

$$\hat{d}_i^{(k',m')} = \sum_{n=0}^{N-1} x_i[n] g\left[n - m'K\right]_N \mathrm{e}^{-j\frac{2\pi k'n}{K}} \overset{(2.43)}{=} d_i^{(k',m')} + \delta_i^{(k',m')} \tag{2.44}$$

where $\delta_i^{(k',m')}$ represents the *self-interference*. This indicates that GFDM is a *non-orthogonal* system. Although, with ZF demodulation, the impact of self-interference can be completely avoided, the two main disadvantages of using ZF detector are (i) the noise enhancement effect and (ii) the inversion of $\mathbf{G}_t$ does not always exist.

Compared to OFDM, the pulse-shaping filter in GFDM can be flexibly designed to suppress the spectral leakage. Furthermore, as a non-orthogonal system, the strict orthogonality

in OFDM is no longer required in GFDM. Similar to OFDM, a CP is also added into the transmitted signal before sending out to a wireless channel. However, the CP in GFDM is applied for the entire block of M symbols instead of every symbol as in OFDM. This results in better spectral efficiency and low latency in GFDM compared to OFDM.

However, the trade-off for allowing non-orthogonal sub-carriers is the self-interference which could significantly degrade performance of GFDM. As such a self-interference cancellation mechanism is usually needed in the receiver of GFDM. To overcome this disadvantage, CFBMC-OQAM shall be presented in the next section.

2.2.4 CFBMC-OQAM

The transmitted signal $\mathbf{d}_i$ in CFBMC-OQAM is constructed from a block-based structure of K sub-carriers and $2M$ time slots such that $N = M \times K$. However, its elements are all *real* instead of complex as in OFDM and GFDM due to the use of offset QAM. Specifically, $\mathbf{d}_i = \begin{bmatrix}\mathbf{d}_i^{(0)} & \mathbf{d}_i^{(1)} & \cdots & \mathbf{d}_i^{(K-1)}\end{bmatrix}^T$ where $\mathbf{d}_i^{(q)} = \begin{bmatrix}d_i^{(q,0)} & d_i^{(q,1)} & \cdots & d_i^{(q,2M-1)}\end{bmatrix}^T$ and $d_i^{(k,m)} \in \mathbb{R}$. After the multi-carrier modulation, $x_i[n]$ can be also written as (2.43) but m is from 0 to $2M-1$ and $g_{k,m}[n] = j^{k+m} g\left[n - mK/2\right]_N \mathrm{e}^{j\frac{2\pi kn}{K}}$. To be rewritten in the forms of (2.27), the $(m+2kM)$th column of $\mathbf{G}_t$ is $\mathbf{G}_t[:, m+2kM] = \begin{bmatrix}g_{k,m}[0] & \cdots & g_{k,m}[N-1]\end{bmatrix}^T$.

To detect the transmitted signal, $\hat{\mathbf{x}}_i$ is passed through a bank of matched filters, i.e., $\mathbf{G}_r = \mathbf{G}_t^H$, and the estimate of $\mathbf{d}_i$ is obtained by taking the real part of the filtered output. When the synchronization is perfect and there is no channel or noise

$$\hat{d}_i^{(k',m')} = \Re\left\{ j^{-(k'+m')} \sum_{n=0}^{N-1} g\left[m'K/2 - n\right]_N \mathrm{e}^{-j\frac{2\pi k'n}{K}} x_i[n] \right\} = d_i^{(k',m')}. \tag{2.45}$$

No self-interference is seen in (2.45) which implies that CFBMC is a real-domain orthogonal system.

2.2.5 Performance of CP-based Multi-Carrier Systems

Fig. 2.13 shows performance of OFDM as an example for CP-based multi-carrier systems in terms of BER with respect to E_b/N_0. This figure shows the performance of OFDM when there is no fading, i.e., $h_f[i] = 1,\ \forall i$ and each sub-channel is an AWGN channel (hence the

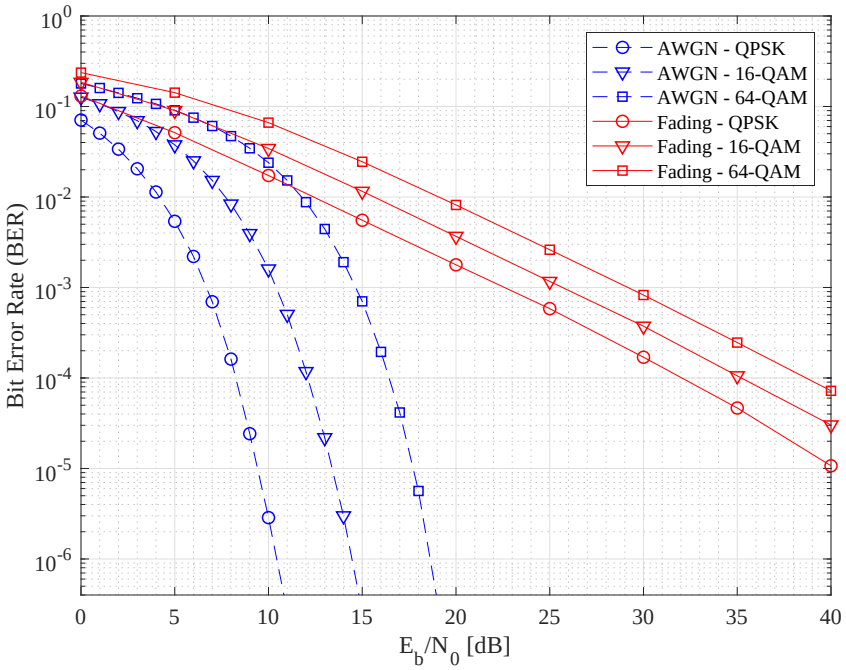

Figure 2.13: BER performance for OFDM systems.

curves are labeled as "AWGN"), and with the presence of fading (labeled as "Fading"). In particular, the discrete-time complex baseband equivalent channel coefficients are assumed to be identically independent complex Gaussian distributed with zero mean and unit variance, i.e., $h[n] \sim \mathcal{CN}(0,1), n = 0, \cdots, \mu-1$. This is known as Rayleigh fading since the magnitude of $h[n]$ follows a Rayleigh distribution [1]. The performance of OFDM is also evaluated with a variety of M-QAM modulations and under the assumption that the channel is known at the receiver. First, it can be seen from Fig. 2.13 that fading dramatically degrades the performance of OFDM systems compared to when there is no fading. Second, for both cases of AWGN and fading channels, the performance of OFDM also degrades as M increases.

2.3 Physical Impairments

As mentioned before, PN, IQ imbalance and nonlinearity are the most common physical impairments which can significantly degrade performance of a communication system. A brief review of these impairments is presented in this section.

2.3.1 Phase Noise

As illustrated in Fig. 2.3, the baseband signal at the transmitter before being transmitted over a channel should be up-converted to an RF carrier $f_c = \omega_c/2\pi$ by an oscillator or a mixer (these two terminologies will be used interchangeably in the following). At the receiver, the received passband signal should be first down-converted to baseband by another oscillator. In practice, those mixers are not perfect. This imperfection, which originates from thermal noise, was identified as one of the major performance limiting factors in multi-carrier systems. The mixer's imperfection causes random deviation of the frequency of the mixer output. These frequency deviations are often modeled as a random excess phase and therefore referred to as PN. At the transmitter, let $x(t)$ and $x_{\mathrm{RF}}(t)$ be the signals before and after RF up-conversion, respectively. Without PN, the RF signal $x_{\mathrm{RF}}(t)$ can be simply written as

$$x_{\mathrm{RF}} = x(t)\mathrm{e}^{j2\pi f_c t}. \tag{2.46}$$

On the other hand, under the presence of PN, the RF signal becomes

$$x_{\mathrm{RF}}(t) = x(t)\mathrm{e}^{j(2\pi f_c t+\theta(t))}, \tag{2.47}$$

where $\theta(t)$ represents PN. This is rewritten in discrete-time baseband equivalent model as

$$x_{\mathrm{b,RF}}[n] = x[n]\mathrm{e}^{j\theta[n]} \tag{2.48}$$

One can obtain a similar equation showing the PN impact in the receiver.

The following briefly reviews two PN models: one is based on an free-running (FR) oscillator [16, 17] and the other is based on a phase-locked loop (PLL) oscillator [17].

FR-PN Model

Let $\alpha_v[n]$ denote the discrete-time phase deviation from an FR oscillator at the nth sampling time. It can be modeled as $\alpha_v[n] = \sum_{i=0}^{n-1} \rho[i]$ where $\rho[i]$ is an i.i.d zero-mean Gaussian random variable with variance $\sigma_\rho^2 = c_v T_s$. Here, c_v is a constant describing the quality of an oscillator, and T_s is the sampling interval. The PN is $\theta[n] = 2\pi f_c \alpha_v[n] = \omega_c \alpha_v[n]$, where f_c is the carrier frequency and $\omega_c = 2\pi f_c$. The variance of $\alpha_v[n]$ is $\mathrm{E}\left[\alpha_v^2[n]\right] =$

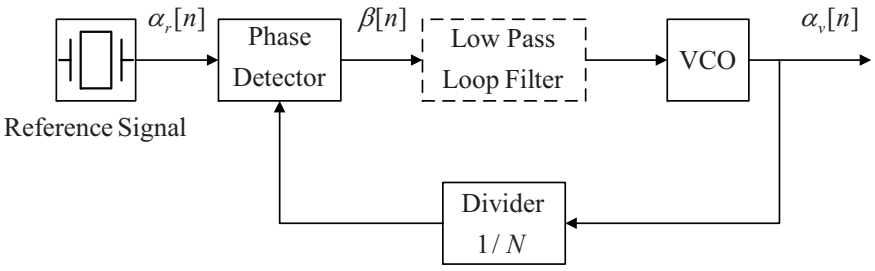

Figure 2.14: A general PLL-based frequency synthesizer.

nc_vT_s, which grows linearly with the sample index n. Furthermore, the autocorrelation function of the phase deviation can be computed as $\mathrm{E}\left[\alpha_v[n_1]\alpha_v[n_2]\right] = c_vT_s \min(n_1, n_2)$ [16]. Define $\mathbf{R}$ as the PN covariance matrix, whose (n_1, n_2)th component is

$$\mathbf{R}[n_1, n_2] = \mathrm{E}\left\{\mathrm{e}^{j(\theta[n_2]-\theta[n_1])}\right\}. \tag{2.49}$$

Since $\theta[n] \sim \mathcal{N}(0, n\omega_c^2 c_v T_s)$ and $\mathrm{E}\left\{\theta[n_1]\theta[n_2]\right\} = \omega_c^2 c_v T_s \min(n_1, n_2)$, one has

$$\mathrm{E}\left\{\theta[n_2] - \theta[n_1]\right\} = 0 \tag{2.50}$$

and

$$\begin{aligned} &\mathrm{E}\left\{(\theta[n_2] - \theta[n_1])^2\right\} \\ &\quad = \mathrm{E}\left\{\theta^2[n_1] + \theta^2[n_2] - 2\theta[n_1]\theta[n_2]\right\} \\ &\quad = (n_1 + n_2 - 2\min(n_1, n_2))\,\omega_c^2 c_v T_s. \end{aligned} \tag{2.51}$$

In order to evaluate (2.49), we make use of the following result. If $X \sim \mathcal{N}(\mu, \sigma^2)$, then its characteristic function $\mathrm{E}\left\{\mathrm{e}^{jtX}\right\} = \mathrm{e}^{jt\mu - \frac{1}{2}\sigma^2 t^2}$ [18]. It then follows that

$$\mathbf{R}[n_1, n_2] = \exp\left\{-\frac{1}{2}(n_1 + n_2 - 2\min(n_1, n_2))\,\omega_c^2 c_v T_s\right\}. \tag{2.52}$$

PLL-PN Model

A general PLL-based frequency synthesizer is illustrated in Fig. 2.14, which models the phase deviation from a reference oscillator having a quality constant c_r as in the FR-PN model. Let $\alpha_r[n]$, $\alpha_v[n]$, and $\beta[n]$ denote the discrete-time phase deviations at the output of the reference oscillator, the frequency synthesizer, and the phase detector, respectively. Then $\alpha_v[n] = \beta[n] + \alpha_r[n]$ [19]. Furthermore, the correlation properties between $\alpha_r[n]$ and $\beta[n]$

are: $\mathrm{E}\{\beta[n_1]\alpha_r[n_2]\} = \sum_{i=1}^{n_o} \mu_i \mathrm{e}^{\lambda_i T_s \min(0,n_2-n_1)}$ and $\mathrm{E}\{\beta[n_1]\beta[n_2]\} = \sum_{i=1}^{n_o} \nu_i \mathrm{e}^{-\lambda_i T_s |n_1-n_2|}$ where $n_o = 1 + o_{\mathrm{lpf}}$, and o_{lpf} represents the order of the loop filter [17,19]. The values of λ_i, μ_i and ν_i are given, for instance in [19], for the PLL-based oscillator with a first-order loop filter.

The statistical characteristics of $(\theta[n_2] - \theta[n_1])$ for the case of PLL-PN can be obtained similarly as follows. First,

$$\mathrm{E}\{\theta[n_2] - \theta[n_1]\} = 0 \tag{2.53}$$

and

$$\begin{aligned}
&\mathrm{E}\left\{(\theta[n_2] - \theta[n_1])^2\right\} \\
&\quad = \mathrm{E}\left\{\theta^2[n_1] + \theta^2[n_2] - 2\theta[n_1]\theta[n_2]\right\} \\
&\quad = \omega_c^2 \mathrm{E}\left\{(\alpha_r[n_1] + \beta[n_1])^2 + (\alpha_r[n_2] + \beta[n_2])^2 - 2(\alpha_r[n_1] + \beta[n_1])(\alpha_r[n_2] + \beta[n_2])\right\} \\
&\quad = \omega_c^2 \mathrm{E}\left\{\left(\alpha_r^2[n_1] + \alpha_r^2[n_2]\right) + \left(\beta^2[n_1] + \beta^2[n_2]\right) + 2\alpha_r[n_1]\beta[n_1] + 2\alpha_r[n_2]\beta[n_2]\right. \\
&\qquad \left. -2\alpha_r[n_1]\alpha_r[n_2] - 2\alpha_r[n_1]\beta[n_2] - 2\beta[n_1]\alpha_r[n_2] - 2\beta[n_1]\beta[n_2]\right\}.
\end{aligned} \tag{2.54}$$

However, $\mathrm{E}\{\beta[n_1]\alpha_r[n_2]\} = \sum_{i=1}^{n_o} \mu_i \mathrm{e}^{\lambda_i T_s \min(0,n_2-n_1)}$ and $\mathrm{E}\{\beta[n_1]\beta[n_2]\} = \sum_{i=1}^{n_o} \nu_i \mathrm{e}^{-\lambda_i T_s |n_1-n_2|}$, thus (2.54) can be rewritten as

$$\begin{aligned}
&\mathrm{E}\left\{(\theta[n_2] - \theta[n_1])^2\right\} \\
&\quad = \omega_c^2 \left[(n_1 + n_2 - 2\min(n_1, n_2)) c_r T_s + 2\sum_{i=1}^{n_o} \nu_i + 4\sum_{i=1}^{n_o} \mu_i \right. \\
&\qquad \left. -2\sum_{i=1}^{n_o} \mu_i \mathrm{e}^{\lambda_i T_s \min(0,n_1-n_2)} - 2\sum_{i=1}^{n_o} \mu_i \mathrm{e}^{\lambda_i T_s \min(0,n_2-n_1)} - 2\sum_{i=1}^{n_o} \nu_i \mathrm{e}^{-\lambda_i T_s |n_1-n_2|}\right] \\
&\quad = \omega_c^2 \left[(n_1 + n_2 - 2\min(n_1, n_2)) c_r T_s + 2\sum_{i=1}^{n_o} (\nu_i + \mu_i)\left(1 - \mathrm{e}^{-\lambda_i T_s |n_1-n_2|}\right)\right].
\end{aligned} \tag{2.55}$$

The last equation in (2.55) is obtained based on

$$\begin{aligned}
\sum_{i=1}^{n_o} \mu_i \mathrm{e}^{\lambda_i T_s \min(0,n_1-n_2)} + \sum_{i=1}^{n_o} \mu_i \mathrm{e}^{\lambda_i T_s \min(0,n_2-n_1)} &= \begin{cases} \sum_{i=1}^{n_o} \mu_i + \sum_{i=1}^{n_o} \mu_i \mathrm{e}^{\lambda_i T_s (n_2-n_1)} & \text{if} \quad n_1 \geq n_2 \\ \sum_{i=1}^{n_o} \mu_i \mathrm{e}^{\lambda_i T_s (n_1-n_2)} + \sum_{i=1}^{n_o} \mu_i & \text{if} \quad n_2 > n_1 \end{cases} \\
&= \sum_{i=1}^{n_o} \mu_i + \sum_{i=1}^{n_o} \mu_i \mathrm{e}^{-\lambda_i T_s |n_1-n_2|}.
\end{aligned} \tag{2.56}$$

Hence, the (n_1, n_2)th component of the PLL-PN covariance matrix $\mathbf{R}$ is

$$\mathbf{R}[n_1, n_2] = \exp\Bigg\{ -\frac{1}{2}\omega_c^2 \Bigg[(n_1 + n_2 - 2\min(n_1, n_2)) c_r T_s + 2\sum_{i=1}^{n_o} (\nu_i + \mu_i) \left(1 - \mathrm{e}^{-\lambda_i T_s |n_1 - n_2|}\right) \Bigg] \Bigg\} \tag{2.57}$$

2.3.2 IQ Imbalance

As discussed in Section 2.1, the transmitted M-QAM passband signal can be represented as (2.1) in which quadrature mixers play an important role of up-converting a baseband signal to a passband signal before transmitting over a wireless channel. In real implementations, however, the quadrature mixers are often impaired by gain and phase mismatches between the I and Q branches. This phenomenon is referred to as IQ imbalance.

It is relevant to point out that the problem of IQ imbalance distortion can be avoided by using different transceiver architectures, such as super-heterodyne transceivers with digital intermediate frequency (IF) [20, 22] and direct sampling transceivers [21, 22]. The first architecture is obtained from the conventional super-heterodyne architecture [21] by removing quadrature mixers and IF filters. Only one DAC and one ADC are used at the transmitter and receiver, respectively. The complexity of this architecture is dominated by the ADC and DAC because they have to handle signals at a higher frequency, which also means higher dynamic-range requirements and higher sensitivity to the clock jitter. In addition, this architecture still requires image rejection filters which are difficult to integrate on-chip at a low cost. The second transceiver architecture does not require any frequency mixing stage as well as IF filtering. Most of the signal processing can be done in the digital domain. However, direct sampling transceivers are mostly limited to applications when the carrier frequency f_c is low and the signal bandwidth is narrow. As the carrier frequency and signal bandwidth go up, the implementation cost significantly increases and the performance of ADC and DAC drops quickly even when under-sampling is applied [21, 22]. As such, this transceiver architecture is not suitable for low-cost applications such as machine-type communications (MTC) [24].

As such, despite of having IQ imbalance, using quadrature mixers can still be a much

cheaper solution compared to the above alternative architectures [20–23]. Furthermore, as shown later, compensation for the IQ imbalance can be conveniently performed in the digital domain at the receiver.

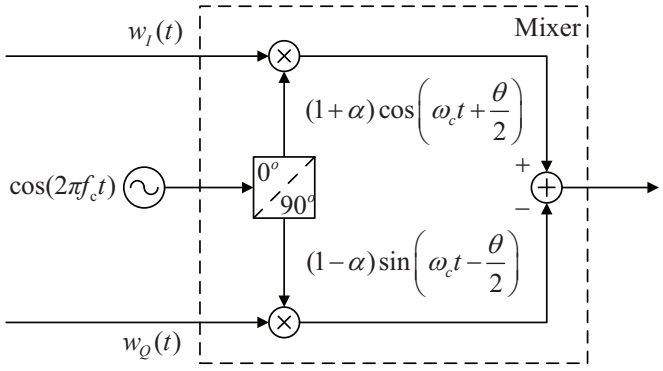

Figure 2.15: Transmit IQ imbalance model.

Consider an IQ imbalance model at the transmitter as in Fig. 2.15. Define $w(t) = w_I(t) + jw_Q(t)$ as the input signal that needs to be up-converted to the carrier frequency f_c by the quadrature mixer, and $z(t)$ as the output of the mixer. Without IQ imbalance, the output of the oscillator would be

$$z(t) = \sqrt{2}w_I(t)\cos(2\pi f_c t) - \sqrt{2}w_Q(t)\sin(2\pi f_c t) = \sqrt{2}\Re\left\{w(t)\mathrm{e}^{j2\pi f_c t}\right\}. \tag{2.58}$$

However, the mixer is not ideal in practice which results in IQ imbalance impairment. Denoting by α_T and θ_T the gain and phase imbalance, respectively. In practice, α_T and θ_T are fixed parameters. Thus, the output of the mixer can be represented as

$$z(t) = \sqrt{2}(1+\alpha_T)w_I(t)\cos\left(2\pi f_c t + \frac{\theta_T}{2}\right) - \sqrt{2}(1-\alpha_T)w_Q(t)\sin\left(2\pi f_c t - \frac{\theta_T}{2}\right). \tag{2.59}$$

The expression in (2.59) can be expanded as

$$\begin{aligned} z(t) = \frac{1}{\sqrt{2}}\mathrm{e}^{j2\pi f_c t}\underbrace{\left((1+\alpha_T)w_I(t)\mathrm{e}^{j\frac{\theta_T}{2}} + j(1-\alpha_T)w_Q(t)\mathrm{e}^{-j\frac{\theta_T}{2}}\right)}_{I_1} + \\ \frac{1}{\sqrt{2}}\mathrm{e}^{-j2\pi f_c t}\underbrace{\left((1+\alpha_T)w_I(t)\mathrm{e}^{-j\frac{\theta_T}{2}} - j(1-\alpha_T)w_Q(t)\mathrm{e}^{j\frac{\theta_T}{2}}\right)}_{I_2}. \end{aligned} \tag{2.60}$$

The term I_1 can be rewritten as

$$I_1 = \xi_T w(t) + \eta_T w^*(t). \tag{2.61}$$

where

$$\begin{aligned}\xi_T &= \cos\frac{\theta_T}{2} + j\alpha_T \sin\frac{\theta_T}{2} \\ \eta_T &= \alpha_T \cos\frac{\theta_T}{2} + j\sin\frac{\theta_T}{2}.\end{aligned} \tag{2.62}$$

A similar expression can be obtained for I_2 and it is simple to show that $I_2 = I_1^*$. Finally,

$$\begin{aligned}z(t) &= \frac{1}{\sqrt{2}}\mathrm{e}^{j2\pi f_c t}\left(\xi_T w(t) + \eta_T w^*(t)\right) + \frac{1}{\sqrt{2}}\mathrm{e}^{-j2\pi f_c t}\left(\xi_T w(t) + \eta_T w^*(t)\right)^* \\ &= \sqrt{2}\Re\left\{\left(\xi_T w(t) + \eta_T w^*(t)\right)\mathrm{e}^{j2\pi f_c t}\right\}.\end{aligned} \tag{2.63}$$

From (2.58) and (2.63), it can be seen that the transmit IQ imbalance results in an "image" signal $w^*(t)$ at the output of the mixer.

Similarly, because of the imperfection of the RF down-conversion mixer, the IQ imbalance happens at the receiver as well. Define α_R and θ_R as the gain and phase imbalance, respectively, of the receive mixer. Also define $\hat{z}(t)$ and $\hat{w}(t)$ as the input and output, respectively, of the mixer. Then, the complex baseband equivalent received signal after the frequency down conversion is

$$\hat{w}(t) = \xi_R \hat{z}(t) + \eta_R \hat{z}^*(t) \tag{2.64}$$

where ξ_R and η_R characterize the effect of the receive IQ imbalance as

$$\begin{aligned}\xi_R &= \cos\frac{\theta_R}{2} - j\alpha_R \sin\frac{\theta_R}{2} \\ \eta_R &= \alpha_R \cos\frac{\theta_R}{2} + j\sin\frac{\theta_R}{2}.\end{aligned} \tag{2.65}$$

Thus, in the presence of the receive IQ imbalance, it can be seen that the output of the mixer contains two components, one is the desired received signal $\hat{z}(t)$ and the other is its "image" signal $\hat{z}^*(t)$.

2.3.3 Nonlinearity

Nonlinearity is generally generated by analog and RF devices like ADC, DAC, oscillators and amplifiers. From communications point of view, this distortion leads to harmonics generation, gain compression, cross modulation, and inter-modulation issues which significantly degrade the performance of either the system itself or other systems working in the contaminated spectrum range [25]. The characteristic of nonlinear devices can be represented

either as memoryless nonlinearity or nonlinearity with memory. Fig. 2.16 illustrates how nonlinearity impairment from a power amplifier can affect the output of a monotonic input system. In this scenario, the impact of nonlinearity is represented by the third-order polynomial $\alpha_1 x + \alpha_2 x^2 - \alpha_3 x^3$. It is assumed that the input of the power amplifier is a sinusoidal signal $x(t) = \cos(2\pi f_1 t)$ which is represented by an impulse at frequency f_1 in the power spectrum density (PSD) plot. The output of the power amplifier can be obtained as

$$\begin{aligned} y(t) &= \alpha_1 \cos(2\pi f_1 t) + \alpha_2 \cos^2(2\pi f_1 t) - \alpha_3 \cos^3(2\pi f_1 t) \\ &= \frac{\alpha_2}{2} + \left(\alpha_1 - \frac{3}{4}\alpha_3\right)\cos(2\pi f_1 t) + \frac{\alpha_2}{2}\cos(4\pi f_1 t) - \frac{\alpha_3}{4}\cos(6\pi f_1 t). \end{aligned} \tag{2.66}$$

It can be seen that the output of this system contains not only the original frequency component, i.e., f_1, but also other frequency components, namely $2f_1$ and $3f_1$, as illustrated in Fig. 2.16.

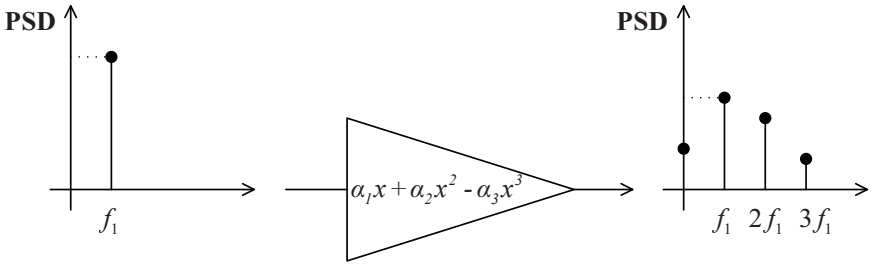

Figure 2.16: Illustration of power amplifier nonlinearity.

The effect of nonlinearities in communication systems has been well studied in the literature [26–30]. The influence of nonlinearities is often negligible in systems employing constant modulus signaling since it makes the linear approximation model valid. However, since multicarrier systems produce signals with large amplitude fluctuations, they significantly suffer from the nonlinearity distortions.

Although nonlinearity distortions can come from many sources, a power amplifier (PA), which is commonly used to amplify the power of a radio frequency signal before being transmitted over a channel, is considered as the major source of nonlinearity distortions in the transmission chain [25]. Thus, only the PA nonlinearity is considered in this research. The output of a PA exhibits different magnitudes of nonlinearities [25], namely AM/AM (Ampli-

tude to Amplitude Modulation) and AM/PM (Amplitude to Phase Modulation) distortions. A PA is often followed by a band-pass filter in practice to cancel any additional unwanted sidebands lying at the harmonics of the carrier frequency. As a result, only in-band nonlinear distortion is considered in this research. In order to model the effects of the in-band nonlinear distortion introduced by the PA, an odd-order polynomial model is commonly used to express the PA's output as follows [31]. Define $z_p(t)$ and $u_p(t)$ as the input and output of a PA, respectively, then $u_p(t)$ can be represented as

$$u_p(t) = \sum_{k=0}^{K} \beta_{2k+1}[z_p(t)]^{2k+1} \tag{2.67}$$

where β_{2k+1} is the coefficient of the polynomial scaling the nonlinearity, which is determined based on interception points. For example, if the effect of PA nonlinearity takes into account up to the third-order distortion, then

$$u_p(t) = \beta_1 z_p(t) + \beta_3[z_p(t)]^3 \tag{2.68}$$

and

$$\left|\frac{\beta_3}{\beta_1}\right| = \frac{4}{3A_{\mathrm{IIP}_3}^2}, \tag{2.69}$$

where A_{IIP_3} refers to the input third order interception point [25].

For ease of representation, the input-output characteristic of a PA can be rewritten as [32]

$$u_p(t) = \alpha z_p(t) + d_p(t) \tag{2.70}$$

where α is a small gain resulting from amplifying, while $d_p(t)$ represents the distortion noise which is statistically independent of $z_p(t)$. Let $u(t)$ and $d(t)$ be the complex baseband equivalent signals of $u_p(t)$ and $d_p(t)$, respectively. Then

$$u(t) = \alpha z(t) + d(t). \tag{2.71}$$

The value of α and the variance of $d(t)$ can be determined by applying the Bussgang's theorem [33] as shown in [25].

In this thesis, the impacts of physical impairments, including PN, IQ imbalance and nonlinearity, are first evaluated in Chapter 3 for an OFDM-based bi-directional full-duplex

communication system. The impact of PN and its compensation in CFBMC-OQAM are studied in Chapter 4 and Chapter 5. Different from Chapter 4 where the compensation of PN is simplified by considering perfect channel estimation at the receiver, the impact of channel estimation error is taken into account in Chapter 5. Finally, in addition to PN, the impact of IQ imbalance is analyzed and compensated in Chapter 6 for a general CP-based multi-carrier system.

2.4 Full-Duplex (FD) Wireless Communications

Full-duplex (FD) communication is an emerging technology for future wireless networks since it achieves much higher spectral efficiency when compared to the conventional half-duplex (HD) communication [34, 35] where the transmission and reception are performed over either different time slots or different frequency bands.

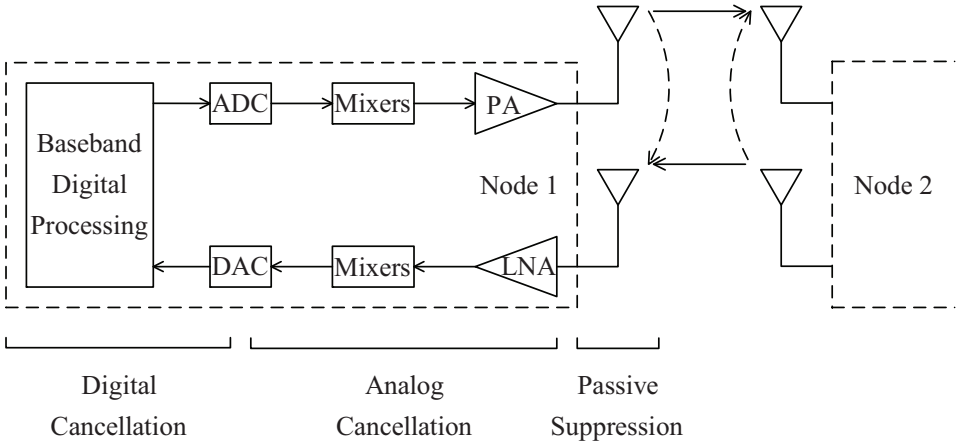

Figure 2.17: A block diagram for full-duplex communications.

Fig. 2.17 illustrates a bi-directional FD communication between two transmission nodes. It is assumed that each node has two antennas, one antenna is for transmitting signal and the other is for receiving signal. In FD communication, the transmission and reception in each node are performed simultaneously at the same time and frequency band. As such, the received signal in Node 1 for example contains not only the transmitted signal from Node 2, which is referred to as the desired signal, but also the transmitted signal from its own device, which is referred to as self-interference (SI). Because the distance between two antennas in

Node 1 is much shorter than the distance between the transmit antenna in Node 2 and the receive antenna in Node 1, the power of the SI signal is typically thousand times higher than the received power of the desired signal. This makes SI become the biggest challenge in realizing FD communication in practice. The channel between two antennas in the same device is also called near-end channel, whereas the channel between the transmit antenna of one device and the receive antenna of the other device is called far-end channel.

In general, self-interference cancellation (SIC) techniques are classified into three main categories, namely passive suppression, analog cancellation and digital cancellation [34, 36] as illustrated in Fig. 2.17. Before performing analog and digital cancellation, a passive suppression technique is required to achieve a high isolation between the transmit antenna and the receive antenna and the amount of cancellation achieved mainly depends on the propagation loss of the wireless channel. As for analog cancellation, a cancelling signal is added to the received signal in the analog domain in order to further attenuate the power of the SI. The residual SI (RSI) after the analog cancellation still remains and can be a bottleneck limiting the implementation of FD devices in practice.

In this thesis, a bi-directional OFDM-based FD communication is studied in Chapter 3, which focuses on digital cancellation of the self interference. The implementation of digital self-interference cancellation is challenging due to the presence of PN, IQ imbalance and PA nonlinearity. As such, the chapter develops an iterative SIC technique such that the impacts of these physical impairments are taken into account in performing SIC.

2.5 Summary

In this chapter, an introduction to single-carrier as well as multi-carrier wireless communication systems has been first presented. By dividing the system's frequency band into many sub-channels whose bandwidths are smaller than the coherence bandwidth of the wireless channel, the frequency-selective fading channel, which causes ISI in single-carrier wireless communications, is converted into a set of flat fading channels in multi-carrier wireless communications. This conversion generally eases the channel equalization task. Second, three CP-based multi-carrier modulation techniques, namely OFDM, CFBMC-OQAM and

GFDM, have been described in detail. Advantages and disadvantages of each multi-carrier technique have been also discussed. Finally, a brief review of physical impairments, including PN, IQ imbalance and nonlinearity, and FD communication technique was given. The next chapters present contributions of this PhD research.

References

[1] H. H. Nguyen and E. Shwedyk: "A First Course in Digital Communications", *Cambridge University Press*, 2009.

[2] Y. S. Cho, J. Kim, W. Y. Yang and C. G. Kang: "MIMO-OFDM Wireless Communications with MATLAB", *John Wiley & Sons (Asia) Pte Ltd*, 2010.

[3] H. Zarrinkoub: "Understanding LTE with MATLAB: From Mathematical Modeling to Simulation and Prototyping", *John Wiley & Sons, Ltd*, 2014.

[4] B. Farhang-Boroujeny: "OFDM Versus Filter Bank Multicarrier", *IEEE Signal Processing Magazine*, vol. 28, no. 3, pp. 92–112, May 2011.

[5] N. Michailow and M. Matth and I. S. Gaspar and A. N. Caldevilla and L. L. Mendes and A. Festag and G. Fettweis: "Generalized Frequency Division Multiplexing for 5th Generation Cellular Networks", *IEEE Transactions on Communications*, vol. 62, no. 9, pp. 3045–3061, Sept. 2014.

[6] G. Fettweis and M. Krondorf and S. Bittner: "GFDM - Generalized Frequency Division Multiplexing", *IEEE 69th Vehicular Technology Conference*, pp. 1–4, April 2009.

[7] G. R. Parsace and A. Yarali and H. Ebrahimzad: "MMSE-DFE equalizer design for OFDM systems with insufficient cyclic prefix", *IEEE 60th Vehicular Technology Conference*, vol. 6, pp. 3828–3832, Sept. 2004.

[8] Y. Jin and X. Xia: "A Robust Precoder Design Based on Channel Statistics for MIMO-OFDM Systems with Insufficient Cyclic Prefix", *IEEE Transactions on Communications*, vol. 62, no. 4, pp. 1249–1257, Apr. 2014.

[9] T. Pham and T. Le-Ngoc and G. K. Woodward and P. A. Martin: "Channel Estimation and Data Detection for Insufficient Cyclic Prefix MIMO-OFDM", *IEEE Transactions on Vehicular Technology*, vol. 66, no. 6, pp. 4756–4768, Jun. 2017.

[10] K. W. Martin: "Small side-lobe filter design for multitone data-communication applications", *IEEE Transactions on Circuits and Systems II: Analog and Digital Signal Processing*, vol. 45, no. 8, pp. 1155–1161, Aug. 1998.

[11] B. Farhang-Boroujeny: "Signal Processing Techniques for Software Radios", *Lulu Publishing House*, vol. 82, 2011.

[12] B. Farhang-Boroujeny: "Filter Bank Multicarrier Modulation: A Waveform Candidate for 5G and Beyond", *Advances in Electrical Engineering*, vol. 2014, pp. 1–25, Feb. 2014.

[13] B. Farhang-Boroujeny: "Filter Bank Multicarrier Modulation: A Waveform Candidate for 5G and Beyond", *Advances in Electrical Engineering*, vol. 2014, pp. 1–25, 2014.

[14] S. Mirabbasi and K. Martin: "Overlapped complex-modulated transmultiplexer filters with simplified design and superior stopbands", *IEEE Transactions on Circuits and Systems II: Analog and Digital Signal Processing*, vol. 50, no. 8, pp. 456–469, Aug. 2003.

[15] A. RezazadehReyhani and B. Farhang-Boroujeny: "An Analytical Study of Circularly Pulse-Shaped FBMC-OQAM Waveforms", *IEEE Signal Processing Letters*, vol. 24, no. 10, pp. 1503–1506, Oct. 2017.

[16] A. Demir and A. Mehrotra and J. Roychowdhury: "Phase noise in oscillators: a unifying theory and numerical methods for characterization", *IEEE Transactions on Circuits and Systems I: Fundamental Theory and Applications*, vol. 47, no. 5, pp. 655–674, May 2000.

[17] D. Petrovic and W. Rave and G. Fettweis: "Effects of Phase Noise on OFDM Systems With and Without PLL: Characterization and Compensation", *IEEE Transactions on Communications*, vol. 55, no. 8, pp. 1607–1616, Aug. 2007.

[18] A. Papoulis and S. U. Pillai: "Probability, Random Variables, and Stochastic Processes", McGraw Hill, Boston (2002).

[19] A. Mehrotra: "Noise analysis of phase-locked loops", *IEEE Transactions on Circuits and Systems I: Fundamental Theory and Applications*, vol. 49, no. 9, pp. 1309–1316, Sept. 2002.

[20] L. Smaini: "RF Analog Impairments Modeling for Communication Systems Simulation", John Wiley & Sons, Ltd, 2012.

[21] I. Robertson, N. Somjit, and M. Chongcheawchamnan: "Microwave and MillimetreWave Design for Wireless Communications", John Wiley & Sons, Ltd, 2016.

[22] H. Zheng: "Designing 4- to 12-GHz Direct Conversion Receiver With LMX8410L IQ Demodulator", Texas Instruments application report, Apr. 2019.

[23] Y. Li and L. Fan and H. Lin and M. Zhao: "A new method to simultaneously estimate TX/RX IQ imbalance and channel for OFDM systems", *2013 IEEE International Conference on Communications (ICC)*, pp. 4551–4555, 2013.

[24] I. B. F. de Almeida and L. L. Mendes and J. J. P. C. Rodrigues and M. A. A. da Cruz: "5G Waveforms for IoT Applications", *IEEE Communications Surveys and Tutorials*, vol. 21, no. 3, pp. 2554–2567, 2019.

[25] T. Schenk: "RF Imperfections in High-rate Wireless Systems: Impact and Digital Compensation". Springer, Netherlands (2008).

[26] S. Li and R. D. Murch: "An Investigation Into Baseband Techniques for Single-Channel Full-Duplex Wireless Communication Systems", *IEEE Transactions on Wireless Communications*, vol. 13, no. 9, pp. 4794–4806, 2014.

[27] E. Ahmed and A. M. Eltawil: "All-Digital Self-Interference Cancellation Technique for Full-Duplex Systems", *IEEE Transactions on Wireless Communications*, vol. 14, no. 7, pp. 3519–3532, 2015.

[28] D. Korpi and L. Anttila and V. Syrjala and M. Valkama: "Widely Linear Digital Self-Interference Cancellation in Direct-Conversion Full-Duplex Transceiver", *IEEE Journal on Selected Areas in Communications*, vol. 32, no. 9, pp. 1674–1687, 2014.

[29] A. C. M. Austin and A. Balatsoukas-Stimming and A. Burg: "Digital predistortion of power amplifier non-linearities for full-duplex transceivers", *2016 IEEE 17th International Workshop on Signal Processing Advances in Wireless Communications*, pp. 1–5 2016.

[30] L. Anttila and D. Korpi and V. Syrjala and M. Valkama: "Cancellation of power amplifier induced nonlinear self-interference in full-duplex transceivers", *2013 Asilomar Conference on Signals, Systems and Computers*, pp. 1193–1198, 2013.

[31] S. Zhao and X. Zhu and H. Wang and L. Wu: "Analysis of joint effect of phase noise, IQ imbalance and amplifier nonlinearity in OFDM system", *International Conference on Wireless Communications and Signal Processing*, pp. 1–6, 2013.

[32] P. Banelli and S. Cacopardi: "Theoretical analysis and performance of OFDM signals in nonlinear AWGN channels", *IEEE Transactions on Communications*, vol. 48, no. 3, pp. 430–441, 2000.

[33] J. J. Bussgang: "Cross-correlation functions of amplitude distorted Gaussian signals". Research laboratory of Electronics, Massachusetts Institute of Technology, 1952.

[34] Z. Zhang and K. Long and A. V. Vasilakos and L. Hanzo: "Full-Duplex Wireless Communications: Challenges, Solutions, and Future Research Directions", *Proceedings of the IEEE*, vol. 104, no. 7, pp. 1369–1409, 2016.

[35] A. Sabharwal and P. Schniter and D. Guo and D. W. Bliss and S. Rangarajan and R. Wichman: "In-Band Full-Duplex Wireless: Challenges and Opportunities", *IEEE Journal on Selected Areas in Communications*, vol. 32, no. 9, pp. 1637–1652, 2014.

[36] M. Duarte and A. Sabharwal: "Full-duplex wireless communications using off-the-shelf radios: Feasibility and first results", *The Forty Fourth Asilomar Conference on Signals, Systems and Computers*, pp. 1558–1562, 2010.

3. Bi-directional OFDM-based Full-Duplex Communications

Published as:

Long D. Le and Ha H. Nguyen, "Iterative Self-Interference Mitigation in Full-Duplex Wireless Communications," *Wireless Personal Communications*, vol. 109, pp. 2663–2682, 2019.

As discussed in the previous chapter, FD communication is a promising technology since it achieves much higher spectral efficiency when compared to the conventional HD communication. However, the trade-off for this spectral advantage is the existence of a massive amount of SI caused by direct coupling of the strong transmit signal to the sensitive receiver chain resided in the same hardware device. This SI poses the biggest challenge in realizing FD communication in practice. There has been extensive research on SIC techniques for FD communications. However, the implementation of SIC is very challenging in practice due to physical impairments of hardware devices such as PN, nonlinearities, and IQ imbalance.

This chapter considers a bi-directional OFDM-based FD communication in the presence of PN, IQ imbalance and PA nonlinearity. In order to effectively mitigate the effect of SI, an iterative SIC technique is proposed which takes into account the impacts of PN, IQ imbalance and PA nonlinearity. Simulation results show that the proposed technique can effectively mitigate the self interference after every iteration. As a consequence, decoding performance of the desired signal is significantly improved. Furthermore, the proposed algorithm is shown to considerably outperform existing algorithms over a practical transmit power range.

Iterative Self-Interference Mitigation in Full-Duplex Wireless Communications

Long D. Le and Ha H. Nguyen

Abstract

This paper considers a full-duplex wireless communication system in which detection of the desired signal is hindered not only by the self-interference (SI), but also phase noise, in-phase and quadrature-phase (IQ) imbalance and power amplifier's nonlinearity distortion. An iterative algorithm is proposed in which the processes of SI cancellation and detection of the desired signal aid each other in each iteration. In each iteration, the SI cancellation process performs widely linear estimation of the SI channel and compensates for physical impairments to improve the detection performance of the desired signal. The detected desired signal is in turn removed from the received signal to improve SI channel estimation and SI cancellation in the next iteration. Simulation results show that the proposed algorithm significantly outperforms existing algorithms in SI cancellation and detection of the desired signal.

Index terms

Full-duplex, self-interference, self-interference cancellation, phase noise, I/Q imbalance, power amplifier's nonlinearity distortion.

3.1 Introduction

Full-duplex (FD) communication is a promising technology for future generations of wireless networks since it achieves much higher spectral efficiency when compared to the conventional half-duplex (HD) communication [1, 2]. Different from HD communication, in which the transmission and reception are performed over different time slots (i.e., time-

domain division – TDD), or over different frequency bands (i.e., frequency-domain division – FDD), FD wireless communication uses the same radio-frequency (RF) band for simultaneous transmission and reception. As such, FD communication utilizes the spectrum resource much more efficiently. However, the trade-off for this spectral advantage is the existence of a massive amount of self-interference (SI) caused by direct coupling of the strong transmit signal to the sensitive receiver chain resided in the same hardware device. The power of the SI signal is typically thousand times higher than the received power of the desired signal. This SI poses the biggest challenge in realizing FD communication in practice.

There has been extensive research on SI cancellation (SIC) techniques for FD communication [3–7]. In general, SIC techniques are classified into three main categories, namely passive suppression, analog cancellation and digital cancellation [1, 3]. Before performing analog and digital cancellation, a passive suppression technique is required to achieve a high isolation between the transmit antenna and the receive antenna and the amount of cancellation achieved mainly depends on the propagation loss of the wireless channel. As for analog cancellation, a cancelling signal is added to the received signal in the analog domain in order to further attenuate the power of the SI. The residual SI (RSI) after the analog cancellation still remains and can be a bottleneck limiting the implementation of FD devices in practice. As demonstrated in [3, 4], digital cancellation has the potential of achieving around additional 6 dB gain after analog cancellation. The implementation of digital SIC is very challenging due to physical impairments of hardware devices. As observed in [5], phase noise (PN), power amplifier (PA) nonlinearity, and in-phase and quadrature-phase (IQ) imbalance are the major factors limiting performance of a digital SIC technique.

The effects of phase noise in SIC are investigated in [7–10]. Specifically, in [9] the impacts of phase noise, which is modeled as a Wiener process, are analyzed under two scenarios: (i) separated oscillators for the transmitter and receiver, and (ii) a common oscillator is shared between the transmitter and receiver. The authors derived closed-form expressions quantifying the digital cancellation capability and its limit in the large interference-to-noise ratio regime. Based on the established digital cancellation capability, the achievable rate region of a two-way FD system is also characterized. A novel digital SIC technique for FD

systems is proposed in [7]. In that paper, a copy of the SI in digital domain is used to cancel out both the SI signal and impairments in the transmitter, including the phase noise. In order to alleviate the receiver's phase noise effect, a common local oscillator (LO) is shared between the auxiliary and ordinary receiver chains.

The impacts of IQ imbalance are considered in [6,10]. In [6], the IQ imbalance is included in both the transmitter and receiver. The observation in this paper is that, under the effect of IQ imbalance, the total SI at the receiver contains not only the linear SI component, but also the complex conjugate SI component. The authors showed that the conjugate SI signal is the most dominant source of distortion under a wide range of transmit power. In some cases the power of conjugate SI is even more powerful than the power of the desired signal. The authors also showed that using a linear digital cancellation technique under the effect of receive IQ imbalance does not yield good performance. Instead, they proposed a technique called widely linear digital cancellation, which takes into account not only the linear SI component but also the conjugate SI component. In [10], an analysis of RSI for a full-duplex OFDM transceiver under the joint impact of both phase noise and IQ imbalance is given. In particular, a closed-form expression for the average RSI power was derived. It was demonstrated that the effects of phase noise and IQ imbalance can be approximately decoupled for small PN and IQ imbalance levels. The average RSI is linearly proportional to the IQ image rejection ratio and the phase noise 3-dB bandwidth.

References [5–7, 11, 12] investigate nonlinearity distortions in FD systems. In general, nonlinearity distortions come from the analog-to-digital converter (ADC), digital-to-analog converter (DAC), mixers and amplifiers (i.e., a PA in the transmitter and a low-noise amplifier (LNA) in the receiver). However, PA is the major source of nonlinearity distortions in the transmission chain [13]. Indeed, a comparison in terms of relative powers of spurious signal components resulting from different RF/analog impairments was given in [5]. In that paper, along with the IQ imbalance, the PA nonlinearity is shown to be the most damaging factor which severely degrades the performance of a SIC technique. The authors in [5] proposed a two-stage iterative SIC scheme based on the output of the PA to substantially mitigate the effect of SI. Simulation results show good performance improvement of the proposed

strategy compared to previously-known digital cancellation schemes. A digital cancellation technique for PA-induced nonlinear SI in a FD transceiver is also studied in [12]. Specifically, a nonlinear digital SIC technique was proposed to handle both the linear and nonlinear SI simultaneously. Simulation results in [12] demonstrate that the proposed canceller is able to extend the usable transmit power range by at least 10 dB, or to allow using a lower-quality PA in the transmitter.

To the authors' best knowledge, there has been no work considering the joint effects of phase noise, IQ imbalance and PA nonlinearity from both the transmitter and receiver in a FD communication system. To fill this gap, this paper considers FD communication between two nodes, Node 1 and Node 2, in which PN, IQ imbalance and PA nonlinearity are present in the transmitter of Node 1, whereas PN and IQ imbalance are considered in its receiver. To focus on signal processing and SI cancellation at Node 1, Node 2 is assumed to be free of impairments. Because of SI, the received signal in Node 1 contains not only the desired signal from Node 2, but also the SI signal from its own transmission. In order to effectively mitigate the effect of SI, the SIC technique proposed in this paper is performed iteratively as follows. First, the SI channel (i.e., the near-end channel) is estimated based on widely linear estimation (WLE). Given the estimated SI channel, the SI signal leaking from its own transceiver is subtracted from the received signal. The resulting signal is further processed to decode the desired signal, i.e., the far-end signal. The impairments are also estimated and compensated to improve the decoding performance. A DFT-based channel estimation method is applied to further mitigate the effect of residual noise and improve the quality of the far-end channel estimation. The decoded desired signal is then removed from the received signal to improve the quality of the SI channel estimation in the next iteration.

Performance evaluation of the proposed algorithm is based on two metrics: Error Vector Magnitude (EVM), and Bit Error Rate (BER) with respect to the transmit power of Node 2. From simulation results, it is observed that the SI signal is effectively mitigated after every iteration, which results in performance improvement in decoding the desired signal. As expected, the decoding performance is much better than that of the case without deploying any SIC technique. Performance of the proposed algorithm is also compared with that of

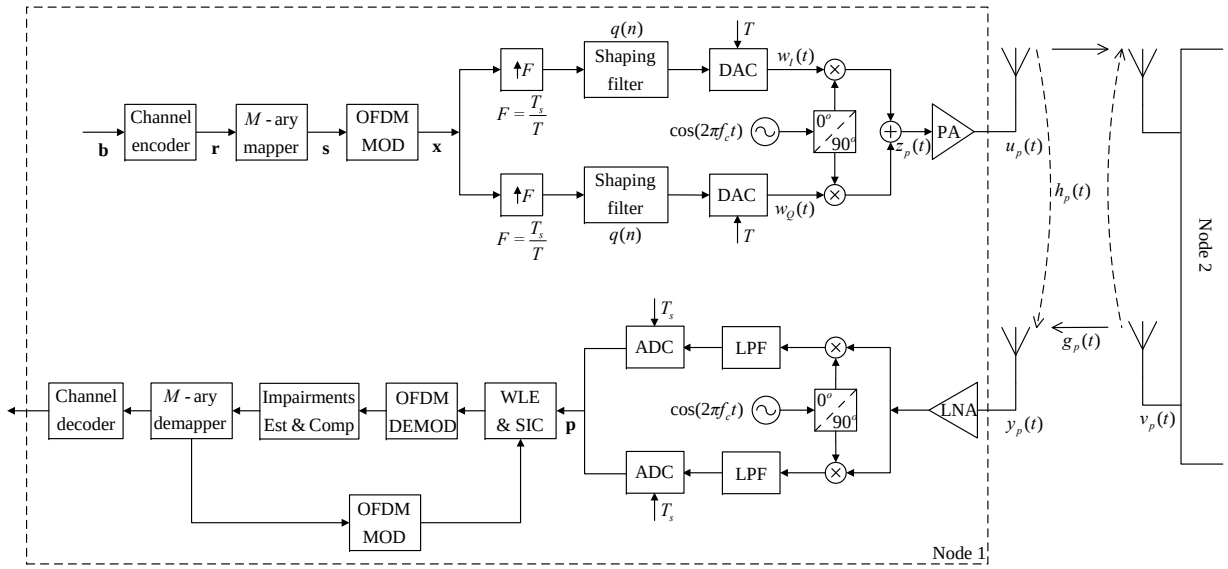

Figure 3.1: System Model.

algorithms proposed in [5] and [6], in which the former uses linear digital estimation and the later uses widely linear digital estimation without considering the iterative decoding and making use of the desired signal in refining the quality of the SI channel estimation. In general, the performance of the proposed SIC technique is considerably better than the existing techniques over the practical transmit power range.

This paper is organized as follows. The system model is presented in Section 3.2. The proposed strategy to iteratively mitigate the effect of SI is described in Section 3.3. Simulation results and performance analysis are provided in Section 3.4. Section 3.5 concludes the paper.

Notation: Lowercase letters are used to denote scalars. Lowercase boldface and uppercase boldface letters stand for vectors and matrices, respectively. $(\cdot)^{\dagger}$, $(\cdot)^{T}$, $(\cdot)^{H}$, $(\cdot)^{*}$, $|\cdot|$, and $\odot$ denote pseudo-inverse, transpose, Hermitian, conjugation, modulus, and element-wise multiplication operations, respectively. $\mathfrak{R}[\cdot]$ and $\mathfrak{I}[\cdot]$ represent the real and imaginary parts of a complex variable.

3.2 System Model

Consider a FD communication system as shown in Fig. 3.1. The information bits of Node 1, represented as vector $\mathbf{b}$, are first encoded to generate coded bits, represented as vector $\mathbf{r}$. The coded bits are then mapped into a sequence of symbols, represented as vector $\mathbf{s}$, based on a QAM constellation and Gray mapping scheme. The sequence of QAM symbols is then serial-to-parallel converted before performing OFDM modulation to obtain the discrete time-domain signal $\mathbf{x} = \begin{bmatrix} x(0) & x(1) & \cdots & x(N-1) \end{bmatrix}^T$, where N is the length of a transmission frame. Each frame contains N_{f} OFDM symbols in which each OFDM symbol consists of N_{fft} time-domain samples (which are the IFFT of N_{fft} subcarriers) and a cyclic prefix (CP) of length N_{cp}. The CP length is chosen long enough to avoid inter-symbol interference between OFDM symbols. It follows that $N = N_{\mathrm{f}}(N_{\mathrm{fft}} + N_{\mathrm{cp}})$. Furthermore, out of N_{fft} subcarriers, there are N_{a} active (i.e., nonzero) subcarriers carrying data and pilots.

The symbol sequence $\mathbf{x}$ is converted to a discrete-time impulse train by upsampling with an oversampling factor F, where F is the ratio of symbol interval, denoted as T_s, to sample interval, denoted as T. Let $q(n)$ be the impulse response of the digital shaping filter. After the discrete-time impulse train passes through the digital shaping filter and DAC, one obtains the following continuous-time complex baseband signal $w(t)$ [14]

$$w(t) = w_I(t) + jw_Q(t) = \sum_{l=0}^{N-1} x(l)q(t - lT_s), \tag{3.1}$$

where $q(t)$ is the impulse response of an equivalent analog pulse shaping filter. It means if B is the bandwidth of the transmitted signal and with an ideal DAC (i.e., band-limited interpolation), then $q(t) = \sum_n q[n]\mathrm{sinc}(2B(t - nT))$, where T is the sampling period. The signal $w(t)$ is up-converted to a carrier frequency f_c by IQ mixers. These mixers are not ideal in practice, which consequently insert the PN and transmit IQ imbalance into the transmitted signal. The RF signal after the mixers is denoted by $z_p(t)$ and its complex baseband equivalent signal is given as [15]

$$z(t) = \mathrm{e}^{j\phi_T(t)} \left(\xi_T w(t) + \eta_T w^*(t)\right) \tag{3.2}$$

where ξ_T and η_T characterize the effect of transmit IQ imbalance. They are given in terms

of gain imbalance α_T and phase imbalance θ_T as

$$\begin{aligned} \xi_T &= \cos\frac{\theta_T}{2} + j\alpha_T \sin\frac{\theta_T}{2} \\ \eta_T &= \alpha_T \cos\frac{\theta_T}{2} + j\sin\frac{\theta_T}{2} \end{aligned} \tag{3.3}$$

The function $\phi_T(t)$ in (3.2) represents the effect of transmit PN impairment. The generation of PN is based on either the free-running oscillator model or phase-locked loop (PLL) synthesizer model [16,17]. Typically, the PN is defined with a power spectral density (PSD) $\mathfrak{L}(f_m)$ [dBc/Hz], where f_m is the frequency offset with respect to the carrier frequency f_c. It can be seen from (3.2) that the impaired signal after mixing contains two components, which are the consequence of the IQ imbalance effect. Each component is further degraded by PN impairment.

The signal $z_p(t)$ is then amplified by a PA, which exhibits different magnitudes of nonlinearities [13], namely AM/AM (Amplitude to Amplitude Modulation) and AM/PM (Amplitude to Phase Modulation) distortions, before finally being transmitted over the wireless channel. The PA is commonly followed by a band-pass filter (BPF) to cancel any additional unwanted sidebands lying at the harmonics of the carrier frequency. As a result, only in-band nonlinear distortion is considered in this paper. In order to model the effects of the in-band nonlinear distortion introduced by the PA, an odd-order polynomial model is commonly used to express the PA's output as [18]

$$u_p(t) = \sum_{k=0}^{K} \beta_{2k+1}[z_p(t)]^{2k+1} \tag{3.4}$$

where β_{2k+1} is the coefficient of the polynomial scaling the nonlinearity, which is determined based on interception points. For example, if the effect of PA nonlinearity takes into account up to the third-order distortion, then

$$u_p(t) = \beta_1 z_p(t) + \beta_3[z_p(t)]^3 \tag{3.5}$$

and

$$\left|\frac{\beta_3}{\beta_1}\right| = \frac{4}{3A^2_{\mathrm{IIP}_3}}, \tag{3.6}$$

where A_{IIP_3} refers to the input third order interception point [13].

For ease of representation, the input-output characteristic of a PA can be rewritten as [19]

$$u_p(t) = \alpha z_p(t) + d_p(t) \tag{3.7}$$

where α is a small gain resulting from amplifying, while $d_p(t)$ represents the distortion noise which is statistically independent of $z_p(t)$. Let $u(t)$ and $d(t)$ be the complex baseband equivalent signals of $u_p(t)$ and $d_p(t)$, respectively. Then

$$u(t) = \alpha z(t) + d(t) \tag{3.8}$$

The value of α and the variance of $d(t)$ can be determined by applying the Bussgang's theorem [20] as shown in [13].

Owing to the SI in FD communications, the received signal in Node 1 contains not only the desired signal (far-end signal) from Node 2, but also the SI signal (near-end signal) from its own transmission. This paper focuses on the SIC in the digital domain under the assumption that the SI has already been partially mitigated by passive suppression and analog cancellation. Thus, the complex baseband equivalent received signal is

$$\begin{aligned} y(t) &= \sqrt{\frac{p_1}{\sigma_u^2}}\kappa_1^{\mathrm{ps}}\kappa_1^{\mathrm{ac}} h(t) * u(t) + \sqrt{\frac{p_2}{\sigma_v^2}}\kappa_2^{\mathrm{ps}} g(t) * v(t) + n(t) \\ &= \gamma \cdot h(t) * u(t) + \theta \cdot g(t) * v(t) + n(t) \\ &= \gamma \int_0^{\infty} h(\tau) u(t-\tau) \mathrm{d}\tau + \theta \int_0^{\infty} g(\tau) v(t-\tau) \mathrm{d}\tau + n(t) \end{aligned} \tag{3.9}$$

in which $v(t)$ denotes the complex baseband equivalent transmitted signal from Node 2; σ_u^2 and σ_v^2 are the powers of $u(t)$ and $v(t)$, respectively; p_i is the transmitted power from Node i, $i = 1, 2$; κ_i^{ps} is the attenuation capturing the propagation path loss and the passive suppression; κ_1^{ac} represents the amount of analog cancellation in Node 1; $\gamma = \sqrt{\frac{p_1}{\sigma_u^2}}\kappa_1^{\mathrm{ps}}\kappa_1^{\mathrm{ac}}$, $\theta = \sqrt{\frac{p_2}{\sigma_v^2}}\kappa_2^{\mathrm{ps}}$; and $n(t)$ denotes a circularly-symmetric complex Gaussian noise with zero mean and variance σ_n^2. Furthermore, $h(t)$ and $g(t)$ in (3.9) are the complex baseband equivalent impulse responses of the SI channel and the channel between Node 2's transmitter and Node 1's receiver, respectively. These channels are assumed to be frequency-selective, represented

by L taps as follows:

$$\begin{aligned} h(t) &= \sum_{m=0}^{L-1} h(m)\delta(t - mT_s) \\ g(t) &= \sum_{m=0}^{L-1} g(m)\delta(t - mT_s) \end{aligned} \tag{3.10}$$

Both the channel tap gains are normalized to unit total power gains, i.e., $\sum_{m=0}^{L-1}|h(m)|^2 = \sum_{m=0}^{L-1}|g(m)|^2 = 1$.

In Node 1, the received signal is first amplified by an ideal LNA, and then frequency down-converted by mixers. Due to imperfection of the mixers, the effects of PN and IQ imbalance are present in the received signal. Thus, the complex baseband equivalent received signal after the frequency down conversion is [21]

$$\tilde{p}(t) = \xi_R \mathrm{e}^{j\phi_R(t)} y(t) + \eta_R \mathrm{e}^{-j\phi_R(t)} y^*(t) \tag{3.11}$$

where $\phi_R(t)$ represents the effect of PN impairment in the receiver, whereas ξ_R and η_R characterize the effect of the receive IQ imbalance in terms of gain imbalance α_R and phase imbalance θ_R

$$\begin{aligned} \xi_R &= \cos\frac{\theta_R}{2} - j\alpha_R \sin\frac{\theta_R}{2} \\ \eta_R &= \alpha_R \cos\frac{\theta_R}{2} + j\sin\frac{\theta_R}{2} \end{aligned} \tag{3.12}$$

After the IQ mixing, T_s-spaced samples of $\tilde{p}(t)$ are produced by the ADC as

$$p(kT_s) = \tilde{p}(t)\Big|_{t=kT_s} = \xi_R \mathrm{e}^{j\phi_R(kT_s)} y(kT_s) + \eta_R \mathrm{e}^{-j\phi_R(kT_s)} y^*(kT_s) \tag{3.13}$$

The expression for $y(kT_s)$ is obtained as in (3.14)

$$\begin{aligned} y(kT_s) &\overset{(3.9)}{=} \gamma \int_0^\infty h(\tau)u(kT_s - \tau)\mathrm{d}\tau + \theta \int_0^\infty g(\tau)v(kT_s - \tau)\mathrm{d}\tau + n(kT_s) \\ &\overset{(3.10)}{=} \gamma \int_0^\infty \sum_{m=0}^{L-1} h(m)\delta(\tau - mT_s)u(kT_s - \tau)\mathrm{d}\tau + \\ &\qquad \theta \int_0^\infty \sum_{m=0}^{L-1} g(m)\delta(\tau - mT_s)v(kT_s - \tau)\mathrm{d}\tau + n(kT_s) \\ &= \gamma \sum_{m=0}^{L-1} h(m)u(kT_s - mT_s) + \theta \sum_{m=0}^{L-1} g(m)v(kT_s - mT_s) + n(kT_s) \end{aligned} \tag{3.14}$$

which simplifies to (3.15) by dropping T_s and treating the sampled values as discrete-time signals

$$\begin{aligned} y(k) &= \gamma \sum_{m=0}^{L-1} h(m)u(k-m) + \theta \sum_{m=0}^{L-1} g(m)v(k-m) + n(k) \\ &= \gamma \cdot \underbrace{h(k) * u(k)}_{y_1(k)} + \theta \cdot \underbrace{g(k) * v(k)}_{y_2(k)} + n(k) \end{aligned} \tag{3.15}$$

Equation (3.15) can be rewritten compactly as

$$\mathbf{y} = \alpha\gamma\xi_T \mathbf{H}\mathbf{P}_T\mathbf{Q}\mathbf{x} + \alpha\gamma\eta_R \mathbf{H}\mathbf{P}_T\mathbf{Q}\mathbf{x}^* + \theta\mathbf{G}\mathbf{Q}\mathbf{c} + \gamma\mathbf{H}\mathbf{d} + \mathbf{n} \tag{3.16}$$

where $\mathbf{y} = \begin{bmatrix} y(0) & y(1) & \cdots & y(N-1) \end{bmatrix}^T$, and

$$\mathbf{Q} = \begin{bmatrix} \tilde{q}(0) & 0 & \cdots & 0 & \cdots & 0 & 0 \\ \tilde{q}(1) & \tilde{q}(0) & \cdots & 0 & \cdots & 0 & 0 \\ \vdots & \vdots & \cdots & \vdots & \cdots & \vdots & \vdots \\ 0 & 0 & \cdots & \tilde{q}(M-1) & \cdots & \tilde{q}(0) & 0 \\ 0 & 0 & \cdots & 0 & \cdots & \tilde{q}(1) & \tilde{q}(0) \end{bmatrix}_{N\times N} \tag{3.17}$$

in which $\tilde{q}(n) = q(nF)$ with $n = 0, \cdots, M-1$. It is pointed that if the digital pulse shaping filter $q(n)$ is designed to satisfy the Nyquist criterion and the sampling times are perfect, $\tilde{q}(0) = 1$, $\tilde{q}(n) = 0$ for $n = 1, \cdots, M-1$ and $\mathbf{Q}$ becomes an identity matrix. The matrix $\mathbf{Q}$ in (3.17), however, applies to the more general case of arbitrary pulse shaping filter and nonzero timing offset. $\mathbf{P}_T = \text{diag}\left(\mathrm{e}^{j\phi_T(0)}; \mathrm{e}^{j\phi_T(1)}; \cdots; \mathrm{e}^{j\phi_T(N-1)}\right)$ represents the discrete-time phase noise impairment. The channel matrices $\mathbf{H}$ and $\mathbf{G}$ are given as

$$\mathbf{H} = \begin{bmatrix} h(0) & 0 & \cdots & 0 & \cdots & 0 & 0 \\ h(1) & h(0) & \cdots & 0 & \cdots & 0 & 0 \\ \vdots & \vdots & \cdots & \vdots & \cdots & \vdots & \vdots \\ 0 & 0 & \cdots & h(L-1) & \cdots & h(0) & 0 \\ 0 & 0 & \cdots & 0 & \cdots & h(1) & h(0) \end{bmatrix}_{N\times N}$$

and

$$\mathbf{G} = \begin{bmatrix} g(0) & 0 & \cdots & 0 & \cdots & 0 & 0 \\ g(1) & g(0) & \cdots & 0 & \cdots & 0 & 0 \\ \vdots & \vdots & \cdots & \vdots & \cdots & \vdots & \vdots \\ 0 & 0 & \cdots & g(L-1) & \cdots & g(0) & 0 \\ 0 & 0 & \cdots & 0 & \cdots & g(1) & g(0) \end{bmatrix}_{N \times N}$$

and $\mathbf{c} = \begin{bmatrix} c(0) & c(1) & \cdots & c(N-1) \end{bmatrix}^T$ is the output of the OFDM modulator in Node 2. The derivation steps for (3.16) are given as in Appendix 3.6.1.

Define $\mathbf{P}_R = \text{diag}\left(\mathrm{e}^{j\phi_R(0)}; \mathrm{e}^{j\phi_R(1)}; \cdots; \mathrm{e}^{j\phi_R(N-1)}\right)$ to represent the effect of PN impairment in the receiver. Thus, (3.13) can be rewritten as (3.18)

$$\begin{aligned} \mathbf{p} &= \xi_R \mathbf{P}_R \left\{ \alpha\gamma\xi_T \mathbf{H}\mathbf{P}_T\mathbf{Q}\mathbf{x} + \alpha\gamma\eta_R \mathbf{H}\mathbf{P}_T\mathbf{Q}\mathbf{x}^* + \theta\mathbf{G}\mathbf{Q}\mathbf{c} + \gamma\mathbf{H}\mathbf{d} + \mathbf{n} \right\} + \\ &\quad \eta_R \mathbf{P}_R^* \left\{ \alpha\gamma\xi_T \mathbf{H}\mathbf{P}_T\mathbf{Q}\mathbf{x} + \alpha\gamma\eta_R \mathbf{H}\mathbf{P}_T\mathbf{Q}\mathbf{x}^* + \theta\mathbf{G}\mathbf{Q}\mathbf{c} + \gamma\mathbf{H}\mathbf{d} + \mathbf{n} \right\}^* \\ &= \left(\alpha\gamma\xi_R\xi_T \mathbf{P}_R\mathbf{H}\mathbf{P}_T\mathbf{Q} + \alpha^*\gamma\eta_R\eta_T^* \mathbf{P}_R^*\mathbf{H}^*\mathbf{P}_T^*\mathbf{Q} \right)\mathbf{x} + \\ &\quad \left(\alpha\gamma\xi_R\eta_T \mathbf{P}_R\mathbf{H}\mathbf{P}_T\mathbf{Q} + \alpha^*\gamma\eta_R\xi_T^* \mathbf{P}_R^*\mathbf{H}^*\mathbf{P}_T^*\mathbf{Q} \right)\mathbf{x}^* + \\ &\quad \left(\theta\xi_R \mathbf{P}_R\mathbf{G}\mathbf{Q}\mathbf{c} + \theta\eta_R \mathbf{P}_R^*\mathbf{G}^*\mathbf{Q}\mathbf{c}^* \right) + \\ &\quad \left(\gamma\xi_R \mathbf{P}_R\mathbf{H}\mathbf{d} + \gamma\eta_R \mathbf{P}_R^*\mathbf{H}^*\mathbf{d}^* + \xi_R\mathbf{P}_R\mathbf{n} + \eta_R\mathbf{P}_R^*\mathbf{n}^* \right) \\ &= \mathbf{K}_1\mathbf{x} + \mathbf{K}_2\mathbf{x}^* + \mathbf{F}_1\mathbf{c} + \mathbf{F}_2\mathbf{c}^* + \tilde{\mathbf{n}} \end{aligned} \tag{3.18}$$

in which

$$\begin{aligned} \mathbf{K}_1 &= \alpha\gamma\xi_R\xi_T \mathbf{P}_R\mathbf{H}\mathbf{P}_T\mathbf{Q} + \alpha^*\gamma\eta_R\eta_T^* \mathbf{P}_R^*\mathbf{H}^*\mathbf{P}_T^*\mathbf{Q} \\ \mathbf{K}_2 &= \alpha\gamma\xi_R\eta_T \mathbf{P}_R\mathbf{H}\mathbf{P}_T\mathbf{Q} + \alpha^*\gamma\eta_R\xi_T^* \mathbf{P}_R^*\mathbf{H}^*\mathbf{P}_T^*\mathbf{Q} \\ \mathbf{F}_1 &= \theta\xi_R \mathbf{P}_R\mathbf{G}\mathbf{Q} \\ \mathbf{F}_2 &= \theta\eta_R \mathbf{P}_R^*\mathbf{G}^*\mathbf{Q} \\ \tilde{\mathbf{n}} &= \gamma\xi_R \mathbf{P}_R\mathbf{H}\mathbf{d} + \gamma\eta_R \mathbf{P}_R^*\mathbf{H}^*\mathbf{d}^* + \xi_R\mathbf{P}_R\mathbf{n} + \eta_R\mathbf{P}_R^*\mathbf{n}^* \end{aligned} \tag{3.19}$$

It can be observed from (3.18) that, due to the impairments in both the transmitter and receiver, the effect of SI is not only manifested in a linear SI component as usual, but also in the conjugate SI component. In addition to the SI, the desired signal, i.e., $\mathbf{c}$, is also degraded by its conjugation. Furthermore, the total distortion noise, i.e., $\tilde{\mathbf{n}}$, contains not only the thermal noise, but also the distortion noise from PA nonlinearity.

It is pointed out that the IQ imbalance in the receiver is the source of conjugate components for the SI, desired signal and noise. Each component is further degraded by other impairments. In [5], the effects of IQ imbalance and PA nonlinearity distortion were considered only from the transmitter. Therefore, the SI signal in the receiver only contains the linear SI component. The SIC algorithm proposed in [5] is performed iteratively in which the SI channel is estimated by least square estimation (LSE). This is also a common estimation method used in many studies to estimate the SI channel. However, as demonstrated later with simulation results, this method does not work well when the conjugate SI component is present.

In the next section, an iterative algorithm is proposed to mitigate the impacts of the SI signal and detect the desired signal. In the proposed algorithm, both the linear SI component and the conjugate SI component are taken into account to estimate the SI channel more effectively. The other impairments are also estimated and compensated for in order to further improve the detection performance of the desired signal. The detected desired signal is the removed from the original received signal in order to improve the SI channel estimation and SI cancellation in the next iteration.

3.3 Proposed Iterative Algorithm

As can be seen from (3.18), the effect of SI on the desired signal is represented in two terms: the transmitted signal $\mathbf{x}$ and its conjugation. On the other hand, the existence of the desired signal and its conjugation in (3.18) complicates the estimation of the SI channel required to perform SI cancellation. The iterative algorithm proposed in this section is grounded on the principle that the processes of SI cancellation and decoding of the desired signal can benefit from each other. The specific steps of the proposed iterative algorithm are presented in the following.

Step 1 – SI channel estimation

To cancel the SI, i.e., the first two terms in (3.18), one could try to estimate the SI channel $[h(0), \ldots, h(L-1)]$ and impairment parameters so that matrices $\mathbf{K}_1$ and $\mathbf{K}_2$ could

be computed as in (3.19). However, a better approach, based on widely-linear estimation, is to rewrite (3.18) as

$$\mathbf{p} = \begin{bmatrix} \mathbf{X} & \mathbf{X}^* \end{bmatrix} \mathbf{k}_{\text{aug}} + \mathbf{F}_1\mathbf{c} + \mathbf{F}_2\mathbf{c}^* + \tilde{\mathbf{n}} = \mathbf{X}_{\text{aug}}\mathbf{k}_{\text{aug}} + \mathbf{F}_1\mathbf{c} + \mathbf{F}_2\mathbf{c}^* + \tilde{\mathbf{n}} \tag{3.20}$$

where $\mathbf{X}$ is given as in (3.21)

$$\mathbf{X} = \begin{bmatrix} x(0) & 0 & \cdots & 0 & 0 \\ x(1) & x(0) & \cdots & 0 & 0 \\ \vdots & \vdots & \cdots & \vdots & \vdots \\ x(N-1) & x(N-2) & \cdots & x(N-L+1) & x(N-L) \end{bmatrix}_{N \times L} \tag{3.21}$$

and $\mathbf{k}_{\text{aug}}$ is a $2L \times 1$ column vector that depends on the SI channel and all impairment parameters. It then follows that, in order to cancel the SI term $\mathbf{X}_{\text{aug}}\mathbf{k}_{\text{aug}}$, the "augmented" SI channel is estimated as [6]:

$$\hat{\mathbf{k}}_{\text{aug}} = \left(\mathbf{X}_{\text{aug}}^H \mathbf{X}_{\text{aug}}\right)^{-1} \mathbf{X}_{\text{aug}}^H \mathbf{p} \tag{3.22}$$

Step 2 – Self interference cancellation (SIC)

Given the estimate of $\mathbf{k}_{\text{aug}}$ in Step 1, the estimated SI is subtracted from the original received signal in preparation for detecting the desired signal. This step yields

$$\tilde{\mathbf{p}} = \mathbf{p} - \mathbf{X}_{\text{aug}}\hat{\mathbf{k}}_{\text{aug}} = \mathbf{F}_1\mathbf{c} + \mathbf{F}_2\mathbf{c}^* + \tilde{\mathbf{n}} + \mathbf{X}_{\text{aug}}\left(\mathbf{k}_{\text{aug}} - \hat{\mathbf{k}}_{\text{aug}}\right) \tag{3.23}$$

Step 3 – Estimation and compensation of the receive IQ imbalance and PN

Before detecting the desired signal $\mathbf{c}$, the effect of receive IQ imbalance shall be compensated first. In particular, the parameters ξ_R and η_R are estimated based on the so-called channel smoothness criterion [22]. In essence, the criterion is based on the fact that the channel response does not change substantially between successive subcarriers in an OFDM system. Hence, the values of ξ_R and η_R are estimated by minimizing the mean square error of channel responses between consecutive subcarriers. These parameters are estimated only once for the whole transmission frame using the training symbol.

Let $\mathbf{\Lambda} = \begin{bmatrix} \lambda(0) & \lambda(1) & \cdots & \lambda(N_\mathrm{a}-1) \end{bmatrix}$ be the known BPSK-modulated training symbol in a transmission frame, $\mathbf{\Lambda}_\mathrm{mirr} = \begin{bmatrix} \lambda(N_\mathrm{a}-1) & \lambda(N_\mathrm{a}-2) & \cdots & \lambda(0) \end{bmatrix}$ is a mirrored version of $\mathbf{\Lambda}$, and $\mathbf{\Lambda}' = \mathbf{\Lambda} \odot \mathbf{\Lambda}_\mathrm{mirr} = \begin{bmatrix} \lambda'(0) & \lambda'(1) & \cdots & \lambda'(N_\mathrm{a}-1) \end{bmatrix}$. Let $\mathbf{\Psi} = \begin{bmatrix} \psi(0) & \psi(1) & \cdots & \psi(N_\mathrm{a}-1) \end{bmatrix}$ represent the estimates of the far-end channel gains obtained from the training symbol and least square estimation. Then the estimates of ξ_R and η_R, denoted $\hat{\xi}_R$ and $\hat{\eta}_R$, can be found as in (3.24) and (3.25), respectively [22].

$$\hat{\eta}_R = \frac{\sum_{l=0}^{N_\mathrm{a}-2} (\psi(l+1) - \psi(l))(\lambda'(N_\mathrm{a}-l-2)\psi(N_\mathrm{a}-l-2) - \lambda'(N_\mathrm{a}-l-1)\psi(N_\mathrm{a}-l-1))}{\sum_{l=0}^{N_\mathrm{a}-2} |\lambda'(N_\mathrm{a}-l-2)\psi(N_\mathrm{a}-l-2) - \lambda'(N_\mathrm{a}-l-1)\psi(N_\mathrm{a}-l-1)|^2} \tag{3.24}$$

and

$$\hat{\xi}_R = \sqrt{1 - \Im^2(\hat{\eta}_R)} - j\frac{\Re(\hat{\eta}_R)\Im(\hat{\eta}_R)}{\sqrt{1 - \Im^2(\hat{\eta}_R)}} \tag{3.25}$$

Given $\hat{\xi}_R$ and $\hat{\eta}_R$, the estimated far-end channel is corrected as

$$\hat{\mathbf{\Psi}} = \frac{\hat{\xi}_R^* \mathbf{\Psi} - \hat{\eta}_R \mathbf{\Lambda}' \odot \mathbf{\Psi}^*_\mathrm{mirr}}{|\hat{\xi}_R|^2 - |\hat{\eta}_R|^2} \tag{3.26}$$

On the other hand, using $\hat{\xi}_R$ and $\hat{\eta}_R$, the time-domain signal in Step 2 for the data portion of a frame is compensated as

$$\hat{\mathbf{p}} = \frac{\hat{\xi}_R^* \tilde{\mathbf{p}} - \hat{\eta}_R \tilde{\mathbf{p}}^*}{|\hat{\xi}_R|^2 - |\hat{\eta}_R|^2}. \tag{3.27}$$

The DFT is then applied to $\hat{\mathbf{p}}$ to convert it to the frequency domain, denoted as DFT($\hat{\mathbf{p}}$).

As for the PN, its impact in the frequency domain consists of two components, namely common phase error (CPE) and inter-carrier interference (ICI) [17]. The former is a phase rotation which is the same for all subcarriers within one symbol and varies slowly from one symbol to the next. On the other hand, the latter is different for all subcarriers and stochastic. As proved in [23], the estimation of ξ_R and η_R is not sensitive to the CPE component. Therefore, the CPE component still remains as a factor in both the channel response in (3.26) and the time-domain signal in (3.27). Furthermore, the value of CPE slightly changes between OFDM symbols. Hence, CPE component can be mitigated by equalization in each information-carrying OFDM symbol.

Step 4 – Improving channel estimation of the far-end channel by a DFT-based method and detecting the desired signal

This step further improves the detection performance of the desired signal by improving the accuracy of far-end channel estimation. To this end, a DFT-based channel estimation method [24–26] is applied. The main idea of this method is to transform the channel estimate in the frequency domain to the time domain and then ignore noise-only samples from L to $N-1$ where L is the number of channel taps in the time domain. By doing so, the RSI, IQ imbalance compensation residual, ICI of PN, PA distortion noise, and thermal noise can be further mitigated. Let $\mathbf{\Phi}$ be the following DFT matrix:

$$\mathbf{\Phi} = \begin{bmatrix} 1 & 1 & 1 & \cdots & 1 \\ 1 & W_{N_{\text{fft}}} & W_{N_{\text{fft}}}^2 & \cdots & W_{N_{\text{fft}}}^{N_{\text{fft}}-1} \\ \vdots & \vdots & \vdots & \cdots & \vdots \\ 1 & W_{N_{\text{fft}}}^{N_{\text{fft}}-1} & W_{N_{\text{fft}}}^{2(N_{\text{fft}}-1)} & \cdots & W_{N_{\text{fft}}}^{(N_{\text{fft}}-1)(N_{\text{fft}}-1)} \end{bmatrix},$$

where $W_{N_{\text{fft}}} = \mathrm{e}^{-j\frac{2\pi}{N_{\text{fft}}}}$. Let $\bar{\mathbf{\Phi}}$ contain the first L columns and the rows corresponding to the nonzero subcarriers of $\mathbf{\Phi}$. The channel estimation can be updated as [27]

$$\hat{\tilde{\mathbf{\Psi}}} = \frac{1}{N_{\text{fft}}}(\bar{\mathbf{\Phi}}^H \bar{\mathbf{\Phi}})^{\dagger} \hat{\mathbf{\Psi}}, \tag{3.28}$$

For example, in the IEEE 802.11a standard, out of $N_{\text{fft}} = 64$ subcarriers, there are $N_{\text{vcl}} = 6$ null-subcarriers on the left, $N_{\text{vcr}} = 5$ null-subcarriers on the right, and 1 null-subcarrier in the middle of an OFDM symbol. Thus $\bar{\mathbf{\Phi}} = \mathbf{\Phi}([(N_{\text{vcl}}+1) : \frac{N_{\text{fft}}}{2}] \cup [(\frac{N_{\text{fft}}}{2}+2) : (N_{\text{fft}} - N_{\text{vcr}})], 1 : L)$.

The updated channel estimate in (3.28) is now used to equalize the frequency-domain information-carrying OFDM symbols from Step 3, i.e., to equalize DFT($\hat{\mathbf{p}}$). Finally, the desired signal is detected after the equalization step.

Step 5 – Subtraction of the desired signal from the original received signal

As can be seen from (3.22) in Step 1, $\mathbf{k}_{\text{aug}}$ is initially estimated based on the original received signal $\mathbf{p}$, which contains not only the SI signal, but also the desired signal. Thus, if the linear and conjugate components of the desired signal can be removed from the original received signal, the estimation accuracy of $\mathbf{k}_{\text{aug}}$ would be improved. This can be done after the detection of the desired signal at the end of Step 4.

Specifically, at the end of Step 4, the desired signal is detected and converted to the time domain and it is denoted as $\hat{\mathbf{c}}$. This signal is then used to construct the transmission matrix, denoted as $\mathbf{C}$, that is similar to (3.21). Given the transmission matrix of the desired signal, the far-end channel experienced by the desired signal is estimated similarly as in (3.22). Next, the contribution of the desired signal is removed from the original received signal to update $\mathbf{p}$ for the next SIC iteration, i.e., the algorithm returns to Step 1.

3.4 Simulation Results

The system parameters used for simulation in this paper is based on the IEEE 802.11a standard. Specifically, the bandwidth and the carrier frequency are 20 MHz and 2.4 GHz, respectively. For OFDM modulation, the FFT size and cyclic prefix length are $N_{\text{fft}} = 64$ and $N_{\text{cp}} = 16$, respectively. Out of 64 subcarriers, there are 52 nonzero subcarriers, including 48 subcarriers occupied for data transmission, and 4 subcarriers used for pilots transmission. The transmission is based on frames. Each frame consists of $N_{\text{f}} = 10$ OFDM symbols in which the first symbol is used for the training purpose and the others are for data and pilots. The training symbol and pilots are all BPSK modulated, whereas the data is transmitted with QPSK. The pulse shaping filter is a raised cosine filter with oversampling factor and roll-off factor of $F = 16$ and 0.5, respectively. In this paper, it is assumed that sampling is performed perfectly in the receiver. A rate-1/2, constraint length-7 nonsystematic feedforward convolutional encoder with generator polynomials $(171_8, 133_8)$ in octal form is employed in the transmitters, whereas the Viterbi decoding algorithm is used at the receiver.

The transmit power of Node 1 is fixed at $p_1 = 15$ dBm, while the transmit power of Node 2, i.e., p_2, varies in the range from 0 dBm to 40 dBm. Path loss between the transmit antenna of Node 2 and the receive antenna of Node 1 is assumed to be 70 dB, i.e., $\kappa_2^{\text{ps}} = 1/\sqrt{10^{70/10}}$, which is approximately equivalent to a distance of 6.5 meters between the two nodes. The passive SI suppression achieved by path loss between the transmit and receive antenna in Node 1 is assumed to be 40 dB, i.e., $\kappa_1^{\text{ps}} = 1/\sqrt{10^{40/10}}$, which is equivalent to a distance of 20 centimeters between the two antennas [3, 5]. It is also assumed that the analog cancellation technique achieves 32 dB cancellation of self interference [3, 6], i.e., $\kappa_1^{\text{ac}} = 1/\sqrt{10^{32/10}}$. The

noise floor is assumed to be -90 dBm [1].

The SI channel is modeled as a Rician fading channel with a K-factor of 37 dB [4] and the power delay profile is chosen as in [28] for the IEEE 802.11a standard, where the relative tap powers are $[0 \quad -5.4 \quad -10.8 \quad -16.2 \quad -21.7]$ dB and the excess tap delays are $[0 \quad 10 \quad 20 \quad 30 \quad 40]$ nanoseconds. The channel experienced by the desired signal is modeled with the same power delay profile as that of the SI channel but with a K-factor of 34 dB [4]. Each signal path has a Bell Doppler spectrum shape [28] with the maximum Doppler shift of 6 Hz.

It is assumed that $\alpha_T = \alpha_R = 0.1$, and $\phi_T = \phi_R = 10^\circ$ [22] to represent the impacts of IQ imbalance in the transmitter and receiver. The effect of PA nonlinearity is considered approximately up to the third order with the third-order interception point of 15 dBm [12]. The effect of the PN impairment is generated based on the PSD function $\mathfrak{L}(f_m) = \begin{bmatrix} -85 & -100 & -110 & -120 & -140 & -160 \end{bmatrix}$ dBc/Hz with the corresponding frequency offsets $\begin{bmatrix} 10^2 & 10^3 & 10^4 & 10^5 & 10^6 & 10^7 \end{bmatrix}$ Hz in both the transmitter and receiver.

Two performance metrics used in this paper are the Error Vector Magnitude (EVM), and Bit Error Rate (BER). The EVM is used to measure the modulation accuracy directly on the constellation points after demodulation [29,30]. In other words, this metric measures the deviation caused by the SI signal and impairments between the estimated constellation points and their ideal locations. Here, EVM is calculated for each frame, in which EVM_i for the ith frame is defined as the root-mean-square of the error between the measured symbols $\hat{s}_m^i$ and the ideal symbols s_m^i, that is $\mathrm{EVM}_i = \sqrt{\sum_{m=1}^{M} |\hat{s}_m^i - s_m^i|^2 / \sum_{m=1}^{M} |s_m^i|^2}$. Then the value of EVM is obtained by averaging over all N_f transmission frames as $\mathrm{EVM} = \frac{1}{N_\mathrm{f}} \sum_{i=1}^{N_\mathrm{f}} \mathrm{EVM}_i$.

In order to illustrate the performance improvement step by step, the two versions of the proposed algorithm are considered. In the first version, named "ISIC", the proposed algorithm is performed without Step 4. This means that the far-end channel estimate is not updated before the equalization. The second version, named "DFT-ISIC", includes Step 4. In all figures, performance of the proposed algorithm is given with the number of iterations ranging from 1 to 3. Performance of the algorithms in [5] and [6] is also included

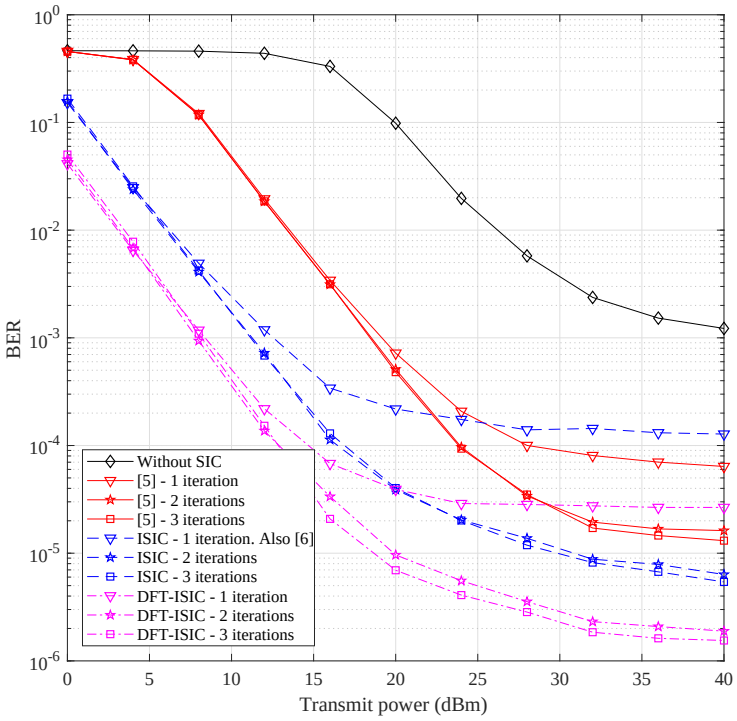

Figure 3.2: Performance comparison in terms of BER between the proposed algorithm and the algorithms in [5], [6], and without deploying any SIC technique.

for comparison. The performance without any compensation of the impairments and SIC, named "Without SIC", is given as well.

First, performance of the proposed algorithm in terms of BER with respect to the transmitted power of Node 2 is presented in Fig. 3.2. It is observed that the SI signal is significantly mitigated after just one iteration, which results in performance improvement in decoding the desired signal. As expected, the decoding performance is much better than in the case without deploying any SIC technique. As seen in Fig. 3.2, after 3 iterations and at BER $= 10^{-3}$, the proposed algorithm gains over 28.0 dB and 32.0 dB in terms of the transmitted power for "ISIC" and "DFT-ISIC" versions, respectively, when compared to the case of "Without SIC".

It is pointed out that the performance of "ISIC" version after 1 iteration is also the performance of the algorithm proposed in [6] using the WLE technique to mitigate the effect

of the SI. It is seen that under the presence of the desired signal, the performance with 1 iteration is not good enough. However, applying the iterative algorithm proposed in this paper significantly improves the performance. In terms of EVM, Fig. 3.3 indicates that, compared to the performance reported in [6], the EVM gain is approximately 5.8 dB and 8.3 dB at the transmitted power of 30 dBm after adding one more cancellation iteration for "ISIC" and "DFT-ISIC", respectively.

The performance of the proposed algorithm is also compared with the algorithm proposed in [5] that uses the linear digital estimation to estimate the SI channel. Generally, the performance of the proposed algorithm is considerably better than the algorithm in [5] over a wide transmitted power range with the same number of iterations. Specifically, if only one iteration is considered for both algorithms, gains of approximately 5.7 dB and 3.1 dB in terms of EVM for "ISIC" are achieved for the transmitted powers of 10 dBm and 15 dBm, respectively. These values increase approximately to 8.8 dB and 6.0 dB, respectively, when "DFT-ISIC" is considered after one iteration. In terms of BER, the proposed algorithm achieves around 7.0 dB and 11.0 dB gains for "ISIC" and "DFT-ISIC", respectively, compared to the algorithm in [5] at BER = 10^{-4} and after 3 iterations. Interestingly, over the considered transmitted power range, when the transmit power in Node 2 is increased, performance of "ISIC" for 1 iteration tends to be worse than the algorithm in [5], particularly when the transmitted power of Node 2 is higher than 25 dBm. The reason for this is the bad quality of the SI channel estimation when the transmitted power of the desired signal is high. It is worthwhile to note that performance improvement of a SIC technique mainly depends on the quality of the SIC channel estimation. The higher the power of SI signal compared to the power of the desired signal is, the better the quality of the SI channel estimation becomes. In other words, when the transmitted power of the desired signal is large, the quality of the SI channel estimation gets worse. Therefore, instead of mitigating the SI signal, the digital SIC actually increases the interference. This fact is also mentioned in [4]. If the number of iterations is not enough, deploying WLE in this transmitted power range seems to raise more interference because it takes both linear SI component and conjugate SI component into account while their powers are much lower than that of the desired signal.

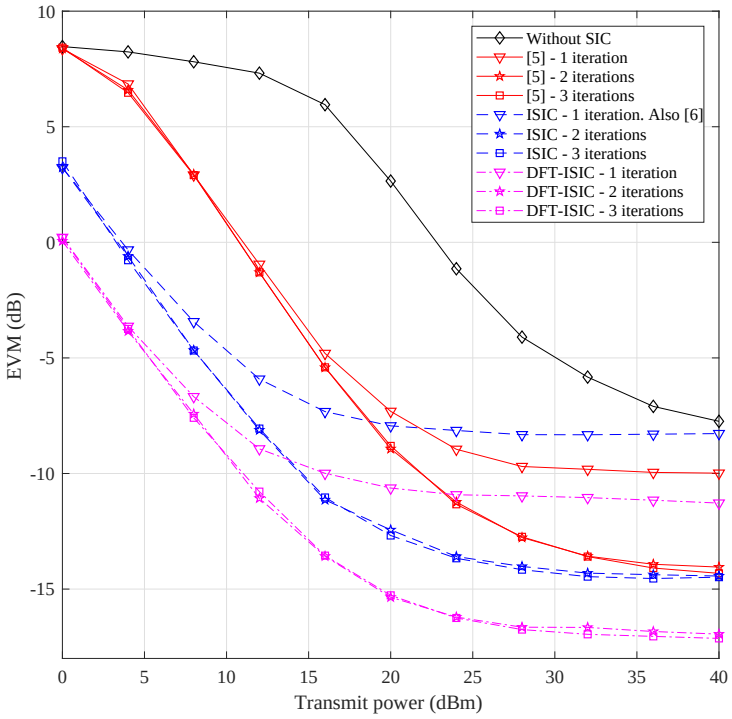

Figure 3.3: EVM comparison between the proposed algorithm and the algorithms in [5], [6], and without deploying any SIC technique.

However, when the number of iterations increases to 2 and 3, it is shown that the algorithm proposed in this paper outperforms the algorithm in [5] over the whole range of considered transmitted power.

It is expected that adding Step 4 can help to further reduce the total amount of noise and thus considerably improve the performance of the proposed algorithm. Indeed, as illustrated in Fig. 3.2, "DFT-ISIC" gains approximately 4.0 dB and 11.2 dB at BER $= 10^{-4}$ and BER $= 10^{-5}$, respectively, compared to "ISIC" after 3 iterations. In terms of EVM, "DFT-ISIC" outperforms "ISIC" nearly 3.0 dB when the transmitted power of Node 2 is 20 dBm.

Finally, it is seen from Fig. 3.3 that the convergence of the algorithm proposed in this paper as well as the algorithm in [5] can be achieved after just 2 to 3 decoding iterations.

3.5 Conclusions

This paper has considered a full-duplex wireless communication system in which the PN, IQ imbalance and PA nonlinearity impairments from the transmitter and receiver are taken into account. An algorithm is proposed to iteratively cancel the SI, compensate for the impairments and detect the desired signal. Simulation results show that the proposed algorithm outperforms existing algorithms over a practical transmit power range.

3.6 Appendices

3.6.1 Appendix A

From (3.1), (3.2), and (2.71) one obtains

$$\begin{aligned} u(t) &= \alpha \mathrm{e}^{j\phi_T(t)} \left(\xi_T w(t) + \eta_T w^*(t)\right) + d(t) \\ &\overset{(3.1)}{=} \alpha \mathrm{e}^{j\phi_T(t)} \left(\xi_T \sum_{l=0}^{N-1} x(l) q(t - lT_s) + \eta_T \sum_{l=0}^{N-1} x^*(l) q(t - lT_s)\right) + d(t) \end{aligned} \tag{3.29}$$

Thus

$$\begin{aligned} u(kT_s) &= u(t)\Big|_{t=kT_s} \\ &= \alpha \mathrm{e}^{j\phi_T(kT_s)} \left(\xi_T \sum_{l=0}^{N-1} x(l) q(kT_s - lT_s) + \eta_T \sum_{l=0}^{N-1} x^*(l) q(kT_s - lT_s)\right) + d(kT_s) \end{aligned} \tag{3.30}$$

Dropping T_s in (3.30) results in

$$u(k) = \alpha \mathrm{e}^{j\phi_T(k)} \left(\xi_T \sum_{l=0}^{N-1} x(l) \tilde{q}(k - l) + \eta_T \sum_{l=0}^{N-1} x^*(l) \tilde{q}(k - l)\right) + d(k) \tag{3.31}$$

in which $\tilde{q}(n)$ is obtained by downsampling $q(n)$ with factor F, $n = 0, \cdots, M-1$.

From (3.31), $y_1(k)$ is written as (3.32)

$$\begin{aligned} y_1(k) &= h(k) * \left(\alpha \mathrm{e}^{j\phi_T(k)} \left(\xi_T \sum_{l=0}^{N-1} x(l)\tilde{q}(k-l) + \eta_T \sum_{l=0}^{N-1} x^*(l)\tilde{q}(k-l) \right) + d(k) \right) \\ &= \alpha\xi_T h(k) * \left(\mathrm{e}^{j\phi_T(k)} \sum_{l=0}^{N-1} x(l)\tilde{q}(k-l) \right) + \\ &\quad \alpha\eta_T h(k) * \left(\mathrm{e}^{j\phi_T(k)} \sum_{l=0}^{N-1} x^*(l)\tilde{q}(k-l) \right) + h(k) * d(k) \\ &= \alpha\xi_T \sum_{i=0}^{N-1} \left(\mathrm{e}^{j\phi_T(i)} \sum_{l=0}^{N-1} x(l)\tilde{q}(i-l) \right) h(k-i) + \\ &\quad \alpha\eta_T \sum_{i=0}^{N-1} \left(\mathrm{e}^{j\phi_T(i)} \sum_{l=0}^{N-1} x^*(l)\tilde{q}(i-l) \right) h(k-i) + h(k) * d(k) \end{aligned} \tag{3.32}$$

With the definition of matrices $\mathbf{Q}$, $\mathbf{H}$ and $\mathbf{P}_T$ in Section 3.2, (3.32) is rewritten compactly as

$$\mathbf{y}_1 = \alpha\xi_T \mathbf{H}\mathbf{P}_T\mathbf{Q}\mathbf{x} + \alpha\eta_T \mathbf{H}\mathbf{P}_T\mathbf{Q}\mathbf{x}^* \tag{3.33}$$

where $\mathbf{y}_1 = \begin{bmatrix} y_1(0) & y_1(1) & \cdots & y_1(N-1) \end{bmatrix}^T$. Similarly, $y_2(k)$ can be compactly written as $\mathbf{y}_2 = \mathbf{G}\mathbf{Q}\mathbf{c}$, where $\mathbf{G}$ and $\mathbf{c}$ are defined as in Section 3.2.

References

[1] Z. Zhang and K. Long and A. V. Vasilakos and L. Hanzo: "Full-Duplex Wireless Communications: Challenges, Solutions, and Future Research Directions", *Proceedings of the IEEE*, vol. 104, no. 7, pp. 1369–1409, 2016.

[2] A. Sabharwal and P. Schniter and D. Guo and D. W. Bliss and S. Rangarajan and R. Wichman: "In-Band Full-Duplex Wireless: Challenges and Opportunities", *IEEE Journal on Selected Areas in Communications*, vol. 32, no. 9, pp. 1637–1652, 2014.

[3] M. Duarte and A. Sabharwal: "Full-duplex wireless communications using off-the-shelf radios: Feasibility and first results", *The Forty Fourth Asilomar Conference on Signals, Systems and Computers*, pp. 1558–1562, 2010.

[4] M. Duarte and C. Dick and A. Sabharwal: "Experiment-Driven Characterization of Full-Duplex Wireless Systems", *IEEE Transactions on Wireless Communications*, vol. 11, no. 12, pp. 4296–4307, 2012.

[5] S. Li and R. D. Murch: "An Investigation Into Baseband Techniques for Single-Channel Full-Duplex Wireless Communication Systems", *IEEE Transactions on Wireless Communications*, vol. 13, no. 9, pp. 4794–4806, 2014.

[6] D. Korpi and L. Anttila and V. Syrjala and M. Valkama: "Widely Linear Digital Self-Interference Cancellation in Direct-Conversion Full-Duplex Transceiver", *IEEE Journal on Selected Areas in Communications*, vol. 32, no. 9, pp. 1674–1687, 2014.

[7] E. Ahmed and A. M. Eltawil: "All-Digital Self-Interference Cancellation Technique for Full-Duplex Systems", *IEEE Transactions on Wireless Communications*, vol. 14, no. 7, pp. 3519–3532, 2015.

[8] V. Syrjala and M. Valkama and L. Anttila and T. Riihonen and D. Korpi: "Analysis of Oscillator Phase-Noise Effects on Self-Interference Cancellation in Full-Duplex OFDM

Radio Transceivers", *IEEE Transactions on Wireless Communications*, vol. 13, no. 6, pp. 2977–2990, 2014.

[9] X. Quan and Y. Liu and S. Shao and C. Huang and Y. Tang: "Impacts of Phase Noise on Digital Self-Interference Cancellation in Full-Duplex Communications", *IEEE Transactions on Signal Processing*, vol. 65, no. 7, pp. 1881–1893, 2017.

[10] L. Samara and M. Mokhtar and O. Ozdemir and R. Hamila and T. Khattab: "Residual Self-Interference Analysis for Full-Duplex OFDM Transceivers Under Phase Noise and I/Q Imbalance", *IEEE Communications Letters*, vol. 21, no. 2, pp. 314–317, 2017.

[11] A. C. M. Austin and A. Balatsoukas-Stimming and A. Burg: "Digital predistortion of power amplifier non-linearities for full-duplex transceivers", *2016 IEEE 17th International Workshop on Signal Processing Advances in Wireless Communications*, pp. 1–5 2016.

[12] L. Anttila and D. Korpi and V. Syrjala and M. Valkama: "Cancellation of power amplifier induced nonlinear self-interference in full-duplex transceivers", *2013 Asilomar Conference on Signals, Systems and Computers*, pp. 1193–1198, 2013.

[13] T. Schenk: "RF Imperfections in High-rate Wireless Systems: Impact and Digital Compensation". Springer, Netherlands, 2008.

[14] M. Rice: "Digital Communications: A Discrete-Time Approach". Pearson Prentice Hall, 2009.

[15] D. Tse and P. Viswanath: "Fundamentals of Wireless Communication". Cambridge University Press, 2005.

[16] A. Demir and A. Mehrotra and J. Roychowdhury: "Phase noise in oscillators: a unifying theory and numerical methods for characterization", *IEEE Transactions on Circuits and Systems I: Fundamental Theory and Applications*, vol. 47, no. 5, pp. 655–674, 2000.

[17] D. Petrovic and W. Rave and G. Fettweis: "Effects of Phase Noise on OFDM Systems With and Without PLL: Characterization and Compensation", *IEEE Transactions on Communications*, vol. 55, no. 8, pp. 1607–1616, 2007.

[18] S. Zhao and X. Zhu and H. Wang and L. Wu: "Analysis of joint effect of phase noise, IQ imbalance and amplifier nonlinearity in OFDM system", *International Conference on Wireless Communications and Signal Processing*, pp. 1–6, 2013.

[19] P. Banelli and S. Cacopardi: "Theoretical analysis and performance of OFDM signals in nonlinear AWGN channels", *IEEE Transactions on Communications*, vol. 48, no. 3, pp. 430–441, 2000.

[20] J. J. Bussgang: "Cross-correlation functions of amplitude distorted Gaussian signals". Research laboratory of Electronics, Massachusetts Institute of Technology, 1952.

[21] Q. Zou: "Signal Processing for RF Distortion Compensation in Wireless Communication Systems", PhD dissertation, University of California, Los Angeles, 2008.

[22] J. Tubbax and B. Come and L. Van der Perre and S. Donnay and M. Engels and H. D. Man and M. Moonen: "Compensation of IQ imbalance and phase noise in OFDM systems", *IEEE Transactions on Wireless Communications*, vol. 4, no. 3, pp. 872–877, 2005.

[23] J. Tubbax and B. Come and L. Van der Perre and S. Donnay and M. Engels and C. Desset: "Joint Compensation of IQ Imbalance and Phase Noise", *The 57th IEEE Semiannual Vehicular Technology Conference*, vol. 3, pp. 1605–1609, 2003.

[24] M. J. Fernandez-Getino Garcia and J. M. Paez-Borrallo and S. Zazo: "DFT-based channel estimation in 2D-pilot-symbol-aided OFDM wireless systems", *53rd IEEE Vehicular Technology Conference*, vol.2, pp. 810–814, 2001.

[25] Y. Kang and K. Kim and H. Park: "Efficient DFT-based channel estimation for OFDM systems on multipath channels", *IET Communications*, vol. 1, no. 2, pp. 197–202, 2007.

[26] X. Hou and Z. Zhang and H. Kayama: "Low-Complexity Enhanced DFT-based Channel Estimation for OFDM Systems with Virtual Subcarriers", *IEEE 18th International Symposium on Personal, Indoor and Mobile Radio Communications*, pp. 1–5, 2007.

[27] X. G. Doukopoulos and R. Legouable: "Robust Channel Estimation via FFT Interpolation for Multicarrier Systems", *IEEE 65th Vehicular Technology Conference*, pp. 1861–1865, 2007.

[28] V. Erceg *et al*: "IEEE P802.11 Wireless LANs", 2004.

[29] W. Li and J. Lilleberg and K. Rikkinen: "On Rate Region Analysis Of Half- and Full-Duplex OFDM Communication Links", *IEEE Journal on Selected Areas in Communications*, vol. 32, no. 9, pp. 1688–1698, 2014.

[30] L. Smaini: "RF Analog Impairments Modeling for Communication Systems Simulation: Application to OFDM-based Transceivers", John Wiley & Sons Ltd, 2012.

4. Impacts of Phase Noise on CFBMC-OQAM

Published as:

Long D. Le and Ha H. Nguyen, "Impacts of Phase Noise on CFBMC-OQAM," *IEEE* 88^{th} *Vehicular Technology Conference (VTC-Fall)*, pp. 1–6, 2018.

In this chapter, the impact of PN on CFBMC-OQAM systems is investigated. Two types of PN are considered: one is FR PN and the another is PLL PN (see Section 2.3.1). As discussed in Section 2.2.4, for CFBMC-OQAM, when the synchronization is perfect and there is no channel or noise, the self-interferences are exactly zeros. However, this chapter shows that the presence of PN increases the self-interferences which significantly degrade the performance of CFBMC-OQAM systems.

An algorithm is then proposed in order to mitigate the impact of PN in this chapter. Specifically, the conjugation of PN is estimated based on the transmission of pilot symbols. The PN conjugation can be represented as a multiplication of a set of known basis vectors with an unknown coefficient vector. The main purpose of this algorithm is to estimate the unknown vector to compensate for the impact of PN given the known pilot symbols. From the simulation results, the PN compensation algorithm is shown to effectively remove the PN impact with a low computational complexity.

Impacts of Phase Noise on CFBMC-OQAM

Long D. Le and Ha H. Nguyen

Abstract

Among many proposed multi-carrier systems, circular filter bank multi-carrier offset quadrature amplitude modulation (CFBMC-OQAM) is one of promising candidates for future wireless networks. This paper studies the impacts of the intrinsic interferences, namely inter-symbol interference (ISI) and inter-carrier interference (ICI), and phase noise (PN) on the performance of CFBMC-OQAM systems. Two types of PN are considered: one is based on a free-running oscillator and the other is based on a phase-locked loop oscillator. Sources of performance degradation are quantified and a closed-form expression is derived for the signal-to-interference ratio (SIR). An algorithm is then applied to mitigate the PN impacts which takes into account the intrinsic interferences. It is observed that while the impact of the self interference can be negligible when there is no PN, the presence of PN significantly degrades performance of CFBMC-OQAM systems. The applied algorithm is shown to effectively remove the PN impacts.

4.1 Introduction

Multi-carrier transmission techniques have been extensively studied over the last few decades [1]. Currently, orthogonal frequency division multiplexing (OFDM) [2] is a popular choice for broadband wireless communication systems because it offers many advantages including resistance to multipath distortions and efficient implementations based on the fast Fourier transform (FFT). However, OFDM also has its own disadvantages. Two major disadvantages are: (i) high spectral leakage to neighboring frequency bands, and (ii) strict orthogonality requirement, which makes OFDM systems more sensitive to impairments like phase noise and frequency offset.

Filter bank multi-carrier offset quadrature amplitude modulation (FBMC-OQAM) is an alternative that can resolve the above problems in OFDM [1,3]. Specifically, with the use of well-designed prototype filters, an FBMC system can avoid the high spectral leakage issue in OFDM. On the other hand, using OQAM splits complex data into real and imaginary parts which consequently relaxes the orthogonality condition to the real field. However, FBMC-OQAM does not have a block-based structure like OFDM which makes it significantly more complicated to implement than OFDM [1].

There are other multi-carrier systems, namely generalized frequency division multiplexing (GFDM) [4] and circular filter bank multi-carrier offset quadrature amplitude modulation (CFBMC-OQAM) [5], that have been recently proposed as candidates for the air interface of 5G networks [6]. GFDM has a block based structure to ease the channel equalization task but it is a non-orthogonal system and thus severely suffers from the impacts of inter-symbol interference (ISI) and inter-carrier interference (ICI) when compared to OFDM. To avoid performance degradation, interference cancellation techniques need to be used, which means high computational complexity [6]. CFBMC-OQAM, on the other hand, is a modified version of FBMC-OQAM by making use of circular convolution as in GFDM. As such, CFBMC-OQAM also has a block based structure to enable the use of cyclic prefix (CP), and to ease channel equalization.

Any multi-carrier systems suffer from physical impairments, especially the phase noise (PN). Impacts of PN in OFDM systems have been extensively studied in the last few decades [7–11]. In the frequency domain, the PN impact can be separated into two components, namely common phase error (CPE) and ICI. Mitigating the PN impacts in OFDM systems can be performed in either the frequency domain [8,9] or the time domain [10,11]. The impacts of PN have recently been considered in [12,13] for FBMC-OQAM and in [14] for GFDM. Different from OFDM, FBMC-OQAM and GFDM suffer from the two intrinsic interferences, namely ISI and ICI. Therefore, these systems generally have additional interference components when PN is taken into account. Consequently, mitigating the impacts of PN in such systems is more complicated than that in OFDM [12]. In [13], two algorithms, which exploit the structure of the interferences, were proposed. However, only the impact of

CPE was studied.

To the best of our knowledge, there is no work investigating the impacts of ICI, ISI, and PN in CFBMC-OQAM systems. Such investigation shall be carried out in this paper. Two common types of PN are considered: one is based on a free-running (FR) oscillator and the another is based on a phase-locked loop (PLL) oscillator. In order to mitigate the impact of PN as well as the intrinsic self interferences, this paper applies an algorithm which was originally proposed in [10] to cancel the impact of PN in an OFDM system. Simulation results show that, without PN the impacts of the intrinsic interferences can be neglected. However, the presence of PN affects every signal components, including the desired signal and the intrinsic interferences. The increased intrinsic interferences significantly degrade performance of CFBMC-OQAM systems. Furthermore, it is observed that the use of circular convolution instead of the conventional linear convolution in CFBMC-OQAM systems and the characteristics of PN result in a variation of the signal-to-interference ratio (SIR) of the received signal with respect to the symbol time index. The PN compensation algorithm effectively removes the PN impact.

This paper is organized as follows. The system model is presented in Section 4.2, which includes brief reviews of CFBMC-OQAM systems and characteristics of two PN types. Evaluation of PN impacts is presented in Section 4.3 for both types of PN. An algorithm to mitigate the PN impacts is presented in Section 4.4. Simulation results are provided in Section 4.5. Section 4.6 concludes the paper.

Notation: Lowercase letters are used to denote scalars. Lowercase boldface and uppercase boldface letters stand for vectors and matrices, respectively. $(\cdot)^{\dagger}$, $(\cdot)^{T}$, $(\cdot)^{H}$, $(\cdot)^{-1}$, $|\cdot|$, $||\cdot||_2$, and $\circledast$ denote pseudo-inverse, transpose, Hermitian, inverse, modulus, ℓ_2-norm and circular convolution operations, respectively. $\mathfrak{R}[\cdot]$, $\mathfrak{I}[\cdot]$, diag$[\cdot]$, and E$[\cdot]$ denote the real and imaginary parts of a complex variable, a diagonal matrix, and expectation operation, respectively.

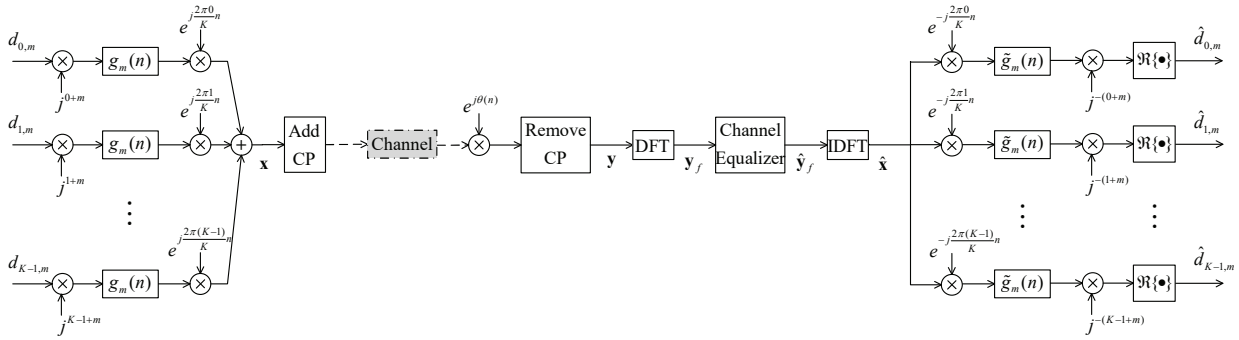

Figure 4.1: A discrete-time complex baseband equivalent CFBMC-OQAM transceiver.

4.2 System Model

4.2.1 CFBMC-OQAM

Consider a discrete-time complex baseband equivalent CFBMC-OQAM system as in Fig. 4.1. Let $N = KM$. Then, the transmitted signal vector $\mathbf{x} = \begin{bmatrix} x(0) & x(1) & \cdots & x(N-1) \end{bmatrix}^T$ is constructed from a $K \times 2M$ block of data defined over K sub-channels and $2M$ time slots as

$$x(n) = \sum_{k=0}^{K-1} \sum_{m=0}^{2M-1} j^{k+m} d_{k,m} g_m(n) \mathrm{e}^{j\frac{2\pi kn}{K}}, \tag{4.1}$$

where $g_m(n) = g\left(n - m\frac{K}{2}\right)_N$ is a cyclic shift version of a length-N real-valued and symmetric prototype filter $g_0(n) = g(n)$. Equation (4.1) can be rewritten as

$$\mathbf{x} = \mathbf{A}\mathbf{d} \tag{4.2}$$

in which $\mathbf{d} = \begin{bmatrix} \mathbf{d}_0 & \mathbf{d}_1 & \cdots & \mathbf{d}_{K-1} \end{bmatrix}^T$ and $\mathbf{d}_i = \begin{bmatrix} d_{i,0} & d_{i,1} & \cdots & d_{i,2M-1} \end{bmatrix}^T$. It is assumed that $d_{k,m}$'s are independent and identically distributed (i.i.d) and $\mathrm{E}\left[d_{k,m}\right] = 0$ and $\mathrm{E}[d_{k,m}^2] = P_d$. $\mathbf{A}$ is called the modulation matrix whose $(m + 2kM)$th column is $\mathbf{A}[:, m + 2kM] = j^{k+m} \begin{bmatrix} g_m(0)\mathrm{e}^{j\frac{2\pi k0}{K}}, & \cdots, & g_m(N-1)\mathrm{e}^{j\frac{2\pi k(N-1)}{K}} \end{bmatrix}^T$ [5]. A CP of length L is added to $\mathbf{x}$ before transmitting.

The channel $\mathbf{h} = \begin{bmatrix} h(0) & h(1) & \cdots & h(\mu-1) \end{bmatrix}^T$ is characterized by μ taps, where $L \geq \mu$. Then, the received signal after removing the CP is

$$\mathbf{y} = \mathbf{H}_{\text{circ}}\mathbf{x} + \mathbf{w} \tag{4.3}$$

where $\mathbf{w}$ represents noise, and $\mathbf{H}_{\text{circ}}$ is a circulant matrix whose columns are circularly shifted versions of vector $\begin{bmatrix} h(0) & h(1) & \cdots & h(\mu-1) & 0 & \cdots & 0 \end{bmatrix}^T_{N\times 1}$. It is noted that $\mathbf{H}_{\text{circ}}$ can be represented as $\mathbf{H}_{\text{circ}} = \mathbf{F}^H \mathbf{\Gamma} \mathbf{F}$ where $\mathbf{F}$ is the normalized DFT matrix. Therefore, to detect the desired signal, the received signal $\mathbf{y}$ is first converted to the frequency domain by a DFT transform, then channel equalized with matrix $\hat{\mathbf{\Gamma}}$ which is an estimate of $\mathbf{\Gamma}$ based on a known preamble, and further IDFT transformed to obtain $\hat{\mathbf{x}}$. Then, $\hat{\mathbf{x}}$ is passed through a bank of matched filters and the estimate of $\mathbf{d}$ is obtained by taking the real part of the filtered output as $\hat{\mathbf{d}} = \Re\left\{\mathbf{A}^H \hat{\mathbf{x}}\right\}$ [5].

4.2.2 Phase Noise

This section briefly reviews two PN models: one is based on an FR oscillator and the other is based on a PLL oscillator.

FR-PN model

Let $\alpha_v(n)$ denote the discrete-time phase deviation from an FR oscillator at the nth sampling time. It can be modeled as $\alpha_v(n) = \sum_{i=0}^{n-1} \rho(i)$ where $\rho(i)$ is an i.i.d zero-mean Gaussian random variable with variance $\sigma_\rho^2 = c_v T_s$. Here, c_v is a constant describing the quality of an oscillator, and T_s is the sampling interval. The PN is $\theta(n) = 2\pi f_c \alpha_v(n) = \omega_c \alpha_v(n)$, where f_c is the carrier frequency. The variance of $\alpha_v(n)$ is $\mathrm{E}\left[\alpha_v^2(n)\right] = n c_v T_s$, which grows linearly with the sample index n. Furthermore, the autocorrelation function of the phase deviation can be computed as $\mathrm{E}\left[\alpha_v(n_1)\alpha_v(n_2)\right] = c_v T_s \min(n_1, n_2)$ [15].

PLL-PN model

A general PLL-based frequency synthesizer is described in [7], which models the phase deviation from a reference oscillator having a quality constant c_r as in the FR-PN model. Let $\alpha_r(n)$, $\alpha_v(n)$, and $\beta(n)$ denote the discrete-time phase deviations at the output of the reference oscillator, the frequency synthesizer, and the phase detector, respectively. Then $\alpha_v(n) = \beta(n) + \alpha_r(n)$ [16]. Furthermore, the correlation properties between $\alpha_r(n)$ and $\beta(n)$ are: $\mathrm{E}\left\{\beta(n_1)\alpha_r(n_2)\right\} = \sum_{i=1}^{n_o} \mu_i \mathrm{e}^{\lambda_i T_s \min(0, n_2 - n_1)}$ and $\mathrm{E}\left\{\beta(n_1)\beta(n_2)\right\} = \sum_{i=1}^{n_o} \nu_i \mathrm{e}^{-\lambda_i T_s |n_1 - n_2|}$ where

$n_o = 1 + o_{\text{lpf}}$, and o_{lpf} represents the order of the loop filter [7, 16]. The values of λ_i, μ_i and ν_i are given, for instance in [16], for the PLL-based oscillator with a first-order loop filter.

4.3 Impacts of PN on CFBMC-OQAM

In the presence of PN, the received signal can be written as

$$y(p) = \mathrm{e}^{j\theta(p)} \left(h(p) \circledast x(p)\right) + w(p) \tag{4.4}$$

where $w(p) \sim \mathcal{CN}(0, \sigma_w^2)$ represents additive white Gaussian noise (AWGN). Note that phase noise does not affect the statistical property of AWGN. Performing the DFT on the received signal results in

$$y_f(l) = \sum_{i=0}^{N-1} H(i)X(i)I(l-i) + W(l) \tag{4.5}$$

where $I(l-i) = \frac{1}{N}\sum_{p=0}^{N-1} \mathrm{e}^{j\theta(p)}\mathrm{e}^{-j\frac{2\pi p(l-i)}{N}}$. As pointed out in [17], $I(l-i)$ is maximum at $l = i$ and its power decreases rapidly around this frequency location. Furthermore, it is assumed that the channel frequency response does not change much over adjacent carriers. Thus (4.5) can be approximated as

$$y_f(l) \approx H(l) \sum_{i=0}^{N-1} X(i)I(l-i) + W(l). \tag{4.6}$$

Assuming that the channel is perfectly estimated, then after channel equalization one obtains:

$$\hat{y}_f(l) = \frac{y_f(l)}{H(l)} \approx \sum_{i=0}^{N-1} X(i)I(l-i) + \frac{W(l)}{H(l)} \tag{4.7}$$

Performing the IDFT on $\hat{y}_f(l)$ results in

$$\hat{x}(n) \approx \frac{1}{N}\sum_{q=0}^{N-1} x(q) \sum_{l=0}^{N-1}\sum_{i=0}^{N-1} I(l-i)\mathrm{e}^{-j\frac{2\pi(qi-ln)}{N}} + \frac{1}{\sqrt{N}}\sum_{l=0}^{N-1}\frac{W(l)}{H(l)}\mathrm{e}^{j\frac{2\pi ln}{N}}. \tag{4.8}$$

Finally, the resulting signal is demodulated with a bank of matched filters to estimate the transmitted data:

$$\hat{d}_{k',m'} = \Re\left\{ j^{-(k'+m')} \sum_{n=0}^{N-1} \tilde{g}_{m'}(n)\mathrm{e}^{-j\frac{2\pi k' n}{K}}\hat{x}(n) \right\} \tag{4.9}$$

where $\tilde{g}_{m'}(n) = g\left(m'K/2 - n\right)_N$ is the matched filter. Equation (4.9) can be further expanded as

$$\hat{d}_{k',m'} \approx \underbrace{d_{k',m'}\Re\left\{\sum_{n=0}^{N-1}\tilde{g}_{m'}(n)g_{m'}(n)\mathrm{e}^{j\theta(n)}\right\}}_{A_{1,1}} + \underbrace{\sum_{\substack{m=0\\m\neq m'}}^{2M-1} d_{k',m}\Re\left\{j^{m-m'}\sum_{n=0}^{N-1}\tilde{g}_{m'}(n)g_{m}(n)\mathrm{e}^{j\theta(n)}\right\}}_{A_{1,2}} +$$
$$\underbrace{\sum_{\substack{k=0\\k\neq k'}}^{K-1}\sum_{m=0}^{2M-1} d_{k,m}\Re\left\{j^{k+m-k'-m'}\sum_{n=0}^{N-1}\tilde{g}_{m'}(n)g_{m}(n)\mathrm{e}^{j\frac{2\pi(k-k')n}{K}}\mathrm{e}^{j\theta(n)}\right\}}_{A_{1,3}} +$$
$$\underbrace{\Re\left\{j^{-(k'+m')}\sum_{n=0}^{N-1}\tilde{g}_{m'}(n)\mathrm{e}^{-j\frac{2\pi k'n}{K}}\frac{1}{N}\sum_{\substack{q=0\\q\neq n}}^{N-1}x(q)\sum_{l=0}^{N-1}\sum_{i=0}^{N-1}I(l-i)\mathrm{e}^{-j\frac{2\pi(qi-ln)}{N}}\right\}}_{A_2=0} +$$
$$\underbrace{\Re\left\{j^{-(k'+m')}\sum_{n=0}^{N-1}\tilde{g}_{m'}(n)\mathrm{e}^{-j\frac{2\pi k'n}{K}}\frac{1}{\sqrt{N}}\sum_{l=0}^{N-1}\frac{W(l)}{H(l)}\mathrm{e}^{j\frac{2\pi ln}{N}}\right\}}_{A_3}. \tag{4.10}$$

Note that the first three signal components depend on the PN process $\theta(n)$ and their powers depend on the following correlation function:

$$\begin{aligned} I_i(a_1,a_2,b_1,b_2,n_1,n_2) &= \mathrm{E}\left[\cos(a_1+b_1\theta(n_1))\cos(a_2+b_2\theta(n_2))\right] \\ &= \frac{1}{2}\cos(a_1+a_2)\mathrm{e}^{-\frac{1}{2}\sigma_i^2(b_1,b_2,n_1,n_2)} + \frac{1}{2}\cos(a_1-a_2)\mathrm{e}^{-\frac{1}{2}\sigma_i^2(b_1,-b_2,n_1,n_2)}, \end{aligned} \tag{4.11}$$

where the subscript i is either 1 or 2, depending on the case of FR-PN or PLL-PN model, respectively. In particular, the function $\sigma_i^2(b_1,b_2,n_1,n_2)$ is given for each PN model as follows. For FR-PN, one has

$$\sigma_1^2(b_1,b_2,n_1,n_2) = \mathrm{E}\left[\left(b_1\theta(n_1)+b_2\theta(n_2)\right)^2\right] = \left(b_1^2n_1 + b_2^2n_2 + 2b_1b_2\min(n_1,n_2)\right)c_v\omega_c^2T_s. \tag{4.12}$$

On the other hand, for PLL-PN one has

$$\sigma_2^2(b_1,b_2,n_1,n_2) = \left(b_1^2\sigma_\alpha^2(n_1) + b_2^2\sigma_\alpha^2(n_2) + 2b_1b_2\delta(n_1,n_2)\right)\omega_c^2$$
$$\sigma_\alpha^2(n) = \sum_{i=1}^{n_o}\nu_i + nc_rT_s + 2\sum_{i=1}^{n_o}\mu_i$$
$$\delta(n_1,n_2) = \sum_{i=1}^{n_o}(\nu_i+\mu_i)\mathrm{e}^{-\lambda_i T_s|n_1-n_2|} + c_rT_s\min(n_1,n_2) + \sum_{i=1}^{n_o}\mu_i$$

The term $A_{1,1}$ is obtained when $m = m'$ and $k = k'$. Therefore, $A_{1,1}$ represents the desired signal component. Because the shaping filter is designed to be real and even symmetric, then $A_{1,1} = d_{k',m'}\sum_{n=0}^{N-1}\left(g_{m'}(n)\right)^2\cos\theta(n)$. Denoting $\sigma_{A_{1,1}}^2$ as the power of this component, then

$$\sigma_{A_{1,1}}^2 = P_d\sum_{n=0}^{N-1}\sum_{l=0}^{N-1}\left(g_{m'}(n)g_{m'}(l)\right)^2 I_i(0,0,1,1,n,l) \tag{4.13}$$

The term $A_{1,2}$ is obtained when $m \neq m'$ and $k = k'$, i.e. $A_{1,2}$ represents the interference from different time slots in the same sub-channel or ISI. Let $\sigma_{A_{1,2}}^2$ denote the power of this component. Similarly, one can obtain

$$\sigma_{A_{1,2}}^2 = P_d\sum_{\substack{m=0\\m\neq m'}}^{2M-1}\sum_{n=0}^{N-1}\sum_{l=0}^{N-1}\tilde{g}_{m'}(n)g_m(n)\tilde{g}_{m'}(l)g_m(l)I_i\left(\frac{\pi}{2}(m-m'),\frac{\pi}{2}(m-m'),1,1,n,l\right) \tag{4.14}$$

The component $A_{1,3}$ is obtained when $k \neq k'$, which therefore represents the interference from symbols transmitted on different sub-channels, i.e., ICI. Denote $\varrho(m,k,m',k',n) = \frac{\pi}{2}(k+m-k'-m') + \frac{2\pi(k-k')n}{K}$, and $\sigma_{A_{1,3}}^2$ as the power of $A_{1,3}$. Then

$$\begin{aligned}\sigma_{A_{1,3}}^2 = P_d\sum_{\substack{k=0\\k\neq k'}}^{K-1}\sum_{m=0}^{2M-1}\sum_{n=0}^{N-1}\sum_{l=0}^{N-1}\tilde{g}_{m'}(n)g_m(n)\tilde{g}_{m'}(l)g_m(l)\times\\ I_i\left(\varrho(m,k,m',k',n),\varrho(m,k,m',k',l),1,1,n,l\right)\end{aligned} \tag{4.15}$$

Ignoring the AWGN component A_3, the impacts of PN are quantified using the signal-to-interference ratio (SIR) as:

$$\mathrm{SIR} = \frac{\sigma_{A_{1,1}}^2}{\sigma_{A_{1,2}}^2 + \sigma_{A_{1,3}}^2} \tag{4.16}$$

4.4 Phase Noise Compensation

It can be seen from (4.10) that the impact of PN is manifested in all the three signal components, which makes PN compensation challenging. From (4.3), the received signal under PN after removing the CP is written as

$$\mathbf{y} = \mathbf{P}\mathbf{H}_{\text{circ}}\mathbf{x} + \mathbf{w} \tag{4.17}$$

where $\mathbf{P} = \text{diag}\begin{bmatrix} \text{e}^{j\theta(L)} & \text{e}^{j\theta(L+1)} & \cdots & \text{e}^{j\theta(N+L-1)} \end{bmatrix}$. Define $\boldsymbol{\Xi} = \begin{bmatrix} \boldsymbol{\xi}_0 & \boldsymbol{\xi}_1 & \cdots & \boldsymbol{\xi}_{F-1} \end{bmatrix}$, which contains F basis vectors, in which $\boldsymbol{\xi}_f = \begin{bmatrix} \xi_{f,0} & \xi_{f,1} & \cdots & \xi_{f,N-1} \end{bmatrix}^T$. The basis vectors are chosen from N eigenvectors of the PN covariance matrix, which correspond to the F largest eigenvalues. Also define $\boldsymbol{\gamma} = \begin{bmatrix} \gamma_0 & \gamma_1 & \cdots & \gamma_{F-1} \end{bmatrix}^T$. In order to compensate the PN effect, the goal is to estimate $\boldsymbol{\gamma}$ such that $\text{diag}\left[\boldsymbol{\Xi}\boldsymbol{\gamma}\right] \simeq \mathbf{P}^H$. Then $\boldsymbol{\Xi}\boldsymbol{\gamma}$ can be used to de-rotate the received signal in the time domain prior to the DFT transform. Specifically, the demodulated signal after PN compensation can be written as

$$\hat{\mathbf{d}} = \Re\left\{\mathbf{A}^H\mathbf{F}^H\boldsymbol{\Gamma}^{-1}\mathbf{F}\text{diag}\left[\mathbf{P}\mathbf{H}_{\text{circ}}\mathbf{A}\mathbf{d} + \mathbf{w}\right]\boldsymbol{\Xi}\boldsymbol{\gamma}\right\} = \Re\left\{\boldsymbol{\Delta}\boldsymbol{\gamma}\right\} \tag{4.18}$$

Denote $\mathbf{p} = \{p_0, p_1, \cdots, p_{Q-1}\}$ as a set of pilot indexes in each transmission block, and the transmitted signal corresponding to the pilot index set as $\mathbf{d}_{\mathbf{p}} = \begin{bmatrix} d_{p_0} & d_{p_1} & \cdots & d_{p_{Q-1}} \end{bmatrix}^T$. Then, $\boldsymbol{\gamma}$ is estimated as [10, 11]

$$\boldsymbol{\gamma} = \arg\min_{\boldsymbol{\gamma}} ||\mathbf{d}_{\mathbf{p}} - \Re\left\{\boldsymbol{\Delta}(\mathbf{p},:)\boldsymbol{\gamma}\right\}||_2^2 \tag{4.19}$$

where $\boldsymbol{\Delta}(\mathbf{p},:)$ is a $Q \times F$ matrix obtained by keeping Q rows of $\boldsymbol{\Delta}$ with respect to pilot indexes. The matrix $\Re\left\{\boldsymbol{\Delta}(\mathbf{p},:)\boldsymbol{\gamma}\right\}$ is expanded as

$$\begin{aligned}\Re\left\{\boldsymbol{\Delta}(\mathbf{p},:)\boldsymbol{\gamma}\right\} &= \begin{bmatrix} \Re\left\{\delta_{0,0}\right\} & \Im\left\{\delta_{0,0}\right\} & \cdots & \Re\left\{\delta_{0,F-1}\right\} & \Im\left\{\delta_{0,F-1}\right\} \\ \Re\left\{\delta_{1,0}\right\} & \Im\left\{\delta_{1,0}\right\} & \cdots & \Re\left\{\delta_{1,F-1}\right\} & \Im\left\{\delta_{1,F-1}\right\} \\ \vdots & \vdots & \cdots & \vdots & \vdots \\ \Re\left\{\delta_{Q-1,0}\right\} & \Im\left\{\delta_{Q-1,0}\right\} & \cdots & \Re\left\{\delta_{Q-1,F-1}\right\} & \Im\left\{\delta_{Q-1,F-1}\right\} \end{bmatrix} \begin{bmatrix} \Re\left\{\gamma_0\right\} \\ -\Im\left\{\gamma_0\right\} \\ \cdots \\ \Re\left\{\gamma_{F-1}\right\} \\ -\Im\left\{\gamma_{F-1}\right\} \end{bmatrix} \\ &= \hat{\boldsymbol{\Delta}}\tilde{\boldsymbol{\gamma}}\end{aligned} \tag{4.20}$$

where $\delta_{i,j}$ denotes the (i,j)th element of matrix $\mathbf{\Delta}(\mathbf{p},:)$.

Vector $\boldsymbol{\gamma}$ is related to $\tilde{\boldsymbol{\gamma}}$ as

$$\boldsymbol{\gamma} = \begin{bmatrix} 1 & -j & 0 & 0 & \cdots & 0 & 0 \\ 0 & 0 & 1 & -j & \cdots & 0 & 0 \\ \vdots & \vdots & \vdots & \vdots & \cdots & \vdots & \vdots \\ 0 & 0 & 0 & 0 & \cdots & 1 & -j \end{bmatrix} \tilde{\boldsymbol{\gamma}}$$

Thus, the estimation of $\boldsymbol{\gamma}$ can be found from

$$\tilde{\boldsymbol{\gamma}} = \arg\min_{\tilde{\boldsymbol{\gamma}}} ||\mathbf{d_p} - \hat{\mathbf{\Delta}}\tilde{\boldsymbol{\gamma}}||_2^2 = \hat{\mathbf{\Delta}}^{\dagger}\mathbf{d_p} \tag{4.21}$$

4.5 Simulation Results

For each transmission block, the numbers of sub-channels K and time slots $2M$ are 128 and 16, respectively. The bandwidth is $B = 100$ MHz and the carrier frequency is $f_c = 6$ GHz [12]. The sampling period is $T_s = 1/B$ s. The Martin shaping filter [3] is employed together with 16-QAM. The CP length is 16 samples. For PN, it is assumed that $c_r = 10^{-23}$ s and $c_v = 5 \times 10^{-18}$ s [16]. All results in this section were obtained with a multi-path channel defined as $\mathbf{h} = [0.390 + 0.105j,\ 0.605 + 0.142j,\ 0.440 + 0.0368j,\ 0.071 + 0.501j]^T$. There are 8 pilots in each time slot and the distance between two adjacent pilots in the same time slot is 16 symbols.

Without PN, the average power of the desired component, i.e., $A_{1,1}$, is normalized to 0 dB and it is the same for every symbol index m'. The average powers of the intrinsic interferences are much smaller than the power of $A_{1,1}$ and they can be practically ignored.

Fig. 4.2 shows the impact of FR-PN on the average power of $A_{1,1}$ with respect to the symbol index in the first transmission block. Plots of $(g_{m'}(n))^2$'s are given on the right-hand side of the figure, which show the same shape but circularly shifted with respect to m'. Since the variance of FR-PN increases linearly in time, $\cos\theta(n)$ tends to decrease in time. Therefore, the average power of $A_{1,1}$ decreases from the first time slot, i.e., $m' = 0$, and then reaches the minimum value at the eighth time slot, i.e., $m' = 7$. After that point, the average power of $A_{1,1}$ increases and reaches to the maximum value at the tenth time slot, i.e.,

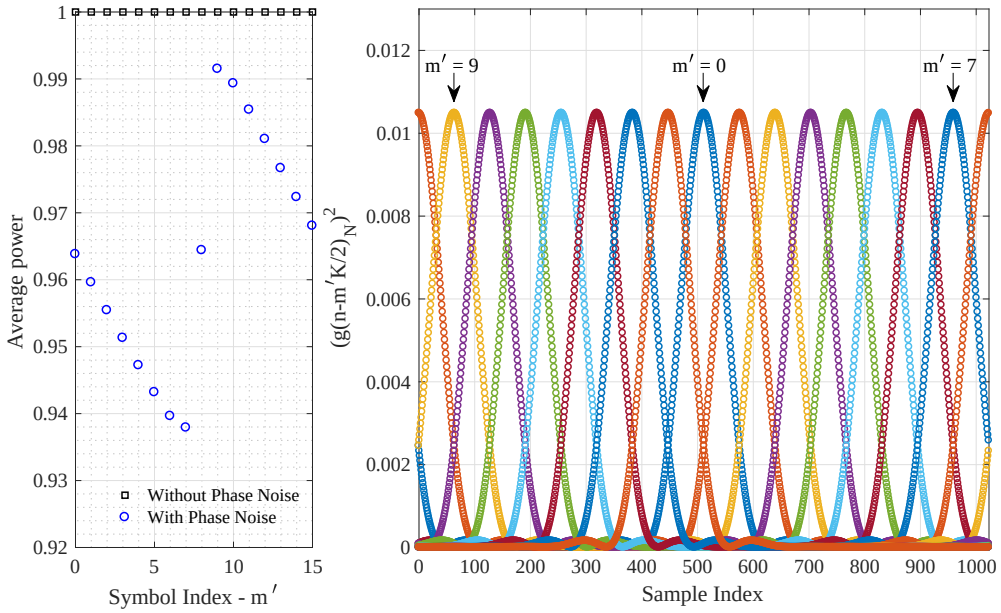

Figure 4.2: Impact of FR-PN on the average power of $A_{1,1}$ in the first transmission block.

$m' = 9$. Then, the average power decreases until $m' = 15$. A similar trend is observed for the next transmission block but the impact of PN is more significant. The impact of PLL-PN on $A_{1,1}$ is similar to that of FR-PN because the variance of PLL-PN also increases in time but at a much slower rate than that of FR-PN when the frequency synthesizer goes into the locked stage. The variation in the average power of $A_{1,1}$ is due to the variation of PN and the use of circular convolution in CFBMC-OQAM systems instead of the conventional linear convolution. This fluctuation happens with other signal components as well.

Fig. 4.3 and Fig. 4.4 show the average powers of the desired signal and intrinsic interferences, respectively, in the presence of PN. It is pointed out that the average powers of $A_{1,1}$ and $A_{1,2}$ depend only on the symbol index m', while the average power of $A_{1,3}$ depends on both m' and k'. However, because the ICI power is mainly contributed by adjacent subchannels, the average power of $A_{1,3}$ is plotted in Fig. 4.4 by setting $|k - k'| = 1$. It can be seen from Fig. 4.3 that, for the case of FR-PN the average power of $A_{1,1}$ drops from 0 to -2.1 dB as the symbol index changes from $m' = 0$ to $m' = 160$, i.e., after 10 transmission blocks. Under FR-PN, the average powers of $A_{1,2}$ and $A_{1,3}$ are about -16 dB and -23 dB at the first time slot, i.e., $m' = 0$, respectively. However, both of these values increase

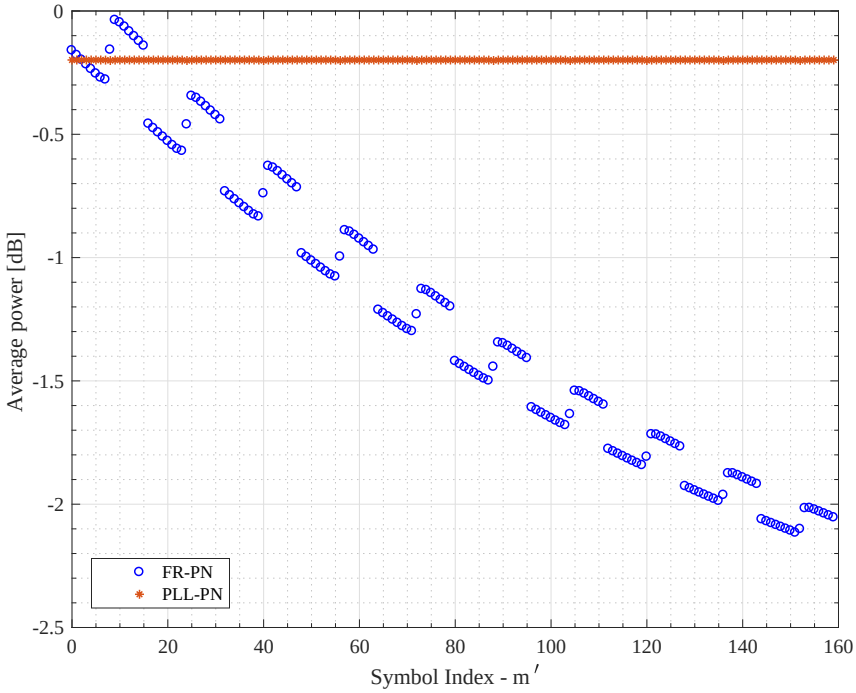

Figure 4.3: Average power of $A_{1,1}$ in the presence of PN.

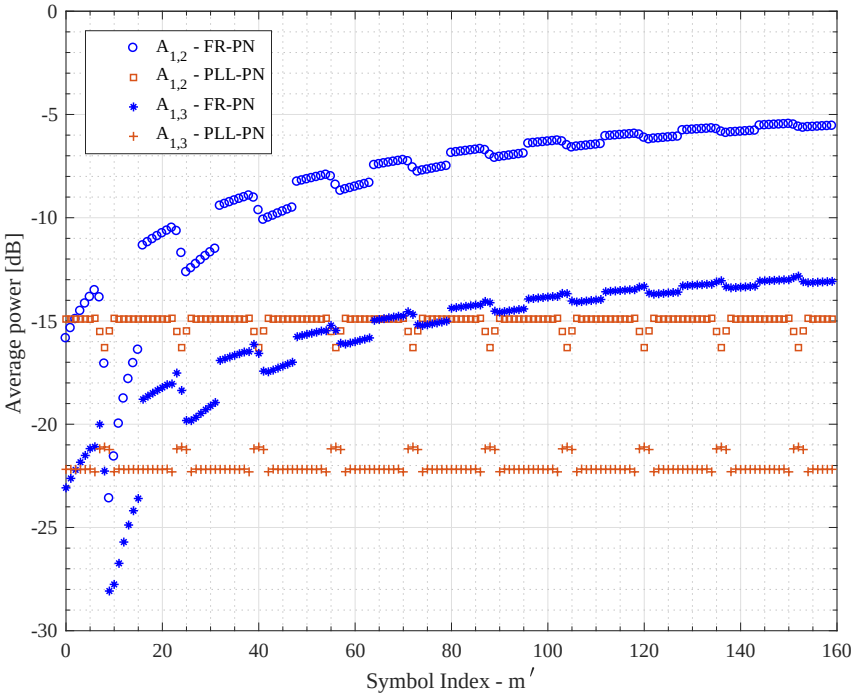

Figure 4.4: Average powers of $A_{1,2}$ and $A_{1,3}$ in the presence of PN.

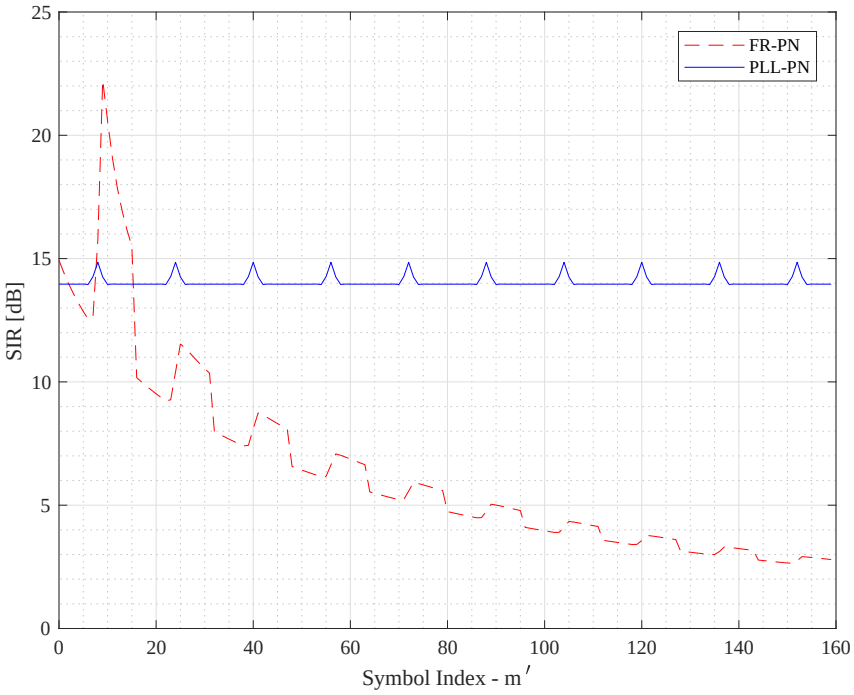

Figure 4.5: SIRs under two PN models.

by approximately 10 dB after 10 transmission blocks, which means that the power of the intrinsic interferences becomes significant and cannot be ignored as when there is no phase noise. Compared to FR-PN, the impacts of PLL-PN on the powers of $A_{1,1}$, $A_{1,2}$ and $A_{1,3}$ are rather consistent over 10 transmission blocks considered. Specifically, the average power of $A_{1,1}$ drops by only 0.2 dB, while the average powers of $A_{1,2}$ and $A_{1,3}$ are approximately -15 dB and -22 dB, respectively.

Fig. 4.5 plots the SIR based on (4.16) for both types of PN. It can be seen that the SIR tends to reduce in time under the case of FR-PN, whereas it is quite stable when PLL-PN is considered. As can be seen from Fig. 4.5, there are periodic fluctuations in the SIR for both cases.

Finally, performance of the CFBMC-OQAM system in terms of the bit error rate (BER) is illustrated in Fig. 4.6. In this figure, the performance in which PN is absent, indicated in the legend as "Without Phase Noise", is included as a reference to compare with the performance under PN with and without deploying the PN compensation algorithm. As expected, the impact of FR-PN is much more severe compared to that of PLL-PN. The performance is

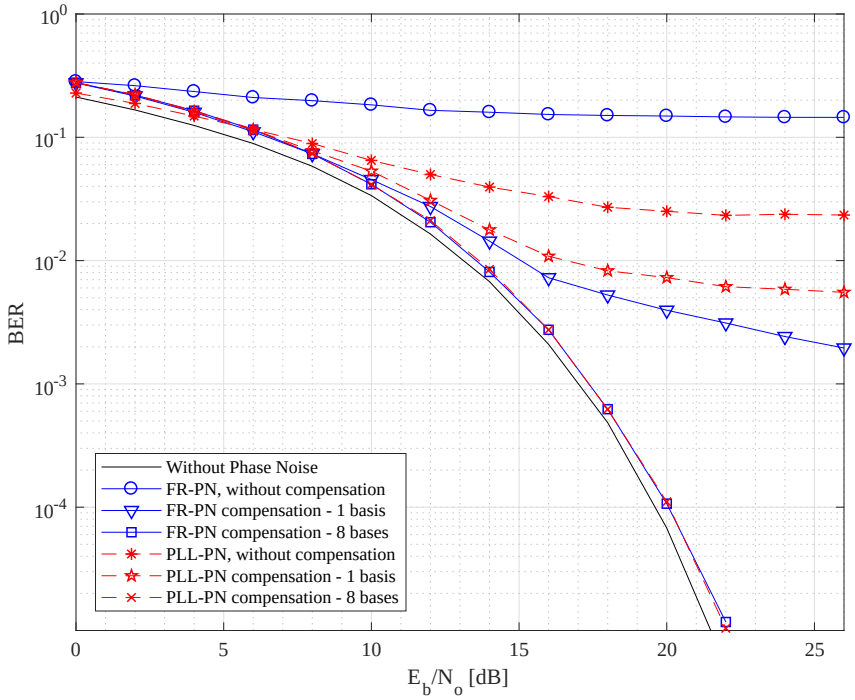

Figure 4.6: BER performance of CFBMC-OQAM.

getting better when the number of bases used in the PN compensation algorithm increases. It is seen from Fig. 4.6 that using 8 bases yields performance very close to the ideal case (i.e., without PN distortion). Specifically, at BER = 10^{-4}, there is a gap of only 0.4 dB between the performance in the ideal case and performance after the PN compensation.

4.6 Conclusions

This paper has considered the impacts of intrinsic self-interferences and phase noise on the performance of a CFBMC-OQAM system. It is shown that PN significantly increase the powers of intrinsic interferences under both PN models considered. Because of the use of circular convolution instead of the conventional linear convolution and PN characteristics, there is a variation in the SIR of the received signal over the symbol time index. The applied PN compensation algorithm effectively mitigates the impact of PN.

References

[1] B. Farhang-Boroujeny: "OFDM Versus Filter Bank Multicarrier", *IEEE Signal Processing Magazine*, vol. 28, no. 3, pp. 92–112, May 2011.

[2] T. Hwang and C. Yang and G. Wu and S. Li and G. Y. Li: "OFDM and Its Wireless Applications: A Survey", *IEEE Transactions on Vehicular Technology*, vol. 58, no. 4, pp. 1673–1694, May 2009.

[3] B. Farhang-Boroujeny: "Filter Bank Multicarrier Modulation: A Waveform Candidate for 5G and Beyond", *Advances in Electrical Engineering*, vol. 2014, pp. 1–25, 2014.

[4] G. Fettweis and M. Krondorf and S. Bittner: "GFDM - Generalized Frequency Division Multiplexing", *IEEE 69th Vehicular Technology Conference*, pp. 1–4, April 2009.

[5] A. RezazadehReyhani and B. Farhang-Boroujeny: "An Analytical Study of Circularly Pulse-Shaped FBMC-OQAM Waveforms", *IEEE Signal Processing Letters*, vol. 24, no. 10, pp. 1503–1506, Oct. 2017.

[6] A. RezazadehReyhani and A. Farhang and B. Farhang-Boroujeny: "Circularly Pulse-Shaped Waveforms for 5G: Options and Comparisons", *IEEE Global Communications Conference*, pp. 1–7, Dec. 2015.

[7] D. Petrovic and W. Rave and G. Fettweis: "Effects of Phase Noise on OFDM Systems With and Without PLL: Characterization and Compensation", *IEEE Transactions on Communications*, vol. 55, no. 8, pp. 1607–1616, Aug. 2007.

[8] S. Wu and P. Liu and Y. Bar-Ness: "Phase Noise Estimation and Mitigation for OFDM Systems", *IEEE Transactions on Wireless Communications*, vol. 5, no. 12, pp. 3616–3625, Dec. 2006.

[9] R. Corvaja and A. G. Armada: "Joint Channel and Phase Noise Compensation for OFDM in Fast-Fading Multipath Applications", *IEEE Transactions on Vehicular Technology*, vol. 58, no. 2, pp. 636–643, Feb. 2009.

[10] R. A. Casas and S. L. Biracree and A. E. Youtz: "Time domain phase noise correction for OFDM signals", *IEEE Transactions on Broadcasting*, vol. 48, no. 3, pp. 230–236, Sept. 2002.

[11] A. Leshem and M. Yemini: "Phase Noise Compensation for OFDM Systems", *IEEE Transactions on Signal Processing*, vol. 65, no. 21, pp. 5675–5686, Nov. 2017.

[12] V. Moles-Cases and A. A. Zaidi and X. Chen and T. J. Oechtering and R. Baldemair: "A comparison of OFDM, QAM-FBMC, and OQAM-FBMC waveforms subject to phase noise", *IEEE International Conference on Communications*, pp. 1–6, May 2017.

[13] A. Kakkavas and M. Castaeda and J. Luo and T. Laas and W. Xu and J. A. Nossek: "FBMC-OQAM with phase noise: Achievable performance and compensation", *IEEE 18th International Workshop on Signal Processing Advances in Wireless Communications*, pp. 1–5, Jul. 2017.

[14] B. Lim and Y. C. Ko: "SIR Analysis of OFDM and GFDM Waveforms With Timing Offset, CFO, and Phase Noise", *IEEE Transactions on Wireless Communications*, vol. 16, no. 10, pp. 6979–6990, Oct. 2017.

[15] A. Demir and A. Mehrotra and J. Roychowdhury: "Phase noise in oscillators: a unifying theory and numerical methods for characterization", *IEEE Transactions on Circuits and Systems I: Fundamental Theory and Applications*, vol. 47, no. 5, pp. 655–674, May 2000.

[16] A. Mehrotra: "Noise analysis of phase-locked loops", *IEEE Transactions on Circuits and Systems I: Fundamental Theory and Applications*, vol. 49, no. 9, pp. 1309–1316, Sept. 2002.

[17] P. Mathecken and T. Riihonen and S. Werner and R. Wichman: "Performance Analysis of OFDM with Wiener Phase Noise and Frequency Selective Fading Channel", *IEEE Transactions on Communications*, vol. 59, no. 5, pp. 1321–1331, May 2011.

5. Phase Noise Compensation for CFBMC-OQAM Systems under Imperfect Channel Estimation

Published as:

Long D. Le and Ha H. Nguyen, "Phase Noise Compensation for CFBMC-OQAM Systems under Imperfect Channel Estimation," *IEEE Access*, vol. 8, pp. 47247–47263, 2020.

In the last chapter, the impact of PN on CFBMC-OQAM systems was investigated assuming that the channel is perfectly known at the receiver. This chapter extends that study by examining the impact of PN and its compensation for CFBMC-OQAM systems under imperfect channel estimation.

It is first shown that, even in the absence of PN, CFBMC-OQAM still suffers from a significant performance degradation due to imperfect channel estimation compared to OFDM. As such, a preamble design is proposed to minimize the channel mean squared error (MSE), and thus mitigate the performance degradation. In the presence of PN, a two-stage PN compensation algorithm is developed. Specifically, in the first stage, the channel frequency response and PN are estimated based on the designed preamble. In the second stage, the estimated channel obtained from the first stage together with pilot symbols are used to compensate for the PN and detect the transmitted signal.

By taking statistical characteristics of both the channel and noise into account, the minimum mean-squared error (MMSE) method is used to improve the channel estimation quality in the first stage. The dependency between the channel frequency response and PN in this stage can be removed by solving an optimization problem to minimize the MSE of

estimated PN. The optimization problem is effectively solved by applying the majorization-minimization algorithm. The second stage basically applies the PN compensation algorithm developed in Chapter 4 to estimate the PN conjugation to compensate for the PN impact.

Simulation results illustrate the performance of the proposed algorithm in a variety of scenarios. Performance of OFDM is also included as the analytical benchmark. It is shown that the proposed algorithm effectively estimates the channel frequency response and compensates for the PN, which results in only a small performance gap in terms of the BER when compared to the ideal case where there is no PN.

Phase Noise Compensation for CFBMC-OQAM Systems under Imperfect Channel Estimation

Long D. Le and Ha H. Nguyen, *Senior Member, IEEE*

Abstract

Among many multi-carrier systems, circular filter-bank multi-carrier offset quadrature amplitude modulation (CFBMC-OQAM) is one of promising candidates for future wireless communications. This paper studies the impact of phase noise and its compensation for CFBMC-OQAM under imperfect channel estimation, which has not been done before. In the presence of phase noise, a two-stage phase noise compensation algorithm is proposed. In the first stage, the channel frequency response and phase noise are estimated based on the transmission of a preamble. Such a preamble is designed to minimize the channel mean squared error. In the second stage, the estimated channel obtained from the first stage together with pilot symbols are used to compensate for the phase noise and detect the transmitted signal. Simulation results obtained under practical scenarios show that the proposed algorithm effectively estimates the channel frequency response and compensates for the phase noise. The proposed algorithm is also shown to outperform an existing algorithm that performs iterative phase noise compensation when phase noise impact is high.

Index terms

FBMC, OFDM, CFBMC-OQAM, phase noise, preamble design, channel estimation.

5.1 Introduction

Multi-carrier transmission techniques have been extensively studied over the last few decades [1]. Currently, cyclic prefix orthogonal frequency-division multiplexing (CP-OFDM)[1]

[1]For brevity, CP-OFDM is simply referred to as OFDM in the paper.

[1, 2] is a popular choice for broadband wireless communication systems because it offers many advantages including resistance to multipath distortions by using CP, and a simple one-tap channel equalization, and efficient implementations based on the fast Fourier transform (FFT). However, OFDM also has its own disadvantages. Two major disadvantages are: (i) the effect of rectangular pulse shaping in the conventional OFDM leads to a high out-of-band emission to neighboring frequency bands [1], and (ii) fairly complicated carrier frequency offset and timing synchronization techniques are needed to establish subcarrier orthogonality at the receiver [3–7].

In the search for more favorable waveforms for the physical layer of the next-generation wireless networks, a number of signaling methods has been suggested. The proposed waveforms can be broadly classified into two groups, one with linear pulse shaping and the other with circular pulse shaping. Filter-bank multi-carrier offset quadrature amplitude modulation (FBMC-OQAM) is one of the signaling methods in the first group that can resolve the above problems in OFDM [1, 8]. Specifically, with the use of well-designed prototype filters [9–11], an FBMC system can avoid the high spectral leakage issue in the conventional OFDM. On the other hand, using OQAM splits complex data into real and imaginary parts which consequently relaxes the orthogonality condition to the real field [1, 8]. However, FBMC-OQAM does not have a block-based structure like OFDM, which makes the channel estimation and equalization tasks significantly more complicated when compared to OFDM.

Recently proposed as candidates for the air interface of 5G networks [12], generalized frequency division multiplexing (GFDM) [13, 14] and circular filter-bank multi-carrier offset quadrature amplitude modulation (CFBMC-OQAM) [15] are signaling methods that use circular pulse shaping. With circular pulse shaping, the length of the CP can be chosen to be the same as the length of the channel impulse response, i.e., independent of the length of the added pulse shaping filter. This is not the case with linear pulse shaping in which the CP length needs to cover both the length of the channel impulse response and the delay introduced by the shaping filter. Similar to the conventional OFDM, the channel estimation and equalization in these systems can be simply performed after removing the CP. However, different from GFDM which is a non-orthogonal system and thus can severely suffer from

the impact of inter-symbol interference (ISI) and inter-carrier interference (ICI), CFBMC-OQAM is an orthogonal system in the real domain.

In practice, to perform the channel equalization task, the channel state information has to be first estimated based on the transmission of either pilots or preambles as in [16–18] for OFDM, and [19–22] for FBMC-OQAM, and [23, 24] for GFDM. However, to the best of our knowledge, all studies on CFBMC-OQAM assume that the channel frequency response is perfectly known for the equalization task [12, 15] and thus the bit-error rate (BER) performance of CFBMC-OQAM is equivalent to that of OFDM under the same system configuration. Such an assumption does not hold in practice.

Any multi-carrier systems suffer from physical impairments, especially the phase noise (PN). Impact of PN on OFDM systems has been extensively studied in the last few decades [25–29]. In the time domain, the effect of PN can be represented as a multiplicative noise in the form of a complex exponential function. In the frequency domain, on the other hand, the PN impact can be separated into two components, namely common phase error (CPE) and ICI. The first component results in a common rotation of all symbols, while the second component is different for every symbol. Mitigating the PN impact in OFDM systems can be performed in either the frequency domain [26,27,30–32] or the time domain [28,29,33–37].

In [31], the frequency-domain PN vector is estimated by solving a constrained quadratic optimization problem. However, the problem is solved under the assumption that PN is very small so that the constraint is relaxed and applied only for the real part of the first frequency-domain PN component. To improve the PN estimation in [31], better constraints are considered in [32] and [34]. The constraint in [32] is derived based on a geometrical structure associated with the frequency-domain PN components, whereas the constraint in [34] relies on the fact that the complex exponential functions of PN have unit magnitudes. Applying the so-called S-procedure, the optimization problem in [32] is solved as a semidefinite programming problem. However, because of the inherently high computational complexity of semidefinite programming, the algorithm in [32] may not work efficiently when the number of sub-carriers is very large as expected in future communication systems. On the other hand, an algorithm known as majorization-minimization [38] is applied to estimate the

channel and PN in [34] with low complexity that allows to deal with systems having a much larger number of sub-carriers.

In [35], an iterative PN compensation algorithm is proposed for OFDM. With this iterative approach, based on the estimated channel and the output of a soft-decision Viterbi decoder, the receiver tries to replicate the PN-free transmitted signal and uses it to estimate the PN in the time domain by a one-tap least mean square (LMS) method. Performance advantage of the iterative PN compensation algorithm over other algorithms is illustrated in terms of the packet-error rate (PER) in [35]. The iterative technique in [35] is further considered in [36] and [37] for 60 GHz and 10 Gbps OFDM experimental systems, respectively.

The impact of PN has recently been considered in [39, 40] for FBMC-OQAM, [41] for GFDM, and [42] for CFBMC-OQAM. Different from OFDM, FBMC-OQAM, GFDM and CFBMC-OQAM suffer from two intrinsic interferences, namely ISI and ICI. Therefore, these systems generally have additional interference components when PN is taken into account. Consequently, mitigating the impact of PN in such systems is more complicated than that in OFDM [39]. In [40], two novel CPE compensation algorithms, one is a pilot-based approach and the other is a blind approach exploiting the interference structure from the neighboring sub-channels, are proposed for FBMC-OQAM. Under the small PN assumption, the paper shows that the proposed algorithms nearly achieve the optimal performance when no PN is considered. The authors in [41] propose a filter for GFDM systems to maximize the signal-to-interference ratio in the presence of timing offset, carrier frequency offset and PN. In our previous study [42], we investigated the impact of two different PN types, one is based on a free-running (FR) oscillator and the other is based on a phase-locked loop (PLL) oscillator, on CFBMC-OQAM systems and proposed an algorithm to effectively compensate the PN impact by taking the intrinsic self-interferences into account. However, the work in [42] assumes that the channel frequency response is perfectly known.

The impact of PN on CFBMC-OQAM and its compensation under imperfect channel estimation shall be studied in this paper. Since CFBMC-OQAM is different from both OFDM and FBMC in terms of signal processing operations, existing techniques developed for OFDM and FBMC might not provide good performance when applied straightforwardly

to CFBMC-OQAM. First, it shall be shown that, compared to OFDM, performance of CFBMC-OQAM is much more susceptive to imperfect channel estimation even when there is no PN. The paper then proposes a preamble design to minimize the channel mean squared error (MSE) and consequently mitigate the performance degradation. In the presence of PN, the paper proposes a two-stage PN compensation algorithm. With the designed preamble, channel and PN are estimated in the first stage. Different from previous works [31, 32, 34] where the channel is estimated based on the least square (LS) method, the channel estimation in this paper is performed based on the minimum mean-squared error (MMSE) method to significantly improve the estimation performance. In the second stage, the estimated channel obtained from the first stage is then utilized together with pilots to compensate for the impact of PN and detect the transmitted data. To avoid error propagation and long latency experienced by iterative PN compensation algorithms [35–37], a non-iterative method is proposed in the second stage. Simulation results obtained under practical scenarios illustrate the effectiveness of the proposed method in compensating for the PN impact in the presence of imperfect channel estimation. Especially, the proposed two-stage algorithm is shown to outperform the iterative PN compensation algorithm in [35] when the PN is large.

It is relevant to point out that paper [43] proposes a two-step algorithm to estimate the carrier frequency offset (CFO) and channel in a multi-input multi-output FBMC-OQAM system. Specifically, in the first step, the CFO is coarsely estimated by using the cross correlation between the received signal and the known preamble. After CFO compensation, the effective channel, which is a combination of the residual CFO and the real channel, is estimated in the second step by either weighted LS or MMSE estimator. The difference between [43] and our paper is that the impact of CFO is represented via a single unknown variable. Once an estimated CFO is obtained from the first step based on preambles, it is used for channel estimation in the second step and data detection for the remaining transmission blocks. However, in our paper, PN needs to be modeled as a random process and it changes from one transmission block to the other. As such, the estimated PN vector obtained based on a preamble block cannot be reused for the data detection in the next blocks.

This paper is organized as follows. The system model is presented in Section 5.2, which

includes a brief review of a CFBMC-OQAM system and characteristics of two PN types. In the first part of Section 5.3, a preamble design is proposed to mitigate the performance degradation in CFBMC-OQAM due to imperfect channel estimation and when PN is absent. Under the presence of PN, the paper proposes a two-stage PN compensation algorithm. The first stage is presented in the second part of Section 5.3 to estimate the channel and PN. The second stage is described in Section 5.4 to compensate for the PN impact and detect the transmitted data. Simulation results are provided in Section 5.5. Section 5.6 concludes the paper.

Notation: Lowercase letters are used to denote scalars. Lowercase boldface and uppercase boldface letters stand for vectors and matrices, respectively. Symbols $(\cdot)^{\dagger}$, $(\cdot)^{T}$, $(\cdot)^{H}$, $(\cdot)^{-1}$, $(\cdot)^{*}$, $|\cdot|$, $||\cdot||_2$, and $\circledast$ denote pseudo-inverse, transpose, Hermitian, inverse, complex conjugate, modulus, ℓ_2-norm and circular convolution operations, respectively. Symbols $\mathfrak{R}\{\cdot\}$, $\mathfrak{I}\{\cdot\}$, diag$[\cdot]$, and E$[\cdot]$ denote the real and imaginary parts of a complex variable, a diagonal matrix if the argument is a vector, or a vector if the argument is a diagonal matrix, and expectation

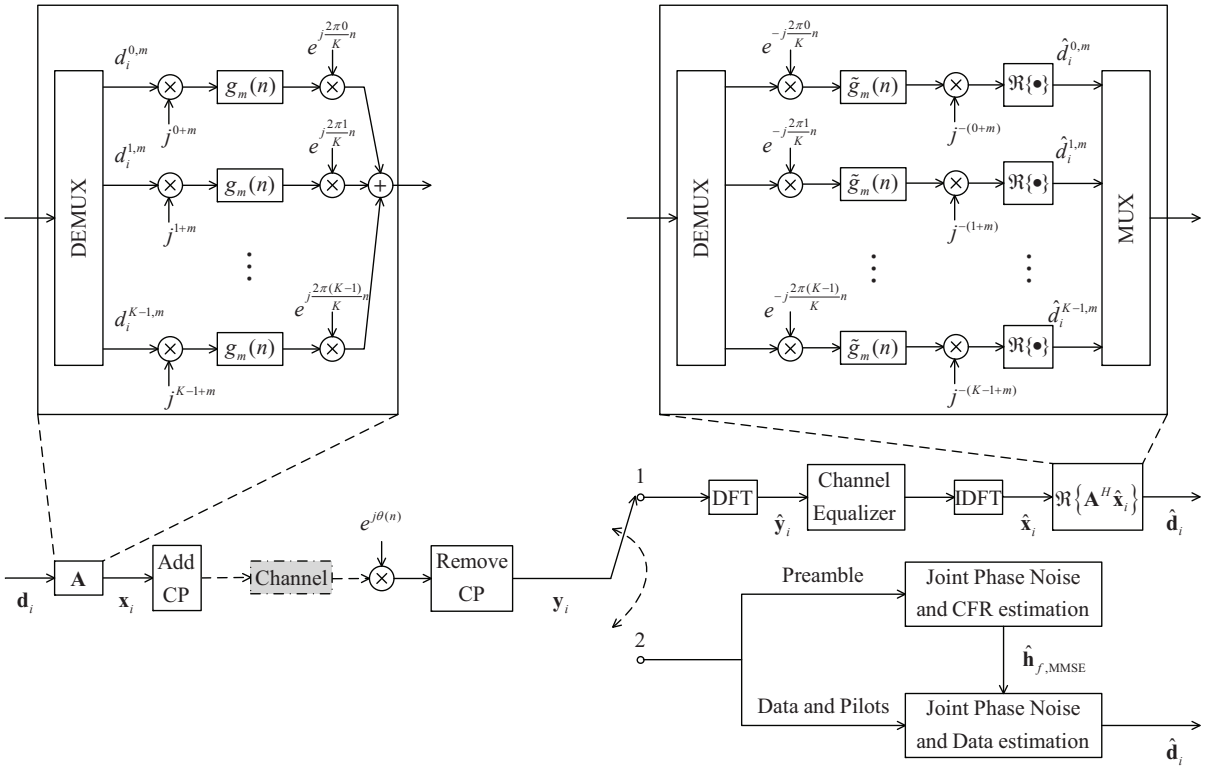

Figure 5.1: A discrete-time complex baseband equivalent CFBMC-OQAM transceiver.

operation, respectively. $\mathbf{1}_{N\times 1}$ denotes a column vector whose N components are all 1's.

5.2 System Model

5.2.1 CFBMC-OQAM

Consider a discrete-time complex baseband equivalent CFBMC-OQAM system as illustrated in Fig. 5.1. Let $N = KM$. Then, the transmitted signal vector corresponding to the ith transmission block $\mathbf{x}_i = \begin{bmatrix} x_i(0) & x_i(1) & \cdots & x_i(N-1) \end{bmatrix}^T$ is constructed from a $K \times 2M$ block of data defined over K sub-carriers and $2M$ time slots as

$$x_i(n) = \sum_{k=0}^{K-1} \sum_{m=0}^{2M-1} j^{k+m} d_i^{k,m} g_m(n) \mathrm{e}^{j\frac{2\pi kn}{K}}, n = 0, 1, \cdots, N-1 \tag{5.1}$$

where $1 \leq i \leq N_b$ and N_b is the number of blocks per one transmission frame, $g_m(n) = g\left(n - m\frac{K}{2}\right)_N$ is a cyclic shift version of a length-N real-valued and symmetric prototype filter $g_0(n) = g(n)$. Equation (5.1) can be rewritten as

$$\mathbf{x}_i = \mathbf{A}\mathbf{d}_i \tag{5.2}$$

in which $\mathbf{d}_i = \begin{bmatrix} \mathbf{d}_i^0 & \mathbf{d}_i^1 & \cdots & \mathbf{d}_i^{K-1} \end{bmatrix}^T$ and $\mathbf{d}_i^q = \begin{bmatrix} d_i^{q,0} & d_i^{q,1} & \cdots & d_i^{q,2M-1} \end{bmatrix}^T$. To enable offset QAM, the real and imaginary parts of a complex QAM symbol in the ith transmission block, $s_i^{k,m} = s_{i,R}^{k,m} + j s_{i,I}^{k,m}$, are separated and arranged as

$$\begin{bmatrix} d_i^{0,0} & d_i^{0,1} & \cdots & d_i^{0,2M-1} \\ d_i^{1,0} & d_i^{1,1} & \cdots & d_i^{1,2M-1} \\ \vdots & \vdots & \ddots & \vdots \\ d_i^{K-1,0} & d_i^{K-1,1} & \cdots & d_i^{K-1,2M-1} \end{bmatrix} = \begin{bmatrix} s_{i,R}^{0,0} & s_{i,I}^{0,0} & \cdots & s_{i,R}^{0,M-1} & s_{i,I}^{0,M-1} \\ s_{i,R}^{1,0} & s_{i,I}^{1,0} & \cdots & s_{i,R}^{1,M-1} & s_{i,I}^{1,M-1} \\ \vdots & \vdots & \cdots & \vdots & \vdots \\ s_{i,R}^{K-1,0} & s_{i,I}^{K-1,0} & \cdots & s_{i,R}^{K-1,M-1} & s_{i,I}^{K-1,M-1} \end{bmatrix}. \tag{5.3}$$

The real-valued vector $\mathbf{d}_i$ is then obtained by vectorizing the matrix on the left of (5.3). $\mathbf{A}$ is called the modulation matrix whose $(m + 2kM)$th column is [15]

$$\mathbf{A}[:, m + 2kM] = j^{k+m}[g_m(0)\mathrm{e}^{j\frac{2\pi k0}{K}}, \cdots, g_m(N-1)\mathrm{e}^{j\frac{2\pi k(N-1)}{K}}]^T.$$

A CP of length L is added to $\mathbf{x}_i$ before transmitting.

The channel $\mathbf{h} = \begin{bmatrix} h(0) & h(1) & \cdots & h(\mu-1) \end{bmatrix}^T$ is characterized by μ taps, where $\mu \leq (L+1)$. It is assumed that $\mathbf{h} \sim \mathcal{CN}(0, \mathbf{\Sigma})$ and $\mathbf{\Sigma} = \mathrm{E}\left[\mathbf{h}\mathbf{h}^H\right]$ is the $\mu \times \mu$ channel covariance

matrix. When there is no PN, the received signal corresponding to the ith block after removing the CP is written as

$$\mathbf{y}_i = \mathbf{H}_{\text{circ}}\mathbf{x}_i + \mathbf{w}_i \tag{5.4}$$

where $\mathbf{w}_i \sim \mathcal{CN}(0, \sigma_{\mathbf{w}}^2\mathbf{I})$ represents noise, and $\mathbf{H}_{\text{circ}}$ is a circulant matrix whose columns are circularly shifted from vector $\begin{bmatrix} h(0) & h(1) & \cdots & h(\mu-1) & 0 & \cdots & 0 \end{bmatrix}^T_{N\times 1}$. It is noted that $\mathbf{H}_{\text{circ}}$ can be represented as $\mathbf{H}_{\text{circ}} = \mathbf{F}^H\mathbf{\Gamma}\mathbf{F}$ where $\mathbf{F}$ is the normalized DFT matrix whose (k,m)th element is given as $[\mathbf{F}]_{k,m} = \frac{1}{\sqrt{N}}\mathrm{e}^{-j\frac{2\pi mk}{N}}$ and $\mathbf{\Gamma}$ is a diagonal matrix whose diagonal elements are subcarrier channel gains in the frequency domain. To detect the desired signal, the received signal $\mathbf{y}_i$ is first converted to the frequency domain by a DFT transform, then channel equalized with matrix $\hat{\mathbf{\Gamma}}$ which is an estimate of $\mathbf{\Gamma}$ based on a known preamble, and further IDFT transformed to obtain $\hat{\mathbf{x}}_i$. Then, $\hat{\mathbf{x}}_i$ is passed through a bank of matched filters and the estimate of $\mathbf{d}_i$ is obtained by taking the real part of the filtered output as $\hat{\mathbf{d}}_i = \Re\left\{\mathbf{A}^H\hat{\mathbf{x}}_i\right\}$ [15].

In the presence of PN, the received signal for the ith block is

$$\mathbf{y}_i = \mathbf{P}_i\mathbf{H}_{\text{circ}}\mathbf{x}_i + \mathbf{w}_i \tag{5.5}$$

where $\mathbf{P}_i = \text{diag}\left[\mathrm{e}^{j\theta(\epsilon)} \quad \mathrm{e}^{j\theta(\epsilon+1)} \quad \cdots \quad \mathrm{e}^{j\theta(\epsilon+N-1)}\right]$ represents the effect of PN on the ith transmission block and $\epsilon = (i-1)N + iL$. It is pointed out that the form of the input/output relation as in (5.4) and (5.5) is common to many multicarrier systems, including OFDM, GFDM and CFBMC-OQAM, which use a CP to overcome the ISI effect of a frequency-selective fading channel. However, different signal processing operations result in either an orthogonal system (such as OFDM), or a non-orthogonal system (such as GFDM), or a real-domain orthogonal system (such as CFBMC-OQAM). Therefore, it is necessary to study different systems in detail when the impacts of PN and imperfect channel estimation are considered.

5.2.2 Phase Noise

This section briefly reviews two PN models: one is based on a free-running oscillator and the other is based on a PLL oscillator.

FR-PN model

Let $\alpha_v(n)$ denote the discrete-time phase deviation from an FR oscillator at the nth sampling time. It can be modeled as $\alpha_v(n) = \sum_{i=0}^{n-1} \rho(i)$ where $\rho(i)$'s are independent and identically distributed (i.i.d) zero-mean Gaussian random variables with variance $\sigma_\rho^2 = c_v T_s$. Here, c_v is a constant describing the quality of an oscillator, and T_s is the sampling interval. The PN is $\theta(n) = 2\pi f_c \alpha_v(n) = \omega_c \alpha_v(n)$, where f_c is the carrier frequency. Thus, the discrete-time FR-PN at the nth sampling time $\theta(n)$ can be modeled as a zero-mean Gaussian distributed random variable with variance $n\omega_c^2 c_v T_s$, which grows linearly with the sample index n. Furthermore, the autocorrelation function of the phase deviation can be computed as $\mathrm{E}\left[\alpha_v(n_1)\alpha_v(n_2)\right] = c_v T_s \min(n_1, n_2)$ [44]. Define $\mathbf{R}$ as the PN covariance matrix, whose (n_1, n_2)th component is [25]:

$$\mathbf{R}(n_1, n_2) = \exp\left\{-\frac{1}{2}\left|n_1 - n_2\right| \omega_c^2 c_v T_s\right\}. \tag{5.6}$$

The above PN covariance matrix will be used later to compensate the impact of PN.

PLL-PN model

A general PLL-based frequency synthesizer is described in [25]. Let $\alpha_r(n)$, $\alpha_v(n)$, and $\beta(n)$ denote the discrete-time phase deviations at the output of the reference oscillator, the frequency synthesizer, and the phase detector, respectively. Then $\alpha_v(n) = \beta(n) + \alpha_r(n)$ [45]. The reference oscillator is basically the same as a FR oscillator which is characterized by a quality factor c_r. The phase deviation output of the phase detector, i.e., $\beta(n)$, is modeled as a one-dimensional Ornstein-Uhlenbeck process [45]. Furthermore, the correlation properties between $\alpha_r(n)$ and $\beta(n)$ are: $\mathrm{E}\left\{\beta(n_1)\alpha_r(n_2)\right\} = \sum_{i=1}^{n_o} \mu_i \mathrm{e}^{\lambda_i T_s \min(0, n_2 - n_1)}$ and $\mathrm{E}\left\{\beta(n_1)\beta(n_2)\right\} = \sum_{i=1}^{n_o} \nu_i \mathrm{e}^{-\lambda_i T_s |n_1 - n_2|}$ where $n_o = 1 + o_{\mathrm{lpf}}$, and o_{lpf} represents the order of the loop filter [25, 45]. The values of λ_i, μ_i and ν_i are given, for instance in [45], for the PLL-based oscillator with a first-order loop filter. The (n_1, n_2)th component of the covariance matrix $\mathbf{R}$ is obtained as [25]

$$\mathbf{R}(n_1, n_2) = \exp\left\{ -\frac{1}{2}\omega_c^2 \left[|n_1 - n_2| c_r T_s + 2\sum_{i=1}^{n_o} (\nu_i + \mu_i)\left(1 - \mathrm{e}^{-\lambda_i T_s |n_1 - n_2|}\right) \right] \right\}. \tag{5.7}$$

5.3 Estimation of Phase Noise and Channel Frequency Response

It is clear that the estimated channel $\hat{\mathbf{\Gamma}}$ plays a critical role in detecting the transmitted signal. In practice, the channel state information can be obtained based on the transmission of preambles or pilot symbols. Specifically, preambles are training blocks which are transmitted at the beginning of each transmission frame, while pilots are known symbols which are embedded into transmission blocks based on a specific pattern and transmitted along with the data. Given known preambles or pilots, channel frequency response can be estimated by dividing the received signal by the corresponding preambles or pilots. Since a preamble occupies the entire transmission block, the channel estimation based on a preamble, if well designed, should be better than that obtained based on pilot symbols. Hence, a preamble is designed and used to estimate the channel in this paper, while pilot symbols are used to compensate for the PN.

Generally, channel estimation can be done in either time or frequency domain [4, 46, 47]. It appears that the frequency-domain approach is more common in practice for a multicarrier system since it can make use of the IFFT/FFT blocks already existing in the system and it also integrates well with the data detection process, which is conveniently performed in the frequency domain. As such, frequency-domain channel estimation is also adopted in this paper.

In this paper, it is assumed that the channel changes slowly during multiple transmission blocks, while PN changes fast and varies from one block to the other. Under this assumption the channel estimation based on the preamble, which is the first transmitted block in a transmission frame, can be used to compensate for the impact of PN and detect the data in the remaining transmission blocks. Thus, this paper proposes an algorithm which has two stages. Specifically, the channel frequency response and PN are estimated in the first stage based on the preamble. Given the estimated channel, data and PN can be estimated based on the pilot symbols in the second stage. To perform this two-stage PN compensation algorithm, the switch in Fig. 5.1 is toggled between the two positions.

5.3.1 Channel estimation and preamble design without the presence of PN in CFBMC-OQAM

First, the received signal corresponding to the first transmission block $\mathbf{y}_1$ is converted to the frequency domain by a DFT transform to as

$$\hat{\mathbf{y}}_1 = \mathbf{F}\mathbf{y}_1 = \mathbf{F}\mathbf{H}_{\text{circ}}\mathbf{A}\mathbf{d}_1 + \mathbf{F}\mathbf{w}_1 = \mathbf{\Gamma}\mathbf{F}\mathbf{A}\mathbf{d}_1 + \hat{\mathbf{w}}_1. \tag{5.8}$$

Define $\mathbf{S}_1 = \text{diag}[\mathbf{F}\mathbf{A}\mathbf{d}_1]$ and $\mathbf{h}_f = \text{diag}[\mathbf{\Gamma}]$. Then (5.8) can be rewritten as

$$\hat{\mathbf{y}}_1 = \mathbf{S}_1\mathbf{h}_f + \hat{\mathbf{w}}_1. \tag{5.9}$$

For channel estimation, a known preamble is transmitted and hence $\mathbf{S}_1$ is known. When the LS estimation method is employed, the estimated channel frequency response $\hat{\mathbf{h}}_{f,\text{LS}}$ is obtained by minimizing the following cost function:

$$C(\hat{\mathbf{h}}_{f,\text{LS}}) = \left|\left|\hat{\mathbf{y}}_1 - \mathbf{S}_1\hat{\mathbf{h}}_{f,\text{LS}}\right|\right|_2^2. \tag{5.10}$$

By setting the derivative of the cost function with respect to $\hat{\mathbf{h}}_{f,\text{LS}}$ to zero, one obtains

$$\hat{\mathbf{h}}_{f,\text{LS}} = \mathbf{S}_1^{-1}\hat{\mathbf{y}}_1. \tag{5.11}$$

It then follows that the MSE between $\hat{\mathbf{h}}_{f,\text{LS}}$ and $\mathbf{h}_f$ is

$$\begin{aligned}
\text{E}[||\hat{\mathbf{h}}_{f,\text{LS}} - \mathbf{h}_f||_2^2] &= \text{E}\left[\text{Tr}\left((\hat{\mathbf{h}}_{f,\text{LS}} - \mathbf{h}_f)(\hat{\mathbf{h}}_{f,\text{LS}} - \mathbf{h}_f)^H\right)\right] \\
&= \text{Tr}\left[\text{E}\left(\mathbf{S}_1^{-1}\hat{\mathbf{y}}_1 - \mathbf{h}_f\right)\left(\mathbf{S}_1^{-1}\hat{\mathbf{y}}_1 - \mathbf{h}_f\right)^H\right] \\
&= \text{Tr}\left[\text{E}\left(\mathbf{S}_1^{-1}\left(\mathbf{S}_1\mathbf{h}_f + \hat{\mathbf{w}}_1\right) - \mathbf{h}_f\right) \times \right. \\
&\qquad \left. \left(\mathbf{S}_1^{-1}\left(\mathbf{S}_1\mathbf{h}_f + \hat{\mathbf{w}}_1\right) - \mathbf{h}_f\right)^H\right] \\
&= \text{Tr}\left[\text{E}\left(\mathbf{S}_1^{-1}\hat{\mathbf{w}}_1\hat{\mathbf{w}}_1^H\left(\mathbf{S}_1^{-1}\right)^H\right)\right] \\
&= \sigma_{\mathbf{w}}^2\,\text{Tr}\left\{\left(\mathbf{S}_1^H\mathbf{S}_1\right)^{-1}\right\}.
\end{aligned} \tag{5.12}$$

As expected the MSE depends on the preamble through the diagonal matrix $\mathbf{S}_1$. This also means that one can design the preamble to minimize the MSE.

Define $\mathbf{\Psi} = \mathbf{S}_1^H \mathbf{S}_1 = \text{diag}\left[\psi_0 \quad \psi_1 \quad \cdots \quad \psi_{N-1}\right]$. Then the preamble design problem is stated as

$$\begin{aligned} \underset{\psi_i}{\text{minimize}} \quad & \sum_{i=0}^{N-1} \frac{1}{\psi_i} \\ \text{subject to} \quad & \psi_i \geq 0 \quad i = 0, 1, \cdots, N-1 \\ & \sum_{i=0}^{N-1} \psi_i \leq N. \end{aligned} \tag{5.13}$$

In (5.13), the first constraint is to guarantee that $\mathbf{\Psi}$ is a positive semi-definite matrix, while the second constraint is to make sure that the total power of $\mathbf{S}_1$ is no more than N. The solution for the optimization problem in (5.13) can be obtained by applying the Karush-Kuhn-Tucker conditions [48] and the solution is $\mathbf{\Psi} = \mathbf{I}$. Thus, $\mathbf{S}_1$ is a diagonal matrix whose diagonal elements are in the forms of exponential functions, i.e.,

$$\mathbf{S}_1 = \text{diag}\left[\mathrm{e}^{j\kappa_0} \quad \mathrm{e}^{j\kappa_1} \quad \cdots \quad \mathrm{e}^{j\kappa_{N-1}}\right]^T. \tag{5.14}$$

Given $\mathbf{S}_1 = \text{diag}\left(\mathbf{F}\mathbf{A}\mathbf{d}_1\right)$ and the fact that $\Re\left\{\mathbf{A}^H\mathbf{A}\right\} = \mathbf{I}$ for a well-designed shaping filter [15], the preamble is finally obtained as

$$\mathbf{d}_1 = \Re\left\{\mathbf{A}^H\mathbf{F}^H \text{diag}\left[\mathbf{S}_1\right]\right\}. \tag{5.15}$$

The above preamble design can be straightforwardly applied to OFDM systems where the modulation matrix $\mathbf{A}$ is replaced by the inverse DFT matrix $\mathbf{F}^H$. This also means that to minimize the channel MSE, the preamble for OFDM under the LS channel estimation has to satisfy the unit-magnitude condition, namely $|\text{diag}[\mathbf{S}_1]| = \mathbf{1}_{N\times 1}$. This is consistent with previous studies for OFDM [16, 18, 49, 50].

It is pointed out that the preamble design in this paper does not take into account either the impact of PN or fading channel. This is a common practice (see e.g., [51, 52]) and is motivated by the fact that preambles are usually used for various purposes, such as establishing synchronization between the transmitter and receiver, estimating system parameters and channel statistics. To be applied ubiquitously, these preambles should be designed or selected without taking into account specific propagation channels and physical impairments. Given the designed preamble, the channel can be estimated based on either

LS or MMSE method depending on whether statistical characteristics of channel and noise are available.

5.3.2 Estimation of PN and channel frequency response

In the presence of PN, this section is performed on the first transmission block, i.e., the designed preamble. Due to PN, the received signal (after removing CP) corresponding to the first transmission block becomes

$$\mathbf{y}_1 = \mathbf{P}_1\mathbf{H}_{\text{circ}}\mathbf{x}_1 + \mathbf{w}_1 = \mathbf{P}_1\mathbf{F}^H\mathbf{S}_1\mathbf{h}_f + \mathbf{w}_1 \tag{5.16}$$

where $\mathbf{P}_1 = \text{diag}\left[\text{e}^{j\theta(L)} \quad \text{e}^{j\theta(L+1)} \quad \dots \quad \text{e}^{j\theta(N+L-1)}\right]$ represents the effect of PN on the first transmission block.

It is seen from (5.16) that there exists an inter-dependency between PN and the channel, i.e., estimation of the channel depends on PN and vice versa. To estimate PN and the channel, the approach in [31, 32, 34] is adopted. In such an approach, the inter-dependency is decoupled by first obtaining the LS-based channel estimate which is a function of the unknown PN matrix. Then, the estimated channel is substituted into the optimization problem which minimizes the MSE for PN estimation. However, different from the previous studies, the MMSE method is used to estimate the channel in this paper. Compared to LS-based channel estimation, the MMSE method takes into account statistical characteristics of both channel and noise to improve the channel estimation quality. To focus on the PN compensation algorithm, it is assumed that the statistical characteristics of channel and noise are known at the receiver.[2]

The MMSE channel estimate $\hat{\mathbf{h}}_{f,\text{MMSE}}$ is found by minimizing $\text{E}\left[||\mathbf{h}_f - \hat{\mathbf{h}}_{f,\text{MMSE}}||_2^2\right]$ [53]. The orthogonality principle states that

$$\text{E}\left[\left(\mathbf{h}_f - \hat{\mathbf{h}}_{f,\text{MMSE}}\right)\hat{\mathbf{h}}_{f,\text{MMSE}}^H\right] = \mathbf{0}, \tag{5.17}$$

[2]In practice, statistical information of channel and noise can be obtained using either data-aided techniques (which require and make use of pilot symbols) or non-data aided techniques (which are based directly on the the received signals).

which results in

$$\hat{\mathbf{h}}_{f,\mathrm{MMSE}} = N\breve{\mathbf{F}}\boldsymbol{\Sigma}\breve{\mathbf{F}}^H\mathbf{S}_1^H\left(N\mathbf{S}_1\breve{\mathbf{F}}\boldsymbol{\Sigma}\breve{\mathbf{F}}^H\mathbf{S}_1^H + \sigma_{\mathbf{w}}^2\mathbf{I}\right)^{-1}\mathbf{F}\mathbf{P}_1^H\mathbf{y}_1 \tag{5.18}$$

where $\breve{\mathbf{F}}$ contains the first μ columns of $\mathbf{F}$. A proof for (5.18) is given in Appendix 5.7.1. Recall that $\hat{\mathbf{h}}_{f,\mathrm{LS}} = \left(\mathbf{P}_1\mathbf{F}^H\mathbf{S}_1\right)^\dagger\mathbf{y}_1 = \mathbf{S}_1^{-1}\mathbf{F}\mathbf{P}_1^H\mathbf{y}_1$. Thus, it can be seen from (5.18) that the MMSE channel estimate can be expressed as a linearly-weighted version of the LS channel estimate, namely $\hat{\mathbf{h}}_{f,\mathrm{MMSE}} = \mathbf{W}\hat{\mathbf{h}}_{f,\mathrm{LS}}$, where

$$\mathbf{W} = N\breve{\mathbf{F}}\boldsymbol{\Sigma}\breve{\mathbf{F}}^H\left(N\breve{\mathbf{F}}\boldsymbol{\Sigma}\breve{\mathbf{F}}^H + \sigma_{\mathbf{w}}^2\left(\mathbf{S}_1^H\mathbf{S}_1\right)^{-1}\right)^{-1}. \tag{5.19}$$

With the expression of the MMSE channel estimate $\hat{\mathbf{h}}_{f,\mathrm{MMSE}}$, PN is then estimated to minimize the following MSE:

$$\mathbf{P}_1 = \arg\min_{\mathbf{P}_1}\left|\left|\left(\mathbf{y}_1 - \mathbf{P}_1\mathbf{F}^H\mathbf{S}_1\mathbf{h}_f\right)\Big|_{\mathbf{h}_f=\hat{\mathbf{h}}_{f,\mathrm{MMSE}}}\right|\right|_2^2. \tag{5.20}$$

Let $\mathbf{B} = N\mathbf{F}^H\mathbf{S}_1\breve{\mathbf{F}}\boldsymbol{\Sigma}\breve{\mathbf{F}}^H\mathbf{S}_1^H\left(N\mathbf{S}_1\breve{\mathbf{F}}\boldsymbol{\Sigma}\breve{\mathbf{F}}^H\mathbf{S}_1^H + \sigma_{\mathbf{w}}^2\mathbf{I}\right)^{-1}\mathbf{F}$. Then the cost function in (5.20) can be rewritten as

$$\begin{aligned} C(\mathbf{P}_1) &= \left|\left|\left(\mathbf{y}_1 - \mathbf{P}_1\mathbf{F}^H\mathbf{S}_1\mathbf{h}_f\right)\Big|_{\mathbf{h}_f=\hat{\mathbf{h}}_{f,\mathrm{MMSE}}}\right|\right|_2^2 \\ &= \left|\left|\mathbf{y}_1 - \mathbf{P}_1\mathbf{B}\mathbf{P}_1^H\mathbf{y}_1\right|\right|_2^2 \\ &= \mathbf{y}_1^H\mathbf{y}_1 - \mathbf{y}_1^H\mathbf{P}_1\left(\mathbf{B}+\mathbf{B}^H\right)\mathbf{P}_1^H\mathbf{y}_1 + \mathbf{y}_1^H\mathbf{P}_1\mathbf{B}^H\mathbf{B}\mathbf{P}_1^H\mathbf{y}_1 \\ &= \mathbf{y}_1^H\mathbf{P}_1\left(\mathbf{I} - 2\mathbf{B} + \mathbf{B}^H\mathbf{B}\right)\mathbf{P}_1^H\mathbf{y}_1. \end{aligned} \tag{5.21}$$

The last equation in (5.21) is derived based on the fact that $\mathbf{P}_1\mathbf{P}_1^H = \mathbf{I}$ and $\mathbf{B}$ is a Hermitian matrix, i.e., $\mathbf{B} = \mathbf{B}^H$. Thus, the optimization problem (5.20) becomes

$$\mathbf{P}_1 = \arg\min_{\mathbf{P}_1}\mathbf{y}_1^H\mathbf{P}_1\left(\mathbf{I} - 2\mathbf{B} + \mathbf{B}^H\mathbf{B}\right)\mathbf{P}_1^H\mathbf{y}_1. \tag{5.22}$$

Define $\mathbf{U} = (\mathbf{I} - 2\mathbf{B} + \mathbf{B}^H\mathbf{B})$, which is a Hermitian matrix, $\mathbf{Y}_1 = \mathrm{diag}\left[\mathbf{y}_1\right]$, and $\boldsymbol{\rho} = \begin{bmatrix}\rho_0 & \rho_1 & \cdots & \rho_{N-1}\end{bmatrix}^T = \mathrm{diag}\left[\mathbf{P}_1\right]^H$. Then the optimization problem (5.22) can be rewritten as

$$\begin{aligned} &\underset{\boldsymbol{\rho}}{\text{minimize}} \quad \boldsymbol{\rho}^H\mathbf{Y}_1^H\mathbf{U}\mathbf{Y}_1\boldsymbol{\rho} \\ &\text{subject to} \quad |\rho_i| = 1; \quad i = 0, 1, \cdots, N-1. \end{aligned} \tag{5.23}$$

A similar form of the optimization problem (5.23) can be found in [31,32,34]. Similar to [34], the majorization-minimization algorithm is applied to solve (5.23). The principle behind the majorization-minimization algorithm is to transform a difficult problem into a series of simpler problems. This algorithm consists of two steps. In the first step, i.e., majorization, a surrogate function needs to be found which locally approximates the objective function at the current point. In the second step, i.e., minimization, the surrogate function is minimized.

From (5.23), define $\mathbf{V} = \mu_{\max}\mathbf{I}_{N\times N}$ where $\mu_{\max}$ is the maximum eigenvalue of $\mathbf{U}$. The surrogate function corresponding to the objective function in (5.23) is [38]

$$g(\boldsymbol{\rho}) = \boldsymbol{\rho}^H\mathbf{Y}_1^H\mathbf{V}\mathbf{Y}_1\boldsymbol{\rho} + 2\Re(\boldsymbol{\rho}^H\mathbf{Y}_1^H(\mathbf{U}-\mathbf{V})\mathbf{Y}_1\boldsymbol{\rho}_t) + \boldsymbol{\rho}_t^H\mathbf{Y}_1^H(\mathbf{V}-\mathbf{U})\mathbf{Y}_1\boldsymbol{\rho}_t \tag{5.24}$$

in which $\boldsymbol{\rho}_t$ is an arbitrary vector. The first and third terms in (5.24) are constants and independent of $\boldsymbol{\rho}$. Thus, minimizing $g(\boldsymbol{\rho})$ in the second step is equivalent to minimizing the second term in (5.24). Hence the optimization problem (5.23) becomes

$$\begin{aligned} \underset{\boldsymbol{\rho}}{\text{minimize}} \quad & \Re(\boldsymbol{\rho}^H\mathbf{Y}_1^H(\mathbf{U}-\mathbf{V})\mathbf{Y}_1\boldsymbol{\rho}_t) \\ \text{subject to} \quad & |\rho_i| = 1; \quad i = 0, 1, \cdots, N-1. \end{aligned} \tag{5.25}$$

A closed-form solution for (5.25) is obtained as:

$$\boldsymbol{\rho}_{t+1} = \mathrm{e}^{j\arg(\mathbf{Y}_1^H(\mathbf{U}-\mathbf{V})\mathbf{Y}_1\boldsymbol{\rho}_t)}. \tag{5.26}$$

A proof for (5.26) is given in Appendix 5.7.2.

In summary, to find a solution for the optimization problem (5.23), $\boldsymbol{\rho}_t$ is first initialized at $t = 0$, i.e., $\boldsymbol{\rho}_0$, and then substituted into (5.26) to obtain $\boldsymbol{\rho}_1$. Next, $\boldsymbol{\rho}_1$ is substituted into (5.26) to obtain $\boldsymbol{\rho}_2$ and so on. The algorithm terminates after a predefined number of iterations N_i or when the squared ℓ_2-norm of the difference over two consecutive iterations is smaller than a predefined threshold. The estimated PN is then substituted into (5.18) to finally obtain the estimated channel frequency response.

The computational complexity of the first stage is proportional to the number of iterations performed on (5.26). It is pointed out that $\mathbf{G} = \mathbf{Y}_1^H(\mathbf{U}-\mathbf{V})\mathbf{Y}_1$ in (5.26) is a constant and is computed once before any iterations. Thus, for each iteration, the computational

complexity is determined by the multiplication between $\mathbf{G}$ and $\boldsymbol{\rho}_t$, which requires N^2 complex multiplications and $N(N-1)$ complex additions. For other parameters, they are also computed once before any iterations. Furthermore, their computational complexities can be reduced by utilizing the facts that: (i) the first stage is performed based on the transmission of the designed preamble which satisfies the condition that $\mathbf{S}_1$ is a diagonal matrix and $\mathbf{S}_1\mathbf{S}_1^H = \mathbf{S}_1^H\mathbf{S}_1 = \mathbf{I}$, and (ii) the statistical characteristics of the channel and noise do not change much from one frame, hence $\boldsymbol{\Sigma}$ and $\sigma_{\mathbf{w}}$ can be considered as constants.

For example, matrix $\mathbf{B}$ can be rewritten as

$$\begin{aligned}\mathbf{B} &= N\mathbf{F}^H\mathbf{S}_1\breve{\mathbf{F}}\boldsymbol{\Sigma}\breve{\mathbf{F}}^H\mathbf{S}_1^H\left(N\mathbf{S}_1\breve{\mathbf{F}}\boldsymbol{\Sigma}\breve{\mathbf{F}}^H\mathbf{S}_1^H + \sigma_{\mathbf{w}}^2\mathbf{I}\right)^{-1}\mathbf{F} \\ &\overset{(5.40)}{=} N\mathbf{F}^H\mathbf{S}_1\breve{\mathbf{F}}\boldsymbol{\Sigma}\left(N\breve{\mathbf{F}}^H\breve{\mathbf{F}}\boldsymbol{\Sigma} + \sigma_{\mathbf{w}}^2\mathbf{I}\right)^{-1}\breve{\mathbf{F}}^H\mathbf{S}_1^H\mathbf{F} \\ &\overset{(5.40)}{=} \mathbf{F}^H\mathbf{S}_1\mathbf{T}\mathbf{S}_1^H\mathbf{F}\end{aligned} \tag{5.27}$$

where $\mathbf{T} = N\breve{\mathbf{F}}\boldsymbol{\Sigma}\breve{\mathbf{F}}^H\left(N\breve{\mathbf{F}}\boldsymbol{\Sigma}\breve{\mathbf{F}}^H + \sigma_{\mathbf{w}}^2\mathbf{I}\right)^{-1}$. In the above equation, the computational complexity due to matrix inversion is significantly reduced from inverting an $N \times N$ matrix to inverting a $\mu \times \mu$ matrix, where $\mu \ll N$. The matrix $\mathbf{T}$ is constant and does not depend on the transmitted preamble. Only the DFT of the preamble, i.e., $\mathbf{F}^H\mathbf{S}_1$, needs to be computed for every frame to update $\mathbf{B}$. Similarly, the computation of $\mathbf{B}^H\mathbf{B}$ is

$$\mathbf{B}^H\mathbf{B} = \mathbf{F}^H\mathbf{S}_1\mathbf{T}^2\mathbf{S}_1^H\mathbf{F} \tag{5.28}$$

which requires the update of $\mathbf{F}^H\mathbf{S}_1$ for every frame only.

5.4 Phase Noise Compensation and Data Detection

In this part, the MMSE-based estimated channel obtained from the previous section shall be used together with pilot symbols to compensate for PN and detect the transmitted signal in the data transmission phase. To estimate and compensate for PN, the PN vector shall be represented using known basis vectors. To this end, define $\boldsymbol{\Xi}_i = \begin{bmatrix}\boldsymbol{\xi}_i^0 & \boldsymbol{\xi}_i^1 & \cdots & \boldsymbol{\xi}_i^{F-1}\end{bmatrix}$, which contains F basis vectors, in which $\boldsymbol{\xi}_i^f = \begin{bmatrix}\xi_i^{f,0} & \xi_i^{f,1} & \cdots & \xi_i^{f,N-1}\end{bmatrix}^T$. The F basis vectors are chosen either from N columns of the DFT matrix or from N eigenvectors corresponding to the F largest eigenvalues of the PN covariance matrices as given in (5.6) and (5.7) for

FR PN and PLL PN, respectively. Also define $\boldsymbol{\gamma}_i = \begin{bmatrix} \gamma_{i,0} & \gamma_{i,1} & \cdots & \gamma_{i,F-1} \end{bmatrix}^T$. In order to compensate for the PN, the goal is to estimate $\boldsymbol{\gamma}_i$ such that $\text{diag}\left[\boldsymbol{\Xi}_i \boldsymbol{\gamma}_i\right] \simeq \mathbf{P}_i^H$. Then, $\boldsymbol{\Xi}_i \boldsymbol{\gamma}_i$ can be used to de-rotate the received signal in the time domain prior to the DFT transform.

Specifically, given the estimated channel frequency response, i.e., $\hat{\boldsymbol{\Gamma}} = \text{diag}[\hat{\mathbf{h}}_{f,\text{MMSE}}]$, the demodulated signal for the ith transmission block after PN compensation can be written as

$$\hat{\mathbf{d}}_i = \Re\left\{\mathbf{A}^H \mathbf{F}^H \hat{\boldsymbol{\Gamma}}^{-1} \mathbf{F} \text{diag}\left[\mathbf{P}_i \mathbf{H}_{\text{circ}} \mathbf{A} \mathbf{d}_i + \mathbf{w}_i\right] \boldsymbol{\Xi}_i \boldsymbol{\gamma}_i\right\} = \Re\left\{\boldsymbol{\Delta}_i \boldsymbol{\gamma}_i\right\}. \tag{5.29}$$

Denote $\mathbf{p} = \{p_0, p_1, \cdots, p_{Q-1}\}$ as a set of pilot indexes in each transmission block, and the transmitted signal corresponding to the pilot index set as $\mathbf{d}_i^{[\mathbf{p}]} = \begin{bmatrix} d_i^{p_0} & d_i^{p_1} & \cdots & d_i^{p_{Q-1}} \end{bmatrix}^T$. Then, $\boldsymbol{\gamma}_i$ can be estimated to minimize the MSE between the originally transmitted pilots and the estimated pilots as

$$\boldsymbol{\gamma}_i = \arg\min_{\boldsymbol{\gamma}_i} \left|\left| \mathbf{d}_i^{[\mathbf{p}]} - \Re\left\{\boldsymbol{\Delta}_i^{[\mathbf{p}]} \boldsymbol{\gamma}_i\right\} \right|\right|_2^2 \tag{5.30}$$

where $\boldsymbol{\Delta}_i^{[\mathbf{p}]}$ is a $Q \times F$ matrix obtained by keeping Q rows of $\boldsymbol{\Delta}_i$ with respect to the pilot index set $\mathbf{p}$. The matrix $\Re\left\{\boldsymbol{\Delta}_i^{[\mathbf{p}]} \boldsymbol{\gamma}_i\right\}$ is expanded as

$$\begin{aligned} \Re\left\{\boldsymbol{\Delta}_i^{[\mathbf{p}]} \boldsymbol{\gamma}_i\right\} &= \begin{bmatrix} \Re\left\{\delta_i^{0,0}\right\} & \Im\left\{\delta_i^{0,0}\right\} & \cdots & \Re\left\{\delta_i^{0,F-1}\right\} & \Im\left\{\delta_i^{0,F-1}\right\} \\ \Re\left\{\delta_i^{1,0}\right\} & \Im\left\{\delta_i^{1,0}\right\} & \cdots & \Re\left\{\delta_i^{1,F-1}\right\} & \Im\left\{\delta_i^{1,F-1}\right\} \\ \vdots & \vdots & \cdots & \vdots & \vdots \\ \Re\left\{\delta_i^{Q-1,0}\right\} & \Im\left\{\delta_i^{Q-1,0}\right\} & \cdots & \Re\left\{\delta_i^{Q-1,F-1}\right\} & \Im\left\{\delta_i^{Q-1,F-1}\right\} \end{bmatrix} \begin{bmatrix} \Re\left\{\gamma_{i,0}\right\} \\ -\Im\left\{\gamma_{i,0}\right\} \\ \cdots \\ \Re\left\{\gamma_{i,F-1}\right\} \\ -\Im\left\{\gamma_{i,F-1}\right\} \end{bmatrix} \\ &= \hat{\boldsymbol{\Delta}}_i \tilde{\boldsymbol{\gamma}}_i \end{aligned} \tag{5.31}$$

where $\delta_i^{k,j}$ denotes the (k,j)th element of matrix $\boldsymbol{\Delta}_i^{[\mathbf{p}]}$. Furthermore, vector $\boldsymbol{\gamma}_i$ is related to $\tilde{\boldsymbol{\gamma}}_i$ as

$$\boldsymbol{\gamma}_i = \begin{bmatrix} 1 & -j & 0 & 0 & \cdots & 0 & 0 \\ 0 & 0 & 1 & -j & \cdots & 0 & 0 \\ \vdots & \vdots & \vdots & \vdots & \cdots & \vdots & \vdots \\ 0 & 0 & 0 & 0 & \cdots & 1 & -j \end{bmatrix} \tilde{\boldsymbol{\gamma}}_i$$

where $\tilde{\boldsymbol{\gamma}}_i$ can be found by solving

$$\tilde{\boldsymbol{\gamma}}_i = \arg\min_{\tilde{\boldsymbol{\gamma}}_i} ||\mathbf{d}_i^{[\mathbf{p}]} - \hat{\boldsymbol{\Delta}}_i \tilde{\boldsymbol{\gamma}}_i||_2^2 \tag{5.32}$$

which yields $\tilde{\boldsymbol{\gamma}}_i = \hat{\boldsymbol{\Delta}}_i^{\dagger}\mathbf{d}_i^{[\mathbf{p}]}$. To avoid the singularity when performing the matrix inverse in $\hat{\boldsymbol{\Delta}}_i^{\dagger}$, the number of pilots should be greater than or equal to the number of bases.

Compared to the iterative PN compensation algorithm proposed in [35], where the PN estimation is based on a one-tap LMS algorithm, the second stage proposed in this paper has higher computational complexity due to the matrix multiplication and inversion in (5.32). It is noted, however, that the complexity in (5.32) only depends on the numbers of bases and pilots which are much smaller than N. As will be shown later, good PN compensation performance can be achieved even when the numbers of bases and pilots are not too large. Furthermore, compared to the iterative PN compensation algorithm in [35], the second stage in our proposed algorithm does not require any iterations. Thus, the proposed algorithm is expected to have lower latency than the one in [35] when a long transmission block is considered.

The proposed PN compensation algorithm is summarized as in Algorithm 1. It contains two stages. The estimation in the first stage is initialized with $\boldsymbol{\rho}_0 = \mathbf{1}$ in order to obtain the PN estimate in (5.26) after N_i iterations. Given the estimated PN, i.e., $\mathbf{P}_1 = \text{diag}[\boldsymbol{\rho}_{N_i}]^H$, the channel then can be estimated based on (5.18). In the second stage, given the estimated channel obtained from the first stage, i.e., $\hat{\boldsymbol{\Gamma}} = \text{diag}[\hat{\mathbf{h}}_{f,\text{MMSE}}]$, as well as the transmitted pilot symbols, which are determined by the pilot index set $\mathbf{p}$, the PN corresponding to the ith data transmission block, which is represented using a known basis matrix $\boldsymbol{\Xi}_i$ and an unknown coefficient vector $\boldsymbol{\gamma}_i$, can be estimated by obtaining an estimate of $\boldsymbol{\gamma}_i$ from (5.32). Given the estimated PN, the impact of PN can be compensated accordingly.

5.5 Simulation Results

In this section, performance of the proposed two-stage PN compensation algorithm is evaluated in different scenarios and with parameters listed in Table A.1. Among many shaping filters [8], the linear-phase square-root raised cosine (SRRC) and Martin [9], which are widely adopted in single-carrier data transmissions, can also be used as prototype filters in FBMC-based systems as long as the underlying channel is slowly varying. As such, the

Algorithm 1 Two-stage phase noise compensation

// Stage 1:

$\mathbf{T} = N\mathbf{S}_1\breve{\mathbf{F}}\mathbf{\Sigma}\breve{\mathbf{F}}^H\mathbf{S}_1^H$;

$\mathbf{B} = \mathbf{F}^H\mathbf{T}\left(\mathbf{T} + \sigma_{\mathbf{w}}^2\mathbf{I}\right)^{-1}\mathbf{F}$;

$\mathbf{U} = \mathbf{I} - 2\mathbf{B} + \mathbf{B}^H\mathbf{B}$;

$\mathbf{V} = \mu_{\max}\mathbf{I}$, $\mu_{\max}$ is the maximum eigenvalue of $\mathbf{U}$;

Initialize: $t \leftarrow 0$; $\boldsymbol{\rho}_t \leftarrow \mathbf{1}$;

while $(t < N_i)$ **do**

    $\boldsymbol{\rho}_{t+1} = \mathrm{e}^{j\arg(\mathbf{Y}_1^H(\mathbf{U}-\mathbf{V})\mathbf{Y}_1\boldsymbol{\rho}_t)}$;

    $t = t + 1$;

end while

return $\boldsymbol{\rho}_{N_i}$;

$\mathbf{P}_1 = \mathrm{diag}[\boldsymbol{\rho}_{N_i}]^H$;

$\hat{\mathbf{h}}_{f,\mathrm{MMSE}} = N\breve{\mathbf{F}}\mathbf{\Sigma}\breve{\mathbf{F}}^H\mathbf{S}_1^H(\mathbf{T} + \sigma_{\mathbf{w}}^2\mathbf{I})^{-1}\mathbf{F}\mathbf{P}_1^H\mathbf{y}_1$;

// Stage 2:

$\hat{\mathbf{\Gamma}} = \mathrm{diag}[\hat{\mathbf{h}}_{f,\mathrm{MMSE}}]$;

for $i = 2$ **to** N_b **do**

    $\mathbf{p} \Rightarrow \mathbf{d}_i^{[\mathbf{p}]}$;

    $\mathbf{\Delta}_i = \mathbf{A}^H\mathbf{F}^H\hat{\mathbf{\Gamma}}^{-1}\mathbf{F}\mathrm{diag}\left[\mathbf{y}_i\right]\mathbf{\Xi}_i$; $\mathbf{\Delta}_i \Rightarrow \hat{\mathbf{\Delta}}_i$;

    $\tilde{\boldsymbol{\gamma}}_i = \hat{\mathbf{\Delta}}_i^{\dagger}\mathbf{d}_i^{[\mathbf{p}]}$; $\tilde{\boldsymbol{\gamma}}_i \Rightarrow \boldsymbol{\gamma}_i$;

    $\mathbf{P}_i^H = \mathrm{diag}\left[\mathbf{\Xi}_i\boldsymbol{\gamma}_i\right]$;

    $\hat{\mathbf{y}}_i = \mathbf{P}_i^H\mathbf{y}_i$;

    Decoding $\hat{\mathbf{y}}_i$;

end for

SRRC and Martin filters shall be considered in this paper[3]. Because of the difference in the signal types being transmitted in the preamble and data blocks, performance in this section is evaluated with respect to the received signal-to-noise ratio (SNR). Two highly frequency-

[3]It might be interesting to examine other prototype filters such as the extended Gaussian filter (EGF) [55, 56], which has better time-frequency localization property.

Table A.1: Simulation parameters

Channel coding	Convolutional code (Rate: 1/3; Constraint length: 7; Generator polynomials: $[133\ 171\ 165]_8$);
Channel decoding	Hard-decision Viterbi decoding;
Modulation	16-QAM;
Block structure	$K = 128; M = 6;$
Prototype filter	Martin; SRRC (Roll-off factor: 0.5);
Number of blocks per frame	$N_b = 10;$
Carrier frequency	$f_c = 6$ GHz; [39]
Bandwidth	$B = 100$ MHz;
Sampling interval	$T_s = 1/B;$
Channel [54]	EPA ($L = 41$); EVA ($L = 251$);
Phase noise [45]	$c_v = 5 \times 10^{-18}$; $c_r = 10^{-23}$

selective channel models, namely the extended pedestrian A (EPA) and extended vehicular A (EVA), are considered in this paper. In the transmitter, a CP length of $L = 41$ or $L = 251$ samples is added into the signal when EPA or EVA is considered, respectively.

5.5.1 Preamble design for channel estimation

First, the preambles designed to mitigate the performance degradation in CFBMC-OQAM compared to OFDM due to imperfect channel estimation corresponding to SRRC and Martin filters are illustrated in Fig. 5.2. To intuitively show the difference between them, a short transmission block is applied where the numbers of sub-carriers and time slots are $K = 64$ and $2M = 6$, respectively. In this figure, $\mathbf{S}_1$ is simply chosen as an identity matrix to satisfy the condition (5.14). As such, the proposed preamble is obtained as

$$\mathbf{d}_1 = \Re\left\{\mathbf{A}^H \mathbf{F}^H \mathbf{1}_{N\times 1}\right\}. \tag{5.33}$$

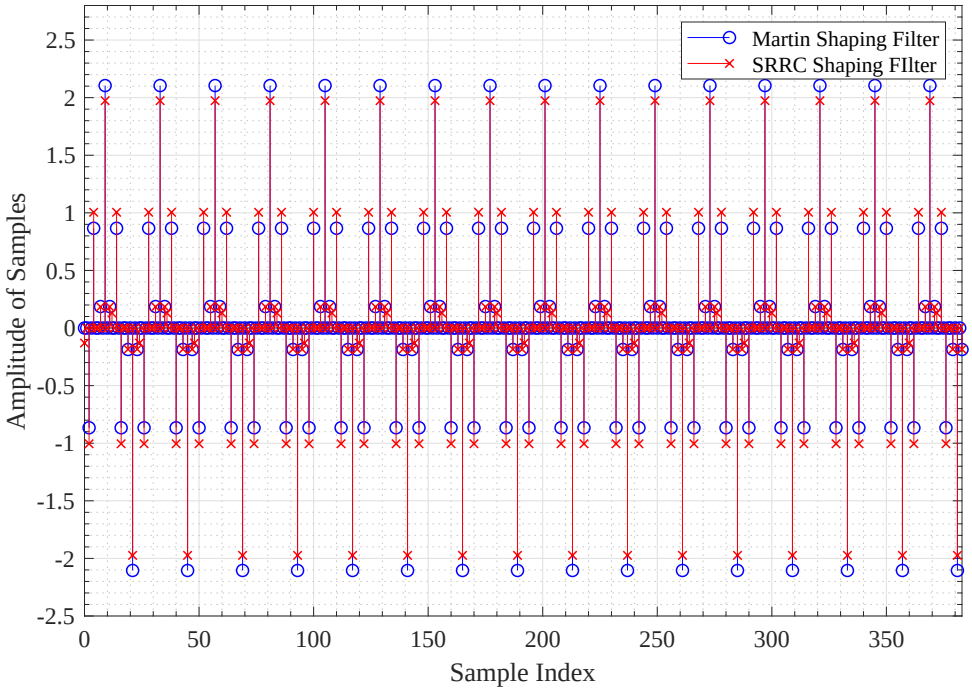

Figure 5.2: The designed preamble $\mathbf{d}_1$ when $K = 64$, $M = 3$, $\mathbf{S}_1 = \mathbf{I}_{N\times N}$, and Martin and SRRC shaping filters are deployed.

In Fig. 5.2, it is observed that applying different prototype shaping filters results in different preamble patterns.

Performance comparisons of different preamble designs in terms of MSE and BER over EPA channel are plotted in Fig. 5.3 when there is no PN (i.e., $\mathbf{P}_1$ is replaced by an identity matrix in (5.18)). Performance curves of OFDM are included as benchmarks. In simulation, "Random Preamble" refers to the case that each symbol in the OFDM preamble is randomly generated from 16-QAM modulation, while each symbol in the CFBMC-OQAM preamble is either a real or an imaginary part of a randomly-generated 16-QAM symbol. On the other hand, "Proposed Preamble" means that the OFDM preamble contains randomly-generated BPSK symbols, while in CFBMC-OQAM, each element in $\mathbf{S}_1$ is a randomly-generated BPSK symbol to satisfy the unit-magnitude condition in (5.14). It is noted that OFDM preamble is a $N \times 1$ vector while it is a $2N \times 1$ vector for CFBMC-OQAM preamble. Also for simplicity, in presenting the following results, only the Martin filter is considered.

It is first observed from Fig. 5.3 that when a "Random Preamble" and LS estimation

are deployed, there is a large performance degradation of about 6.8 dB at MSE = 10^{-3} in CFBMC-OQAM compared to that in OFDM. While in terms of BER, the performance loss of CFBMC-OQAM is approximately 4.1 dB at BER = 10^{-5} compared to that in OFDM under the same configuration. However, when the proposed preambles are applied in both OFDM and CFBMC-OQAM, the performance of CFBMC-OQAM in terms of MSE is almost the same as that in OFDM for both LS and MMSE channel estimation methods. For BER performance, there are only about 1.1 dB and 0.6 dB losses at BER = 10^{-5} for CBMC-OQAM compared to OFDM when LS and MMSE methods are deployed, respectively.

For CFBMC-OQAM, the proposed preamble helps to gain approximately 9.6 dB and 30.0 dB at MSE = 10^{-3} when LS and MMSE are used, respectively, compared to when a random preamble is deployed. While in terms of BER performance, these gains are around 4.2 dB and 7.9 dB at BER = 10^{-5}, respectively.

It is pointed out that at high SNR, performance of the MMSE channel estimator approaches that of the LS channel estimator, provided that these estimators operate in the time domain and that the channel taps are statistically independent (which is a common assumption in the literature). The behavior is, however, different for the MMSE and LS

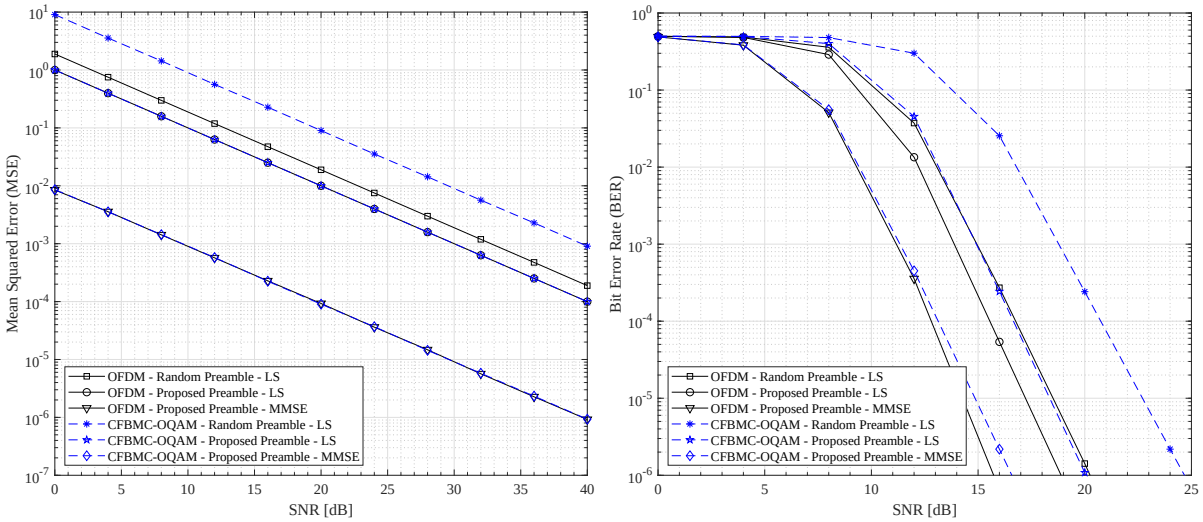

(a) MSE (b) BER

Figure 5.3: Performance comparisons in terms of (a) MSE and (b) BER for different preamble designs over EPA channel when $K = 128$, $M = 6$ and Martin shaping filter is deployed.

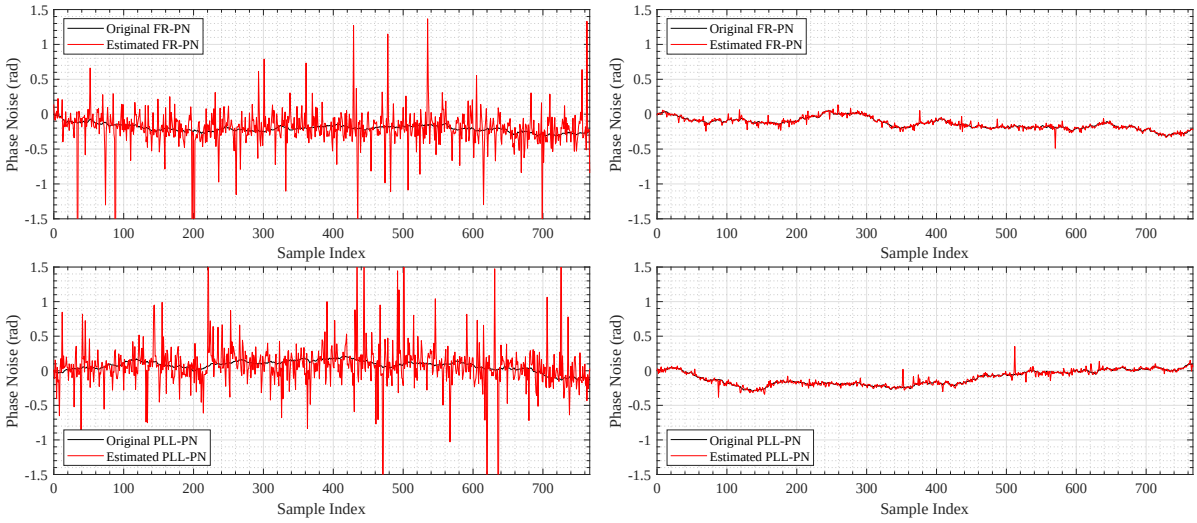

(a) SNR = 15 dB (b) SNR = 35 dB

Figure 5.4: Estimated PN in the first stage over EPA channel when $K = 128$, $M = 6$ and Martin shaping filter is deployed.

channel estimators operating in the frequency domain, as in this paper. This is because, as long as the number of subchannels in the frequency domain is larger than the number of channel taps in the time domain (which is typically the case in practice), the subchannels in the frequency domain are correlated. Since the MMSE estimator takes into account the correlation of the subchannels as well as the noise statistics, it consistently outperforms the LS estimator (which does not make use of the subchannels correlation or noise statistics). In fact, a similar performance gap (even at high SNR) between the frequency-domain MMSE and LS channel estimators is also observed for the OFDM systems in [46].

5.5.2 Stage 1: Estimation of PN and channel frequency response

From this part, impact of PN is included in simulation results. The PN estimation algorithm in Section 5.3.2 is initialized with $\boldsymbol{\rho}_0 = \mathbf{1}_{N\times 1}$. The number of iterations is set to $N_i = 150$. First, the estimated PN from the first stage is illustrated in Fig. 5.4 for SNR = 15 dB and SNR = 35 dB for both types of PN. In this figure, EPA channel is considered. It can be seen that although SNR = 15 dB is quite low, the algorithm can generally track the PN, but there are large fluctuations in the estimated PN. However, when increasing SNR to

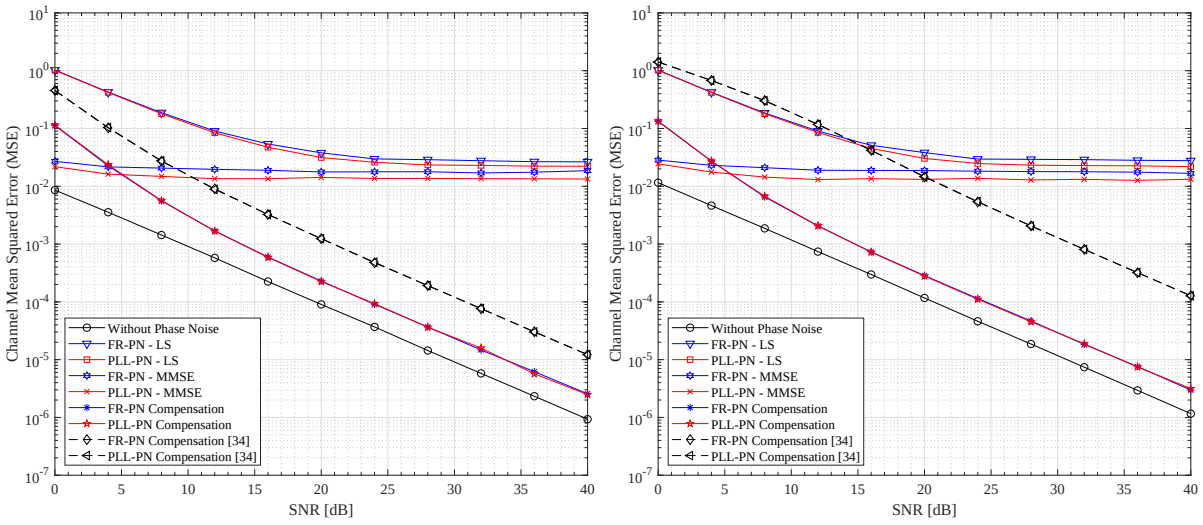

(a) EPA channel

(b) EVA channel

Figure 5.5: Channel MSE from the first stage under two PN models when $K = 128$, $M = 6$ and Martin shaping filter is deployed.

35 dB, the PN is estimated almost perfectly.

After obtaining the PN estimation in (5.26), the estimated PN is substituted into (5.18) to estimate the channel frequency response. An evaluation in terms of MSE for the channel estimation is demonstrated in Fig. 5.5 which contains two sub-figures 5.5a and 5.5b corresponding to EPA and EVA channels, respectively. In Fig. 5.5, the performance for the case when there is no PN and the MMSE-based channel estimate is employed (labeled as "Without Phase Noise"), serves as the lower bound. The performance curves under the presence of two PN types without PN compensation deploying LS and MMSE channel estimations are also included. Performance of the proposed algorithm in [34] is also added for two PN types. It is recalled that different from [34] in which the channel is estimated based on LS method, the channel is estimated based on MMSE method in this paper.

It can be seen from Fig. 5.5 that without PN compensation the system basically fails in estimating the channel as the channel MSE is always above 10^{-2} for the whole range of SNR in both sub-figures. It is also observed that the channel MSE performance when PLL-PN is present and no compensation is applied is lower than that when FR-PN is present for both LS and MMSE channel estimation methods. This is expected because the impact of FR-PN

is more significant than that of PLL-PN.

By applying the channel and PN estimation in the first stage of the two-stage algorithm, the channel MSE is significantly improved. Specifically, for EPA channel, there is only approximately 4.4 dB performance loss compared to the ideal case ("Without Phase Noise") at MSE $= 10^{-3}$. For EVA channel, this performance gap is around 4.1 dB at MSE $= 10^{-3}$. It can be observed that performances of the proposed channel estimation in the first stage are almost the same for two types of PN in both Figs. 5.5a and 5.5b.

The results in Fig. 5.5 show that, compared to the algorithm in [34], the proposed algorithm in this paper yields significant gains. Specifically, under the case of EPA channel, approximately 6.9 dB performance gain is achieved at MSE $= 10^{-3}$. This improvement is further increased to approximately 16.3 dB when the EVA channel is considered. It will be seen later that the performance gain brought by channel estimation in this stage significantly improves the PN compensation in the second stage of the proposed algorithm.

On the other hand, the degraded channel MSE in the low SNR observed from Fig. 5.5 is similar to the observation in [34]. This is caused by the susceptibility of the estimation in the first stage to the under-determination problem in the low SNR range, where the number of unknown variables is larger than the number of equations provided by the received signal.

It is interesting to see from Fig. 5.4a that, although there is a high fluctuation in the estimated PN compared to the real PN, the first stage still results in a better channel MSE performance compared to the case when no PN compensation is applied, i.e., by ignoring PN, as shown in Fig. 5.5. To explain this, define $\bar{\mathbf{y}}_1 = \mathbf{P}_1^H \mathbf{y}_1$ and $\tilde{\mathbf{y}}_1 = \hat{\mathbf{P}}_1^H \mathbf{y}_1$, where $\mathbf{P}_1$ and $\hat{\mathbf{P}}_1$ are the true PN and the estimated PN obtained from (5.26), respectively. This means that $\bar{\mathbf{y}}_1$ is the received signal without any effect of PN, whereas $\tilde{\mathbf{y}}_1$ is the received signal that experiences PN impact and PN compensation. From (5.18), without PN, the estimated channel is $\hat{\mathbf{h}}_{f,\text{MMSE}}^{(1)} = \mathbf{C}\bar{\mathbf{y}}_1$ where $\mathbf{C} = N\breve{\mathbf{F}}\mathbf{\Sigma}\breve{\mathbf{F}}^H\mathbf{S}_1^H \left(N\mathbf{S}_1\breve{\mathbf{F}}\mathbf{\Sigma}\breve{\mathbf{F}}^H\mathbf{S}_1^H + \sigma_{\mathbf{w}}^2\mathbf{I}\right)^{-1}\mathbf{F}$. In the presence of PN but without PN compensation, the estimated channel is obtained as $\hat{\mathbf{h}}_{f,\text{MMSE}}^{(2)} = \mathbf{C}\mathbf{y}_1$. However, if the first stage is deployed, i.e., the estimated PN in (5.26) is substituted into (5.18), the estimated channel is $\hat{\mathbf{h}}_{f,\text{MMSE}}^{(3)} = \mathbf{C}\tilde{\mathbf{y}}_1$. Obviously, whether channel

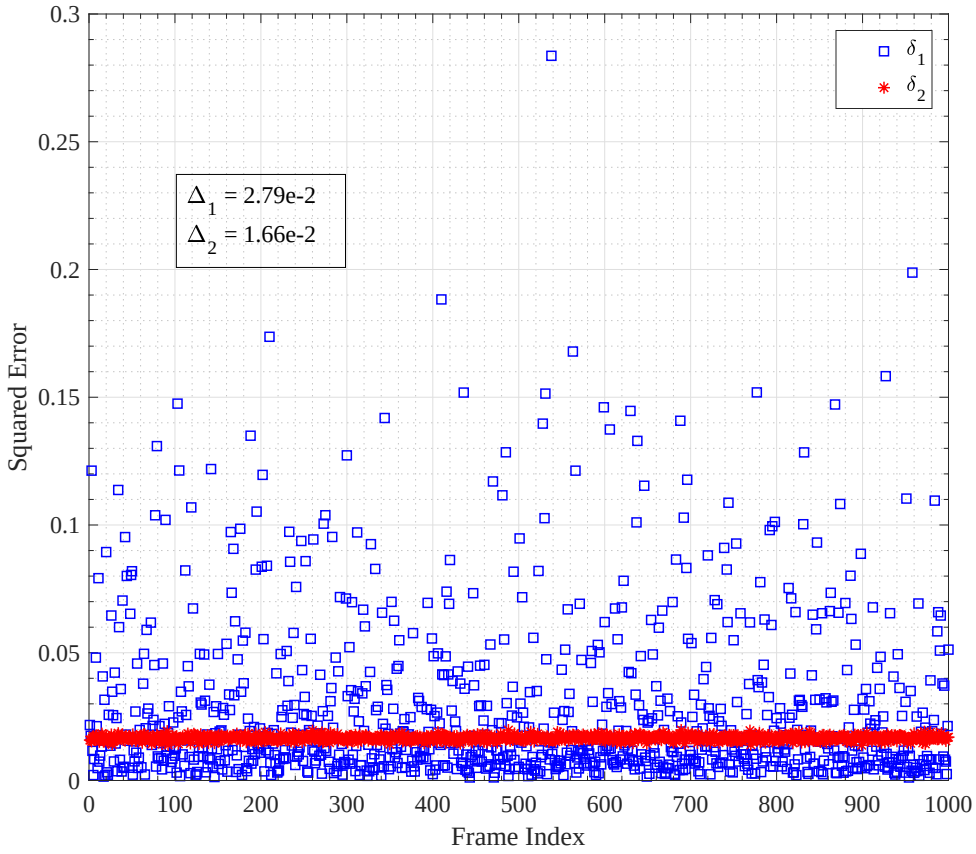

Figure 5.6: A comparison of squared errors between ($\mathbf{y}_1$, $\bar{\mathbf{y}}_1$) and ($\tilde{\mathbf{y}}_1$, $\bar{\mathbf{y}}_1$) over 1000 preamble frames at SNR = 15 dB.

estimate $\hat{\mathbf{h}}^{(2)}_{f,\text{MMSE}}$ or $\hat{\mathbf{h}}^{(3)}_{f,\text{MMSE}}$ is closer to $\hat{\mathbf{h}}^{(1)}_{f,\text{MMSE}}$ depends on whether $\mathbf{y}_1$ or $\tilde{\mathbf{y}}_1$ is closer to $\bar{\mathbf{y}}_1$ in the mean squared error sense. To see this, Fig. 5.6 displays squared errors between ($\mathbf{y}_1$, $\bar{\mathbf{y}}_1$), denoted as δ_1, and ($\tilde{\mathbf{y}}_1$, $\bar{\mathbf{y}}_1$), denoted as δ_2, over 1000 preamble frames and for SNR = 15 dB. It can be seen that there are cases where δ_1 is lower than δ_2, which means that the estimated PN in the first stage sometimes does not help to improve the received signal quality after performing PN compensation and thus does not improve channel estimation. However, the average value of δ_2, indicated in the figure as Δ_2, is considerably lower than the average value of δ_1, indicated as Δ_1. Therefore, on the average, the estimated PN still results in a lower MSE of the estimated channel as observed in Fig. 5.5.

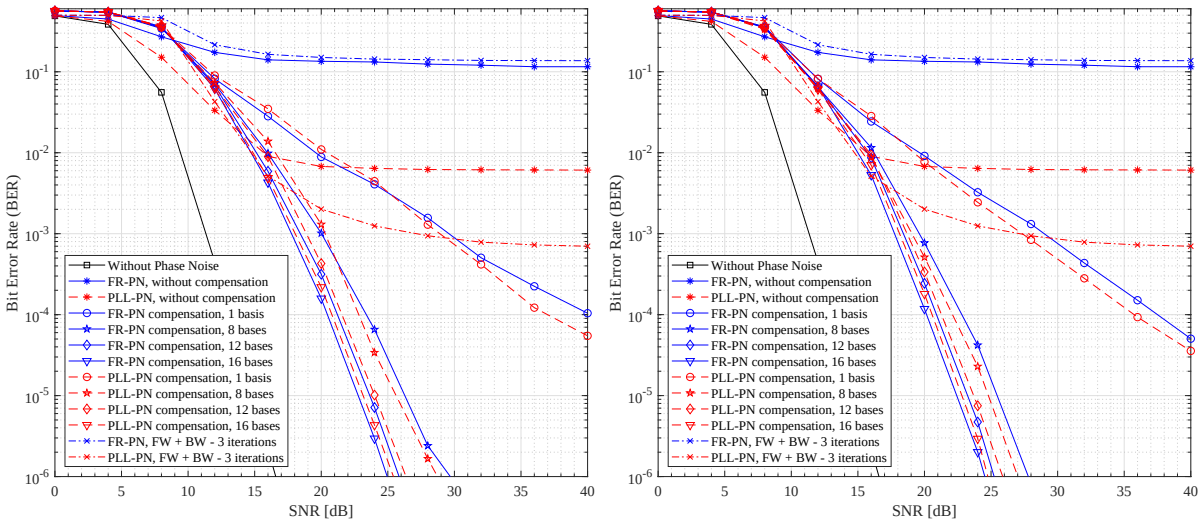

(a) Bases are from DFT matrix (b) Bases are from the PN covariance matrix

Figure 5.7: BER performance of the two-stage algorithm over EPA channel when $K = 128$, $M = 6$ and Martin shaping filter is deployed. The pilot ratio is 1/8.

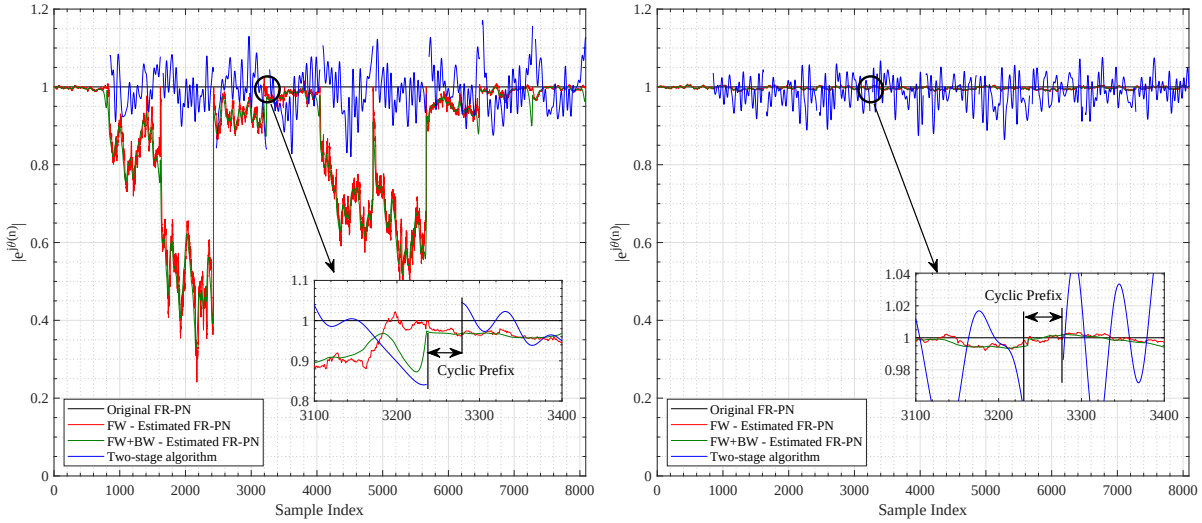

(a) $c_v = 5 \times 10^{-18}$ (b) $c_v = 1 \times 10^{-19}$

Figure 5.8: A comparison in the PN estimation between the proposed algorithm in this paper and the iterative algorithm in [35]. For the proposed algorithm in this paper, 16 bases are deployed which are taken from DFT matrix. The pilot ratio is 1/8 and SNR = 25 dB.

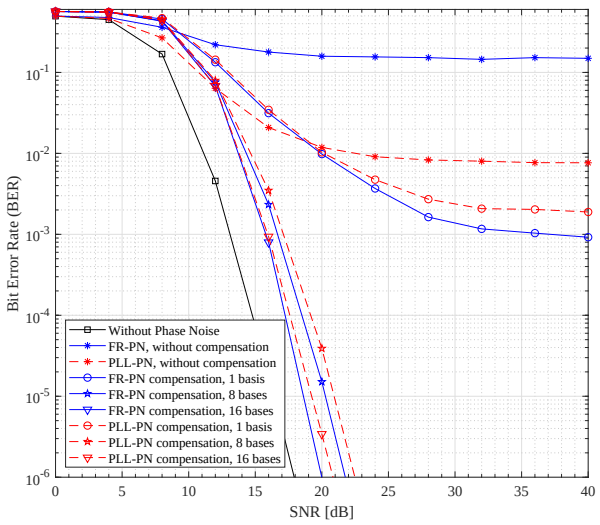

Figure 5.9: BER performance of the two-stage algorithm over EVA channel when $K = 128$, $M = 6$ and Martin shaping filter is deployed. Basis vectors are from the PN covariance matrix. The pilot ratio is 1/8.

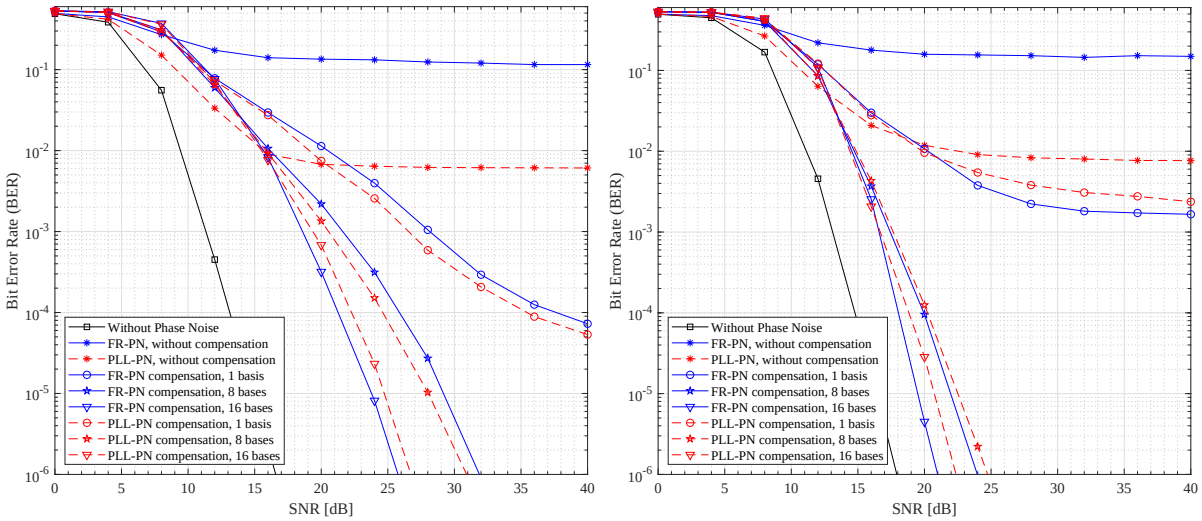

(a) EPA channel (b) EVA channel

Figure 5.10: BER performance of the two-stage algorithm when $K = 128$, $M = 6$ and Martin shaping filter is deployed. Basis vectors are from the PN covariance matrix. The pilot ratio is 1/16.

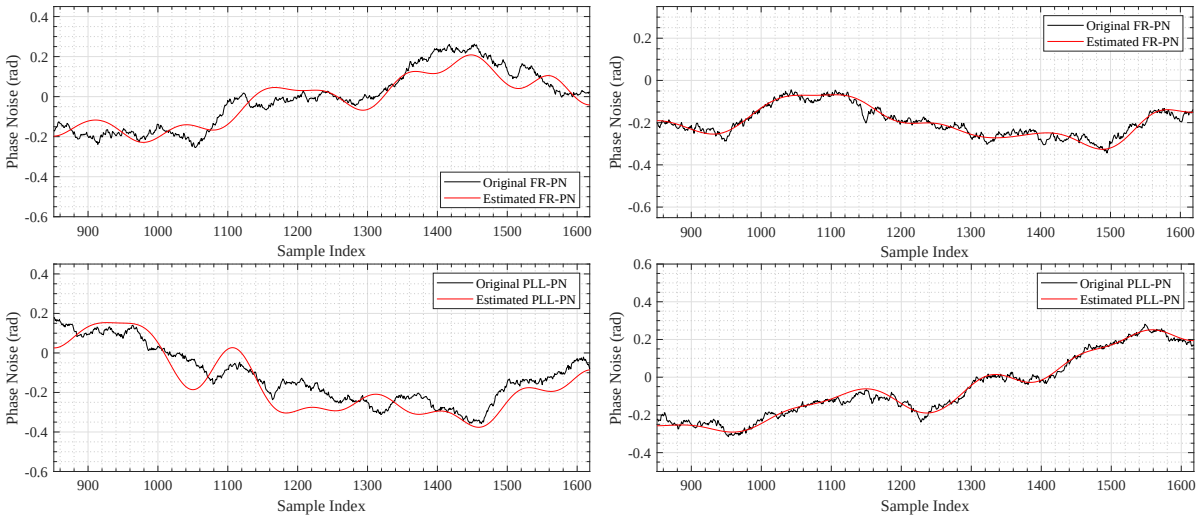

(a) SNR = 15 dB (b) SNR = 35 dB

Figure 5.11: Estimated PN from the second stage when $K = 128$, $M = 6$, $F = 16$ and basis vectors are from the PN covariance matrix. The pilot ratio is 1/8.

5.5.3 Stage 2: Data detection and phase noise compensation

To compensate for the PN and detect data, pilots are inserted into transmission frames. Two pilot patterns are considered in this paper. For the first pattern, which corresponds to the pilot ratio of approximately 1/8, 15 pilot symbols are inserted into each time slot of data transmission blocks at positions [7, 15, 23, 31, 39, 47, 55, 63, 71, 79, 87, 95, 103, 111, 119]. The second pattern has a pilot ratio of 1/16 in which 8 pilots are added at positions [7, 23, 39, 55, 71, 87, 103, 119].

BER performance of CFBMC-OQAM is first illustrated in Fig. 5.7 corresponding to when EPA channel is considered and the pilot ratio is 1/8. In this figure, performance of the case labeled as "Without Phase Noise" where PN is absent serves as the lower bound. There are two sub-figures in Fig. 5.7. The sub-figure on the left is for the case that F basis vectors are taken from N columns of the DFT matrix, while the sub-figure on the right is for the case when F basis vectors are taken from N eigenvectors of the PN covariance matrix $\mathbf{R}$ corresponding to the largest eigenvalues.

For comparison, Fig. 5.7 also includes performance obtained after 3 iterations of the

iterative PN compensation algorithm proposed in [35]. In each iteration of such an algorithm, a forward LMS procedure is first applied to estimate the PN which is then smoothened by a backward procedure. As such, the algorithm proposed in [35] is referred to as "FW+BW" in Fig. 5.7. As suggested in [35], the estimation step sizes for the forward and backward procedures are selected as $\mu_\phi = 0.1$ and $\lambda_\phi = 1 - \mu_\phi$, respectively.

First, without PN compensation, the impact of FR-PN is much more severe than that from PLL-PN as expected. It can be seen from Fig. 5.7 that PN compensation performance is significantly improved when the number of bases increases. Specifically, for FR-PN distortion, at BER = 10^{-5}, performance gap between the ideal case, i.e., "Without Phase Noise", and "FR-PN compensation" reduces from 11.4 dB to 7.9 dB when 8 and 16 DFT-matrix-based basis vectors are considered, respectively. Similarly, for PLL-PN distortion, approximately 2.5 dB performance gain is obtained when the number of DFT-based bases increases from 8 to 16 vectors. About 8.3 dB performance gap is observed between the ideal case and "PLL-PN compensation, 16 bases". A similar trend can be seen in Fig. 5.7b when the basis vectors are taken from the PN covariance matrix. However, performance of the proposed algorithm using the PN covariance matrix tends to be better than using DFT matrix, especially when a low number of basis vectors is considered. It can also be seen that increasing the number of bases from 12 to 16 does not improve much the performance of the proposed two-stage PN compensation algorithm. In particular, when the bases are obtained from the PN covariance matrices, only approximately 0.8 dB gain is observed at BER = 10^{-5} for both PN models.

Fig. 5.7 shows that applying the algorithm proposed in [35] does not result in good performance. To explain this, Fig. 5.8 (which contains two sub-figures) illustrate magnitudes of the estimated FR-PN in the forms of exponential function obtained from the proposed algorithm in the second stage in this paper (labeled as "Two-stage algorithm"), the algorithm in [35] when only the FW procedure is considered (labeled as "FW - Estimated FR-PN"), and the algorithm in [35] when both FW and BW procedures are considered (labeled as "FW+BW - Estimated FR-PN"). The sub-figure on the left is obtained when the quality factor $c_v = 5 \times 10^{-18}$, while the right sub-figure is for $c_v = 1 \times 10^{-19}$. The first quality factor

corresponds to FR-PN having a 3-dB bandwidth $\Delta f_{3\text{dB}}$ of over one thousand hertz, whereas the second quality factor corresponds to $\Delta f_{3\text{dB}}$ of dozens hertz.[4]

As can be seen from Fig. 5.8b, when the PN is small, the algorithm in [35] outperforms the algorithm proposed in this paper in tracking the PN. However, when the PN is large, significant fluctuations are observed for the estimated PN obtained from [35] in some specific positions as highlighted in Fig. 5.8a. It is worth noting that in [35], the PN compensation algorithm is performed for every transmission block and the PN corresponding to a symbol interval is estimated based on the estimated PN obtained for the previous symbol interval and the decoded signal. Thus, having decoding errors at the output of the channel decoder results in poor estimates of the PN. These errors consequently affect the PN estimation for the next symbol intervals. At the end, the errors are spread all over the whole transmission block. This error propagation phenomenon often happens when the decoding output is reused in an iterative algorithm. Consistent with the results illustrated in [35], performance of the iterative algorithm in terms of PER is still high due to the in-block error spreading. Another disadvantage of the iterative algorithm in [35] is the long latency.

Fig. 5.9 illustrates performance of the proposed algorithm when the EVA channel is considered. For this figure, the basis vectors are generated from the PN covariance matrix and the pilot ratio is 1/8. It can be seen that increasing the number of bases improves the performance and the improvement is better than when the EPA channel is considered. At BER = 10^{-5}, only about 2.5 dB performance gap is observed when 16 basis vectors are applied for two PN types compared to the ideal case.

Performance of the proposed algorithm for both EPA and EVA channels when the pilot ratio is 1/16 is presented in Fig. 5.10. In this figure, all bases are from the PN covariance matrix. As expected, decreasing the pilot ratio from 1/8 to 1/16 degrades performance of the proposed algorithm. For the EPA channel, the performance gaps between the proposed algorithm with 16 basis vectors and the ideal case without PN are about 8.9 dB and 9.9 dB for FR-PN and PLL-PN, respectively, at BER = 10^{-5} as seen in Fig. 5.10a. For the

[4]In FR-PN model, the 3-dB bandwidth $\Delta f_{3\text{dB}}$ is related to the quality factor c_v as $\Delta f_{3\text{dB}} \sim 2\pi c_v f_c^2$ [25,34].

EVA channel in Fig. 5.10b, these gaps are 3.1 dB and 4.3 dB for FR-PN and PLL-PN, respectively.

It can be seen from Figs. 5.7, 5.9 and 5.10 that the BER performance of the proposed two-stage algorithm is degraded in the low SNR range compared to when no compensation algorithm is deployed. First, this phenomenon comes directly from the degradation of the estimated channel MSE in the first stage due to the under-determination problem discussed earlier. Furthermore, the proposed PN estimation in the second stage is essentially similar to the approximation problem in which the PN is approximated by a high-degree polynomial based on a set of equispaced interpolation points which are the pilot symbols in this paper. It will be shown later that this approximation results in a high fluctuation of the estimated PN in the low SNR range and thus degrades the compensation performance.

Finally, the PN estimation based on pilots in the second stage is evaluated in Fig. 5.11 when SNR = 15 dB and SNR = 35 dB. Specifically, the PN in the second transmission block is plotted in Fig. 5.11. Thus, the symbol index in Fig. 5.11 runs from 851 to 1618. It can be seen that while the PN distortion is estimated very coarsely when SNR = 15 dB, the PN estimation is getting much better for both types of PN when SNR increases to 35 dB. From the results in Fig. 5.11, it appears that the PN is approximated by a high-degree curve. This is inline with the previous discussion on the similarity between the proposed PN estimation in the second stage and the approximation problem based on a set of equispaced interpolation points.

5.5.4 Spectral efficiency

In general, the proposed algorithm trades bandwidth efficiency for better PN compensation. For the specific system parameters considered in the simulation with $K = 128$ subcarriers, $2 \times M = 12$ time slots, there are $N = K \times M = 768$ QAM symbols in each block, which also means that $N = 768$ QAM symbols are used in the preamble for the first stage. For the simulation results in Fig. 5.7 with a pilot ratio of $1/8$, $N_p = 15 \times 6 = 90$ QAM pilot symbols are transmitted to estimate the PN in the second stage. Overall, the total number of QAM symbols used as preamble and pilots in the proposed two-stage algorithm

is:

$$N_{\text{tot}}^{(1)} = N + (N_b - 1) \times N_p = 768 + (10 - 1) \times 90 = 1578. \tag{5.34}$$

In [35], before performing the iterative PN compensation, initial channel estimation is performed based on the transmission of preambles. Then a CPE compensation operation is performed for every remaining transmission block in a frame based on the transmission of pilots. It is presented in [35] that a two-symbol preamble, which is equivalent to two transmission blocks in this paper, is transmitted in each frame for initial channel estimation. Using the pilot ratio of 1/32 as in [35], $N_p = 1/32 \times 768 = 24$ pilots are needed for CPE compensation per each transmission block. Therefore, the total number of QAM symbols used as preamble and pilots in the algorithm in [35] is:

$$N_{\text{tot}}^{(2)} = 2 \times N + (N_b - 2) \times N_p = 1728. \tag{5.35}$$

It can be seen from (5.34) and (5.35) that in this particular case the algorithm proposed in this paper has a better overall spectral efficiency than the one in [35]. However, if the number of blocks per frame increases, the algorithm in [35] will be better than the proposed two-state algorithm in terms of the spectral efficiency.

5.6 Conclusions

This paper has investigated the impact of PN on CFBMC-OQAM systems in the presence of imperfect channel estimation. First, it has been shown that there is a considerable performance gap between CFBMC-OQAM and OFDM under imperfect channel estimation. As such, a preamble design based on LS estimation has been proposed to reduce such performance gap. Simulation results indicated that applying the designed preamble results in a similar performance between CFBMC-OQAM and OFDM in terms of BER and MSE. In the presence of PN, the paper also proposed a two-stage algorithm to effectively estimate the channel frequency response and compensate for the PN impact. In particular, given the designed preamble, the channel frequency response and PN have been estimated in the first stage, in which the MMSE estimation method is employed to improve the channel estimation. In the second stage, the PN and data are estimated and detected based on the estimated

channel obtained in the first stage and pilot symbols. Performance of the proposed two-stage PN compensation algorithm has been verified in a various number of practical simulation scenarios. Simulation results clearly shown that the two-stage algorithm effectively estimates the channel frequency response and compensates for the impact of PN.

5.7 Appendix

5.7.1 Appendix B

Based on the received signal in (5.16), the MMSE channel is $\hat{\mathbf{h}}_{f,\text{MMSE}} = \hat{\mathbf{W}}\mathbf{y}_1$ where $\hat{\mathbf{W}}$ is a $N \times N$ weighting matrix that minimizes $\text{E}\left[||\mathbf{h}_f - \hat{\mathbf{h}}_{f,\text{MMSE}}||_2^2\right]$. Substituting $\hat{\mathbf{h}}_{f,\text{MMSE}} = \hat{\mathbf{W}}\mathbf{y}_1$ into the orthogonality condition in (5.17) results in

$$\begin{aligned} &\text{E}\left[\left(\mathbf{h}_f - \hat{\mathbf{W}}\mathbf{y}_1\right)\mathbf{y}_1^H\right] = \mathbf{0} \\ \Leftrightarrow\ &\text{E}\left[\mathbf{h}_f\mathbf{y}_1^H\right] - \hat{\mathbf{W}}\text{E}\left[\mathbf{y}_1\mathbf{y}_1^H\right] = \mathbf{0} \end{aligned} \tag{5.36}$$

Considering the first term in (5.36), one has

$$\begin{aligned} \text{E}\left[\mathbf{h}_f\mathbf{y}_1^H\right] &\overset{(5.16)}{=} \text{E}\left[\mathbf{h}_f\left(\mathbf{P}_1\mathbf{F}^H\mathbf{S}_1\mathbf{h}_f + \mathbf{w}_1\right)^H\right] \\ &= \text{E}\left[\mathbf{h}_f\mathbf{h}_f^H\right]\mathbf{S}_1^H\mathbf{F}\mathbf{P}_1^H \\ &= N\breve{\mathbf{F}}\mathbf{\Sigma}\breve{\mathbf{F}}^H\mathbf{S}_1^H\mathbf{F}\mathbf{P}_1^H \end{aligned} \tag{5.37}$$

The last equation in (5.37) is obtained based on the fact that $\mathbf{h}_f = \sqrt{N}\breve{\mathbf{F}}\mathbf{h}$.

The second term in (5.36) can be derived as

$$\begin{aligned} &\hat{\mathbf{W}}\text{E}\left[\mathbf{y}_1\mathbf{y}_1^H\right] \\ &\quad\overset{(5.16)}{=} \hat{\mathbf{W}}\text{E}\left[\left(\mathbf{P}_1\mathbf{F}^H\mathbf{S}_1\mathbf{h}_f + \mathbf{w}_1\right)\left(\mathbf{P}_1\mathbf{F}^H\mathbf{S}_1\mathbf{h}_f + \mathbf{w}_1\right)^H\right] \\ &\quad= \hat{\mathbf{W}}\text{E}\left[\mathbf{P}_1\mathbf{F}^H\mathbf{S}_1\mathbf{h}_f\mathbf{h}_f^H\mathbf{S}_1^H\mathbf{F}\mathbf{P}_1^H + \mathbf{w}_1\mathbf{w}_1^H\right] \\ &\quad= \hat{\mathbf{W}}\left(N\mathbf{P}_1\mathbf{F}^H\mathbf{S}_1\breve{\mathbf{F}}\mathbf{\Sigma}\breve{\mathbf{F}}^H\mathbf{S}_1^H\mathbf{F}\mathbf{P}_1^H + \sigma_{\mathbf{w}}^2\mathbf{I}\right) \end{aligned} \tag{5.38}$$

From (5.36), (5.37), and (5.38), one obtains the weighting matrix $\hat{\mathbf{W}}$ as (5.39). The last equation in (5.39) is derived based on the fact that given two arbitrary matrices $\mathbf{R} \in \mathbb{C}^{N\times M}$

$$\begin{aligned}\hat{\mathbf{W}} &= N\breve{\mathbf{F}}\boldsymbol{\Sigma}\breve{\mathbf{F}}^H\mathbf{S}_1^H\mathbf{F}\mathbf{P}_1^H\left(N\mathbf{P}_1\mathbf{F}^H\mathbf{S}_1\breve{\mathbf{F}}\boldsymbol{\Sigma}\breve{\mathbf{F}}^H\mathbf{S}_1^H\mathbf{F}\mathbf{P}_1^H+\sigma_{\mathbf{w}}^2\mathbf{I}\right)^{-1}\\ &= N\breve{\mathbf{F}}\boldsymbol{\Sigma}\breve{\mathbf{F}}^H\mathbf{S}_1^H\left(N\mathbf{S}_1\breve{\mathbf{F}}\boldsymbol{\Sigma}\breve{\mathbf{F}}^H\mathbf{S}_1^H+\sigma_{\mathbf{w}}^2\mathbf{I}\right)^{-1}\mathbf{F}\mathbf{P}_1^H\end{aligned} \tag{5.39}$$

---

and $\mathbf{Q}\in\mathbb{C}^{M\times N}$, then the following identity is always true:

$$\left(\mathbf{I}_{N\times N}+\mathbf{R}\mathbf{Q}\right)^{-1}\mathbf{R}=\mathbf{R}\left(\mathbf{I}_{M\times M}+\mathbf{Q}\mathbf{R}\right)^{-1} \tag{5.40}$$

Therefore, the MMSE channel estimate is finally given as in (5.18).

5.7.2 Appendix C

Define $\mathbf{z}=\mathbf{Y}_1^H(\mathbf{U}-\mathbf{V})\mathbf{Y}_1\boldsymbol{\rho}_t$. Then the optimization problem in (5.25) can be rewritten as

$$\begin{aligned}\underset{\boldsymbol{\rho}}{\text{minimize}} \quad & \frac{1}{2}\left(\boldsymbol{\rho}^H\mathbf{z}+\mathbf{z}^H\boldsymbol{\rho}\right)\\ \text{subject to} \quad & |\rho_i|=1; \quad i=0,1,\cdots,N-1\end{aligned} \tag{5.41}$$

Because of the constraint in (5.41), the solution, if exist, should be in the form of an exponential function. Define ε_i where $i=0,1,\cdots,N-1$, as Lagrange multipliers. Then the Lagrange function can be written as

$$\begin{aligned}C(\boldsymbol{\rho},\boldsymbol{\varepsilon}) &= \frac{1}{2}\left(\boldsymbol{\rho}^H\mathbf{z}+\mathbf{z}^H\boldsymbol{\rho}\right)+\sum_{i=0}^{N-1}\varepsilon_i\left(||\rho_i||_2^2-1\right)\\ &= \frac{1}{2}\sum_{i=0}^{N-1}\left(\rho_i^*z_i+z_i^*\rho_i\right)+\sum_{i=0}^{N-1}\varepsilon_i\left(||\rho_i||_2^2-1\right)\\ &= \frac{1}{2}\sum_{i=0}^{N-1}\left(\left(\Re(\rho_i)-j\Im(\rho_i)\right)z_i+\right.\\ &\quad \left.z_i^*\left(\Re(\rho_i)+j\Im(\rho_i)\right)\right)+\\ &\quad \sum_{i=0}^{N-1}\varepsilon_i\left(\Re^2(\rho_i)+\Im^2(\rho_i)-1\right)\end{aligned} \tag{5.42}$$

Taking the partial derivative of $C(\boldsymbol{\rho},\boldsymbol{\varepsilon})$ with respect to $\Re(\rho_i)$ and $\Im(\rho_i)$ results in

$$\frac{\partial C(\boldsymbol{\rho},\boldsymbol{\varepsilon})}{\partial\Re(\rho_i)}=\frac{1}{2}\left(z_i+z_i^*\right)+2\varepsilon_i\Re(\rho_i)=0 \tag{5.43a}$$

$$\frac{\partial C(\boldsymbol{\rho},\boldsymbol{\varepsilon})}{\partial\Im(\rho_i)}=\frac{1}{2}j\left(-z_i+z_i^*\right)+2\varepsilon_i\Im(\rho_i)=0 \tag{5.43b}$$

which yields

$$\mathfrak{R}(\rho_i) = -\frac{\mathfrak{R}(z_i)}{2\varepsilon_i} \tag{5.44a}$$

$$\mathfrak{I}(\rho_i) = -\frac{\mathfrak{I}(z_i)}{2\varepsilon_i} \tag{5.44b}$$

where $i = 0, 1, \cdots, N-1$. Thus

$$\arg(\rho_i) = \frac{\mathfrak{I}(\rho_i)}{\mathfrak{R}(\rho_i)} = \frac{\mathfrak{I}(z_i)}{\mathfrak{R}(z_i)} = \arg(z_i) \tag{5.45}$$

Hence, the solution for the optimization problem in (5.25) is

$$\boldsymbol{\rho}_{t+1} = \mathrm{e}^{j\arg(\mathbf{z})} = \mathrm{e}^{j\arg(\mathbf{Y}_1^H(\mathbf{U}-\mathbf{V})\mathbf{Y}_1\boldsymbol{\rho}_t)} \tag{5.46}$$

References

[1] B. Farhang-Boroujeny: "OFDM Versus Filter Bank Multicarrier", *IEEE Signal Processing Magazine*, vol. 28, no. 3, pp. 92–112, May 2011.

[2] T. Hwang and C. Yang and G. Wu and S. Li and G. Y. Li: "OFDM and Its Wireless Applications: A Survey", *IEEE Transactions on Vehicular Technology*, vol. 58, no. 4, pp. 1673–1694, May 2009.

[3] M. Morelli and C. -C. J. Kuo and M. Pun: "Synchronization Techniques for Orthogonal Frequency Division Multiple Access (OFDMA): A Tutorial Review", *Proceedings of the IEEE*, vol. 95, no. 7, pp. 1394–1427, Jul. 2007.

[4] K. Vasudevan: "Coherent detection of turbo coded OFDM signals transmitted through frequency selective Rayleigh fading channels", *2013 IEEE International Conference on Signal Processing, Computing and Control (ISPCC)*, pp. 1–6, Sept. 2013.

[5] E. P. Simon and L. Ros and H. Hijazi and M. Ghogho: "Joint Carrier Frequency Offset and Channel Estimation for OFDM Systems via the EM Algorithm in the Presence of Very High Mobility", *IEEE Transactions on Signal Processing*, vol. 60, no. 2, pp. 754–765, Feb. 2012.

[6] O. Weikert: "Joint estimation of Carrier and Sampling Frequency Offset, phase noise, IQ Offset and MIMO channel for LTE Advanced UL MIMO", *2013 IEEE 14th Workshop on Signal Processing Advances in Wireless Communications (SPAWC)*, pp. 520–524, Jun. 2013.

[7] K. Vasudevan: "Coherent Detection of Turbo-Coded OFDM Signals Transmitted Through Frequency Selective Rayleigh Fading Channels with Receiver Diversity and Increased Throughput", *Wireless Personal Communications*, vol. 82, pp. 1623–1642, Feb. 2015.

[8] B. Farhang-Boroujeny: "Filter Bank Multicarrier Modulation: A Waveform Candidate for 5G and Beyond", *Advances in Electrical Engineering*, vol. 2014, pp. 1–25, Feb. 2014.

[9] K. W. Martin: "Small side-lobe filter design for multitone data-communication applications", *IEEE Transactions on Circuits and Systems II: Analog and Digital Signal Processing*, vol. 45, no. 8, pp. 1155–1161, Aug. 1998.

[10] K. Vasudevan: "Digital Communications and Signal Processing", *Universities Press*, 2010.

[11] B. Farhang-Boroujeny: "Signal Processing Techniques for Software Radios", *Lulu Publishing House*, vol. 82, 2011.

[12] A. RezazadehReyhani and A. Farhang and B. Farhang-Boroujeny: "Circularly Pulse-Shaped Waveforms for 5G: Options and Comparisons", *2015 IEEE Global Communications Conference (GLOBECOM)*, pp. 1–7, Dec. 2015.

[13] G. Fettweis and M. Krondorf and S. Bittner: "GFDM - Generalized Frequency Division Multiplexing", *IEEE 69th Vehicular Technology Conference*, pp. 1–4, April 2009.

[14] N. Michailow and M. Matth and I. S. Gaspar and A. N. Caldevilla and L. L. Mendes and A. Festag and G. Fettweis: "Generalized Frequency Division Multiplexing for 5th Generation Cellular Networks", *IEEE Transactions on Communications*, vol. 62, no. 9, pp. 3045–3061, Sept. 2014.

[15] A. RezazadehReyhani and B. Farhang-Boroujeny: "An Analytical Study of Circularly Pulse-Shaped FBMC-OQAM Waveforms", *IEEE Signal Processing Letters*, vol. 24, no. 10, pp. 1503–1506, Oct. 2017.

[16] S. Adireddy and L. Tong and H. Viswanathan: "Optimal placement of training for frequency-selective block-fading channels", *IEEE Transactions on Information Theory*, vol. 48, no. 8, pp. 2338–2353, Aug. 2002.

[17] W. Zhang and X. Xia and P. C. Ching: "Optimal Training and Pilot Pattern Design for OFDM Systems in Rayleigh Fading", *IEEE Transactions on Broadcasting*, vol. 52, no. 4, pp. 505–514, Dec. 2006.

[18] D. Katselis and E. Kofidis and A. Rontogiannis and S. Theodoridis: "Preamble-Based Channel Estimation for CP-OFDM and OFDM/OQAM Systems: A Comparative Study", *IEEE Transactions on Signal Processing*, vol. 58, no. 5, pp. 2911–2916, May 2010.

[19] E. Kofidis: "Preamble-Based Estimation of Highly Frequency Selective Channels in FBMC/OQAM Systems", *IEEE Transactions on Signal Processing*, vol. 65, no. 7, pp. 1855–1868, April 2017.

[20] J. Choi and Y. Oh and H. Lee and J. Seo: "Pilot-Aided Channel Estimation Utilizing Intrinsic Interference for FBMC/OQAM Systems", *IEEE Transactions on Broadcasting*, vol. 63, no. 4, pp. 644–655, Dec. 2017.

[21] P. Singh and H. B. Mishra and A. K. Jagannatham and K. Vasudevan: "Semi-Blind, Training, and Data-Aided Channel Estimation Schemes for MIMO-FBMC-OQAM Systems", *IEEE Transactions on Signal Processing*, vol. 67, no. 18, pp. 4668–4682, Sept. 2019.

[22] P. Singh and H. B. Mishra and A. K. Jagannatham and K. Vasudevand and L. Hanzo: "Uplink Sum-Rate and Power Scaling Laws for Multi-User Massive MIMO-FBMC Systems", *IEEE Transactions on Communications*, vol. 68, no. 1, pp. 161–176, Jan. 2020.

[23] S. Ehsanfar and M. Matthe and D. Zhang and G. Fettweis: "Theoretical Analysis and CRLB Evaluation for Pilot-Aided Channel Estimation in GFDM", *2016 IEEE Global Communications Conference (GLOBECOM)*, pp. 1–7, Dec. 2016.

[24] S. Ehsanfar and M. Matthe and D. Zhang and G. Fettweis: "Interference-Free Pilots Insertion for MIMO-GFDM Channel Estimation", *2017 IEEE Wireless Communications and Networking Conference (WCNC)*, pp. 1–6, Mar. 2017.

[25] D. Petrovic and W. Rave and G. Fettweis: "Effects of Phase Noise on OFDM Systems With and Without PLL: Characterization and Compensation", *IEEE Transactions on Communications*, vol. 55, no. 8, pp. 1607–1616, Aug. 2007.

[26] S. Wu and P. Liu and Y. Bar-Ness: "Phase Noise Estimation and Mitigation for OFDM Systems", *IEEE Transactions on Wireless Communications*, vol. 5, no. 12, pp. 3616–3625, Dec. 2006.

[27] R. Corvaja and A. G. Armada: "Joint Channel and Phase Noise Compensation for OFDM in Fast-Fading Multipath Applications", *IEEE Transactions on Vehicular Technology*, vol. 58, no. 2, pp. 636–643, Feb. 2009.

[28] R. A. Casas and S. L. Biracree and A. E. Youtz: "Time domain phase noise correction for OFDM signals", *IEEE Transactions on Broadcasting*, vol. 48, no. 3, pp. 230–236, Sept. 2002.

[29] A. Leshem and M. Yemini: "Phase Noise Compensation for OFDM Systems", *IEEE Transactions on Signal Processing*, vol. 65, no. 21, pp. 5675–5686, Nov. 2017.

[30] S. Wu and Y. Bar-Ness: "A phase noise suppression algorithm for OFDM-based WLANs", *IEEE Communications Letters*, vol. 6, no. 12, pp. 535–537, Dec. 2002.

[31] P. Rabiei and W. Namgoong and N. Al-Dhahir: "A Non-Iterative Technique for Phase Noise ICI Mitigation in Packet-Based OFDM Systems", *IEEE Transactions on Signal Processing*, vol. 58, no. 11, pp. 5945–5950, Nov. 2010.

[32] P. Mathecken and T. Riihonen and S. Werner and R. Wichman: "Phase Noise Estimation in OFDM: Utilizing Its Associated Spectral Geometry", *IEEE Transactions on Signal Processing*, vol. 64, no. 8, pp. 1999–2012, Apr. 2016.

[33] Q. Zou and A. Tarighat and A. H. Sayed: "Compensation of Phase Noise in OFDM Wireless Systems", *IEEE Transactions on Signal Processing*, vol. 55, no. 11, pp. 5407–5424, Nov. 2007.

[34] Z. Wang and P. Babu and D. P. Palomar: "Effective Low-Complexity Optimization Methods for Joint Phase Noise and Channel Estimation in OFDM", *IEEE Transactions on Signal Processing*, vol. 65, no. 12, pp. 3247–3260, Jun. 2017.

[35] S. Suyama and H. Suzuki and K. Fukawa and J. Izumi: "Iterative receiver employing phase noise compensation and channel estimation for millimeter-wave OFDM systems", *IEEE Journal on Selected Areas in Communications*, vol. 27, no. 8, pp. 1358–1366, Oct. 2009.

[36] S. Suyama and Y. Hashimoto and H. Suzuki and K. Fukawa: "60 GHz OFDM experimental system employing decision-directed phase noise compensation", *2012 IEEE Radio and Wireless Symposium*, pp. 191–194, Jan. 2012.

[37] D. Shin and S. Suyama and H. Suzuki and K. Fukawa: "10 Gbps millimeter-wave OFDM experimental system with iterative phase noise compensation", *2013 IEEE Radio and Wireless Symposium*, pp. 184–186, Jan. 2013.

[38] Y. Sun and P. Babu and D. P. Palomar: "Majorization-Minimization Algorithms in Signal Processing, Communications, and Machine Learning", *IEEE Transactions on Signal Processing*, vol. 65, no. 3, pp. 794–816, Feb. 2017.

[39] V. Moles-Cases and A. A. Zaidi and X. Chen and T. J. Oechtering and R. Baldemair: "A comparison of OFDM, QAM-FBMC, and OQAM-FBMC waveforms subject to phase noise", *IEEE International Conference on Communications*, pp. 1–6, May 2017.

[40] A. Kakkavas and M. Castaeda and J. Luo and T. Laas and W. Xu and J. A. Nossek: "FBMC-OQAM with phase noise: Achievable performance and compensation", *IEEE 18th International Workshop on Signal Processing Advances in Wireless Communications*, pp. 1–5, Jul. 2017.

[41] B. Lim and Y. C. Ko: "SIR Analysis of OFDM and GFDM Waveforms With Timing Offset, CFO, and Phase Noise", *IEEE Transactions on Wireless Communications*, vol. 16, no. 10, pp. 6979–6990, Oct. 2017.

[42] L. D. Le and H. H. Nguyen: "Impacts of Phase Noise on CFBMC-OQAM", *2018 IEEE 88th Vehicular Technology Conference (VTC)*, pp. 1–6, Aug. 2018.

[43] P. Singh and E. Sharma and K. Vasudevan and R. Budhiraja: "CFO and Channel Estimation for Frequency Selective MIMO-FBMC/OQAM Systems", *IEEE Wireless Communications Letters*, vol. 7, no. 5, pp. 844–847, Oct. 2018.

[44] A. Demir and A. Mehrotra and J. Roychowdhury: "Phase noise in oscillators: a unifying theory and numerical methods for characterization", *IEEE Transactions on Circuits and Systems I: Fundamental Theory and Applications*, vol. 47, no. 5, pp. 655–674, May 2000.

[45] A. Mehrotra: "Noise analysis of phase-locked loops", *IEEE Transactions on Circuits and Systems I: Fundamental Theory and Applications*, vol. 49, no. 9, pp. 1309–1316, Sept. 2002.

[46] J. -J. van de Beek and O. Edfors and M. Sandell and S. K. Wilson and P. O. Borjesson: "On channel estimation in OFDM systems", *IEEE 45th Vehicular Technology Conference*, vol. 2, pp. 815–819, Jul. 1995.

[47] Z. Cheng and D. Dahlhaus: "Time versus frequency domain channel estimation for OFDM systems with antenna arrays", *6th International Conference on Signal Processing*, vol. 2, pp. 1340–1343, Aug. 2002.

[48] S. Boyd and L. Vandenberghe: "Convex Optimization", *Cambridge University Press*, 2004.

[49] S. Ohno: "Preamble and Pilot Symbol Design for Channel Estimation in OFDM", *2007 IEEE International Conference on Acoustics, Speech and Signal Processing*, vol. 3, pp. III-281–III-284, Apr. 2007.

[50] D. Katselis: "Some Preamble Design Aspects in CP-OFDM Systems", *IEEE Communications Letters*, vol. 16, no. 3, pp. 356–359, Mar. 2012.

[51] 3rd Generation Partnership Project (3GPP): "Evolved Universal Terrestrial Radio Access (E-UTRA); Physical channels and modulation", *Technical Specification (TS)*, no. 36.211, Feb. 2015, version 12.4.0.

[52] D. Katselis: "IEEE Standard for Information Technology – Local and metropolitan area networks – Specific requirements – Part 11: Wireless LAN Medium Access Control (MAC)and Physical Layer (PHY) Specifications Amendment 5: Enhancements for Higher Throughput", *IEEE Std 802.11n-2009 (Amendment to IEEE Std 802.11-2007 as amended by IEEE Std 802.11k-2008, IEEE Std 802.11r-2008, IEEE Std 802.11y-2008, and IEEE Std 802.11w-2009)*, pp. 1–565, Oct. 2009.

[53] Y. S. Cho, J. Kim, W. Y. Yang and C. G. Kang: "MIMO-OFDM Wireless Communications with MATLAB", *John Wiley & Sons (Asia) Pte Ltd*, 2010.

[54] 3rd Generation Partnership Project (3GPP): "Evolved Universal Terrestrial Radio Access (E-UTRA); User Equipment (UE) radio transmission and reception", *Technical Specification (TS)*, no. 36.101, Apr. 2017, version 14.3.0.

[55] L. Zhang and P. Xiao and A. Zafar and A. U. Quddus and R. Tafazolli: "FBMC System: An Insight Into Doubly Dispersive Channel Impact", *IEEE Transactions on Vehicular Technology*, vol. 66, no. 5, pp. 3942–3956, May 2017.

[56] J. Zhang and M. Zhao and L. Zhang and J. Zhong and T. Yu: "Circular Convolution Filter Bank Multicarrier (FBMC) System with Index Modulation", *2017 IEEE 86th Vehicular Technology Conference (VTC-Fall)*, pp. 1–5, Sep. 2017.

6. Compensation of Phase Noise and IQ Imbalance in Multi-Carrier Systems

Published as:

Long D. Le and Ha H. Nguyen, "Compensation of Phase Noise and IQ Imbalance in Multi-Carrier Systems," *IEEE Access*, vol. 8, pp. 191263–191277, 2020.

Besides PN, IQ imbalance is also a common physical impairment which can significantly degrade performance of a communication system. As such, the impacts of both PN and IQ imbalance is considered in this chapter. A two-stage algorithm is proposed to compensate for these two impairments in a general multi-carrier modulation system. Specifically, in the first stage, the IQ imbalance parameters and channel impulse response are estimated based on a preamble. The preamble is designed such that the estimation of IQ imbalance parameters does not depend on the channel and PN estimation errors. The proposed design is based on the observation that the impact of PN in the frequency domain can be well captured by a certain number of factors. Given the estimates from the first stage, the IQ imbalance and PN are subsequently compensated in the second stage for data transmission blocks.

The proposed algorithm is further extended to a multiple-input multiple-output (MIMO) system that employs a diversity technique. It is shown that only one preamble block is needed to estimate the IQ imbalances as well as impulse responses of multiple MIMO channels. This means that the proposed algorithm is spectrally efficient. The computational complexity of the proposed algorithm is also analyzed. Simulation results illustrate the effectiveness of the proposed algorithm in a variety of scenarios and for different CP-based multi-carrier systems, including OFDM, GFDM, and CFBMC-OQAM.

Compensation of Phase Noise and IQ Imbalance in Multi-Carrier Systems

Long D. Le and Ha H. Nguyen, *Senior Member, IEEE*

Abstract

Compensation for the impacts of phase noise (PN) and in-phase and quadrature (IQ) imbalance on cyclic-prefix (CP) based multi-carrier modulation systems in the presence of imperfect channel estimation is considered in this paper. A unified two-stage algorithm is proposed. In the first stage, IQ imbalance parameters and channel impulse response are estimated based on the transmission of a preamble which is designed in such a way that the estimation of IQ imbalance does not require any knowledge about the channel and PN. Given the estimates from the first stage, the impacts of IQ imbalance and PN are subsequently compensated in the second stage based on the transmission of pilot symbols. The proposed algorithm is further extended to a MIMO system that employs a diversity technique. Simulation results are presented for a wide range of PN and IQ imbalance scenarios to corroborate the effectiveness of the proposed algorithm.

Index terms

Multi-carrier systems, OFDM, CFBMC-OQAM, GFDM, phase noise, IQ imbalance, channel estimation, cyclic prefix.

6.1 Introduction

The next generation of wireless communication systems is expected to support not only a wide range of data rates, but also a large number of devices sharing a limited transmission bandwidth [1]. Recent studies on transmission technologies emphasize the need of new multi-carrier modulation techniques to support these requirements [2, 3]. Among multi-carrier

transmission techniques, orthogonal frequency-division multiplexing (OFDM) is currently a popular choice for many communication systems due to its numerous advantages [4, 5]. However, OFDM also has disadvantages such as (i) the high out-of-band (OOB) emission of OFDM poses a challenge for opportunistic and dynamic spectrum access, and (ii) a strict orthogonal synchronization between sub-carriers makes OFDM less attractive in low-power communication systems.

Generalized frequency division multiplexing (GFDM) [6, 7] and circular filter-bank multi-carrier offset quadrature amplitude modulation (CFBMC-OQAM) [8, 9] have been recently proposed as promising candidates for the next generation wireless networks that can resolve the disadvantages in OFDM. In particular, with the use of well-designed prototype filters [10, 11], these systems can avoid the high spectral leakage in the conventional OFDM. Furthermore, the strict orthogonal requirement in OFDM is relaxed in GFDM and CFBMC-OQAM.

A common approach in multi-carrier techniques, including OFDM, GFDM and CFBMC-OQAM, is that a proper-length cyclic prefix (CP) is added into the signal before sending out to the channel. By doing so, the interference induced from the multipath (frequency-selective) fading channel is completely removed in the receiver. This also makes the channel estimation and equalization significantly simplified. However, different from OFDM where a CP is added into each sub-symbol, the overhead induced from CP is kept minimum in GFDM and CFBMC-OQAM since a single CP is added for the entire block that contains multiple sub-symbols.

Physical impairments like phase noise (PN), and in-phase and quadrature (IQ) imbalance are major sources limiting performance of multi-carrier systems [12]. The impact of PN can be separated into two components, namely common phase error (CPE) and inter-carrier interference (ICI), in the frequency domain [13]. While the first component results in a common rotation of all symbols in the same transmission block, the second component is different for every symbol. To compensate for the PN impact, many papers estimate CPE and assume ICI as Gaussian noise [14–17]. This assumption does not always hold true in practice, especially when PN is not small. Moreover, iterative PN compensation algorithms

are proposed to replicate the PN-free transmitted signal and then use it to estimate the PN in the time domain [18, 19]. However, these algorithms do not work well for large PN due to error propagation, an inherent problem of an iterative algorithm. Another disadvantage of iterative algorithms is their long latency. In [14, 20–22], the authors propose non-iterative algorithms to compensate for the PN impact. Specifically, in [14], the PN and channel are first jointly estimated by solving a constrained quadratic optimization problem, but under overly simplified constraints. The optimization problem in [14] is revisited in [20–22] with more realistic constraints. Compared to [20], the proposed algorithms in [21, 22] have lower complexity.

Different from PN which is randomly varying, IQ imbalance is a static impairment [12,23]. As such, the IQ imbalance parameters are estimated only once for the whole transmission. It is shown in [23–26] that in the presence of IQ imbalance, the received signal contains not only the linear component, which is a linear convolution between the transmitted signal and the channel, but also the complex conjugate of the linear component which significantly degrades the system performance. Algorithms are proposed in [16,23,24] to estimate the IQ imbalance parameters based on an assumption that without IQ imbalance, the channel has a "smooth" frequency response since the coherence bandwidth of the channel is commonly larger than the inter-carrier spacing. In [27], the authors propose a novel approach to estimate the mixer's IQ imbalance which is isolated from the fading channel estimation by exploiting the channel coherence in both time and frequency domains. However, in order to achieve a reasonable performance, multiple training symbols are used.

In the presence of both PN and IQ imbalance, an algorithm is proposed in [15, 28, 29] to compensate for the impairments. In these papers, the PN and channel impulse response are first estimated based on a transmitted preamble. Given the estimates, the IQ imbalance parameters can be found. Such an algorithm is further extended when multiple-input multiple-output (MIMO) transmission is considered. The estimation of IQ imbalance in [15, 28, 29] highly depends on the estimation errors of PN and the channel. This consequently results in a performance degradation when the estimated IQ imbalance is used for compensation in the rest of data blocks. As a further development of the work in [23, 24], the impact of PN

is included in [16, 30]. Given the IQ imbalance compensation, the PN is estimated and then compensated for the data blocks. A simple joint estimation and compensation technique to estimate channel, PN and IQ imbalance is proposed in [17]. A sub-carrier multiplexed preamble structure having a minimum overhead is introduced and used in the estimation of IQ imbalance parameters as well as the initial estimation of the effective channel matrix, including CPE. Then, a novel tracking method based on the second-order statistics of ICI and noise is used to update the effective channel matrix throughout a transmission frame.

Main Contributions: In this paper, a generalized model of signal processing for CP-based multi-carrier modulation systems, including but not limited to OFDM, GFDM and CFBMC-OQAM, is first presented. We then introduce a unified algorithm which contains two stages to estimate and then compensate for the impacts of PN and IQ imbalance. In the first stage, the channel impulse response and IQ imbalance parameters are first estimated based on the transmission of a preamble. Given the estimates from the first stage, in the second stage the IQ imbalance and PN are compensated in that order based on the pilot symbols for the rest of data transmission blocks. The preamble is designed such that the estimation of IQ imbalance does not depend on the estimated channel and PN. Given the estimated IQ imbalance, the channel impulse response is estimated. The computational complexity of the first stage is analyzed and reduced based on the structure of the proposed preamble. The proposed algorithm is then further extended to a MIMO system with a transmit diversity technique. A general scenario is considered in which each receive antenna suffers from a different impact of IQ imbalance and PN. The preamble design is then generalized for the MIMO system so that the IQ imbalances as well as channel impulse responses can be easily estimated while only one transmission block is needed for the preamble. The developed algorithm makes no assumption about having small IQ imbalance or PN. Simulation results are provided in a variety of scenarios to show the effectiveness of the proposed algorithm.

Notations: Lowercase letters are used to denote scalars. Lowercase boldface and uppercase boldface letters stand for vectors and matrices, respectively. Symbols $(\cdot)^{\dagger}$, $(\cdot)^{T}$, $(\cdot)^{H}$, $(\cdot)^{-1}$, $(\cdot)^{*}$, $|\cdot|$, $||\cdot||_2$, $*$, and $\circledast$ denote pseudo-inverse, transpose, Hermitian, inverse, complex conjugate, modulus, ℓ_2-norm, linear convolution, and circular convolution operations,

respectively. Symbols $\Re\{\cdot\}$, $\Im\{\cdot\}$, diag[·], and E[·] denote the real and imaginary parts of a complex variable, a diagonal matrix if the argument is a vector, or a vector if the argument is a diagonal matrix, and expectation operation, respectively. $\mathbf{1}_{N\times 1}$ denotes a column vector whose N components are all 1's. $\mathcal{CN}(\boldsymbol{\mu}, \boldsymbol{\Sigma})$ represents a circularly symmetric Gaussian random vector with mean $\boldsymbol{\mu}$ and covariance matrix $\boldsymbol{\Sigma}$. This paper use (t) to denote the continuous time signal and $[n]$ to denote discrete-time signals.

6.2 System Model

6.2.1 CP-Based Multi-Carrier Systems

Figure 6.1 illustrates a CP-based multi-carrier system under consideration. An information bit sequence $\mathbf{b}_i$ corresponding to the ith transmission block is first encoded to obtain a coded-bit sequence $\mathbf{u}_i$, which is then mapped into a symbol sequence $\mathbf{d}_i$ by quadrature-amplitude modulation (QAM) mapper. Next, the symbol sequence $\mathbf{d}_i$ is modulated by multiplying with a general multi-carrier modulation matrix $\mathbf{G}_t$ to obtain

$$\mathbf{x}_i = \begin{bmatrix} x_i[0] & x_i[1] & \cdots & x_i[N-1] \end{bmatrix}^T = \mathbf{G}_t \mathbf{d}_i. \tag{6.1}$$

Before transmitting over a wireless channel, a CP of length N_g is added into $\mathbf{x}_i$ to obtain $\tilde{\mathbf{x}}_i = \begin{bmatrix} x_i[N-N_g] & \cdots & x_i[N-1] & x_i[0] & \cdots & x_i[N-1] \end{bmatrix}^T$. To overcome the inter-symbol interference (ISI) induced from the multipath fading channel, N_g is chosen such that $N_g \geq N_c - 1$, where N_c is the length of the channel impulse response. The signal $\tilde{\mathbf{x}}_i$ then goes through the D/A converter and is up-converted to a passband signal $x_i(t)$. The received passband signal is

$$y_i(t) = h(t) * x_i(t) + w_i(t), \tag{6.2}$$

where $h(t)$ is the impulse response of the channel and $w_i(t)$ is thermal noise.

At the receiver, $y_i(t)$ is first down-converted to baseband, filtered and sampled (by the A/D converter). After removing CP, the received signal $\mathbf{y}_i = \begin{bmatrix} y_i[0] & y_i[1] & \cdots & y_i[N-1] \end{bmatrix}^T$ can be written as

$$\mathbf{y}_i = \mathbf{H}\mathbf{x}_i + \mathbf{w}_i \tag{6.3}$$

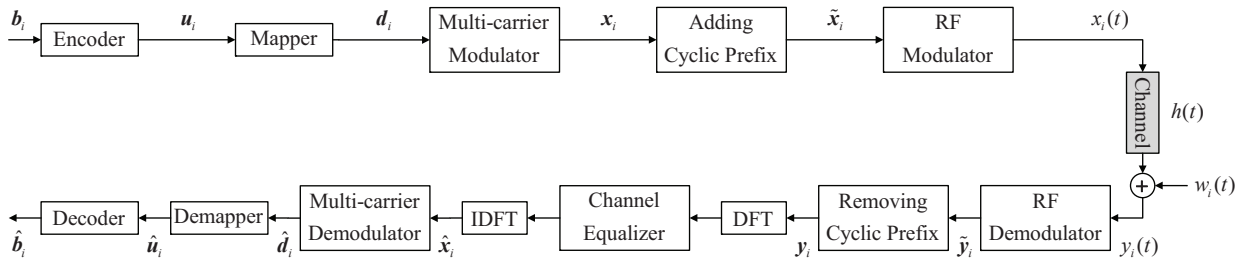

Figure 6.1: A CP-based multi-carrier transceiver.

where $\mathbf{H}$ is an $N \times N$ circulant matrix whose columns are the shifted versions of the first column $\begin{bmatrix}\mathbf{h}^T & 0 & \cdots & 0\end{bmatrix}^T$ with $\mathbf{h} = \begin{bmatrix}h[0] & h[1] & \cdots & h[N_c-1]\end{bmatrix}^T$ is the complex-baseband discrete-time equivalent channel impulse response of $h(t)$. It is assumed that $\mathbf{h} \sim \mathcal{CN}(\mathbf{0}, \mathbf{\Sigma})$. For all CP-based multi-carrier systems, $\mathbf{H}$ can always be written as $\mathbf{H} = \mathbf{F}^H \mathbf{\Gamma} \mathbf{F}$ where $\mathbf{F}$ is the normalized DFT matrix whose (k,m)th element is given as $[\mathbf{F}]_{k,m} = \frac{1}{\sqrt{N}} \mathrm{e}^{-j\frac{2\pi mk}{N}}$ and $\mathbf{\Gamma}$ is a diagonal matrix whose diagonal is the channel frequency response $\mathbf{h}_f$. The vector $\mathbf{w}_i \sim \mathcal{CN}(0, \sigma_{\mathbf{w}}^2 \mathbf{I})$ represents Gaussian noise in the ith transmission block.

To detect the transmitted signal, $\mathbf{y}_i$ is passed through a DFT, then a channel equalizer and an IDFT to obtain $\hat{\mathbf{x}}_i$. The output signal of the IDFT block is demodulated with a bank of filters to obtain

$$\hat{\mathbf{d}}_i = \mathbf{G}_r \hat{\mathbf{x}}_i \tag{6.4}$$

where the multi-carrier demodulation is represented by matrix $\mathbf{G}_r$. The output $\hat{\mathbf{d}}_i$ is finally passed through a demapper and then a decoder to obtain $\hat{\mathbf{u}}_i$ and $\hat{\mathbf{b}}_i$, respectively.

For OFDM, $\mathbf{G}_t = \mathbf{F}^H$, $\mathbf{G}_r = \mathbf{F}$ and $\mathbf{d}_i$ is a column vector of N *complex* QAM symbols. For GFDM, $\mathbf{d}_i$ is also a set of N *complex* QAM symbols but it is generated differently from OFDM. Specifically, the symbol sequence after the mapper is first arranged into a block-based structure of M time slots and K sub-carriers so that $N = M \times K$. Then, $\mathbf{d}_i$ is obtained by vectorizing that block-based structure. In GFDM, $\mathbf{G}_r = \mathbf{G}_t^H$ for matched-filter (MF) demodulation and $\mathbf{G}_r = \mathbf{G}_t^{-1}$ for zero-forcing (ZF) demodulation. For CFBMC, $\mathbf{d}_i$ is a $2N \times 1$ *real*-valued column vector which is constructed similarly as in GFDM but from a $K \times 2M$ structure. For the receiver of CFBMC, $\mathbf{G}_r = \mathbf{G}_t^H$. Thanks to the real-domain orthogonality, the estimate of $\mathbf{d}_i$ is obtained by taking the real part of the multi-carrier demodulation output.

6.2.2 PN and IQ Imbalance

PN and IQ imbalance mainly come from imperfect mixers in both transmitter and receiver. However, this paper assumes that only the receive mixer is impaired. This assumption is commonly adopted in the downlink transmission from a base station to a mobile user where the impact of PN and IQ imbalance is more severe at the receiver.

Define $\mathbf{s}_i = \mathbf{F}\mathbf{x}_i$ and $\bar{\mathbf{s}}_i$ is the complex-conjugate mirroring version of $\mathbf{s}_i$. Then the presence of PN and IQ imbalance results in the following received signal:

$$\mathbf{z}_i = \mu\mathbf{P}_i\mathbf{y}_i + \epsilon\mathbf{P}_i^H\mathbf{y}_i^* \overset{(6.3)}{=} \mu\mathbf{P}_i\mathbf{F}^H\mathbf{\Gamma}\mathbf{s}_i + \epsilon\mathbf{P}_i^H\mathbf{F}^H\overline{\mathbf{\Gamma}}\bar{\mathbf{s}}_i + \mathbf{v}_i \tag{6.5}$$

in which $\mathbf{v}_i = \mu\mathbf{P}_i\mathbf{w}_i + \epsilon\mathbf{P}_i^H\mathbf{w}_i^*$ and $\overline{\mathbf{\Gamma}}$ is a diagonal matrix whose diagonal is $\overline{\mathbf{h}}_f$ which is obtained from $\mathbf{h}_f$ by the complex-conjugate mirroring operation. The diagonal matrix $\mathbf{P}_i = \text{diag}\left[\text{e}^{j\phi_i[0]} \quad \text{e}^{j\phi_i[1]} \quad \dots \quad \text{e}^{j\phi_i[N-1]}\right]$ represents the PN corresponding to the ith transmission block. In this paper, $\phi_i[n]$ is simply generated as a Wiener process [31, 32]. As such, the discrete-time PN from an oscillator can be modeled as $\phi_i[n] = 2\pi f_c \sum_{i=0}^{n-1} \beta[i]$ where f_c is the carrier frequency and $\beta[i]$'s are independent and identically distributed zero-mean Gaussian random variables with variance $\sigma_\beta^2 = c_v T_s$, c_v is a constant describing the quality of the oscillator[1] and T_s is the sampling interval. For the asymmetrical IQ imbalance model [12], the constants μ and ϵ are given as

$$\mu = \frac{1}{2}(1 - g\text{e}^{-j\psi}) \quad \text{and} \quad \epsilon = \frac{1}{2}(1 + g\text{e}^{j\psi}), \tag{6.6}$$

where g and ψ denote the amplitude and phase offsets from IQ imbalance.

Performing DFT on $\mathbf{z}_i$ results in

$$\mathbf{z}_i^{(\text{f})} = \mu\mathbf{Q}_i\mathbf{\Gamma}\mathbf{s}_i + \epsilon\overline{\mathbf{Q}}_i\overline{\mathbf{\Gamma}}\bar{\mathbf{s}}_i + \mathbf{v}_i^{(\text{f})} \tag{6.7}$$

where $\mathbf{v}_i^{(\text{f})} = \mathbf{F}\mathbf{v}_i$, $\mathbf{Q}_i = \mathbf{F}\mathbf{P}_i\mathbf{F}^H$ and $\overline{\mathbf{Q}}_i = \mathbf{F}\mathbf{P}_i^H\mathbf{F}^H$. Both $\mathbf{Q}_i$ and $\overline{\mathbf{Q}}_i$ are circular matrices. Define $I_i[l-q]$ and $J_i[l-q]$ as elements at the lth row and the qth column of $\mathbf{Q}_i$ and $\overline{\mathbf{Q}}_i$,

[1]The 3-dB bandwidth $\Delta f_{3\text{dB}}$ is related to the quality factor c_v as $\Delta f_{3\text{dB}} \sim 2\pi c_v f_c^2$ [21, 32].

respectively. Then

$$\begin{aligned} I_i[l-q] &= \frac{1}{N}\sum_{p=0}^{N-1} \mathrm{e}^{j\phi_i[p]}\mathrm{e}^{-j\frac{2\pi p}{N}(l-q)_N} \\ J_i[l-q] &= \frac{1}{N}\sum_{p=0}^{N-1} \mathrm{e}^{-j\phi_i[p]}\mathrm{e}^{-j\frac{2\pi p}{N}(l-q)_N} \\ J_i[l-q] &= I_i^*[q-l]. \end{aligned} \tag{6.8}$$

Matrix $\mathbf{Q}_i$ now can be written as

$$\mathbf{Q}_i = \begin{bmatrix} I_i[0] & I_i[-1] & \cdots & I_i[2-N] & I_i[1-N] \\ I_i[1] & I_i[0] & \cdots & I_i[3-N] & I_i[2-N] \\ \vdots & \vdots & \ddots & \vdots & \vdots \\ I_i[N-1] & I_i[N-2] & \cdots & I_i[1] & I_i[0] \end{bmatrix}. \tag{6.9}$$

A similar expression can be obtained for $\overline{\mathbf{Q}}_i$ by replacing I_i by J_i.

It is worth pointing out that $I_i[l-q]$ reflects the impact of PN on the received signal in the frequency domain. When $l=q$, $I_i[0] = \frac{1}{N}\sum_{p=0}^{N-1} \mathrm{e}^{j\phi_i[p]}$ is known as CPE [32]. This value is constant for all sub-carriers in the same block, but different from one block to the other. When $l \neq q$, $I_i[l-q]$ represents the interference induced by the qth sub-carrier on the lth sub-carrier, i.e., ICI interference. This term randomly changes from one sub-carrier to the next.

Define $\boldsymbol{\rho}_i = \mathbf{z}_i + \mathbf{z}_i^*$ and $\boldsymbol{\rho}_i^{(\mathrm{f})}$ the corresponding DFT of $\boldsymbol{\rho}_i$. Given $\mu + \epsilon^* = \mu^* + \epsilon = 1$, one can obtain

$$\boldsymbol{\rho}_i^{(\mathrm{f})} = \mathbf{Q}_i\boldsymbol{\Gamma}\mathbf{s}_i + \overline{\mathbf{Q}}_i\overline{\boldsymbol{\Gamma}}\overline{\mathbf{s}}_i + \tilde{\mathbf{v}}_i^{(\mathrm{f})} \tag{6.10}$$

where $\tilde{\mathbf{v}}_i^{(\mathrm{f})} = \mathbf{F}\mathbf{P}_i\mathbf{w}_i + \mathbf{F}\mathbf{P}_i^H\mathbf{w}_i^*$.

6.3 Proposed Algorithm for PN and IQ Imbalance Compensation

The proposed algorithm has two stages. In the first stage, the channel and IQ imbalance parameters, i.e., μ and ϵ, are estimated based on the transmission of a preamble. Different from [15, 28, 29], here the preamble is designed such that the estimation of IQ imbalance parameters is not affected by the estimation errors of the PN and channel. Given the estimates

from the first stage and pilot symbols, the PN and IQ imbalance can be subsequently compensated for the rest of data transmission blocks. In this paper, the preamble is transmitted in the first block, i.e., $i = 1$, and the first stage is operated on the preamble only.

6.3.1 Stage 1: Estimation of IQ Imbalance, PN and Channel

Preamble Design and IQ Imbalance Estimation

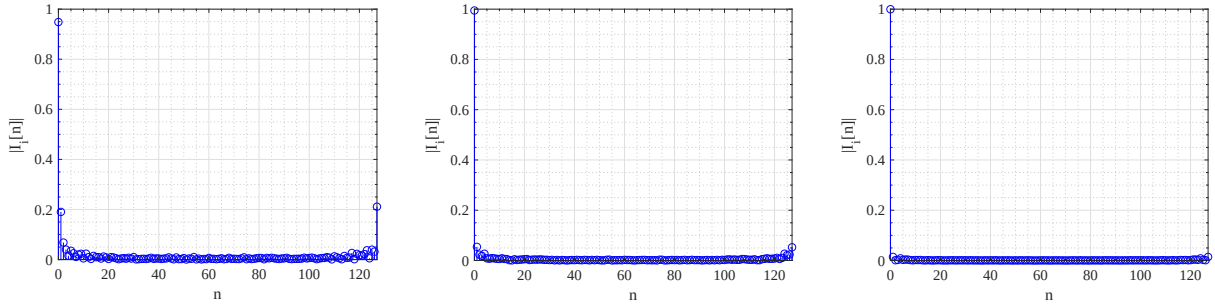

(a) $c_v = 2 \times 10^{-17}$ (b) $c_v = 5 \times 10^{-18}$ (c) $c_v = 5 \times 10^{-19}$

Figure 6.2: The first column of $\mathbf{Q}_i$. The values of c_v are chosen such as $\Delta f_{3\text{dB}}$ is in the order of ten thousands hertz (a), thousands hertz (b) and hundreds hertz (c).

Fig. 6.2 shows the *absolute values* of the first column of $\mathbf{Q}_i$, which is the frequency-domain representation of PN for the ith transmission block. The figure is obtained with 3 different values of c_v, corresponding to $\Delta f_{3\text{dB}}$ in the order of ten thousands, thousands and hundreds hertz. It can be seen that when the PN is small, the CPE, i.e., $I_i[0]$, dominates the other components, hence the impact of ICI is negligible. However, when the PN is large, the impact of ICI cannot be ignored. Interestingly, even when the PN is very large, the impact of PN in the frequency domain can be well captured by a few components around $I_i[0]$.

It is assumed that the frequency-domain PN corresponding to the preamble, i.e., $i = 1$, can be approximately represented by $\begin{bmatrix} I_1[-N_\diamond] & \cdots & I_1[-1] & I_1[0] & I_1[1] & \cdots & I_1[N_\diamond] \end{bmatrix}$, where $N_\diamond$ is the approximation order of PN. As such, $\mathbf{Q}_1$ and $\overline{\mathbf{Q}}_1$ can be rewritten approximately

as ,.

$$\mathbf{Q}_1 \approx \begin{bmatrix} I_1[0] & I_1[-1] & \cdots & 0 & \cdots & 0 & I_1[N_\diamond] & I_1[N_\diamond-1] & \cdots & I_1[2] & I_1[1] \\ I_1[1] & I_1[0] & \cdots & I_1[-N_\diamond] & \cdots & 0 & 0 & I_1[N_\diamond] & \cdots & I_1[3] & I_1[2] \\ \vdots & \vdots & \ddots & \vdots & \ddots & \vdots & \vdots & \vdots & \ddots & \vdots & \vdots \\ I_1[-1] & I_1[-2] & \cdots & 0 & \cdots & I_1[N_\diamond] & I_1[N_\diamond-1] & I_1[N_\diamond-2] & \cdots & I_1[1] & I_1[0] \end{bmatrix} \tag{6.11}$$

and

$$\overline{\mathbf{Q}}_1 \approx \begin{bmatrix} I_1^*[0] & I_1^*[1] & \cdots & 0 & \cdots & 0 & I_1^*[-N_\diamond] & I_1^*[1-N_\diamond] & \cdots & I_1^*[-2] & I_1^*[-1] \\ I_1^*[-1] & I_1^*[0] & \cdots & I_1^*[N_\diamond] & \cdots & 0 & 0 & I_1^*[-N_\diamond] & \cdots & I_1^*[-3] & I_1^*[-2] \\ \vdots & \vdots & \ddots & \vdots & \ddots & \vdots & \vdots & \vdots & \ddots & \vdots & \vdots \\ I_1^*[1] & I_1^*[2] & \cdots & 0 & \cdots & I_1^*[-N_\diamond] & I_1^*[1-N_\diamond] & I_1^*[2-N_\diamond] & \cdots & I_1^*[-1] & I_1^*[0] \end{bmatrix}, \tag{6.12}$$

respectively. Given $\mathbf{Q}_1$ and $\overline{\mathbf{Q}}_1$, the received signal in (6.7) for the preamble can be derived as

$$\begin{aligned} z_1^{(\mathrm{f})}[N_\diamond+1] &= \mu\left\{I_1[-N_\diamond]h_f[2N_\diamond+1]s_1[2N_\diamond+1]\cdots+I_1[N_\diamond]h_f[1]s_1[1]\right\}+ \\ &\quad \epsilon\left\{I_1^*[N_\diamond]h_f^*[N-2N_\diamond-1]s_1^*[N-2N_\diamond-1]+\cdots+\right. \\ &\quad \left. I_1^*[-N_\diamond]h_f^*[N-1]s_1^*[N-1]\right\}+v_1^{(\mathrm{f})}[N_\diamond+1] \\ &\vdots \\ z_1^{(\mathrm{f})}\left[\frac{N}{2}-N_\diamond-1\right] &= \mu\left\{I_1[-N_\diamond]h_f\left[\frac{N}{2}-1\right]s_1\left[\frac{N}{2}-1\right]+\cdots+\right. \\ &\quad \left. I_1[N_\diamond]h_f\left[\frac{N}{2}-2N_\diamond-1\right]s_1\left[\frac{N}{2}-2N_\diamond-1\right]\right\}+ \\ &\quad \epsilon\left\{I_1^*[N_\diamond]h_f^*\left[\frac{N}{2}+1\right]s_1^*\left[\frac{N}{2}+1\right]+\cdots+\right. \\ &\quad \left. I_1^*[-N_\diamond]h_f^*\left[\frac{N}{2}+2N_\diamond+1\right]s_1^*\left[\frac{N}{2}+2N_\diamond+1\right]\right\}+v_1^{(\mathrm{f})}\left[\frac{N}{2}-N_\diamond-1\right] \end{aligned} \tag{6.13}$$

from the $(N_\diamond+1)$th sample to $\left(\frac{N}{2}-N_\diamond-1\right)$th sample. Furthermore, given (6.10), $\boldsymbol{\rho}_1^{(\mathrm{f})}$ can

be rewritten as

$$\begin{aligned}
\rho_1^{(\mathrm{f})}[N_\diamond+1] &= \{I_1[-N_\diamond]h_f[2N_\diamond+1]s_1[2N_\diamond+1]\cdots+I_1[N_\diamond]h_f[1]s_1[1]\}+\\
&\quad\left\{I_1^*[N_\diamond]h_f^*[N-2N_\diamond-1]s_1^*[N-2N_\diamond-1]+\cdots+\right.\\
&\quad\left.I_1^*[-N_\diamond]h_f^*[N-1]s_1^*[N-1]\right\}+\tilde{v}_1^{(\mathrm{f})}[N_\diamond+1]\\
&\vdots\\
\rho_1^{(\mathrm{f})}\left[\frac{N}{2}-N_\diamond-1\right] &= \left\{I_1[-N_\diamond]h_f\left[\frac{N}{2}-1\right]s_1\left[\frac{N}{2}-1\right]+\cdots+\right.\\
&\quad\left.I_1[N_\diamond]h_f\left[\frac{N}{2}-2N_\diamond-1\right]s_1\left[\frac{N}{2}-2N_\diamond-1\right]\right\}+\\
&\quad\left\{I_1^*[N_\diamond]h_f^*\left[\frac{N}{2}+1\right]s_1^*\left[\frac{N}{2}+1\right]+\cdots+\right.\\
&\quad\left.I_1^*[-N_\diamond]h_f^*\left[\frac{N}{2}+2N_\diamond+1\right]s_1^*\left[\frac{N}{2}+2N_\diamond+1\right]\right\}+\tilde{v}_1^{(\mathrm{f})}\left[\frac{N}{2}-N_\diamond-1\right]
\end{aligned} \tag{6.14}$$

from the $(N_\diamond+1)$th sample to $\left(\frac{N}{2}-N_\diamond-1\right)$th sample.

It can be observed that, for each expression in (6.13) and (6.14), while the terms inside the first curly brackets, which are related to μ, only contain symbols from the first half of the preamble, i.e., between $s_1[1]$ and $s_1\left[\frac{N}{2}-1\right]$, the terms inside the second curly brackets, which are related to ϵ, only contain symbols from the second half of the preamble, i.e., between $s_1\left[\frac{N}{2}+1\right]$ and $s_1[N-1]$. As such, if either the first half or the second half of $\mathbf{s}_1$ contains all zero elements, then either ϵ or μ can be estimated, respectively. Specifically, making the second half of the preamble all zeros, i.e., $s_1[n]=0$ for $n=\left(\frac{N}{2}+1\right),\cdots,(N-1)$, then (6.13) and (6.14) can be respectively rewritten as

$$\begin{aligned}
z_1^{(\mathrm{f})}[N_\diamond+1] &= \mu\{I_1[-N_\diamond]h_f[2N_\diamond+1]s_1[2N_\diamond+1]\cdots+I_1[N_\diamond]h_f[1]s_1[1]\}+v_1^{(\mathrm{f})}[N_\diamond+1]\\
&\vdots\\
z_1^{(\mathrm{f})}\left[\frac{N}{2}-N_\diamond-1\right] &= \mu\left\{I_1[-N_\diamond]h_f\left[\frac{N}{2}-1\right]s_1\left[\frac{N}{2}-1\right]+\cdots+\right.\\
&\quad\left.I_1[N_\diamond]h_f\left[\frac{N}{2}-2N_\diamond-1\right]s_1\left[\frac{N}{2}-2N_\diamond-1\right]\right\}+v_1^{(\mathrm{f})}\left[\frac{N}{2}-N_\diamond-1\right]
\end{aligned} \tag{6.15}$$

and

$$\begin{aligned}
\rho_1^{(\mathrm{f})}[N_\diamond+1] &= \{I_1[-N_\diamond]h_f[2N_\diamond+1]s_1[2N_\diamond+1]\cdots+I_1[N_\diamond]h_f[1]s_1[1]\}+\tilde{v}_1^{(\mathrm{f})}[N_\diamond+1]\\
&\vdots\\
\rho_1^{(\mathrm{f})}\left[\frac{N}{2}-N_\diamond-1\right] &= \left\{I_1[-N_\diamond]h_f\left[\frac{N}{2}-1\right]s_1\left[\frac{N}{2}-1\right]+\cdots+\right.\\
&\qquad \left. I_1[N_\diamond]h_f\left[\frac{N}{2}-2N_\diamond-1\right]s_1\left[\frac{N}{2}-2N_\diamond-1\right]\right\}+\tilde{v}_1^{(\mathrm{f})}\left[\frac{N}{2}-N_\diamond-1\right]
\end{aligned} \tag{6.16}$$

and the relationship between $z_1^{(\mathrm{f})}$ and $\rho_1^{(\mathrm{f})}$ can be obtained as

$$\begin{aligned}
z_1^{(\mathrm{f})}[N_\diamond+1] &= \mu\rho_1^{(\mathrm{f})}[N_\diamond+1]+\left(v_1^{(\mathrm{f})}[N_\diamond+1]-\mu\tilde{v}_1^{(\mathrm{f})}[N_\diamond+1]\right)\\
&\vdots\\
z_1^{(\mathrm{f})}\left[\frac{N}{2}-N_\diamond-1\right] &= \mu\rho_1^{(\mathrm{f})}\left[\frac{N}{2}-N_\diamond-1\right]+\left(v_1^{(\mathrm{f})}\left[\frac{N}{2}-N_\diamond-1\right]-\mu\tilde{v}_1^{(\mathrm{f})}\left[\frac{N}{2}-N_\diamond-1\right]\right).
\end{aligned} \tag{6.17}$$

From (6.17), μ can be estimated as

$$\hat{\mu}=\frac{1}{\frac{N}{2}-2N_\diamond-1}\sum_{n=N_\diamond+1}^{\frac{N}{2}-N_\diamond-1}\frac{z_1^{(\mathrm{f})}[n]}{\rho_1^{(\mathrm{f})}[n]}. \tag{6.18}$$

With the estimate of μ, ϵ can be estimated as

$$\hat{\epsilon}=1-\hat{\mu}^*. \tag{6.19}$$

The performance of IQ imbalance estimation can be evaluated in terms of the mean squared error (MSE) as

$$\mathrm{MSE}_{\mathrm{IQ}}=\mathrm{E}\left\{|\hat{\mu}-\mu|^2\right\}. \tag{6.20}$$

Remarks:

- Similarly, ϵ can be estimated first by designing the preamble such that the first half of $\mathbf{s}_1$ contains all zeros, i.e., $s_1[n]=0$ for $n=0,\cdots,\left(\frac{N}{2}-1\right)$.
- The previous analysis is performed for the $(N_\diamond+1)$th sample to the $\left(\frac{N}{2}-N_\diamond-1\right)$th sample, i.e., they belong to the first half of the received signal $\mathbf{z}_1^{(\mathrm{f})}$. A similar analysis

can be done for the second half of $\mathbf{z}_1^{(\mathrm{f})}$. However, the same conclusion related to how $\mathbf{s}_1$ is designed would be reached.

- $(2N_\diamond + 1)$ samples in the first half of the received signal $\mathbf{z}_1^{(\mathrm{f})}$ are not used in estimating the IQ imbalance parameters.

- Depending on how large $\Delta f_{3\mathrm{dB}}$ is, $N_\diamond$ can be chosen appropriately so that the PN impact can be well captured. For instance, when $\Delta f_{3\mathrm{dB}}$ is in the order from hundreds to thousands hertz, $N_\diamond = 2$ would be enough to capture the PN impact as illustrated in Figs. 6.2b and 6.2c. However, when $\Delta f_{3\mathrm{dB}}$ is very high, as in the order of ten thousands hertz as shown in Fig. 6.2a, $N_\diamond = 4$ is a better choice.

- The estimation of IQ imbalance does not require any knowledge about the fading channel and PN.

PN and Channel Estimation

Given $\hat{\mu}$ and $\hat{\epsilon}$, IQ imbalance can be compensated from the received signal corresponding to the preamble as

$$\mathbf{r}_1 = \frac{\hat{\mu}^* \mathbf{z}_1 - \hat{\epsilon} \mathbf{z}_1^*}{|\hat{\mu}|^2 - |\hat{\epsilon}|^2} \approx \mathbf{P}_1 \mathbf{H} \mathbf{x}_1 + \hat{\mathbf{w}}_1 = \sqrt{N} \mathbf{P}_1 \mathbf{F}^H \mathbf{S}_1 \breve{\mathbf{F}} \mathbf{h} + \hat{\mathbf{w}}_1 \tag{6.21}$$

where $\hat{\mathbf{w}}_1 = \mathbf{P}_1 \mathbf{w}_1$, $\mathbf{S}_1 = \mathrm{diag}[\mathbf{s}_1]$ and $\breve{\mathbf{F}}$ is obtained from $\mathbf{F}$ by keeping the first N_c columns.

To estimate the channel impulse response, the inter-dependency between the channel $\mathbf{h}$ and the PN $\mathbf{P}_1$ in (6.21) has to be resolved. Similar to [14, 20–22], the inter-dependency can be decoupled by first obtaining an estimate of the channel which is a function of $\mathbf{P}_1$. The estimated channel is then substituted into the optimization problem which minimizes the MSE of PN estimate. The PN estimated from solving the optimization problem is then used to finally obtain the estimated channel. It is pointed out that, to improve the quality of the estimated channel, the minimum mean squared error (MMSE) method is used in this paper rather than the least square (LS) method as in [14, 20, 21]. Furthermore, the proposed algorithm estimates the channel impulse response rather than the channel frequency response as proposed in [22]. The reason is that the length of a channel impulse response is usually

much shorter than the length of its corresponding channel frequency response, and as such, estimating the channel impulse response usually requires less transmitted pilots than that from estimating the channel frequency response. This is especially useful when the MIMO scenario is considered later where only one preamble is used to estimate multiple channel impulse responses.

From (6.21), the estimated channel impulse response obtained with the MMSE method is

$$\mathbf{h}_{\text{MMSE}} = \sqrt{N}\boldsymbol{\Sigma}\breve{\mathbf{F}}^H\mathbf{S}_1^H(N\mathbf{S}_1\breve{\mathbf{F}}\boldsymbol{\Sigma}\breve{\mathbf{F}}^H\mathbf{S}_1^H + \sigma_{\mathbf{w}}^2\mathbf{I})^{-1}\mathbf{F}\mathbf{P}_1^H\mathbf{r}_1. \tag{6.22}$$

Given $\mathbf{h}_{\text{MMSE}}$, PN is then estimated by minimizing

$$\begin{aligned}\mathscr{C}(\mathbf{P}_1) &= \left|\left|\left(\mathbf{r}_1 - \sqrt{N}\mathbf{P}_1\mathbf{F}^H\mathbf{S}_1\breve{\mathbf{F}}\mathbf{h}\right)\Big|_{\mathbf{h}=\mathbf{h}_{\text{MMSE}}}\right|\right|_2^2 \\ &= \mathbf{r}_1^H\mathbf{P}_1\left(\mathbf{I} - 2\boldsymbol{\Lambda} + \boldsymbol{\Lambda}\boldsymbol{\Lambda}\right)\mathbf{P}_1^H\mathbf{r}_1\end{aligned} \tag{6.23}$$

where $\boldsymbol{\Lambda} = N\mathbf{F}^H\mathbf{S}_1\breve{\mathbf{F}}\boldsymbol{\Sigma}\breve{\mathbf{F}}^H\mathbf{S}_1^H\left(N\mathbf{S}_1\breve{\mathbf{F}}\boldsymbol{\Sigma}\breve{\mathbf{F}}^H\mathbf{S}_1^H + \sigma_{\mathbf{w}}^2\mathbf{I}\right)^{-1}\mathbf{F}$.

Let $\mathbf{F}_1$ and $\breve{\mathbf{F}}_1$ be obtained from $\mathbf{F}$ and $\breve{\mathbf{F}}$, respectively, by keeping the first $N/4$ rows, and $\mathbf{A}$ be a diagonal matrix whose diagonal contains all the non-zero elements from the first half of the preamble designed in the previous subsection. As such, $\boldsymbol{\Lambda}$ can be simplified as $\boldsymbol{\Lambda} = N\mathbf{F}_1^H\mathbf{A}\breve{\mathbf{F}}_1\boldsymbol{\Sigma}\breve{\mathbf{F}}_1^H\mathbf{A}^H\left(N\mathbf{A}\breve{\mathbf{F}}_1\boldsymbol{\Sigma}\breve{\mathbf{F}}_1^H\mathbf{A}^H + \sigma_{\mathbf{w}}^2\mathbf{I}_{N/2}\right)^{-1}\mathbf{F}_1$. It can be seen that the most complicated operations in computing $\boldsymbol{\Lambda}$ related to matrix inversion and multiplication are reduced from N-dimensional matrices to only $N/2$-dimensional matrices. The matrix inversion in $\boldsymbol{\Lambda}$ can be further simplified if the preamble is designed such as $\mathbf{A}^H\mathbf{A} = \mathbf{I}_{N/2}$ [22] and the length of the channel impulse response is much shorter than the half length of the preamble $\mathbf{s}_1$. Specifically, $\boldsymbol{\Lambda}$ can be rewritten as

$$\boldsymbol{\Lambda} = N\mathbf{F}_1^H\mathbf{A}\breve{\mathbf{F}}_1\boldsymbol{\Sigma}\left(N\breve{\mathbf{F}}_1^H\breve{\mathbf{F}}_1\boldsymbol{\Sigma} + \sigma_{\mathbf{w}}^2\mathbf{I}_{N_c}\right)^{-1}\breve{\mathbf{F}}_1^H\mathbf{A}^H\mathbf{F}_1. \tag{6.24}$$

In (6.24), the inversion complexity of an $N/2$-dimensional matrix is reduced to that of an N_c-dimensional matrix. Furthermore, the matrix inversion does not depend on the preamble. This means that it needs to be computed once only, provided that the statistics of channel and noise do not change.

Define $\mathbf{U} = (\mathbf{I} - 2\mathbf{\Lambda} + \mathbf{\Lambda}\mathbf{\Lambda})$, $\mathbf{R} = \text{diag}\,[\mathbf{r}_1]$, and $\boldsymbol{\eta} = \begin{bmatrix} \eta_0 & \eta_1 & \cdots & \eta_{N-1} \end{bmatrix}^T = \text{diag}\,[\mathbf{P}_1]^H$. Then the PN can be estimated by solving the following optimization problem:

$$\begin{aligned} &\underset{\boldsymbol{\eta}}{\text{minimize}} \quad \boldsymbol{\eta}^H \mathbf{R}^H \mathbf{U} \mathbf{R} \boldsymbol{\eta} \\ &\text{subject to} \quad |\eta_j| = 1; \quad j = 0, 1, \cdots, N-1. \end{aligned} \tag{6.25}$$

Similar to [21,22], the majorization-minimization algorithm is applied to solve (6.25). Define $\mathbf{V} = \lambda_{\max} \mathbf{I}_N$ where $\lambda_{\max}$ is the maximum eigenvalue of $\mathbf{U}$. A closed-form solution for (6.25) is obtained as

$$\boldsymbol{\eta}_{t+1} = \mathrm{e}^{j \arg(\mathbf{R}_1^H (\mathbf{U} - \mathbf{V}) \mathbf{R}_1 \boldsymbol{\eta}_t)}. \tag{6.26}$$

In summary, to find a solution for the optimization problem (6.25), it is first initialized at $t = 0$, i.e., $\boldsymbol{\eta}_0$, and then substituted into (6.26) to obtain $\boldsymbol{\eta}_1$. Next, $\boldsymbol{\eta}_1$ is substituted into (6.26) to obtain $\boldsymbol{\eta}_2$ and so on. The algorithm terminates after a predefined number of iterations, say N_{iter}. The estimated PN is then substituted into (6.22) to finally obtain the estimated channel impulse response. It is pointed out that, given the prposed preamble design, the first stage can be carried out in the same way for all CP-based multi-carrier systems considered in this paper.

6.3.2 Stage 2: Data Detection

In the second stage of the proposed algorithm, the impact of IQ imbalance and PN shall be subsequently compensated for the data blocks. With the estimated IQ imbalance parameters, the IQ imbalance is first compensated for the received signal corresponding to the ith transmission block as

$$\mathbf{r}_i = \frac{\hat{\mu}^* \mathbf{z}_i - \hat{\epsilon} \mathbf{z}_i^*}{|\hat{\mu}|^2 - |\hat{\epsilon}|^2} \approx \mathbf{P}_i \mathbf{F}^H \mathbf{\Gamma} \mathbf{F} \mathbf{G}_t \mathbf{d}_i + \hat{\mathbf{w}}_i \tag{6.27}$$

where $2 \leq i \leq N_f$ and N_f is the number of blocks in each frame. The IQ imbalance-compensated signal $\mathbf{r}_i$ then enters the PN compensation procedure. It is assumed that the conjugate of PN, namely $\mathbf{P}_i^H$, can be approximately represented as a multiplication of a known basis matrix $\mathbf{\Omega}_i = \begin{bmatrix} \boldsymbol{\omega}_i^{(0)} & \boldsymbol{\omega}_i^{(1)} & \cdots & \boldsymbol{\omega}_i^{(N_b-1)} \end{bmatrix}$ which contains N_b column vectors $\boldsymbol{\omega}_i^{(n)} = \begin{bmatrix} \omega_i^{(n,0)} & \cdots & \omega_i^{(n,N-1)} \end{bmatrix}^T$ and an unknown vector $\boldsymbol{\gamma}_i = \begin{bmatrix} \gamma_i^{(0)} & \cdots & \gamma_i^{(N_b-1)} \end{bmatrix}^T$. Of course

$\boldsymbol{\gamma}_i$ should be estimated (which shall be discussed shortly) so that $\boldsymbol{\Omega}_i\boldsymbol{\gamma}_i$ can be used to de-rotate the PN impact in the receiver. After the PN compensation, the output signal is further processed to detect the transmitted signal as $\hat{\mathbf{d}}_i = \boldsymbol{\Delta}_i\boldsymbol{\gamma}_i$ where $\boldsymbol{\Delta}_i = \mathbf{G}_r\mathbf{F}^H\hat{\boldsymbol{\Gamma}}^{-1}\mathbf{F}\text{diag}\left[\mathbf{r}_i\right]\boldsymbol{\Omega}_i$ and $\hat{\boldsymbol{\Gamma}} = \sqrt{N}\text{diag}[\breve{\mathbf{F}}\mathbf{h}_{\text{MMSE}}]$.

Let $\mathbf{p} = \begin{bmatrix} p_0 & p_1 & \cdots & p_{T-1} \end{bmatrix}$ be a set of pilot indexes in each transmission block, and $\mathbf{d}_i^{[\mathbf{p}]} = \begin{bmatrix} d_i^{[p_0]} & d_i^{[p_1]} & \cdots & d_i^{[p_{T-1}]} \end{bmatrix}^T$ be the transmitted signal corresponding to the pilot index set. Define $\boldsymbol{\Delta}_i^{[\mathbf{p}]}$ as the matrix which is obtained from $\boldsymbol{\Delta}_i$ by keeping the rows corresponding to the pilot indexes. Thus, the received signal for the pilot symbols can be written as

$$\mathbf{d}_i^{[\mathbf{p}]} = \boldsymbol{\Delta}_i^{[\mathbf{p}]}\boldsymbol{\gamma}_i. \tag{6.28}$$

To estimate $\boldsymbol{\gamma}_i$, LS estimation is used for simplicity.

For CFBMC, the received signal corresponding to the pilot symbols is written as $\mathbf{d}_i^{[\mathbf{p}]} = \Re\left\{\boldsymbol{\Delta}_i^{[\mathbf{p}]}\boldsymbol{\gamma}_i\right\}$, which can be further rewritten as

$$\begin{aligned}\Re\left\{\boldsymbol{\Delta}_i^{[\mathbf{p}]}\boldsymbol{\gamma}_i\right\} &= \begin{bmatrix} \Re\left\{\delta_i^{(0,0)}\right\} & \Im\left\{\delta_i^{(0,0)}\right\} & \cdots & \Re\left\{\delta_i^{(0,F-1)}\right\} & \Im\left\{\delta_i^{(0,F-1)}\right\} \\ \Re\left\{\delta_i^{(1,0)}\right\} & \Im\left\{\delta_i^{(1,0)}\right\} & \cdots & \Re\left\{\delta_i^{(1,F-1)}\right\} & \Im\left\{\delta_i^{(1,F-1)}\right\} \\ \vdots & \vdots & \cdots & \vdots & \vdots \\ \Re\left\{\delta_i^{(Q-1,0)}\right\} & \Im\left\{\delta_i^{(Q-1,0)}\right\} & \cdots & \Re\left\{\delta_i^{(Q-1,F-1)}\right\} & \Im\left\{\delta_i^{(Q-1,F-1)}\right\} \end{bmatrix} \begin{bmatrix} \Re\left\{\gamma_{i,0}\right\} \\ -\Im\left\{\gamma_{i,0}\right\} \\ \cdots \\ \Re\left\{\gamma_{i,F-1}\right\} \\ -\Im\left\{\gamma_{i,F-1}\right\} \end{bmatrix} \\ &= \tilde{\boldsymbol{\Delta}}_i\tilde{\boldsymbol{\gamma}}_i \end{aligned} \tag{6.29}$$

which is in the form of (6.28), where $\delta_i^{(k,j)}$ denotes the (k,j)th element of matrix $\boldsymbol{\Delta}_i^{[\mathbf{p}]}$ and $\boldsymbol{\gamma}_i$ is related to $\tilde{\boldsymbol{\gamma}}_i$ as

$$\boldsymbol{\gamma}_i = \begin{bmatrix} 1 & -j & 0 & 0 & \cdots & 0 & 0 \\ 0 & 0 & 1 & -j & \cdots & 0 & 0 \\ \vdots & \vdots & \vdots & \vdots & \cdots & \vdots & \vdots \\ 0 & 0 & 0 & 0 & \cdots & 1 & -j \end{bmatrix}_{N_b \times 2N_b} \tilde{\boldsymbol{\gamma}}_i. \tag{6.30}$$

The proposed algorithm in the second stage does not require any iterations as the ones proposed in [18, 19, 33]. As such, the unwanted effects of an iterative algorithm such as high

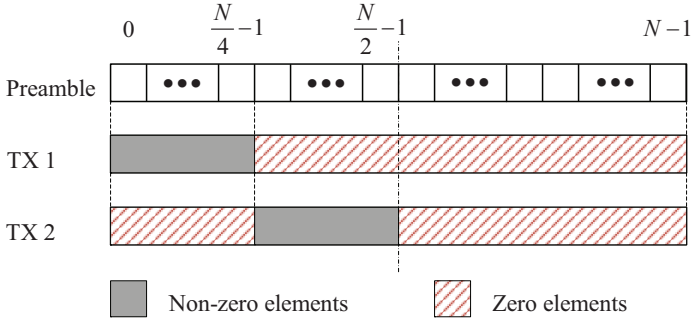

Figure 6.3: Proposed preamble when $N_t = 2$.

latency and error propagation can be effectively avoided. Furthermore, different from the existing literature, the PN is estimated in the second stage without making any assumptions to simplify the PN model.

6.4 Extension to MIMO Systems

This section extends the algorithm proposed in the previous section to the MIMO systems. Consider a MIMO system equipped with N_t transmit and N_r receive antennas. The channel impulse response between the pth transmit antenna and the qth receive antenna is denoted as $\mathbf{h}_{p,q}$ and modeled as $\mathbf{h}_{p,q} \sim \mathcal{CN}(\mathbf{0}, \mathbf{\Sigma}_{p,q})$. Define $\mathbf{x}_{p,i}$ and $\mathbf{z}_{q,i}$ as the transmitted signal and the received signal corresponding to the ith transmission block at the pth transmit antenna and the qth receive antenna, respectively. Let $\mathbf{P}_{q,i}$ and (μ_q, ϵ_q) represent the impact of PN and IQ imbalance corresponding to the qth receive antenna and the ith transmission block. Then, the received signal at the qth antenna after removing CP is

$$\mathbf{z}_{q,i} = \mu_q \mathbf{P}_{q,i} \sum_{p=1}^{N_t} \mathbf{H}_{p,q} \mathbf{x}_{p,i} + \epsilon_q \mathbf{P}_{q,i}^H \sum_{p=1}^{N_t} \mathbf{H}_{p,q}^* \mathbf{x}_{p,i}^* + \mathbf{v}_{q,i} \tag{6.31}$$

where $\mathbf{v}_{q,i} = \mu_q \mathbf{P}_{q,i} \mathbf{w}_{q,i} + \epsilon_q \mathbf{P}_{q,i}^H \mathbf{w}_{q,i}^*$ and $\mathbf{w}_{q,i}$ represents Gaussian noise in the ideal case, i.e., without PN and IQ imbalance, and $\mathbf{H}_{p,q}$ is a circulant matrix built from $\mathbf{h}_{p,q}$.

6.4.1 Stage 1: IQ Imbalance, PN and Channel Estimation

Preamble Design and IQ Imbalance Estimation

Observe from (6.31) that all the transmitted signals appear as pairs of linear components, namely $\mathbf{H}_{p,q}\mathbf{x}_{p,i}$ and $\mathbf{H}_{p,q}^*\mathbf{x}_{p,i}^*$ in the received signal. Such observation motivates us to propose

a preamble as illustrated in Fig. 6.3 for the case $N_t = 2$. Specifically, there is one preamble for each transmit antenna which contains only one transmission block. The transmitted preamble from each transmit antenna shall be non-overlapped with the ones from the other transmit antennas. Furthermore, each transmitted preamble is designed by following the same principle presented in Section 6.3.1.

The received signal at the qth antenna corresponding to the preamble and after removing CP can be derived as

$$\mathbf{z}_{q,1} = \mu_q \mathbf{P}_{q,1} \sum_{p=1}^{2} \mathbf{H}_{p,q} \mathbf{x}_{p,1} + \epsilon_q \mathbf{P}_{q,1}^{H} \sum_{p=1}^{2} \mathbf{H}_{p,q}^{*} \mathbf{x}_{p,1}^{*} + \mathbf{v}_{q,1} \tag{6.32}$$

Performing DFT, one obtains

$$\mathbf{z}_{q,1}^{(\mathrm{f})} = \mu_q \mathbf{Q}_{q,1} \sum_{p=1}^{2} \mathbf{\Gamma}_{p,q} \mathbf{s}_{p,1} + \epsilon_q \overline{\mathbf{Q}}_{q,1} \sum_{p=1}^{2} \overline{\mathbf{\Gamma}}_{p,q} \overline{\mathbf{s}}_{p,1} + \mathbf{v}_{q,1}^{(\mathrm{f})} \tag{6.33}$$

$$\boldsymbol{\rho}_{q,1}^{(\mathrm{f})} = \mathbf{Q}_{q,1} \sum_{p=1}^{2} \mathbf{\Gamma}_{p,q} \mathbf{s}_{p,1} + \overline{\mathbf{Q}}_{q,1} \sum_{p=1}^{2} \overline{\mathbf{\Gamma}}_{p,q} \overline{\mathbf{s}}_{p,1} + \tilde{\mathbf{v}}_{q,1}^{(\mathrm{f})}. \tag{6.34}$$

With the proposed preamble design in Fig. 6.3, where $s_{1,1}[n] \neq 0$ when $n = 0, \cdots, \frac{N}{4} - 1$ and $s_{2,1}[n] \neq 0$ when $n = \frac{N}{4}, \cdots, \frac{N}{2} - 1$, equations (6.15), (6.16) and (6.17) can be further

rewritten respectively as

$$
\begin{aligned}
z^{(\mathrm{f})}_{q,1}[N_\diamond+1] &= \mu_q\left\{I^q_1[-N_\diamond]h^{(\mathrm{f})}_{1,q}[2N_\diamond+1]s_{1,1}[2N_\diamond+1]\cdots+I^q_1[N_\diamond]h^{(\mathrm{f})}_{1,q}[1]s_{1,1}[1]\right\}+v^{(\mathrm{f})}_{q,1}[N_\diamond+1]\\
&\vdots\\
z^{(\mathrm{f})}_{q,1}\left[\frac{N}{4}-N_\diamond-1\right] &= \mu_q\left\{I^q_1[-N_\diamond]h^{(\mathrm{f})}_{1,q}\left[\frac{N}{4}-1\right]s_{1,1}\left[\frac{N}{4}-1\right]+\cdots+\right.\\
&\qquad \left. I^q_1[N_\diamond]h^{(\mathrm{f})}_{1,q}\left[\frac{N}{4}-2N_\diamond-1\right]s_{1,1}\left[\frac{N}{4}-2N_\diamond-1\right]\right\}+v^{(\mathrm{f})}_{q,1}\left[\frac{N}{2}-N_\diamond-1\right]\\
&\vdots\\
z^{(\mathrm{f})}_{q,1}\left[\frac{N}{4}+N_\diamond\right] &= \mu_q\left\{I^q_1[-N_\diamond]h^{(\mathrm{f})}_{2,q}\left[\frac{N}{4}+2N_\diamond\right]s_{2,1}\left[\frac{N}{4}+2N_\diamond\right]+\cdots+\right.\\
&\qquad \left. I^q_1[N_\diamond]h^{(\mathrm{f})}_{2,q}\left[\frac{N}{4}\right]s_{2,1}\left[\frac{N}{4}\right]\right\}+v^{(\mathrm{f})}_{q,1}\left[\frac{N}{4}+N_\diamond\right]\\
&\vdots\\
z^{(\mathrm{f})}_{q,1}\left[\frac{N}{2}-N_\diamond-1\right] &= \mu_q\left\{I^q_1[-N_\diamond]h^{(\mathrm{f})}_{2,q}\left[\frac{N}{2}-1\right]s_{2,1}\left[\frac{N}{2}-1\right]+\cdots+\right.\\
&\qquad \left. I^q_1[N_\diamond]h^{(\mathrm{f})}_{2,q}\left[\frac{N}{2}-2N_\diamond-1\right]s_{2,1}\left[\frac{N}{2}-2N_\diamond-1\right]\right\}+v^{(\mathrm{f})}_{q,1}\left[\frac{N}{2}-N_\diamond-1\right]
\end{aligned}
\tag{6.35}
$$

and

$$
\begin{aligned}
\rho^{(\mathrm{f})}_{q,1}[N_\diamond+1] &= I^q_1[-N_\diamond]h^{(\mathrm{f})}_{1,q}[2N_\diamond+1]s_{1,1}[2N_\diamond+1]\cdots+I^q_1[N_\diamond]h^{(\mathrm{f})}_{1,q}[1]s_{1,1}[1]+\tilde{v}^{(\mathrm{f})}_{q,1}[N_\diamond+1]\\
&\vdots\\
\rho^{(\mathrm{f})}_{q,1}\left[\frac{N}{4}-N_\diamond-1\right] &= I^q_1[-N_\diamond]h^{(\mathrm{f})}_{1,q}\left[\frac{N}{4}-1\right]s_{1,1}\left[\frac{N}{4}-1\right]+\cdots+\\
&\qquad I^q_1[N_\diamond]h^{(\mathrm{f})}_{1,q}\left[\frac{N}{4}-2N_\diamond-1\right]s_{1,1}\left[\frac{N}{4}-2N_\diamond-1\right]+\tilde{v}^{(\mathrm{f})}_{q,1}\left[\frac{N}{2}-N_\diamond-1\right]\\
&\vdots\\
\rho^{(\mathrm{f})}_{q,1}\left[\frac{N}{4}+N_\diamond\right] &= I^q_1[-N_\diamond]h^{(\mathrm{f})}_{2,q}\left[\frac{N}{4}+2N_\diamond\right]s_{2,1}\left[\frac{N}{4}+2N_\diamond\right]+\cdots+\\
&\qquad I^q_1[N_\diamond]h^{(\mathrm{f})}_{2,q}\left[\frac{N}{4}\right]s_{2,1}\left[\frac{N}{4}\right]+\tilde{v}^{(\mathrm{f})}_{q,1}\left[\frac{N}{4}+N_\diamond\right]\\
&\vdots\\
\rho^{(\mathrm{f})}_{q,1}\left[\frac{N}{2}-N_\diamond-1\right] &= I^q_1[-N_\diamond]h^{(\mathrm{f})}_{2,q}\left[\frac{N}{2}-1\right]s_{2,1}\left[\frac{N}{2}-1\right]+\cdots+\\
&\qquad I^q_1[N_\diamond]h^{(\mathrm{f})}_{2,q}\left[\frac{N}{2}-2N_\diamond-1\right]s_{2,1}\left[\frac{N}{2}-2N_\diamond-1\right]+\tilde{v}^{(\mathrm{f})}_{q,1}\left[\frac{N}{2}-N_\diamond-1\right]
\end{aligned}
\tag{6.36}
$$

and

$$
\begin{aligned}
z_{q,1}^{(\mathrm{f})}[N_\diamond+1] &= \mu_q \rho_{q,1}^{(\mathrm{f})}[N_\diamond+1] + \left(v_{q,1}^{(\mathrm{f})}[N_\diamond+1] - \mu_q \tilde{v}_{q,1}^{(\mathrm{f})}[N_\diamond+1]\right) \\
&\vdots \\
z_{q,1}^{(\mathrm{f})}\left[\frac{N}{4}-N_\diamond-1\right] &= \mu_q \rho_{q,1}^{(\mathrm{f})}\left[\frac{N}{4}-N_\diamond-1\right] + \left(v_{q,1}^{(\mathrm{f})}\left[\frac{N}{4}-N_\diamond-1\right] - \mu_q \tilde{v}_{q,1}^{(\mathrm{f})}\left[\frac{N}{4}-N_\diamond-1\right]\right) \\
&\vdots \\
z_{q,1}^{(\mathrm{f})}\left[\frac{N}{4}+N_\diamond\right] &= \mu_q \rho_{q,1}^{(\mathrm{f})}\left[\frac{N}{4}+N_\diamond\right] + \left(v_{q,1}^{(\mathrm{f})}\left[\frac{N}{4}+N_\diamond\right] - \mu_q \tilde{v}_{q,1}^{(\mathrm{f})}\left[\frac{N}{4}+N_\diamond\right]\right) \\
&\vdots \\
z_{q,1}^{(\mathrm{f})}\left[\frac{N}{2}-N_\diamond-1\right] &= \mu_q \rho_{q,1}^{(\mathrm{f})}\left[\frac{N}{2}-N_\diamond-1\right] + \left(v_{q,1}^{(\mathrm{f})}\left[\frac{N}{2}-N_\diamond-1\right] - \mu_q \tilde{v}_{q,1}^{(\mathrm{f})}\left[\frac{N}{2}-N_\diamond-1\right]\right)
\end{aligned}
\tag{6.37}
$$

Remarks:

- From (6.35) and (6.36), the received signal samples from the $(N_\diamond+1)$th sample to the $\left(\frac{N}{4}-N_\diamond-1\right)$th sample do not depend on the non-zero elements in $\mathbf{s}_{2,1}$. Similarly, the received signal samples from the $\left(\frac{N}{4}+N_\diamond\right)$th sample to the $\left(\frac{N}{2}-N_\diamond-1\right)$th sample do not depend on the non-zero elements in $\mathbf{s}_{1,1}$.

- From (6.37), the IQ imbalance parameters can be estimated as

$$
\begin{aligned}
\hat{\mu}_q &= \frac{1}{|\vartheta|}\sum_{n\in\vartheta}\frac{z_{q,1}^{(\mathrm{f})}[n]}{\rho_{q,1}^{(\mathrm{f})}[n]} \\
\hat{\epsilon}_q &= 1-\hat{\mu}_q^*
\end{aligned}
\tag{6.38}
$$

  in which $\vartheta = \left[(N_\diamond+1):\left(\frac{N}{4}-N_\diamond-1\right)\right] \cup \left[\left(\frac{N}{4}+N_\diamond\right):\left(\frac{N}{2}-N_\diamond-1\right)\right]$ and $|\vartheta|$ returns the cardinality of ϑ.

- The received signal samples from the $\left(\frac{N}{4}-N_\diamond\right)$th sample to the $\left(\frac{N}{4}+N_\diamond-1\right)$th sample depend on the non-zero elements from both $\mathbf{s}_{1,1}$ and $\mathbf{s}_{2,1}$. As such, they cannot be used to estimate the IQ imbalance parameters. Compared to the SISO scenario, $2N_\diamond$ samples cannot be used to estimate the IQ imbalance parameters which, therefore, results in a degradation in the quality of IQ imbalance estimation. However, when the number of samples is large enough, this degradation can be negligible.

- The preamble design can be straightforwardly extended when the number of transmit antennas is greater than two. In general, with N_t transmit antennas, $(2^{N_t-1}N_\diamond+2N_\diamond+1)$ samples in the first half of the preamble cannot be used in estimating the IQ imbalance parameters.

PN and Channel Estimation

Once $\hat{\mu}_q$ and $\hat{\epsilon}_q$ are obtained, the IQ imbalance compensation is performed on the preamble of the qth receive antenna to obtain

$$\mathbf{r}_{q,1} = \frac{\hat{\mu}_q^* \mathbf{z}_{q,1} - \hat{\epsilon}_q \mathbf{z}_{q,1}^*}{|\hat{\mu}_q|^2 - |\hat{\epsilon}_q|^2} \approx \mathbf{P}_{q,1} \sum_{p=1}^{N_t} \mathbf{H}_{p,q} \mathbf{x}_{p,1} + \hat{\mathbf{w}}_{q,1} \tag{6.39}$$

where $\hat{\mathbf{w}}_{q,1} = \mathbf{P}_{q,1}\mathbf{w}_{q,1}$. The above equation can be rewritten as follows:

$$\mathbf{r}_{q,1} \approx \mathbf{P}_{q,1}\mathbf{K}\mathbf{h}_q + \hat{\mathbf{w}}_{q,1} \tag{6.40}$$

where $\mathbf{h}_q = \begin{bmatrix} \mathbf{h}_{1,q}^T & \mathbf{h}_{2,q}^T & \cdots & \mathbf{h}_{N_t,q}^T \end{bmatrix}^T$ and $\mathbf{K} = \begin{bmatrix} \mathbf{K}_1 & \mathbf{K}_2 & \cdots & \mathbf{K}_{N_t} \end{bmatrix}$ with $\mathbf{K}_p = \sqrt{N}\mathbf{F}^H \mathbf{S}_{p,1} \breve{\mathbf{F}}$ and $\mathbf{S}_{p,1} = \text{diag}[\mathbf{s}_{p,1}]$. Equation (6.40) is now similar to (6.21). As such, the channel can be first estimated based on the MMSE method as

$$\mathbf{h}_{q,\text{MMSE}} = \mathbf{\Sigma}_{\mathbf{h}_q} \mathbf{K}^H \left(\mathbf{K} \mathbf{\Sigma}_{\mathbf{h}_q} \mathbf{K}^H + \sigma_{\mathbf{w}}^2 \mathbf{I} \right)^{-1} \mathbf{P}_{q,1}^H \mathbf{r}_{q,1} \tag{6.41}$$

where $\mathbf{\Sigma}_{\mathbf{h}_q} = \text{E}\left[\mathbf{h}_q \mathbf{h}_q^H\right] = \text{diag}\left[\mathbf{\Sigma}_{1,q} \quad \mathbf{\Sigma}_{2,q} \quad \cdots \quad \mathbf{\Sigma}_{N_t,q}\right]$.

Define $\mathbf{U}_q = \mathbf{I} - 2\mathbf{\Lambda}_q + \mathbf{\Lambda}_q\mathbf{\Lambda}_q$ where $\mathbf{\Lambda}_q = \mathbf{K}\mathbf{\Sigma}_{\mathbf{h}_q}\mathbf{K}^H \left(\mathbf{K}\mathbf{\Sigma}_{\mathbf{h}_q}\mathbf{K}^H + \sigma_{\mathbf{w}}^2\mathbf{I} \right)^{-1}$ and $\mathbf{V}_q = \lambda_{q,\max}\mathbf{I}_{N\times N}$ where $\lambda_{q,\max}$ is the maximum eigenvalue of $\mathbf{U}_q$. Let $\mathbf{R}_q = \text{diag}\left[\mathbf{r}_{q,1}\right]$, and $\boldsymbol{\eta}_q = \begin{bmatrix} \eta_{q,0} & \eta_{q,1} & \cdots & \eta_{q,N-1} \end{bmatrix}^T = \text{diag}\left[\mathbf{P}_{q,1}\right]^H$. Then, the PN from the qth receive mixer corresponding to the preamble can be estimated by solving the following optimization problem:

$$\begin{aligned} &\underset{\boldsymbol{\eta}_q}{\text{minimize}} \quad \boldsymbol{\eta}_q^H \mathbf{R}_q^H \mathbf{U}_q \mathbf{R}_q \boldsymbol{\eta}_q \\ &\text{subject to} \quad |\eta_{q,n}| = 1; \quad n = 0, 1, \cdots, N-1. \end{aligned} \tag{6.42}$$

A closed-form solution for (6.42) is obtained as

$$\boldsymbol{\eta}_{q,t+1} = \text{e}^{j \arg(\mathbf{R}_q^H(\mathbf{U}_q - \mathbf{V}_q)\mathbf{R}_q \boldsymbol{\eta}_{q,t})}. \tag{6.43}$$

The estimated PN obtained from the optimization problem is then substituted back into (6.41) to find $\mathbf{h}_{q,\mathrm{MMSE}}$.

Remarks:

- Only one transmission block is required as a preamble to perform the first stage of the proposed algorithm, making it spectrally efficient.
- With the proposed preamble, estimation of IQ imbalance parameters as well as the set of channel impulse responses corresponding to a given receive antenna can be performed as (6.38) and (6.41), respectively.
- The algorithm in the first stage can be significantly simplified based on the structure of the preamble. For example, when $N_t = 2$, one has

$$\begin{aligned} \mathbf{K}_1 &= \sqrt{N}\mathbf{F}^H\mathbf{S}_{1,1}\breve{\mathbf{F}} = \sqrt{N}\mathbf{F}_1^H\mathbf{A}\breve{\mathbf{F}}_1 \\ \mathbf{K}_2 &= \sqrt{N}\mathbf{F}^H\mathbf{S}_{2,1}\breve{\mathbf{F}} = \sqrt{N}\mathbf{F}_2^H\mathbf{A}\breve{\mathbf{F}}_2 \end{aligned} \tag{6.44}$$

  where $\mathbf{A}$ is the $N/4 \times N/4$ diagonal matrix whose diagonal contains all the non-zero elements of the preamble. Matrices $\mathbf{F}_1$ and $\breve{\mathbf{F}}_1$ are obtained from $\mathbf{F}$ and $\breve{\mathbf{F}}$, respectively, by keeping the first $N/4$ rows. On the other hand, matrices $\mathbf{F}_2$ and $\breve{\mathbf{F}}_2$ are obtained from $\mathbf{F}$ and $\breve{\mathbf{F}}$, respectively, by taking the rows from $\left(\frac{N}{4}+1\right)$ to $\frac{N}{2}$.

6.4.2 Stage 2: Data Detection

For a MIMO system, the use of multiple antennas can be broadly classified into two categories: spatial multiplexing techniques and spatial diversity techniques [34, 35]. While the first class aims to increase the transmission rate, the second class is to improve the transmission reliability. This paper focuses on a diversity technique, namely space-frequency block code (SFBC) [34, 35].

Generation of SFBC for CP-Based Multi-Carrier Systems

To implement SFBC for CP-based multi-carrier systems, this paper proposes a strategy as illustrated in Fig. 6.4 for the simple case of $N_t = 2$. Specifically, the modulated signal

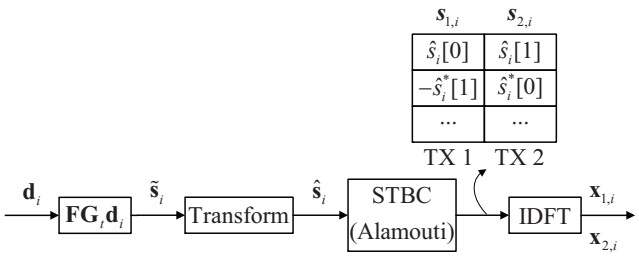

Figure 6.4: SFBC in CP-based multi-carrier systems when $N_t = 2$.

$\mathbf{d}_i$ is first transformed to $\tilde{\mathbf{s}}_i = \mathbf{F}\mathbf{G}_t\mathbf{d}_i$. Then $\tilde{\mathbf{s}}_i = \begin{bmatrix} \tilde{s}_i[0] & \tilde{s}_i[1] & \cdots & \tilde{s}_i[N-1] \end{bmatrix}^T$ is converted to $\hat{\mathbf{s}}_i = \begin{bmatrix} \tilde{s}_i[0] & -\tilde{s}_i^*[1] & \cdots & -\tilde{s}_i^*[N-1] \end{bmatrix}^T$. Finally, $\hat{\mathbf{s}}_i$ is passed through a space-time block code (STBC), which can be the Alamouti code [34] for $N_t = 2$. The generated signals $\mathbf{s}_{1,i}$ and $\mathbf{s}_{2,i}$ for two transmit antennas which are finally passed through an IDFT block to obtain $\mathbf{x}_{1,i}$ and $\mathbf{x}_{2,i}$, respectively.

The transmitted signal on the first transmit antenna is the same as in the single-antenna system, i.e., $\mathbf{G}_t\mathbf{d}_i$, whereas the transmitted signal on the second transmit antenna is an orthogonally transformed version of the one from the first antenna. For OFDM, $\mathbf{G}_t = \mathbf{F}^H$, so that $\tilde{\mathbf{s}}_i = \mathbf{d}_i$. Compared to the conventional MIMO-OFDM with SFBC [34, 35], the proposed strategy is different in the way that a new block, namely $\mathbf{F}\mathbf{G}_t\mathbf{d}_i$, is added in order to adapt to the general multi-carrier modulation matrix $\mathbf{G}_t$.

At the receiver, signal processing can be carried out in a similar manner as in the SISO system. However, the channel equalizer is replaced by an SFBC combiner. The estimate corresponding to $\hat{\mathbf{s}}_i$ can be derived as

$$\begin{bmatrix} \hat{s}_i[n] \\ \hat{s}_i[n+1] \end{bmatrix} = \hat{\mathbf{L}}_{n,n+1} \begin{bmatrix} \tilde{r}_{1,i}[n] \\ \tilde{r}_{2,i}[n] \\ \tilde{r}_{1,i}^*[n+1] \\ \tilde{r}_{2,i}^*[n+1] \end{bmatrix} \tag{6.45}$$

where

$$\hat{\mathbf{L}}_{n,n+1} = \left(\mathbf{L}_{n,n+1}^H \mathbf{L}_{n,n+1}\right)^{-1} \mathbf{L}_{n,n+1}^H \tag{6.46}$$

and

$$\mathbf{L}_{n,n+1} = \begin{bmatrix} h_{1,1}^{(\mathrm{f})}[n] & h_{2,1}^{(\mathrm{f})}[n] \\ h_{1,2}^{(\mathrm{f})}[n] & h_{2,2}^{(\mathrm{f})}[n] \\ (h_{1,1}^{(\mathrm{f})}[n+1])^* & -(h_{1,1}^{(\mathrm{f})}[n+1])^* \\ (h_{2,2}^{(\mathrm{f})}[n+1])^* & -(h_{1,2}^{(\mathrm{f})}[n+1])^* \end{bmatrix} \tag{6.47}$$

and $\tilde{\mathbf{r}}_{q,i}$ is the received signal corresponding to the ith transmission block at the qth receive antenna after DFT. From (6.45), the transmitted signal $\mathbf{d}_i$ can be finally recovered.

Data Detection

The received signal at the qth receive antenna corresponding to the ith data transmission block after the IQ imbalance compensation is written as

$$\mathbf{r}_{q,i} = \frac{\hat{\mu}_q^* \mathbf{z}_{q,i} - \hat{\epsilon}_q \mathbf{z}_{q,i}^*}{|\hat{\mu}_q|^2 - |\hat{\epsilon}_q|^2} \approx \mathbf{P}_{q,i} \mathbf{F}^H \sum_{p=1}^{N_t} \mathbf{\Gamma}_{p,q} \mathbf{s}_{p,i} + \hat{\mathbf{w}}_{q,i} \tag{6.48}$$

where $\hat{\mathbf{w}}_{q,i} = \mathbf{P}_{q,i}\mathbf{w}_{q,i}$, $\mathbf{s}_{p,i} = \mathbf{F}\mathbf{x}_{p,i}$ and $2 \leq i \leq N_f$.

Similar to the SISO scenario, it is assumed that the conjugate PN at the qth receive antenna corresponding to the ith transmission block, i.e., $\mathbf{P}_{q,i}^H$, can be approximately represented as a multiplication of a known basis matrix $\mathbf{\Omega}_{q,i} = \begin{bmatrix} \boldsymbol{\omega}_{q,i}^{(0)} & \boldsymbol{\omega}_{q,i}^{(1)} & \cdots & \boldsymbol{\omega}_{q,i}^{(N_b-1)} \end{bmatrix}$ containing N_b column vectors $\boldsymbol{\omega}_{q,i}^{(n)} = \begin{bmatrix} \omega_{q,i}^{(n,0)} & \cdots & \omega_{q,i}^{(n,N-1)} \end{bmatrix}^T$ and an unknown vector $\boldsymbol{\gamma}_{q,i} = \begin{bmatrix} \gamma_{q,i}^{(0)} & \cdots & \gamma_{q,i}^{(N_b-1)} \end{bmatrix}^T$. The goal is to estimate $\boldsymbol{\gamma}_{q,i}$ so that $\mathbf{\Omega}_{q,i}\boldsymbol{\gamma}_{q,i}$ can be used to multiply with the received signal $\mathbf{r}_{q,i}$ to compensate for the PN impact.

After the PN compensation, the output signal is approximately written as

$$\mathrm{diag}[\mathbf{r}_{q,i}]\mathbf{\Omega}_{q,i}\boldsymbol{\gamma}_{q,i} \approx \mathbf{F}^H \sum_{p=1}^{N_t} \mathbf{\Gamma}_{p,q} \mathbf{s}_{p,i} + \bar{\mathbf{w}}_{q,i} \tag{6.49}$$

where $\bar{\mathbf{w}}_{q,i} = \mathrm{diag}[\hat{\mathbf{w}}_{q,i}]\mathbf{\Omega}_{q,i}\boldsymbol{\gamma}_{q,i}$. The received signal is further processed to detect the transmitted signal by first passing through a DFT. Define $\mathbf{\Upsilon}_{q,i} = \mathbf{F}\mathrm{diag}[\mathbf{r}_{q,i}]\mathbf{\Omega}_{q,i}$ and $\tilde{\mathbf{w}}_{q,i} = \mathbf{F}\bar{\mathbf{w}}_{q,i}$. Then the signal after DFT is written as

$$\tilde{\mathbf{r}}_{q,i} = \mathbf{\Upsilon}_{q,i}\boldsymbol{\gamma}_{q,i} \approx \sum_{p=1}^{N_t} \mathbf{\Gamma}_{p,q} \mathbf{s}_{q,i} + \tilde{\mathbf{w}}_{q,i}. \tag{6.50}$$

To illustrate how $\boldsymbol{\gamma}_{q,i}$ can be estimated based on the transmitted pilot symbols, a 2×2 MIMO system is considered. Given the PN-compensated received signal $\tilde{\mathbf{r}}_{q,i}$, the transmitted signal $\hat{\mathbf{s}}_i$ can be detected as

$$\begin{bmatrix} \hat{s}_i[0] \\ \hat{s}_i[1] \\ \vdots \\ \hat{s}_i[N-2] \\ \hat{s}_i[N-1] \end{bmatrix} \overset{(6.45)}{=} \underbrace{\begin{bmatrix} \hat{\mathbf{L}}_{0,1} & \mathbf{0} & \cdots & \mathbf{0} & \mathbf{0} \\ \mathbf{0} & \hat{\mathbf{L}}_{2,3} & \cdots & \mathbf{0} & \mathbf{0} \\ \vdots & \vdots & \ddots & \vdots & \vdots \\ \mathbf{0} & \mathbf{0} & \cdots & \hat{\mathbf{L}}_{N-4,N-3} & \mathbf{0} \\ \mathbf{0} & \mathbf{0} & \cdots & \mathbf{0} & \hat{\mathbf{L}}_{N-2,N-1} \end{bmatrix}}_{\hat{\mathbf{L}}} \begin{bmatrix} \tilde{r}_{1,i}[0] \\ \tilde{r}_{2,i}[0] \\ \tilde{r}^*_{1,i}[1] \\ \tilde{r}^*_{2,i}[1] \\ \vdots \\ \tilde{r}_{1,i}[N-2] \\ \tilde{r}_{2,i}[N-2] \\ \tilde{r}^*_{1,i}[N-1] \\ \tilde{r}^*_{2,i}[N-1] \end{bmatrix}. \tag{6.51}$$

It is worth pointing out that the channel frequency responses in $\hat{\mathbf{L}}$ are from the estimated channel in (6.41). Given that the right-hand side of (6.51) is derived as

$$\begin{aligned} \begin{bmatrix} \tilde{r}_{1,i}[0] \\ \tilde{r}_{2,i}[0] \\ \tilde{r}^*_{1,i}[1] \\ \tilde{r}^*_{2,i}[1] \\ \vdots \\ \tilde{r}_{1,i}[N-2] \\ \tilde{r}_{2,i}[N-2] \\ \tilde{r}^*_{1,i}[N-1] \\ \tilde{r}^*_{2,i}[N-1] \end{bmatrix} &\overset{(6.50)}{=} \underbrace{\begin{bmatrix} \boldsymbol{\Upsilon}_{1,i}[0,:] \\ \mathbf{0} \\ \mathbf{0} \\ \mathbf{0} \\ \vdots \\ \boldsymbol{\Upsilon}_{1,i}[N-2,:] \\ \mathbf{0} \\ \mathbf{0} \\ \mathbf{0} \end{bmatrix}}_{\ddot{\boldsymbol{\Delta}}_{1,i}} \gamma_{1,i} + \underbrace{\begin{bmatrix} \mathbf{0} \\ \boldsymbol{\Upsilon}_{2,i}[0,:] \\ \mathbf{0} \\ \mathbf{0} \\ \vdots \\ \mathbf{0} \\ \boldsymbol{\Upsilon}_{2,i}[N-2,:] \\ \mathbf{0} \\ \mathbf{0} \end{bmatrix}}_{\ddot{\boldsymbol{\Delta}}_{2,i}} \gamma_{2,i} + \underbrace{\begin{bmatrix} \mathbf{0} \\ \mathbf{0} \\ \boldsymbol{\Upsilon}^*_{1,i}[1,:] \\ \mathbf{0} \\ \vdots \\ \mathbf{0} \\ \mathbf{0} \\ \boldsymbol{\Upsilon}^*_{1,i}[N-1,:] \\ \mathbf{0} \end{bmatrix}}_{\ddot{\boldsymbol{\Delta}}_{c,1,i}} \gamma^*_{1,i} + \underbrace{\begin{bmatrix} \mathbf{0} \\ \mathbf{0} \\ \mathbf{0} \\ \boldsymbol{\Upsilon}^*_{2,i}[1,:] \\ \vdots \\ \mathbf{0} \\ \mathbf{0} \\ \mathbf{0} \\ \boldsymbol{\Upsilon}^*_{2,i}[N-1,:] \end{bmatrix}}_{\ddot{\boldsymbol{\Delta}}_{c,2,i}} \gamma^*_{2,i} \\ &= \begin{bmatrix} \ddot{\boldsymbol{\Delta}}_{1,i} & \ddot{\boldsymbol{\Delta}}_{2,i} & \ddot{\boldsymbol{\Delta}}_{c,1,i} & \ddot{\boldsymbol{\Delta}}_{c,2,i} \end{bmatrix} \begin{bmatrix} \gamma_{1,i} \\ \gamma_{2,i} \\ \gamma^*_{1,i} \\ \gamma^*_{2,i} \end{bmatrix} = \ddot{\boldsymbol{\Delta}}_i \hat{\boldsymbol{\gamma}}_i. \end{aligned} \tag{6.52}$$

Equation (6.51) can be rewritten as

$$\hat{\mathbf{s}}_i = \boldsymbol{\Delta}_i \hat{\boldsymbol{\gamma}}_i \tag{6.53}$$

where $\boldsymbol{\Delta}_i = \hat{\mathbf{L}}\ddot{\boldsymbol{\Delta}}_i$. Given the estimate of $\hat{\mathbf{s}}_i$, $\tilde{\mathbf{s}}_i$ can be derived as

$$\tilde{\mathbf{s}}_i = \begin{bmatrix} \hat{s}_i[0] \\ -\hat{s}_i^*[1] \\ \vdots \\ \hat{s}_i[N-2] \\ -\hat{s}_i^*[N-1] \end{bmatrix} = \begin{bmatrix} \boldsymbol{\Delta}_i[0,:] \\ -\bar{\boldsymbol{\Delta}}_i[1,:] \\ \vdots \\ \boldsymbol{\Delta}_i[N-2,:] \\ -\bar{\boldsymbol{\Delta}}_i[N-1,:] \end{bmatrix} \hat{\boldsymbol{\gamma}}_i = \hat{\boldsymbol{\Delta}}_i \hat{\boldsymbol{\gamma}}_i \tag{6.54}$$

in which $\bar{\boldsymbol{\Delta}}_i[n,:]$ is obtained from $\boldsymbol{\Delta}_i[n,:]$ by first conjugating $\boldsymbol{\Delta}_i[n,:]$ and then swapping locations of the first half and the second half of the conjugated result.

Define $\mathbf{p} = \begin{bmatrix} p_0 & p_1 & \cdots & p_{T-1} \end{bmatrix}$ as a set of pilot indexes in each transmission block, and $\mathbf{d}_i^{[\mathbf{p}]} = \begin{bmatrix} d_i^{[p_0]} & d_i^{[p_1]} & \cdots & d_i^{[p_{T-1}]} \end{bmatrix}^T$ as the transmitted signal corresponding to the pilot index set for the ith transmission block. Furthermore, define $\breve{\boldsymbol{\Delta}}_i^{[\mathbf{p}]}$ as the matrix obtained from $\breve{\boldsymbol{\Delta}}_i = \mathbf{G}_r \mathbf{F}^H \hat{\boldsymbol{\Delta}}_i$ by keeping the rows corresponding to the pilot indexes. Thus, $\hat{\boldsymbol{\gamma}}_i$ can be estimated as

$$\hat{\boldsymbol{\gamma}}_i = \left(\breve{\boldsymbol{\Delta}}_i^{[\mathbf{p}]} \right)^{\dagger} \mathbf{d}_i^{[\mathbf{p}]}. \tag{6.55}$$

For CFBMC, a similar adjustment as presented in Section 6.3.2 needs to be performed in order to estimate $\hat{\boldsymbol{\gamma}}_i$. Given $\hat{\boldsymbol{\gamma}}_i$, $\boldsymbol{\gamma}_{q,i}$ for the qth receive antenna can be derived as

$$\begin{aligned} \boldsymbol{\gamma}_{1,i} &= \frac{1}{2} \left(\hat{\boldsymbol{\gamma}}_i \left[1 : N_b \right] + \hat{\boldsymbol{\gamma}}_i^* \left[2N_b + 1 : 3N_b \right] \right) \\ \boldsymbol{\gamma}_{2,i} &= \frac{1}{2} \left(\hat{\boldsymbol{\gamma}}_i \left[N_b + 1 : 2N_b \right] + \hat{\boldsymbol{\gamma}}_i^* \left[3N_b + 1 : 4N_b \right] \right). \end{aligned} \tag{6.56}$$

Before closing this section, it is pointed out that the proposed algorithm can be applied to the general case where each receive antenna experiences different IQ imbalance and PN impact. In the special case when all receive antennas are using the same mixer to down-convert the received signal and thus experience from the same IQ imbalance and PN, then the estimation of IQ imbalance, PN, and channel impulse responses can be further improved by averaging (6.38), (6.43), and (6.56).

6.5 Simulation Results

In this section, performance of the proposed two-stage PN and IQ imbalance compensation algorithm is evaluated in various scenarios and with parameters listed in Ta-

Table A.2: Simulation parameters.

Channel coding	Convolutional code (Rate: 1/3; Constraint length: 7; Generator polynomials: $[133\ 171\ 165]_8$);
Channel decoding	Hard-decision Viterbi decoding;
Modulation	16-QAM;
Block structure	$N = 768$ (OFDM); $K = 256; M = 3$ (GFDM, CFBMC);
Prototype filter	CFBMC: Martin; GFDM: Raised Cosine (Roll-off factor: 0.1);
Blocks/Frame	$N_f = 10$;
Carrier frequency	$f_c = 6$ GHz;
Bandwidth	$B = 100$ MHz;
Sampling interval	$T_s = 1/B$;
Channel	EVA ($N_g = 251$);
MIMO	$N_t = 2; N_r = 2$; SFBC;
Phase noise	$c_v = \{5 \times 10^{-19}; 5 \times 10^{-18}; 2 \times 10^{-17}\}$;
IQ imbalance	SISO: $g = 1.1; \psi \sim \mathbb{U}[-\pi/36; \pi/36]$; MIMO: $\mathbf{g} = [1.1; 1.05]; \boldsymbol{\psi} \sim \mathbb{U}[-\pi/36; \pi/36]$;

ble A.2. Among many CP-based multi-carrier modulation systems, this paper investigates OFDM, GFDM and CFBMC-OQAM as they represent different classes of multi-carrier systems, namely, orthogonal, non-orthogonal and real-domain orthogonal systems, respectively. The simulation results are first presented for SISO, and then for MIMO systems. When $c_v = 5 \times 10^{-19}$ and $c_v = 5 \times 10^{-18}$, $N_\diamond = 2$ is chosen. However, when $c_v = 2 \times 10^{-17}$, i.e., more severe PN, $N_\diamond = 4$ is chosen.

The PN estimation in the first stage is initialized with $\boldsymbol{\eta}_0 = \mathbf{1}_{N\times 1}$ and the number of iterations is set to $N_{\text{iter}} = 10$. To perform the second stage, pilots are inserted into each transmission block at positions $q_1 = 2 + 4n_1$ where $n_1 = 0 : 191$ for OFDM and $n_2 = 0 : 63$ in each time slot for CFBMC and GFDM. It is pointed out that, different from OFDM, CFBMC and GFDM have block-based structures. Therefore, the above pilot configuration in each time slot results in 192 total pilot symbols in CFBMC and GFDM, which is the same number of pilots for OFDM. This pilot configuration corresponds to a pilot ratio 1/4. For simplicity the ZF demodulator is used for GFDM.

6.5.1 SISO Scenario

For the preamble $\mathbf{s}_1$, a length–$\frac{N}{2}$ Zadoff-Chu sequence with the sequence index $u = 25$ is generated for the first half, and all zero elements are set for the second half.

Stage 1

Performance of the first stage is illustrated in Fig. 6.5 for the IQ imbalance estimation, PN estimation, and channel impulse response estimation. Recall that with the proposed preamble design, the first stage can be performed in the same way for all CP-based multi-carrier systems. As such, the performance in Fig. 6.5 would apply for all three CP-based multi-carrier systems considered in this paper. In the simulation, PN is varied from medium when $c_v = 5 \times 10^{-19}$ to very high when $c_v = 2 \times 10^{-17}$. For the IQ imbalance, while the amplitude imbalance is set to $g = 1.1$, the phase imbalance is generated as a uniformly distributed random variable over $-\pi/36$ to $\pi/36$. When the proposed algorithm is employed, its performance is labeled based on the value of c_v. On the other hand, "No PN and IQ"

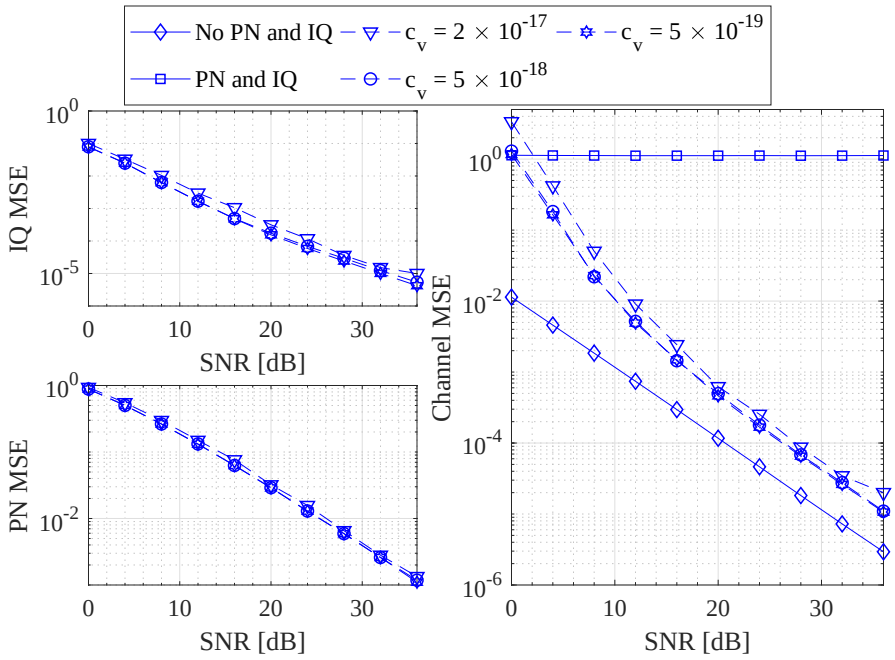

Figure 6.5: MSE performance of CP-based SISO multi-carrier systems in the presence of PN and IQ imbalance.

refers to the ideal case where there is no PN and IQ imbalance at the receive mixer, "PN and IQ" is obtained under the impact of IQ imbalance and PN with $c_v = 5 \times 10^{-19}$ and without performing any compensation.

First, for the channel MSE performance, it can be seen that the system completely fails on estimating the channel impulse response in the presence of PN and IQ imbalance even under the lowest level of PN [2]. However, when the first stage is applied, the channel MSE performance is significantly improved. Specifically, only approximately 5.5 dB performance gap is observed at MSE $= 10^{-4}$ between "No PN and IQ" and the proposed algorithm when $c_v = 5 \times 10^{-19}$. When the PN level is increased by 10 times, i.e., $c_v = 5 \times 10^{-18}$, only additional 0.2 dB loss is seen. When $c_v = 2 \times 10^{-17}$, the performance gap is further increased by around 1.3 dB.

By adaptively choosing $N_\diamond$, the MSE performance of IQ imbalance and PN estimations is not much different when varying the PN level. In particular, for the IQ imbalance estimation,

[2]This is the reason why the performance curves for "PN and IQ" when $c_v = 5 \times 10^{-18}$ or $c_v = 2 \times 10^{-17}$ are not shown in Fig. 6.5.

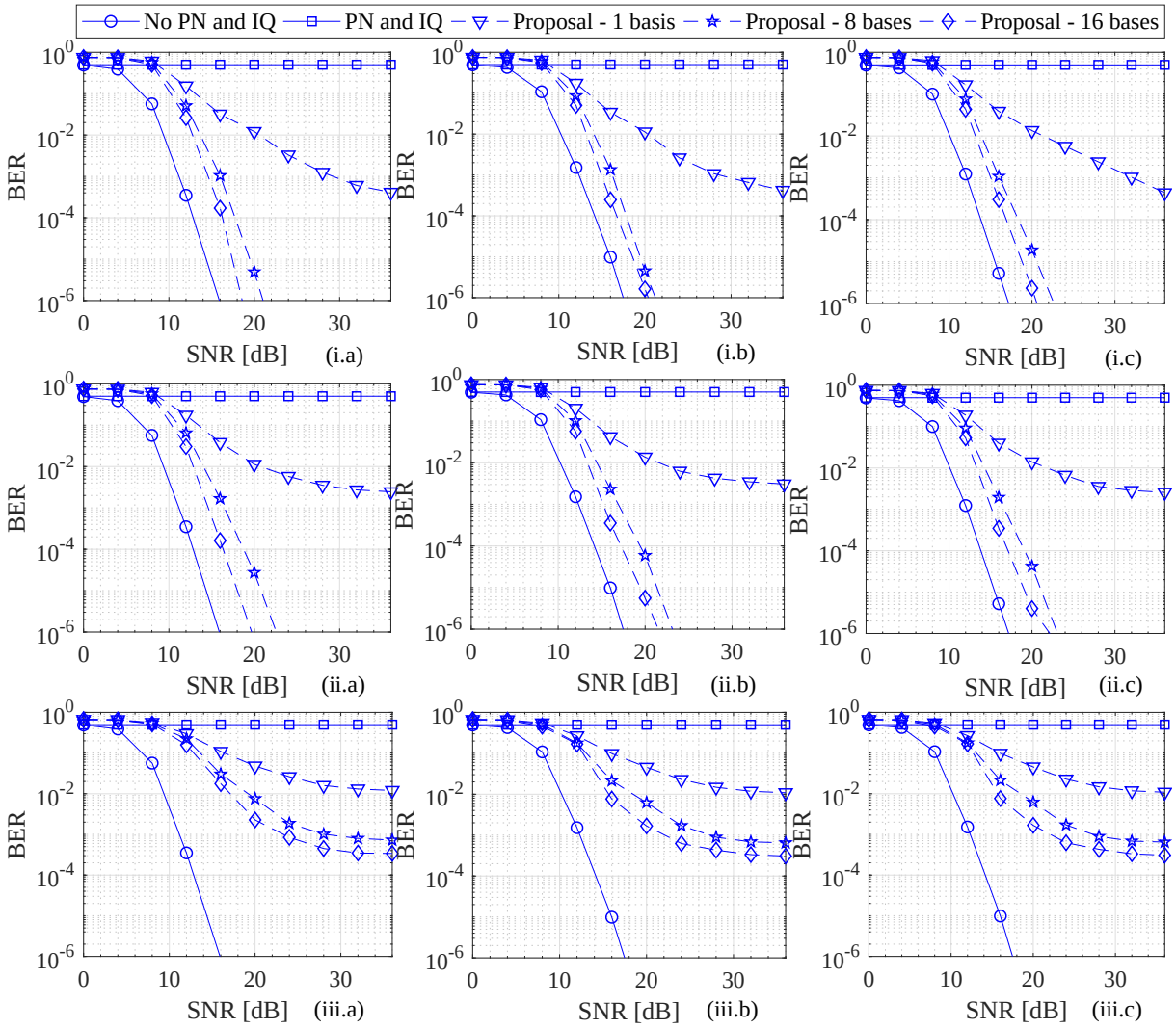

Figure 6.6: Bit-error rate performance of CP-based SISO multi-carrier systems in the presence of PN and IQ imbalance. (a) OFDM, (b) CFBMC, (c) GFDM, (i) $c_v = 5 \times 10^{-19}$, (ii) $c_v = 5 \times 10^{-18}$, and (iii) $c_v = 2 \times 10^{-17}$.

only 0.6 dB and 2.7 dB performance losses are observed when the PN level increases from $c_v = 5 \times 10^{-19}$ to $c_v = 5 \times 10^{-18}$ and from $c_v = 5 \times 10^{-19}$ to $c_v = 2 \times 10^{-17}$, respectively, at MSE $= 10^{-4}$. For the PN estimation, the performance gap between $c_v = 5 \times 10^{-19}$ and $c_v = 2 \times 10^{-17}$ is only 0.8 dB at MSE $= 10^{-2}$. The MSE performances when $c_v = 5 \times 10^{-19}$ and $c_v = 5 \times 10^{-18}$ are almost the same.

Stage 2

Performance of the second stage in terms of the bit-error rate (BER) is shown in Fig. 6.6. For the second stage, it is assumed that all bases are generated from a DFT matrix. First, it can be seen that in the ideal case, i.e., "No PN and IQ", the BER performance of OFDM is slightly better than that of CFBMC and GFDM. In particular, at BER $= 10^{-5}$, the degradations are approximately 1.6 dB and 1.2 dB for CFBMC and GFDM, respectively. These degradations are due to, respectively, noise enhancement induced from the use of ZF demodulator in GFDM [7] and the self-interference in CFBMC [22]. Similar to channel estimation performance, in the presence of PN and IQ imbalance, all the considered CP-based multi-carrier systems fail on detecting the received signal without any compensation. By deploying the proposed algorithm, performance of the systems is clearly improved. When $c_v = 5 \times 10^{-19}$, increasing the number of bases from 8 to 16 helps to further gain 2.0 dB for OFDM, 0.9 dB for CFBMC and 1.8 dB for GFDM at BER $= 10^{-5}$. Compared to the ideal case, only 3.1 dB, 2.6 dB, and 3.3 dB performance losses are observed for OFDM, CFBMC, and GFDM, respectively, when 16 bases are used in the proposed algorithm.

When $c_v = 5 \times 10^{-18}$, the performance gaps between "No PN and IQ" and the proposed algorithm using 16 bases are 3.7 dB, 3.5 dB and 3.7 dB for OFDM, CFBMC, and GFDM, respectively, at BER $= 10^{-5}$. Therefore, only around 0.6 dB, 0.9 dB and 0.4 dB losses are observed even when compared to the case $c_v = 5 \times 10^{-19}$. When $c_v = 2 \times 10^{-17}$, although increasing the number of bases still considerably improves the detection, performance of all three systems is saturated above BER $= 10^{-4}$.

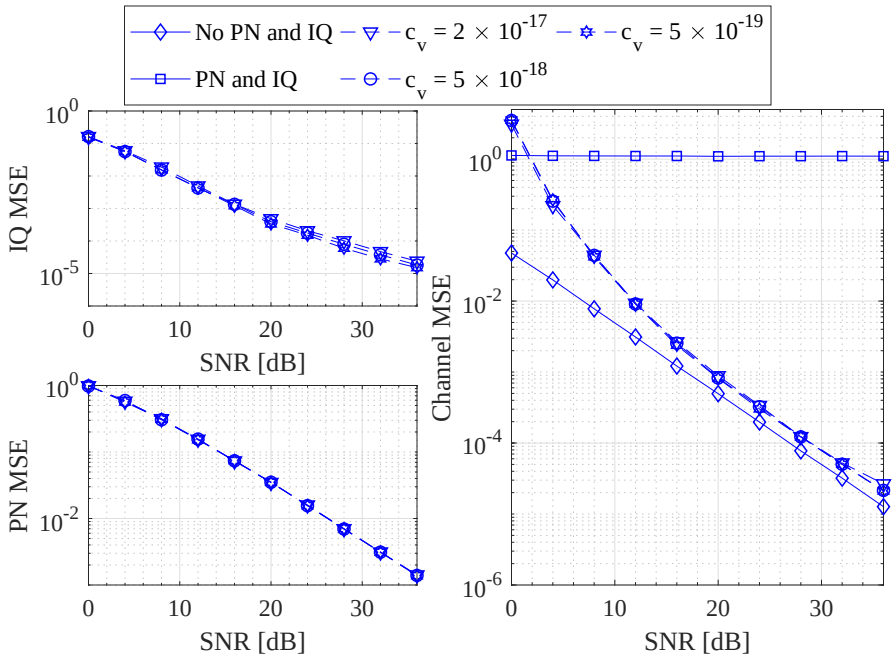

Figure 6.7: MSE performance of CP-based 2×2 multi-carrier systems in the presence of PN and IQ imbalance.

6.5.2 MIMO Scenario

For the MIMO scenario, it is assumed that $N_t = N_r = 2$. The preamble is designed such that $s_{1,1}[n] \neq 0$ when $n = 0, \cdots, \frac{N}{4} - 1$ and $s_{2,1}[n] \neq 0$ when $n = \frac{N}{4}, \cdots, \frac{N}{2} - 1$. The non-zero portions in $\mathbf{s}_{1,1}$ and $\mathbf{s}_{2,1}$ are generated from a length–$\frac{N}{4}$ Zadoff-Chu sequence with the sequence index $u = 25$. Here, PN and IQ imbalance are generated differently for each receive antenna. Specifically, $\mathbf{g} = \begin{bmatrix} 1.1 & 1.05 \end{bmatrix}$ and $\boldsymbol{\psi} \sim \mathbb{U}[-\pi/36; \pi/36]$.

Stage 1

To evaluate the MSE performance of the first stage, the Frobenius norm is used for the estimated channel impulse responses, estimated IQ imbalances and estimated PNs. Performance of the first stage is shown in Fig. 6.7. There is not much difference in the MSE performances when $c_v = 5 \times 10^{-19}$ and $c_v = 2 \times 10^{-17}$. For the channel estimation, approximately 1.9 dB performance loss is observed at MSE $= 10^{-4}$ between the ideal case and the proposed algorithm when $c_v = 5 \times 10^{-19}$. For the IQ imbalance estimation, about 1.1 dB and 2.3 dB gaps are seen when the PN level increases from $c_v = 5 \times 10^{-19}$ to $c_v = 5 \times 10^{-18}$

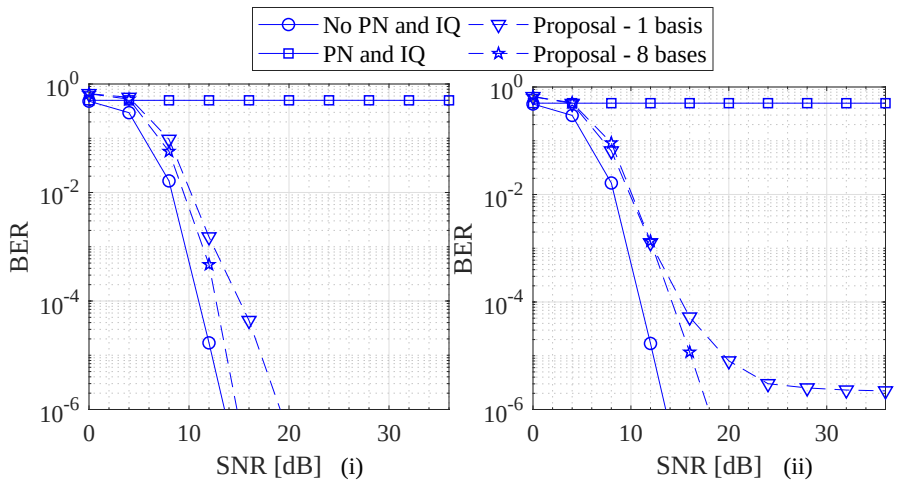

Figure 6.8: Bit-error rate performance of 2×2 MIMO-OFDM in the presence of PN and IQ imbalance. (i) $c_v = 5 \times 10^{-18}$, and (ii) $c_v = 2 \times 10^{-17}$.

and from $c_v = 5 \times 10^{-19}$ to 2×10^{-17}, respectively. The difference is unnoticeable for PN estimation.

Stage 2

Performance of the second stage is shown in Fig. 6.8. Since there is a strong similarity in the BER performance of the considered CP-based multi-carrier systems in the SISO scenario (see Fig. 6.6), only performance of the OFDM system is presented in Fig. 6.8 for the MIMO scenario. Furthermore, the performance when $c_v = 5 \times 10^{-19}$ is not shown since it is very similar to the performance when $c_v = 5 \times 10^{-18}$. First, observe that by using SFBC the proposed algorithm substantially enhances the decoding performance. In particular, compared to the SISO case, the compensation performance is significantly improved even when only one basis is deployed. When $c_v = 5 \times 10^{-18}$, increasing the number of bases from 1 to 8 helps to gain approximately 3.5 dB at BER $= 10^{-5}$. The performance gap between the ideal case and the proposed algorithm is only about 1.3 dB at BER $= 10^{-5}$ when 8 bases are used.

While there is a performance saturation when $c_v = 2 \times 10^{-17}$ in the SISO case (see Fig. 6.6), with the help of the diversity technique the error performance of the proposed algorithm is not saturated and is much better in the MIMO scenario. Only approximately 3.8 dB gap

at BER $= 10^{-5}$ is seen between "No PN and IQ" and the proposed algorithm using 8 bases.

6.6 Conclusions

In this paper, the impacts of PN and IQ imbalance are first analyzed for CP-based multi-carrier modulation systems, including but not limited to OFDM, GFDM and CFBMC. Then, a unified two-stage algorithm was proposed to compensate for the impacts of PN and IQ imbalance. Specifically, the IQ imbalance parameters and channel impulse response are estimated in the first stage based on the transmission of a preamble which is designed such that the estimation of IQ imbalance does not depend on the estimation errors of the estimated channel and PN. Given the estimates from the first stage, the IQ imbalance and PN are compensated subsequently in the second stage. The proposed algorithm is further extended to a spatial-diversity MIMO system where the IQ imbalance and PN are different for each receive antenna. Simulation results were presented and discussed in detail to demonstrate the effectiveness of the proposed algorithm in a variety of PN and IQ imbalance conditions.

References

[1] J. G. Andrews and S. Buzzi and W. Choi and S. V. Hanly and A. Lozano and A. C. K. Soong and J. C. Zhang: "What Will 5G Be?", *IEEE Journal on Selected Areas in Communications*, vol. 32, no. 6, pp. 1065–1082, 2014.

[2] B. Farhang-Boroujeny: "Filter Bank Multicarrier Modulation: A Waveform Candidate for 5G and Beyond", *Advances in Electrical Engineering*, vol. 2014, pp. 1–25, Feb. 2014.

[3] R. Nissel and S. Schwarz and M. Rupp: "Filter Bank Multicarrier Modulation Schemes for Future Mobile Communications", *IEEE Journal on Selected Areas in Communications*, vol. 35, no. 8, pp. 1768–1782, Feb. 2017.

[4] B. Farhang-Boroujeny: "OFDM Versus Filter Bank Multicarrier", *IEEE Signal Processing Magazine*, vol. 28, no. 3, pp. 92–112, May 2011.

[5] T. Hwang and C. Yang and G. Wu and S. Li and G. Y. Li: "OFDM and Its Wireless Applications: A Survey", *IEEE Transactions on Vehicular Technology*, vol. 58, no. 4, pp. 1673–1694, May 2009.

[6] G. Fettweis and M. Krondorf and S. Bittner: "GFDM - Generalized Frequency Division Multiplexing", *IEEE 69th Vehicular Technology Conference*, pp. 1–4, April 2009.

[7] N. Michailow and M. Matth and I. S. Gaspar and A. N. Caldevilla and L. L. Mendes and A. Festag and G. Fettweis: "Generalized Frequency Division Multiplexing for 5th Generation Cellular Networks", *IEEE Transactions on Communications*, vol. 62, no. 9, pp. 3045–3061, Sept. 2014.

[8] A. RezazadehReyhani and A. Farhang and B. Farhang-Boroujeny: "Circularly Pulse-Shaped Waveforms for 5G: Options and Comparisons", *2015 IEEE Global Communications Conference (GLOBECOM)*, pp. 1–7, Dec. 2015.

[9] A. RezazadehReyhani and B. Farhang-Boroujeny: "An Analytical Study of Circularly Pulse-Shaped FBMC-OQAM Waveforms", *IEEE Signal Processing Letters*, vol. 24, no. 10, pp. 1503–1506, Oct. 2017.

[10] K. W. Martin: "Small side-lobe filter design for multitone data-communication applications", *IEEE Transactions on Circuits and Systems II: Analog and Digital Signal Processing*, vol. 45, no. 8, pp. 1155–1161, Aug. 1998.

[11] B. Farhang-Boroujeny: "Signal Processing Techniques for Software Radios", *Lulu Publishing House*, vol. 82, 2011.

[12] T. Schenk: "RF Imperfections in High-rate Wireless Systems: Impact and Digital Compensation". Springer, Netherlands (2008).

[13] S. Wu and Y. Bar-Ness: "A phase noise suppression algorithm for OFDM-based WLANs", *IEEE Communications Letters*, vol. 6, no. 12, pp. 535–537, Dec. 2002.

[14] P. Rabiei and W. Namgoong and N. Al-Dhahir: "A Non-Iterative Technique for Phase Noise ICI Mitigation in Packet-Based OFDM Systems", *IEEE Transactions on Signal Processing*, vol. 58, no. 11, pp. 5945–5950, Nov. 2010.

[15] P. Rabiei and W. Namgoong and N. Al-Dhahir: "Reduced-Complexity Joint Baseband Compensation of Phase Noise and I/Q Imbalance for MIMO-OFDM Systems", *IEEE Transactions on Wireless Communications*, vol. 9, no. 11, pp. 3450–3460, 2010.

[16] J. Tubbax and B. Come and L. Van der Perre and S. Donnay and M. Engels and H. D. Man and M. Moonen: "Compensation of IQ imbalance and phase noise in OFDM systems", *IEEE Transactions on Wireless Communications*, vol. 4, no. 3, pp. 872–877, 2005.

[17] S. Jnawali and S. Beygi and H. R. Bahrami: "A Low-Complexity Method to Compensate IQ-Imbalance and Phase Noise in MIMO-OFDM Systems", *2011 IEEE Global Telecommunications Conference - GLOBECOM 2011*, pp. 1–6, 2011.

[18] S. Suyama and H. Suzuki and K. Fukawa and J. Izumi: "Iterative receiver employing phase noise compensation and channel estimation for millimeter-wave OFDM systems", *IEEE Journal on Selected Areas in Communications*, vol. 27, no. 8, pp. 1358–1366, Oct. 2009.

[19] S. Suyama and Y. Hashimoto and H. Suzuki and K. Fukawa: "60 GHz OFDM experimental system employing decision-directed phase noise compensation", *2012 IEEE Radio and Wireless Symposium*, pp. 191–194, Jan. 2012.

[20] P. Mathecken and T. Riihonen and S. Werner and R. Wichman: "Phase Noise Estimation in OFDM: Utilizing Its Associated Spectral Geometry", *IEEE Transactions on Signal Processing*, vol. 64, no. 8, pp. 1999–2012, Apr. 2016.

[21] Z. Wang and P. Babu and D. P. Palomar: "Effective Low-Complexity Optimization Methods for Joint Phase Noise and Channel Estimation in OFDM", *IEEE Transactions on Signal Processing*, vol. 65, no. 12, pp. 3247–3260, Jun. 2017.

[22] L. D. Le and H. H. Nguyen: "Phase Noise Compensation for CFBMC-OQAM Systems Under Imperfect Channel Estimation", *IEEE Access*, vol. 8, pp. 47247–47263, 2020.

[23] J. Tubbax and B. Come and L. Van der Perre and L. Deneire and S. Donnay and M. Engels: "Compensation of IQ imbalance in OFDM systems", *2003 IEEE International Conference on Communications*, vol. 5, pp. 3403–3407, May 2003.

[24] J. Tubbax and B. Come and L. Van der Perre and S. Donnay and M. Moonen and H. D. Man: "Compensation of transmitter IQ imbalance for OFDM systems", *2004 IEEE International Conference on Acoustics, Speech, and Signal Processing*, vol. 2, pp. 325–328, May 2004.

[25] H. Cheng and Y. Xia and Y. Huang and L. Yang and Z. Xiong and D. P. Mandic: "Improperness Based SINR Analysis of GFDM Systems Under Joint Tx and Rx I/Q Imbalance", *2020 IEEE Wireless Communications and Networking Conference (WCNC)*, pp. 1–6, 2020.

[26] M. Lupupa and J. Qi: "I/Q imbalance in generalized frequency division multiplexing under Weibull fading", *2015 IEEE 26th Annual International Symposium on Personal, Indoor, and Mobile Radio Communications (PIMRC)*, pp. 471–476, 2015.

[27] A. Gomaa and L. M. A. Jalloul: "Data-Aided I/Q Imbalance Estimation and Compensation in OFDM Systems", *IEEE Communications Letters*, vol. 18, no. 3, pp. 459–462, 2014.

[28] P. Rabiei and W. Namgoong and N. Al-Dhahir: "Low-Complexity OFDM Channel Estimation in the Presence of I/Q Imbalance and Phase Noise", *IEEE Global Telecommunications Conference*, pp. 1–5, 2009.

[29] P. Rabiei and W. Namgoong and N. Al-Dhahir: "MIMO-OFDM channel estimation in the presence of I/Q imbalance and phase noise for IEEE 802.11N", *IEEE International Conference on Acoustics, Speech and Signal Processing*, pp. 3190–3193, 2010.

[30] J. Tubbax and B. Come and L. Van der Perre and S. Donnay and M. Engels and C. Desset: "Joint Compensation of IQ Imbalance and Phase Noise", *The 57th IEEE Semiannual Vehicular Technology Conference*, vol. 3, pp. 1605–1609, Apr. 2003.

[31] A. Demir and A. Mehrotra and J. Roychowdhury: "Phase noise in oscillators: a unifying theory and numerical methods for characterization", *IEEE Transactions on Circuits and Systems I: Fundamental Theory and Applications*, vol. 47, no. 5, pp. 655–674, May 2000.

[32] D. Petrovic and W. Rave and G. Fettweis: "Effects of Phase Noise on OFDM Systems With and Without PLL: Characterization and Compensation", *IEEE Transactions on Communications*, vol. 55, no. 8, pp. 1607–1616, Aug. 2007.

[33] D. Shin and S. Suyama and H. Suzuki and K. Fukawa: "10 Gbps millimeter-wave OFDM experimental system with iterative phase noise compensation", *2013 IEEE Radio and Wireless Symposium*, pp. 184–186, Jan. 2013.

[34] Y. S. Cho, J. Kim, W. Y. Yang and C. G. Kang: "MIMO-OFDM Wireless Communications with MATLAB", *John Wiley & Sons (Asia) Pte Ltd*, 2010.

[35] H. Zarrinkoub: "Understanding LTE with MATLAB: From Mathematical Modeling to Simulation and Prototyping", *John Wiley & Sons, Ltd*, 2014.

7. Summary and Suggestions for Further Studies

7.1 Summary

Due to the low complexity implementation of channel estimation and equalization, CP-based multi-carrier modulation techniques including OFDM, CFBMC-OQAM and GFDM have become popular choices in many communication systems. This thesis focused on two main topics: (i) the integration of CP-based multi-carrier systems with the other techniques and (ii) the impacts of physical impairments and their compensation in CP-based multi-carrier systems.

In the first contribution, an OFDM-based FD communication scenario between two nodes in the presence of the most relevant physical impairments, namely PN, IQ imbalance and nonlinearity, is considered. The impact of physical impairments on the received signal in FD communication scenario is first analyzed. Based on that analysis, an iterative SIC algorithm is proposed in which the SIC and data detection benefit from each other. To improve the quality of the SIC, the physical impairments are estimated and compensated. Performance of the proposed algorithm is shown to outperform the existing algorithms.

In the second contribution, the impact of PN is evaluated in CFBMC-OQAM systems. It is first shown that in the presence of PN, the self-interferences, namely ISI and ICI, drastically degrade performance of CFBMC-OQAM. Then, an algorithm is proposed to compensate for the PN impact in CFBMC-OQAM in which channel frequency response is assumed to be known at the receiver. In this algorithm, the impact of PN in the conjugation form can be captured by a multiplication of a known basis matrix and an unknown vector which is then estimated based on pilot symbols. Only a small performance gap is observed between the

proposed algorithm and the ideal case where there is no PN.

As an extension of the second contribution, the impact of imperfect channel estimation is considered in the third part of this research. In order to take into account channel estimation, a two-stage PN compensation algorithm is proposed in which the channel frequency response is estimated in the first stage based on the transmission of a preamble. Given the estimated channel, the PN impact can be compensated for the rest of data transmission blocks in the second stage. The strategy to design the preamble is also presented in this part of the research. From the simulation results, the proposed algorithm is shown to effectively estimate the channel information as well as compensate for the PN impact.

In the last contribution, the impact of IQ imbalance is also included in addition to PN and imperfect channel estimation. A two-stage algorithm is developed to take the impact of IQ imbalance into account. Along with the channel, the IQ imbalance parameters are estimated in the first stage. The preamble in this chapter is designed to be spectrally efficient and the estimation of IQ imbalance does not depend on the estimation errors of estimated channel and PN. Given the estimate from the first stage, the IQ imbalance and PN are subsequently compensated in the second stage. The proposed algorithm is further extended to a MIMO system where the PN and IQ imbalance are different in each receive antenna. The preamble design is also generalized for the MIMO system. Only one transmission symbol is needed to be transmitted as the preamble. To further improve performance of the proposed algorithm, a diversity technique is considered in the MIMO system. Simulation results are presented for three systems, namely OFDM, GFDM and CFBMC-OQAM. The proposed algorithm is shown to effectively compensate for PN and IQ imbalance impacts.

7.2 Suggestions for Further Studies

As a further development of the first contribution, the combination of a general CP-based multi-carrier system and FD communication under the impact of physical impairments could be studied. Different from the first contribution which considers an orthogonal system, i.e., OFDM, the other classes of CP-based multi-carrier systems can be considered as well. Without a strict orthogonal condition, more challenging issues are expected related to the

impact of SI. For example, as described in Section 2.2.3, because GFDM is a non-orthogonal system, it suffers from the self-interference even under the ideal transmission condition. As such, when integrated with FD communications, an SIC should be designed such that it can handle not only the ordinary SI resulting from the FD communications, but also the SI due to the non-orthogonality. Including physical impairments would further complicate the design of an effective SIC algorithm.

Second, it was shown that the use of CP can eliminate the IBI, provided that its length is chosen sufficiently large compared to the channel length. While a long CP leads to a significant reduction in both bandwidth and power efficiencies since the CP does not carry any useful information, a CP whose length is shorter than the length of the channel impulse response results in ICI and IBI [3, 4]. In general, while the CP length is usually specified based on a standard, the channel length could change randomly. This possibly results in a CP insufficiency. As such, the impact of insufficient CP could be studied in a general CP-based multi-carrier system. The compensation of insufficient CP generally requires knowledge of not only the transmitted signal from the previous block to remove the IBI, but also the channel state information to remove the ICI impact. When physical impairments are also included in the insufficient CP scenario, it further complicates the design of compensation algorithms.

Third, not only PN and IQ imbalance, nonlinearity is also shown to be a critical factor that significantly degrades performance of a multi-carrier system in general. However, the impact of nonlinearity has only been considered for OFDM systems in conjunction with FD communications in this thesis. As relatively new multi-carrier techniques, there have not been many studies that examine performance of CFBMC-OQAM and GFDM in the presence of nonlinearities. To evaluate performance degradation induced from nonlinearities, the Bussgang decomposition can be applied [5, 6]. This decomposition provides an exact probabilistic relationship between the output and the input of a nonlinear system. Specifically, the output is equal to a scaled version of the input plus uncorrelated distortion. Applying this decomposition would help to analytically derive performance of the new waveforms in the presence of nonlinearities in terms of achievable datat rate, BER, etc.

Last, to further improve the applicability as well as the validity of all the studies in this research, additional works need to be considered. For example, in the first contribution, the BER performance obtained from the proposed algorithm should be compared with the BER performance when HD is considered and there are no physical impairments (which serves as the lower bound), to further show the effectiveness of the proposed algorithm in canceling SI and compensating physical impairments. Second, to simplify the development of the proposed algorithm, the remote device is assumed to be free of physical impairments. This assumption may not hold true in practice. Furthermore, the trade-off between the computational complexity and processing latency of the proposed iterative SI compensation algorithm is needed. In the second and third studies where the impact of PN and its compensation are considered for CFBMC-OQAM systems, to improve the quality of the estimated channel and thus the PN compensation, statistics of channel and noise are assumed to be known and MMSE estimation can be performed. In practice, this information needs to be estimated and thus its estimation error should also be taken into account. Furthermore, since the first stage of the proposed algorithm is performed iteratively, the latency induced from the first stage should be analyzed. In the last study where IQ imbalance is considered together with PN and imperfect channel estimation, the IQ imbalance distortion is assumed to be from mixers only, which is commonly known as frequency-independent IQ imbalance. However, the mismatches between the I and Q branches due to transmit/receive analog filters and DAC or ADC, which is frequency-dependent IQ imbalance, has not been considered. Additionally, the impacts of PN and IQ imbalance should also be considered at the transmitter for the last three studies in this thesis.

References

[1] N. Michailow and M. Matth and I. S. Gaspar and A. N. Caldevilla and L. L. Mendes and A. Festag and G. Fettweis: "Generalized Frequency Division Multiplexing for 5th Generation Cellular Networks", *IEEE Transactions on Communications*, vol. 62, no. 9, pp. 3045–3061, Sept. 2014.

[2] G. Fettweis and M. Krondorf and S. Bittner: "GFDM - Generalized Frequency Division Multiplexing", *IEEE 69th Vehicular Technology Conference*, pp. 1–4, April 2009.

[3] Y. Jin and X. Xia: "A Robust Precoder Design Based on Channel Statistics for MIMO-OFDM Systems with Insufficient Cyclic Prefix", *IEEE Transactions on Communications*, vol. 62, no. 4, pp. 1249–1257, Apr. 2014.

[4] T. Pham and T. Le-Ngoc and G. K. Woodward and P. A. Martin: "Channel Estimation and Data Detection for Insufficient Cyclic Prefix MIMO-OFDM", *IEEE Transactions on Vehicular Technology*, vol. 66, no. 6, pp. 4756–4768, Jun. 2017.

[5] J. J. Bussgang: "Cross-correlation functions of amplitude distorted Gaussian signals". Research laboratory of Electronics, Massachusetts Institute of Technology, 1952.

[6] O. T. Demir and E. Bjornson, "The Bussgang Decomposition of Nonlinear Systems: Basic Theory and MIMO Extensions [Lecture Notes]," *IEEE Signal Processing Magazine*, vol. 38, no. 1, pp. 131–136, Jan. 2021.

Thank you for your order with RightsLink / Springer Nature

no-reply@copyright.com <no-reply@copyright.com>

Sun 2020-10-11 5:54 PM

To: Le, Long <long.le@usask.ca>

SPRINGER NATURE

Thank you for your order!

Dear Mr. Long Le,

Thank you for placing your order through Copyright Clearance Center's RightsLink® service.

Order Summary

Licensee:	Mr. Long Le
Order Date:	Oct 11, 2020
Order Number:	4926160676351
Publication:	Wireless Personal Communications
Title:	Iterative Self-Interference Mitigation in Full-Duplex Wireless Communications
Type of Use:	Thesis/Dissertation
Order Total:	0.00 CAD

View or print complete details of your order and the publisher's terms and conditions.

Sincerely,

Copyright Clearance Center

Tel: +1-855-239-3415 / +1-978-646-2777
customercare@copyright.com

https://myaccount.copyright.com

Impacts of Phase Noise on CFBMC-OQAM

Conference Proceedings: 2018 IEEE 88th Vehicular Technology Conference (VTC-Fall)

Author: Long D. Le

Publisher: IEEE

Date: Aug. 2018

Thesis / Dissertation Reuse

The IEEE does not require individuals working on a thesis to obtain a formal reuse license, however, you may print out this statement to be used as a permission grant:

Requirements to be followed when using any portion (e.g., figure, graph, table, or textual material) of an IEEE copyrighted paper in a thesis:

1) In the case of textual material (e.g., using short quotes or referring to the work within these papers) users must give full credit to the original source (author, paper, publication) followed by the IEEE copyright line © 2011 IEEE.
2) In the case of illustrations or tabular material, we require that the copyright line © [Year of original publication] IEEE appear prominently with each reprinted figure and/or table.
3) If a substantial portion of the original paper is to be used, and if you are not the senior author, also obtain the senior author's approval.

Requirements to be followed when using an entire IEEE copyrighted paper in a thesis:

1) The following IEEE copyright/ credit notice should be placed prominently in the references: © [year of original publication] IEEE. Reprinted, with permission, from [author names, paper title, IEEE publication title, and month/year of publication]
2) Only the accepted version of an IEEE copyrighted paper can be used when posting the paper or your thesis on-line.
3) In placing the thesis on the author's university website, please display the following message in a prominent place on the website: In reference to IEEE copyrighted material which is used with permission in this thesis, the IEEE does not endorse any of [university/educational entity's name goes here]'s products or services. Internal or personal use of this material is permitted. If interested in reprinting/republishing IEEE copyrighted material for advertising or promotional purposes or for creating new collective works for resale or redistribution, please go to http://www.ieee.org/publications_standards/publications/rights/rights_link.html to learn how to obtain a License from RightsLink.

If applicable, University Microfilms and/or ProQuest Library, or the Archives of Canada may supply single copies of the dissertation.

BACK CLOSE WINDOW